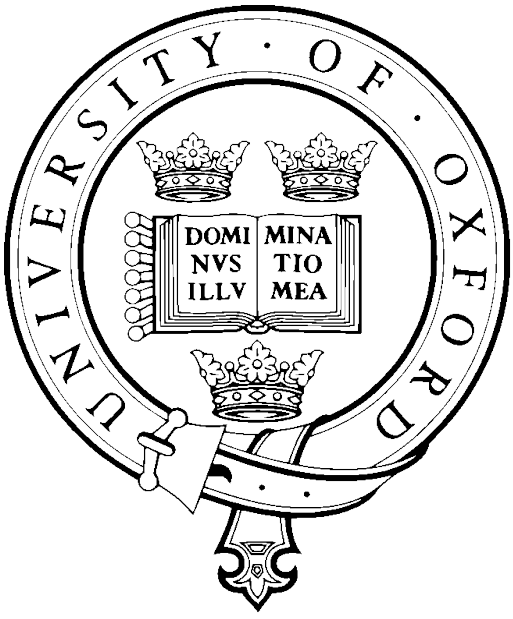
Estimates of the size-fractionated primary production of UK Shelf Seas from satellite

By

Kieran Francis Curran

A thesis submitted to the University of Oxford for the degree of Doctor of Philosophy in Earth Sciences



Department of Earth Sciences and Wolfson College
University of Oxford
2018

Supervised by Dr. Gavin H. Tilstone, Dr Heather A. Bouman, Dr Anna E. Hickman, Dr Bob Brewin, Dr Shubha Sathyendranath, Dr Will Homoky

Estimates of the size-fractionated primary production of UK Shelf Seas from satellite

Kieran Francis Curran, Wolfson College

Thesis submitted to the University of Oxford for the degree of Doctor of Philosophy in Earth Sciences

Abstract

Estimates of size-fractionated (S-F) primary production are valuable to marine ecologists, biogeochemists and policymakers, as the productivity of individual fractions are important to populations of grazers and processes of nutrient cycling and carbon export. This thesis aims to provide a means to estimate S-F PP in UK Shelf Seas, using *in situ* measurements of photosynthesis-irradiance (*PE*) parameters to tune an existing remote sensing model of S-F PP. A large dataset from the Celtic Sea and the Western English Channel shows that photosynthetic rates of picophytoplankton are markedly higher than larger nano- and microphytoplankton, and that *PE* parameter values for this size fraction are higher than observed in open-ocean environments. This leads to picophytoplankton accounting for a greater proportion of shelf-sea PP than previously assumed. Bio-optical measurements conducted in the Celtic Sea allowed the correction of α^Bvalues and calculation of φ_{max} using more representative S-F chlorophyll-specific absorption ($a_{ph}^*(\lambda)$) spectra. However, a significant number of data gaps and lack of reliable microphytoplankton spectra necessitated using average or modelled values of $a_{ph}^*(\lambda)$. Testing approaches of estimating $a_{ph}^*(\lambda)$ revealed that using some modelled spectra produced reasonable estimates of water-column

PP. However, the vertical distribution of PP changed considerably between model runs using different estimated spectra, which may hinder our ability to assess the shape of the PP profile and the contribution of subsurface populations to integrated PP.

This study provides a synthesis of the largest dataset of measured S-F chlorophyll concentrations, phytoplankton *PE* parameters, and absorption spectra for UK Shelf Seas, incorporating data from across a variety of shelf environments in multiple years, often at weekly resolution for Western English Channel sites, allowing us to explore the relationship between the photophysiology of shelf-sea phytoplankton and environmental variables. Developing a regionally-tuned model to map S-F PP in UK Shelf Seas from space represents a useful advance in the monitoring of ecology and biogeochemistry of shelf-sea systems.

Estimates of the size-fractionated primary production of UK Shelf Seas from satellite

Kieran Francis Curran, Wolfson College

Thesis submitted to the University of Oxford for the degree of Doctor of Philosophy in Earth Sciences

Extended abstract

The fate of carbon fixed during photosynthesis in the pelagic food chain, and regional biogeochemistry is often determined by the size of single-celled microalgae collectively known as phytoplankton, which vary over nine orders of magnitude in cell volume. Thus there is a growing interest to understand not only the dynamics of the bulk phytoplankton biomass and primary production, but also how the size structure of phytoplankton communities change and how ocean productivity is divided amongst the phytoplankton size classes which requires measurements of the photophysiology of each size range of interest. Existing datasets of size-fractionated (S-F) photosynthesis-irradiance (*PE*) parameters are extremely rare, particularly in shelf seas, given that the experimental measurement of the S-F primary production is time consuming and labour intensive. Thus previous studies that have attempted to estimate S-F productivity on basin-to-global scales use indirect methods to estimate the biomass of individual size fractions, most commonly diagnostic pigment concentrations (Uitz et al. (2010).

The *PE* parameters are used in light-driven models of primary production (PP) to describe the photosynthetic response of phytoplankton to absorbed or available light. It is essential to specify the PE parameters at every pixel for computation of primary production using

satellite data. In order to minimize the errors in the computed production fields for a given region, it is necessary to optimise the assignment of *PE* parameters by using field measurements. As the hydrodynamics, nutrient availability and ecology of shelf seas are often distinct from the open ocean, it is likely that an approach for parameter assignment based on an open-ocean dataset may not be appropriate for shelf waters.

This study seeks to address this lack of (S-F) bio-optical data from shelf seas, and provide a basis to test the applicability of generic S-F PP algorithms to UK shelf waters. To this end, S-F measurements of chlorophyll concentration, photosynthesis-irradiance response curves and phytoplankton light absorption were taken along with hydrographic measurements during spring and summer cruises in the Celtic Sea and from two time-series stations of the Western English Channel Observatory (WCO). The effect of abiotic variables such as light and temperature on photosynthetic rates was also investigated to establish whether empirical relationships found in other regions are common to the UK shelf and assess their utility as environmental predictors of the *PE* parameters (Bouman et al. 2005; Bouman et al. 2003; Robinson et al. 2018; Uitz et al. 2008).

Analysis of the *PE* parameters P_m^B and α^B collected from the Celtic Sea and Western English Channel Observatory reveal a clear size dependence: both parameters increase with decreasing cell size, consistent with culture and field studies (including shelf seas (de Madariaga and Joint 1994; Morán and Scharek 2015)), with the magnitude of P_m^B and α^B generally being greater than those reported in open-ocean waters (Brewin et al. 2017b; Uitz et al. 2008). Nanophytoplankton and picophytoplankton chlorophyll-specific absorption coefficients (a_{ph}^*) measured on the UK shelf were lower than most other studies, particularly those based on open-ocean optical datasets. These regional differences in a_{ph}^*coefficients were likely due to differences in phytoplankton taxonomic and pigment composition.

To address the sparsity of S-F absorption spectra, various models were tested to predict the shape and magnitude of $a_{ph}^{*}(\lambda)$. Marked differences in the spectral shape and magnitude of $a_{ph}^{*}(\lambda)$ observed between models meant that in order to fill data gaps by using estimated $a_{ph}^{*}(\lambda)$ in spectrally-resolved models of PP without increasing errors, the effect of the choice of $a_{ph}^{*}(\lambda)$ on estimates of PP was examined. Results were surprising, with the low spectral resolution model of Varunan and Shanmugam (2015) outperforming the models of Ciotti et al. (2002) and Uitz et al. (2008) which produced estimates of $a_{ph}^{*}(\lambda)$ at a high spectral resolution based on *in situ* data (Tables 3.2, 3.3). However, the spectral shapes produced by the taxon-specific model of Ciotti et al. (2002) most closely resembled the phytoplankton absorption spectra measured in the Celtic Sea, and were thus used to estimate phytoplankton $a_{ph}^{*}(\lambda)$ in PP model runs in Chapter 3.

In order to scale up station-by-station estimates of S-F PP to regional scales, the S-F chlorophyll and *PE* parameter data alongside hydrographic measurements described in Chapter 1 were used to regionally tune the remote sensing PP model of Brewin et al. (2017b). My results show that the retuned model was more representative of the estimates presented on a station-by-station basis in Chapter 1 during periods of high chlorophyll concentration. However, the retuned model overestimated PP during periods of low chlorophyll concentration and this bias may be due to a seasonal bias in the sampling of the Celtic Sea and Western Channel, which took place primarily from the spring bloom to late summer (Fig 4.13). The model results also show that estimates of PP in UK shelf seas are particularly sensitive to the shape of the sub-surface biomass profile and is extremely difficult to predict using satellite-observable variables. Although model performance was improved by assuming permanent stratification for the region, this is an unrealistic assumption when modelling PP between autumn to early spring when these waters are vertically mixed.

Results from Chapter 4 have demonstrated that current models of S-F PP can be used in shelf seas with some success, however their satisfactory performance relies on being regionally tuned by *in situ* measurements collected in UK shelf seas. The bio-optical dataset generated by my thesis work suggest that S-F *PE* parameters derived from shelf communities are distinct from open-ocean communities in terms of their light-limited photosynthetic rates (α^B), which in the UK shelf dataset are markedly higher. These differences in α^B were shown to have pronounced impacts on estimates of PP near the sub-surface chlorophyll maximum. Moreover, the shelf-sea dataset exhibited high values of P_m^B for the picophytoplankton size fraction, which were reflected in their significant contribution to total PP in UK shelf seas.

Table of Contents

Abstract....ii

Extended abstract....iv

List of figures....xiv

List of Tables....**Error! Bookmark not defined.**

List of Parameter and variable symbols and abbreviations....xix

1 Introduction....1

1.1 The importance of shelf seas for marine primary production....1

1.2 The importance of phytoplankton community structure in ocean biogeochemistry....3

1.3 Separating the phytoplankton community....5

1.3.1 Taxonomic-based methods....5

1.3.2 Phytoplankton pigment markers....6

1.3.3 Size-fractionation....8

1.4 Phytoplankton photophysiology....8

1.4.1 Photosynthesis-irradiance (*PE*) parameters....9

1.4.2 Photoacclimation of phytoplankton....11

1.4.3 Influence of underwater light field on phytoplankton absorption....14

1.5 The underwater light field of shelf seas....17

1.6 Modelling primary production in shelf seas....20

1.6.1 PP as a key environmental indicator....20

1.6.2 Estimating PP simple functions to complex spectral models....21

1.7 Estimating PP from satellite observations 22

1.7.1 Incorporating PE parameters in satellite models of PP 23

1.8 Thesis objectives 24

2 Variability of size-fractionated photophysiology and primary production in UK shelf seas 27

2.1 Introduction 27

2.1.1 Heterogeneity of shelf seas 27

2.1.2 Modelling of primary production 30

2.1.3 Importance of photophysiological measurements for satellite models of PP 34

2.1.4 Objectives of this chapter 35

2.2 Methods 36

2.2.1 Study area and sampling 36

2.2.2 Size-fractionated chlorophyll–a concentrations 38

2.2.3 Size-fractionated phytoplankton and particulate absorption spectra (PABS) 39

2.2.4 Size-fractionated PE and photo-physiological parameters 40

2.2.5 Spectral correction of light-limited photosynthesis 41

2.2.6 Estimates of daily depth-integrated primary production 42

2.2.7 Phytoplankton taxonomy 43

2.2.7.1 Light microscopy 44

2.2.7.2 Flow cytometry 44

2.2.7.3 Statistical Analysis 45

2.3 Results 46

2.3.1 Seasonal variability at WCO and Celtic Sea – stratification and nutrients 46

2.3.2 Seasonal variability at WCO – phytoplankton biomass and taxonomy 50

2.3.5 Seasonal variability at WCO – size-fractionated PE parameters 53

2.3.3 The Celtic Sea spring bloom – Stratification, biomass and taxonomy.....54

2.3.4 Seasonal variability in the Celtic Sea – size-fractionated chlorophyll 58

2.3.5 Seasonal variability in the Celtic Sea - size-fractionated phytoplankton light absorption spectra.....61

2.3.6 Variability with depth – size-fractionated PE parameters at L4, E1 and the Celtic Sea 63

2.3.7 Statistical analyses.....70

2.3.7.1 Principal component analyses (PCA).....70

2.3.7.1 Relationships of photophysiological parameters with physical variables.....72

2.3.8 Variability in modelled size-fractionated primary production 74

2.7 Discussion.....78

2.7.1 Differences in photo-physiology between size fractions in shelf seas 78

2.7.2 Seasonal and regional variability in phytoplankton biomass and photo-physiology .80

2.7.3 Seasonal and regional variability in Biomass and Primary production.....84

2.8 Conclusions 90

3 Estimating the light absorption properties of different size classes of phytoplankton for use in shelf sea primary production models.....93

3.1 Introduction 93

3.1.1 Estimating size-fractionated light absorption from total measurements using diagnostic pigments 95

3.1.1 Estimating size-fractionated light absorption from phytoplankton pigments 95

3.1.2 Estimating size-fractionated light absorption using pigment reconstruction 96

3.1.3 Estimating size-fractionated light absorption from ocean colour remote sensing data 97

3.1.4 Estimating size-fractionated light absorption from dominant taxa 98

3.1.5 Measuring size-fractionated light absorption *in vivo* 99

3.1.6 Objectives 100

3.2 Methods 101

3.2.1 Study area and sampling.....101

3.2.2 Size-fractionated chlorophyll–a concentrations and phytoplankton light absorption 101

3.2.3 Estimation of size-fractionated light absorption from phytoplankton pigments (Uitz et al 2008) 103

3.2.4 Estimation of light absorption by pigment reconstruction (Bidigare et al 1990) 103

3.2.5 Estimation of light absorption using ocean colour remote sensing data (Varunan and Shanmugam 2015) 106

3.2.6 Estimation of light absorption from dominant taxa (Ciotti et al 2002) 107

3.2.7 Comparisons of PP estimates using modelled and measured $a_{ph}(\lambda)$ 108

3.3 Results 110

3.3.1 Measured total and chlorophyll-specific phytoplankton absorption.....110

3.3.2 The model of Uitz et al (2008): scaling size-fractionated values of $aph*(\lambda)$ with ζ 117

3.3.3 Modelled phytoplankton absorption spectra using the pigment reconstruction method (Bidigare et al. 1990) 118

3.3.5 Size-fractionated light absorption using ocean-colour remote-sensing data (Varunan & Shanmugam 2015) 122

3.3.6 Comparison between models of $aph*(\lambda)$ 123

3.4 How do modelled phytoplankton absorption spectra affect estimates of primary production in shelf seas? 126

3.5 Discussion 132

3.5.1 How well do modelled size-fractionated specific absorption coefficients match measured spectra? 132

3.5.3 To what extent do differences in modelled phytoplankton absorption spectra influence calculated size-fractionated primary productivity? 136

3.8 Conclusions 138

4 Estimates of size-fractionated primary production from satellite 141

4.1 Introduction 141

4.1.1 Previous efforts to estimate S-F PP 141

4.1.2 Estimating phytoplankton size distribution from satellite 142

4.2 Methods 144

4.2.1 Estimating primary production using the available light model of Brewin et al (2017) 144

4.2.2 Euphotic Depth 146

4.2.3 Vertical variability in chlorophyll-a concentration 146

4.2.4 Photophysiological parameters 147

4.2.5 Irradiance 148

4.2.6 Satellite datasets 149

4.3 Objectives 150

4.4 Results 150

4.4.1 Modelling size-fractionated chlorophyll from total chlorophyll 150

4.4.2 Comparison of measured and modelled photo-physiological parameters 153

4.4.3 Estimates of euphotic depth from surface chlorophyll 155

4.4.5 Vertical distribution of phytoplankton biomass 156

4.4.6 Estimates of annual PP from ocean colour data 158

4.4.7 Differences with open ocean parameterisation (Open Sat) of Brewin et al (2017) model 162

4.4.8 Annual patterns of size-fractionated PP in UK shelf seas: estimates from satellite models compared with a bio-optical model using measured photophysiology. 165

4.5 Discussion 171

4.5.1 How accurate are satellite estimates of size-fractionated PP using a retuned model? 171

4.5.2 Photo physiological parameters and biomass distribution 173

4.5.3 Effect of hydrographic differences between open ocean and shelf seas on modelled PP 174

4.5.4 Optics 175

4.6 Conclusions 177

5 Conclusions and future directions 178

5.1 Do Shelf Sea phytoplankton communities require separate parameterisation of photophysiology? 178

5.2 Estimating PP for the UK shelf – improvements in model performance and steps for improvement.....185

5.3 Improvements to estimates of the vertical distribution of phytoplankton 187

REFERENCES 190

List of figures

Figure 1.1 Photosynthesis-irradiance (*PE*) curve showing α^B, P_m^B, E_k ……...10

Figure 1.2 Light absorption spectrum of pure water of Pope and Fry (1997)..…….….17

Figure 1.3 Hierarchy of approaches to modelling primary production of Platt and Sathyendranath (2009)…… ……21

Figure 2.1 Schematic of variables and parameters required to estimate primary production using measurements of *PE* parameters……..……31

Figure 2.2 Example size-fractionated *PE* curves measured in the Celtic Sea April 2015…….. 32

Figure 2.3 Map showing the sample sites visited during August 2014 and April 2015 cruises to the Celtic Sea and from two sites of Western English Channel Observatory…….37

Figure 2.4 Climatological time series of temperature, salinity and PAR at station L4……48

Figure 2.5 Climatological time series of macronutrient concentrations at stations L4 and E1…...49

Figure 2.6 Time series of macronutrient concentrations in the Celtic sea at two stations: Celtic Deep (Mar 2014 – Aug 2015) and Central Celtic Sea (Mar 2014 – Jul 2015)……..… …..….50

Figure 2.7 Mean monthly total and size-fractionated chlorophyll concentrations at L4 during 2009-2015……...…51

Figure 2.8 Mean monthly phytoplankton carbon concentration at L4 by functional type Estimated using light microscopy cell count data from 2009-2016……52

Figure 2.9 Climatologies of monthly mean P_m^B and α^B values of micro, nano and picophytoplankton measured at station L4 2009-2015……..……54

Figure 2.10 Time series of total chlorophyll concentration and water temperature at the Central Celtic Sea during April 2015……..……55

Figure 2.11 Time series of cellular carbon concentrations of diatoms, dinoflagellates and phytoflagellates at the Central Celtic Sea during April 2015……..…….……57

Figure 2.12 Mean values of chlorophyll concentrations at nominal depths during the August 2014 and April 2015 Celtic Sea cruises……..……58

Figure 2.13 Chlorophyll-normalized size-fractionated phytoplankton light absorption spectra (a_{ph}^*) measured during August 2014 and April 2015 Celtic Sea cruises…….…..…..61

Figure 2.14 Size-fractionated measurements of P_m^B at each sampling depth taken during 2014 and 2015 at stations L4 & E1, and at each nominal depth during Celtic Sea cruises ……..…64

Figure 2.15 Size-fractionated measurements of α^B at each sampling depth taken during 2014 and 2015 at stations L4 & E1, and at each nominal depth during Celtic Sea cruises…….……67

Figure 2.16 Principal components loading plot for abiotic variables, taxon-specific cell carbon concentrations and photosynthetic parameters for L4 and April 2015 Celtic Sea cruise…….70

Figure 2.17 Principal components loading plot for abiotic variables and photosynthetic parameters for L4 and April 2015 Celtic Sea cruise……71

Figure 2.18 Time series of size-fractionated primary production using *in situ* measurements of biomass and the *PE* parameters with the primary production model of Tilstone et al. (2003)……75

Figure 2.19 16 year time series of surface chlorophyll-a concentration measured at station L4 and from ESA OCCI v3.1 chlorophyll product……83

Figure 3.1 Specific light absorption coefficients of phytoplankton pigments of Bidigare et al (1990) ……..104

Figure 3.2 Total and size-fractionated light absorption spectra measured during August 2014 and April 2015 Celtic Sea cruises and Total absorption measured for L4 2014-2015…….…….112

Figure 3.3 Total and size-fractionated chlorophyll-specific light absorption spectra measured during August 2014 and April 2015 Celtic Sea cruises and total absorption measured for L4 2014-2015……..113

Figure 3.4 Average nano- and picophytoplankton chlorophyll-specific absorption spectra split by surface mixed layer and thermocline communities measured during August 2014 and April 2015 Celtic Sea cruises and average red-normalised absorption of nano- and picophytoplankton …..114

Figure 3.5 5 $a_{ph}^*(443)$ values of different size fractions measured during the April 2015 Celtic Sea cruise plotted against ζ (dimensionless depth) consistent with the model of Uitz et al (2008)……..….115

Figure 3.6 Size-fractionated $a_{ph}(\lambda)$ calculated for August 2014 and April 2015 Celtic Sea cruises using the approach of Uitz et al (2008) and *in situ* S-F chlorophyll concentrations……....118

Figure 3.7 Total $a_{ph}(\lambda)$ calculated using the pigment reconstruction technique of Bidigare et al (1990) with phytoplankton pigment concentrations from station L4……..….118

Fig 3.8 Analysis of difference between pigment-reconstructed total $a_{ph}(\lambda)$ ($a_{rec}(\lambda)$) and measured total $a_{ph}(\lambda)$ for station L4……..……..119

Figure 3.9 Linear regression of $a_{ph}(443)$ $a_{ph}(665)$ for measured (a_{ph}) and pigment-reconstructed (a_{rec}) absorption spectra for coincident samples depths at station L4……..……120

Figure 3.10 Linear regression of the mean absorption coefficient of phytoplankton computed from measured ($\bar{a}_{ph}$) and pigment-reconstructed ($\bar{a}_{rec}$) spectra for station L4…….121

Figure 3.11 Size-fractionated $a_{ph}(\square)$ reconstructed using the Varunan & Shanmugam (2015) method using size-fractionated chlorophyll data from the August 2014 and April 2015 Celtic Sea cruises.....122

Figure 3.12 Spectra of the average (mean) difference between $a_{ph}(\square)$ estimated using the values of Varunan & Shanmugam (2015), and those measured during the August 2014 and April 2015 Celtic Sea cruises……..…123

Figure 3.13 Specific absorption coefficient spectra from the models of Ciotti et al (2002), Uitz et al (2008), Brewin et al (2011), Varunan & Shanmugam (2015) and measured values from this study (nano- and picophytoplankton only)…… ……..……..……124

Figure 3.14 Daily integrated primary production estimated using the model of Tilstone et al (2005). Where $a_{ph}(\lambda)$ values from (a) measurements of *in vivo* absorption (b) the Uitz et al (2008) model, (c) the Ciotti et al (2002) model and (d) the Varunan & Shanmugam (2015) are used to calculate α^B and φ_{max}……127

Figure 3.15 Modelled volumetric primary production (mg C m^{-3} d^{-1}) estimated using the model of Tilstone et al (2005) using (a) measured $a_{ph}(\lambda)$ during April 2015 Celtic Sea cruise with corresponding plots for the models of (b) Uitz et al (2008), (c) Varunan & Shanmugam (2015) and (d) Ciotti et al (2002) showing the percentage difference in modelled volumetric primary production when using $a_{ph}(\lambda)$ spectra of each model versus measured $a_{ph}(\lambda)$ spectra……..……..130

Figure 4.1 Variables and parameters required to calculate size-fractionated primary production using the model of Brewin et al (2017)…….. ……..……145

Figure 4.2 Brewin et al. (2017b) model of size-fractionated chlorophyll scaled to total chlorophyll concentration showing the original North Atlantic dataset and model relationships overlaid with observed values taken from the Celtic Sea and Western English Channel during this study……..152

Figure 4.3 Relationship of P_m^B and α^B with respect to ζ for each size class using the retuned shelf model (black lines) with the models of Uitz et al. (2008) (dotted lines) and Brewin et al. (2017b) (dashed lines)……...154

Figure 4.4 *In situ* measurements of surface chlorophyll and euphotic depth Z_{eu} measured in the Western English Channel and Celtic Sea during four separate cruises…….155

Figure 4.5 Log regression of modelled sub-surface chlorophyll calculated using equation 4.3 assuming a well-mixed water column vs profiles of *in situ* measurements of chlorophyll from UK shelf seas…….156

Figure 4.6 Log regression of modelled sub-surface chlorophyll calculated using equation 4.3 assuming a stratified water column vs profiles of *in situ* measurements of chlorophyll from UK shelf seas…….157

Figure 4.7 Profiles of relative biomass (B^{Bs}) with respect to dimensionless depth (ζ) and surface chlorophyll concentration(B_s) and (b) the absolute concentration of chlorophyll at specific depths across a range of surface chlorophyll values……..158

Figure 4.8 Estimates of total and size-fractionated PP using the retuned shelf model run with the monthly composites of ESA OC-CCI chlorophyll product data (Jackson et al. 2017) and NASA MODIS-Aqua PAR…….160

Figure 4.9 Differences in total PP using the retuned shelf model (Shelf Sat) (Fig 4.8) compared to the original North Atlantic model tune (Open Sat)……. ……..162

Figure 4.10 Estimates of monthly micro + nanophytoplankton PP using the Shelf Sat and the difference in micro + nanophytoplankton PP estimated by the Shelf Sat and Open Sat models……..163

Figure 4.11 Differences in estimated monthly picophytoplankton PP between the Shelf Sat and Open Sat model tunes…….…….…..…164

Figure 4.12 Monthly average total PP calculated using in situ data from station L4 2009-2015 (black line), with estimated PP from the Open sat and Shelf sat tunes…….…….166

Figure 4.13 Climatological means of total and size-fractionated PP for station L4 2009-2015 with standard error plotted with estimates by the Shelf sat tune using chlorophyll imagery for 2016…….166

Figure 4.14 Climatological means of picophytoplankton and micro + nanophytoplankton PP for station L4 2009-2015 with standard error plotted for estimates by the Shelf sat and Open sat tunes using OC-CCI v3.1 chlorophyll imagery for 2016……..168

Figure 4.15 Linear regression of daily integrated PP from Shelf sat and Open sat model tunes against calculated values for stations L4, Central Celtic Sea (CCS) off the Celtic Shelf (Off shelf)……169

List of Tables

Table 1.1 Phytoplankton pigments indicative of specific phytoplankton taxa and their respective size classes……..…7

Table 2.1 Sampling periods for station L4 with number of days sampled within each year……..…38

Table 2.2 Size-fractionated chlorophyll concentrations (B) and photo-physiological parameter values with ± one standard deviation measured at the WCO sites……69

Table 2.3 Results of quadratic regression fit between physical variables and *PE* parameters for L4 data (2009-2015) and for August 2014 and April 2015 Celtic Sea cruises…….……...73

Table 2.4 Results of multiple stepwise linear regression between all physical variables and PE parameters for L4 data (2009-2015) and for August 2014 and April 2015 Celtic Sea cruises……...74

Table 2.5 Mean size-fractionated photo-physiological parameters measured bring this study and other shelf sea studies……..…79

Table 2.6 Measurements of daily integrated primary production from previous studies in UK shelf seas…….84

Table 2.7 The contribution of individual size fractions to total community primary production at station L4 and Celtic Sea…….....…86

Table 3.1 Median size fractionated chlorophyll values measured during Celtic Sea cruises……..……...113

Table 3.2 Summary of regressions of PP estimates when α^B is corrected for the spectrum of the lamp using different modelled a_{ph}spectra against PP estimated using measured spectra……...……...…128

Table 3.3 Summary of regressions of PP using modelled a_{ph} values and with measured α^B values……..128

Table 4.1 Average surface values of α^B and P_m^B and their slope values S^{Bs} and S^{α_s} with respect to dimensionless depth ζ for UK shelf data (this study) and under the original parameterisation using Atlantic data Brewin et al. (2017b)…….……..…….148

Table 4.2 Number of total daily PP estimates for Station L4 2009-2015 used in constructing the climatology presented in Fig 4.12…….165

Table 4.3 Regression statistics for Shelf sat and Open sat models using data from station L4, CCS and Off the shelf edge……169

List of Parameter and variable symbols and abbreviations

Symbols and abbreviations used throughout the text with corresponding units descriptions. Definitions with further detail are given where parameters are first used in the relevant chapters

Parameter, variable or name	Abbreviation or Symbol	Units
Absorption of light by phytoplankton	a_{ph}	m^{-1}
Chlorophyll-specific absorption of light by phytoplankton	a^*_{ph}	m^2 mg Chl-a^{-1}
Pigment-reconstructed a_{ph}	a_{rec}	m^{-1}
Integrated absorption (400-700nm)	a^{int}_{ph}	m^{-1}
Chlorophyll concentration	B	mg m^{-3}
Chlorophyll concentration at surface	B_s	mg m^{-3}
Chlorophyll concentration in a vertical profile normalised to B_s	B^{B_s}	mg m^{-3}
Maximum chlorophyll concentration in a vertical profile normalised B_s	$B^{B_s}_m$	mg m^{-3}
Maximum photosynthetic rate	P^B_m	mg C mg Chl-a^{-1} h^{-1}
Maximum photosynthetic rate for size class i	$P^B_{m,i}$	mg C mg Chl-a^{-1} h^{-1}
Maximum photosynthetic rate for size class i at surface	$P^{B_s}_{m,i}$	mg C mg Chl-a^{-1} h^{-1}
Light-limited photosynthetic rate	α^B	mg C mg Chl-a^{-1} h^{-1}(µE m^{-2} s^{-1})$^{-1}$
Light-limited photosynthetic rate for size class i	α^B_i	mg C mg Chl-a^{-1} h^{-1}(µE m^{-2} s^{-1})$^{-1}$
Light-limited photosynthetic rate for size class i at surface	$\alpha^{B_s}_i$	mg C mg Chl-a^{-1} h^{-1}(µE m^{-2} s^{-1})$^{-1}$
Slope of change in B^{B_s} with ζ	S^{B_s}	Dimensionless
Dimensionless depth at which $B^{B_s}_m$ occurs	ζ_m	Dimensionless
Maximum quantum yield of photosynthesis	φ_{max}	mol C mol absorbed photons^{-1}
Central Celtic Sea	CCS	
Chlorophyll-a	Chl-a	mg
Coloured dissolved organic matter	CDOM	
Conductivity, temperature & depth sensor	CTD	
Deep chlorophyll maximum	DCM	
Depth	z	m
Depth divided by euphotic depth	ζ	Dimensionless
Diffuse attenuation coefficient of PAR	K_d	m^{-1}
Dissolved inorganic carbon	DIC	
Dissolved organic carbon	DOC	
Dissolved organic matter	DOM	
Euphotic depth	Z_{eu}	m
High performance liquid chromatography	HPLC	
Inherent optical properties	IOPs	
Irradiance	E	µE m^{-2} s^{-1}
Particulate organic carbon	POC	
Photoprotective carotenoids	PPC	
Photosynthesis vs irradiance	PE	
Photosynthetic carotenoids	PSC	
Photosynthetically active radiation	PAR	µE m^{-2} s^{-1}
Photosynthetically useable radiation	E_{PUR}	µE m^{-2} s^{-1}
Integrated primary production	PP	mg C m^{-2} d^{-1}

Depth-specific primary production	PP(z)	mg C m^{-3} d^{-1}
Remote sensing reflectance	R_{rs}	
Sea surface temperature	SST	^{o}C
Size-fractionated	S-F	
Sub-surface chlorophyll maximum	SCM	
Spring Celtic Sea cruise	DY029	
Summer Celtic Sea cruise	DY026	
Surface mixed layer	SML	
Time	t	s
Total suspended material	TSM	
Water optics dominated by phytoplankton	Case 1	
Water optics not dominated by phytoplankton	Case 2	
Western English Channel Observatory	WCO	
Coastal WCO site	L4	
Offshore WCO site	E1	
Wavelength of light	(λ)	nm

1 Introduction

1.1 The importance of shelf seas for marine primary production

Though only occupying ~7% of Earth's surface, the shelf seas constitute one of its most productive environments, with 2 to 5 times the annual production (g C m^{-2} y^{-1}) of the open ocean, allowing these seas to support 90% of global fisheries (Pauly et al. 2002). Photosynthesis by phytoplankton is the principal source of organic carbon for pelagic ecosystems in shelf seas (de Haas et al. 2002), supporting secondary production by heterotrophic protozoan and metazoan grazers and regenerative production by a range of heterotrophic bacteria (Pace et al. 1984). The cycling of dissolved organic material (DOM) by heterotrophic bacteria – sourced from phytoplankton cell lysis and grazing – into compounds more readily absorbed by phytoplankton is termed the "microbial loop" (Azam et al. 1983; Pomeroy et al. 2007), a process which fuels a significant amount of phytoplankton photosynthesis through regenerative production (Lancelot and Billen 1984; Sherr and Sherr 1988).

Phytoplankton community size structure is a key determinant of particulate carbon export to bottom waters and sediments (Boyd et al. 2000; Laurenceau-Cornec et al. 2015). Larger microalgae, such as biomineralizing diatoms, sink more quickly and are less likely to be fully grazed than smaller cells. The largest phytoplankton cells are typically grazed by larger metazoan zooplankton (e.g. copepods, decapod larvae and krill), which enhance export of carbon from surface waters in two ways. Firstly, metazoan zooplankton package some carbon as faecal pellets, which may sink quickly below the thermocline, particularly when grazing at the sub-surface chlorophyll maximum (SCM) (Giering et al. 2016; Manno et al.

2015). In addition, many zooplankton undergo diel vertical migration, residing at depth during the day to avoid predation, and thus add to the sub-thermocline dissolved inorganic carbon (DIC) pool (Dam et al. 1995; Longhurst et al. 1990; Steinberg et al. 2000), though the influence of zooplankton respiration is small compared with bacterial and protist respiration (García-Martín et al. 2017; Legendre et al. 2015).

The hydrography of shelf seas often allows the efficient export of labile material to benthic ecosystems as particulate organic carbon (POC) (Grebmeier and McRoy 1989; Grebmeier et al. 1988; Lee et al. 2002; Warwick and Joint 1987), with some carbon being exported from the shelf to deeper oceanic waters as dissolved inorganic carbon (DIC) and dissolved organic carbon (DOC) referred to as the "shelf pump" (Thomas et al. 2004). Due to the productivity and high carbon export potential of shelf seas, they may be considered carbon sinks if regional hydrography permits quick sinking of POC to the benthos or off-shelf advection of bottom water. Shelf seas exhibit heightened productivity though the increased stocks of nitrate and phosphate due to anthropogenic activity (Muller-Karger et al. 2005; Thomas et al. 2004), with many coastal regions exhibiting eutrophication. The influence increased macronutrient supply may have further elevated the role of shelf seas as carbon sinks from natural post-glacial rates (Walsh et al. 1981).

This introductory chapter sets out the importance of phytoplankton to shelf sea biogeochemistry and the various "roles" that different phytoplankton functional types play in mediating shelf sea pelagic ecology and biogeochemistry, and why assumptions of their physiology and distribution made from open ocean observations may not be applicable to shelf regions. Different methods of separating the phytoplankton community are discussed including the use of size-fractionation to estimate the photosynthetic parameters and absorption properties for the three size classes of marine phytoplankton. The key parameters and variables necessary to estimate primary production using bio-optical models are

introduced including the methods for their measurement. I then conclude by discussing the use of satellite ocean-colour radiometry data to estimate phytoplankton biomass (chlorophyll) and monitor their spatio-temporal distribution and explain how this information can be combined with photosynthetic rate measurements and irradiances to estimate primary production over scales not possible with *in situ* data.

1.2 The importance of phytoplankton community structure in ocean biogeochemistry

Given the ecological and biogeochemical significance of shelf-sea primary producers, it is critical to develop an understanding of the environmental factors governing their community structure. As marine phytoplankton have competed for a limited number of resources (nutrients and light) from as long ago as the Paleoproterozoic (cyanobacteria) to Mesoproterozoic (eukaryotes) (Falkowski et al. 2004), a low diversity of species would be expected as organisms with competitive advantages would dominate (Hardin 1960). Yet phytoplankton display extremely diverse taxonomy (Hutchinson 1961). In addition to the 5000 known species of phytoplankton (Tett and Barton 1995), many genera are made up of physiologically- and genetically-distinct subpopulations or ecotypes in order to adapt to specific hydrodynamic niches (Bouman et al. 2006; Johnson et al. 2006; Simmons et al. 2016), increasing this biodiversity further still.

There are three ways to separate the phytoplankton community into subgroups for ecological and biogeochemical studies: 1) Taxonomic Groups (e.g. diatoms, dinoflagellates, coccolithophores, cyanobacteria) 2) Phytoplankton Functional Types (e.g. calcifiers, regenerative producers, particulate carbon exporters) and 3) Size Classes (e.g micro-, nano- and picophytoplankton). Ecological and biogeochemical models may also use a combination of groupings to parameterise specific taxonomic or functional groups of

particular regional interest of relevance (Butenschön et al. 2016), for example separating one taxon that influences a particular aspect of biogeochemistry within a wider size fraction, such as fast-sinking diatoms (microphytoplankton) or calcifying coccolithophores (nanophytoplankton). This taxonomic and physiological diversity is matched by a profound range of phytoplankton cell sizes: nine orders of magnitude separate the cell volumes of the smallest cyanobacterium *Prochlorococcus* and the largest unicellular diatoms, such as *Coscinodiscus wailesii* (Finkel et al. 2009). Compared with marine metazoans, this range is broadly equivalent to the difference between euphasiid krill and the blue whale, highlighting the oversimplification implicit in treating the phytoplankton community as a single entity in biogeochemical or ecological processes. Indeed phytoplankton provide a nutrient source for similarly varied range of grazers - from phagotrophic protozoans key to the microbial loop, to the aforementioned krill, perhaps the most important marine prey species in terms of biomass (Atkinson et al. 2009).

Phytoplankton size may be considered the most powerful generalised explanatory variable of phytoplankton functional diversity; cell size affects not only photophysiology, nutrient uptake, elemental stoichiometry and grazing dynamics, but also rates of growth, photosynthesis and respiration, and is therefore indicative of the effect a phytoplankton community will have on the *in situ* DIC, DOM and POC pools (Cermeño et al. 2005; Finkel et al. 2004; Follows et al. 2007; Irwin et al. 2006; Kempes et al. 2012; Verdy et al. 2009). Size-fractionation is therefore not merely a convenient means of providing more detailed information of the gross size structure of natural assemblages than measurements of total biomass, but is a way to apportion experimental rates to functionally-meaningful groups, which have relevance to wider studies of pelagic biogeochemistry.

As we seek to model phytoplankton dynamics and their interaction with the wider biogeochemistry of shelf seas, it is necessary to incorporate this diversity of the primary

producers, where possible using measurements of their characteristics at a sub-community level. When models contain information on the rates, elemental stoichiometry and photophysiology of different groups, they may produce more useful output than broader, generalised values (Follows et al. 2007; Friedlingstein et al. 2006; Iglesias-Rodríguez et al. 2002)

In the following section I examine the various methodological approaches used to subdivide phytoplankton biomass into various subgroups and discuss their advantages and limitations.

1.3 Separating the phytoplankton community

1.3.1 Taxonomic-based methods

Taxonomic discrimination and enumeration through light microscopy (Widdicombe et al. 2010) and flow cytometry (Tarran et al. 2006) provide valuable information on phytoplankton community structure across the entire size spectrum and can therefore be an instructive means by which to apportion photophysiological measurements to certain taxonomic groups. Indeed, by measuring the forward and side scattering properties and fluorescence emission of cells cytometric sorting can also be used to make subsequent measurements of individual or groups of similar cells within a mixed community. Cell sorting during flow cytometry is particularly useful when employing molecular methods such as qunatifying intracellular responses to environmental variables. Molecular methods also provide a reliable means to identify community structure and are particularly useful when identifying the structure of smaller nano- and picophytoplankton, which are difficult to discriminate using conventional light microscopy (Vaulot et al. 2008). However, molecular probes designed to detect specific taxa are based primarily on sequences obtained from cultured species, and as such are biased towards identifying groups of interest, such as

harmful algae, or cryptic species not identifiable by other means (Sathyendranath et al. 2014); some molecular techniques will therefore resolve phytoplankton to different taxonomic levels, which may be problematic when there is a high degree of phenotypic or functional diversity within a taxon.

Species-specific rates have been derived from natural phytoplankton samples by conducting bulk primary productivity experiments during mono-specific blooms. Although such rates are likely more representative for the region of interest than lab-maintained cultures, it could also be argued that measurements taken from mono-specific blooms may not be indicative of a species' photophysiology within a mixed community, however this caveat may not be too constraining for species which are typically found to dominate the phytoplankton biomass in large blooms when present within shelf seas, such as *Phaeocystis.*

Dijkman and Kromkamp (2006) introduce pulse-amplitude modulated microscopy as a way of measuring the photosynthetic efficiency of individual cells rather than water samples containing mixed communities a significant development in the application of fluorescence-based measurements of photophysiology of different phytoplankton groups. This method is of great value to research into the differences in photophysiology between groups or between cells of the same species growing under different conditions.

1.3.2 Phytoplankton pigment markers

A method of resolving community structure from bulk measurements is the use of diagnostic phytoplankton pigments. Pigment-based methods use a suite of accessory pigments common to certain functional types to characterise the gross taxonomic and size composition

of the phytoplankton community (Table 1.1) (Coupel et al. 2015; Schl et al. 2000; Uitz et al. 2008; Vidussi et al. 2001; Wright et al. 2005).

Table 1.1 Phytoplankton pigments indicative of specific phytoplankton taxa and their respective size classes (Vidussi et al. 2001)

Pigment	**Taxa**	**Size class**
Zeaxanthin	Cyanobacteria	Pico
Divinyl-chlorophyll a	*Prochlorococcus*	Pico
Chlorophyll *b*, Divinyl-chlorophyll *b*	*Prochlorococcus*, green flagellates	Pico
19′-hexanoyloxyfucoxanthin	Chromophytes, nanoflagellates	Nano
19′-butanoyloxyfucoxanthin	Chromophytes, nanoflagellates	Nano
Alloxanthin	Cryptophytes	Nano
Fucoxanthin	Diatoms	Micro
Peridinin	Dinoflagellates	Micro

Through the use of high performance liquid chromatography (HPLC), concentrations of pigments can be measured accurately even at low concentrations (Abaychi and Riley 1979; Barlow et al. 1997), and the resulting stoichiometric differences in different pigment ratios can provide information of phytoplankton photoacclimatory, stress and photosynthetic potential, and may be used to estimate $a_{ph}(\lambda)$ when their pigment-specific absorption coefficients are known (Bidigare et al. 1990). The advantage of this method is its analytical consistency; concentrations can be measured in a repeatable and accurate manner using specific protocols (Claustre et al. 2004), with lower sensitivity to operator skill than some taxonomic techniques. However, pigments are shared between some taxa across cell size groupings and functional types. Fucoxanthin, for instance, is a key indicator of diatom (microphytoplankon) abundance (Uitz et al. 2008; Vidussi et al. 2001), but is also common to the haptophyte class, given their common heterokont lineage. This means that using

pigment analyses to subsequently discriminate functional types or cell sizes present within a phytoplankton community may be sensitive to errors where taxa that share diagnostic pigments co-occur e.g. diatoms and *Phaoecystis* in UK shelf seas.

1.3.3 Size-fractionation

Size fractionation provides a more robust way to divide the phytoplankton community into distinct groups that bear some relevance to wider biogeochemistry, as phytoplankton functional types can generally be apportioned to specific size fractions as used in pigment analyses (Brewin et al. 2017b; Joint et al. 1993; Maguer et al. 2015; Uitz et al. 2008; Vidussi et al. 2001). The size fractionation of phytoplankton cells is typically performed using sequential vacuum filtration using filters of decreasing pore sizes corresponding to the bounds of the phytoplankton size fractions. Fractionation is usually performed to separate three size classes: microphytoplankton (>20 μm), nanophytoplankton (2-20 μm) and picophytoplankton (>2 μm). Size fractionation rate measurements are usually made after incubation, which allows the activity of a size class within a natural community to be measured. This type of sequential filtration of cells may be problematic as it could lead to some smaller size classes beinge retained on larger filters due to clogging at high biomass, flocculation of particulate material and cells, or have varied retention due to irregular cell geometry such as pennate diatoms or colonial prymnesiophytes.

1.4 Phytoplankton photophysiology

In order to estimate primary production of different phytoplankton size classes, information on their photosynthetic response of each group to different levels of light is required as well as the wavelengths of light harvested by cells for use in photosynthesis, as the spectrum of

available light varies through the water column as different constituents absorb different wavelengths more strongly

Photophysiology describes the physiological response of photosynthetic organisms to light, and is expressed by changes in both their photosynthetic and photoprotective apparatus. The acclimation of phytoplankton cells to growth irradiance, in terms of both intensity and spectral quality, is commonly exhibited through the modification of intracellular pigment composition and photochemical pathways (Dubinsky and Stambler 2009; MacIntyre et al. 2002b; Moore et al. 2006). However, in addition to photoacclimatory changes in response to changes in the underwater light field, variability in the photosynthetic characteristics of microalgal cells can be influenced by changes in nutrient availability and temperature (Bouman et al. 2005; Bouman et al. 2003; Harrison and Platt 1980). The effect of different abiotic variables (salinity, temperature, irradiance) on phytoplankton photophysiology in UK Shelf seas is investigated in Chapter 2.

1.4.1 Photosynthesis-irradiance (*PE*) parameters

In order to model carbon fixation by phytoplankton as a function of light intensity, measurements of the photosynthetic response of each size fraction are required. The rate of photosynthesis as a function of light available or absorption is encapsulated by the photosynthesis-irradiance or *PE* parameters, which describe the curvilinear relationship between carbon fixation and light and are frequently normalised to chlorophyll concentration (mg Chl m^{-3}) to allow carbon uptake rates to be scaled with this pigment-based measure of phytoplankton biomass. Details on how the photosynthesis-irradiance curves are generated through lab incubations is described in section 2.2.4. As with many biochemical processes, the rate of carbon fixation reaches an asymptotic maximum (Fig 1.1) where light is no longer limiting photosynthesis as all reaction centres are saturated: this is deemed the

maximum rate of photosynthesis, or light-saturated photosynthesis denoted P_m^B (mg C mg Chl-a^{-1} h^{-1}) (Jassby and Platt 1976) and is not considered to be spectrally dependent.

When light is limiting, the photosynthetic rate can be expressed as the amount of carbon dioxide fixed per chlorophyll concentration per unit time as a linear function of available or absorbed irradiance (mg C mg Chl-a^{-1} h^{-1}(µmol photons m^{-2} s^{-1})$^{-1}$). This light-limited slope is termed the light-limited photosynthetic rate or the initial slope of photosynthesis-irradiance response curve, denoted α^B (Fig 1.1) (Jassby and Platt 1976). α^B is sensitive to the spectral quality of the growth irradiance and how well it matches the spectral absorption properties of the cell. The energy of photons at photosynthetically available radiation wavelengths (PAR) varies from 1.8 eV at 700nm to 3.1eV at 400 nm, with longer wavelengths being more strongly attenuated by seawater. Phytoplankton pigments therefore harvest most light energy used in photosynthesis from blue to blue-green wavelengths. Consequently, when light is limited, the rate of the light-dependent reactions of photosynthesis (slope shown in Fig 1.1) will vary based on the wavelengths of incident photons.

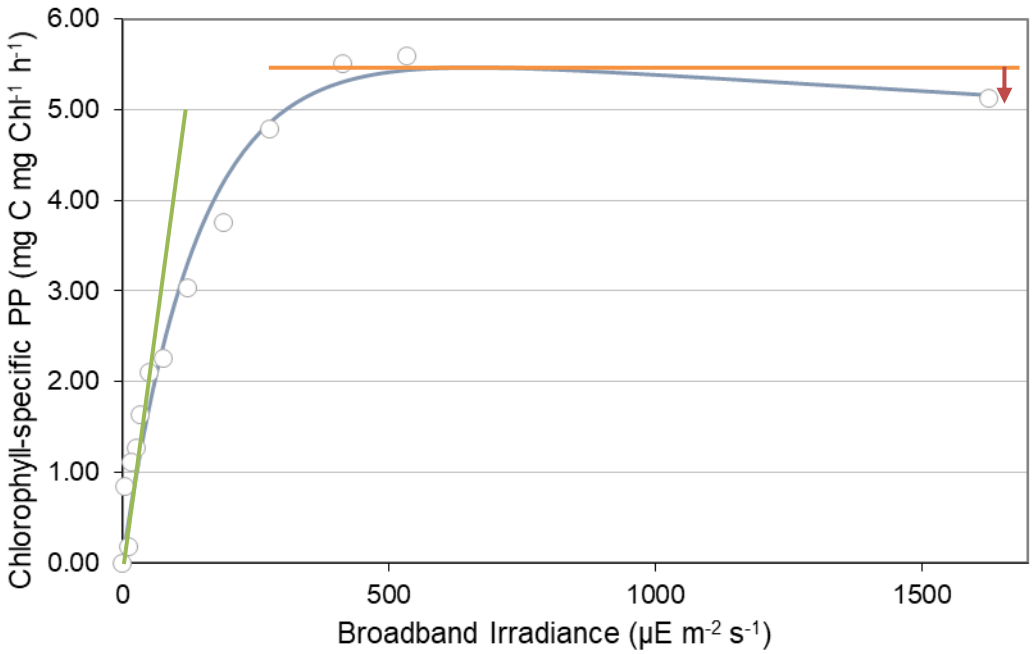


Fig 1.1 Photosynthesis-irradiance (PE) curve showing the initial slope (α^B) (green line), the asymptotic maximum photosynthetic rate (P_m^B) (orange line) the photoinhibition parameter (β) which quantifies the reduction in productivity from P_m^B at high irradiances (red arrow). Points are measurements made after sample incubation and blue curve is the model of Platt (1980).

1.4.2 Photoacclimation of phytoplankton

Photoacclimation by phytoplankton to an ambient light field is typically driven by two processes which both involve changes in the intracellular pigmentation suite:

(1) Maximising the efficiency of photosynthesis for a given light field through the synthesis of chlorophyll and photosynthetic accessory pigments.

(2) Protecting the cells photosynthetic apparatus from high irradiances of visible light and ultraviolet (UV) radiation by the synthesis of photoprotective pigments and other compounds.

Photosynthetic accessory pigments e.g peridinin, fucoxanthin, 19′-hexanoyloxyfucoxanthin and 19′-butanoyloxyfucoxanthin – extend the light-harvesting wavelength spectrum of cells beyond that of chlorophyll pigments alone into the blue-green spectrum (Barlow et al. 2002), allowing increased photosynthetic efficiency at a given broadband light intensity. Other pigments and light-absorbing compounds are involved in the protection of the photosynthetic apparatus against damaging levels of visible and UV radiation. The synthesis of mycosporine-like amino acids (MAAs) and xanthophyll cycling by algal cells is a key process used by marine phytoplankton to invoke non-photosynthetic quenching of excess visible and UV radiation into heat, protecting photosynthetic reaction centres (Müller et al. 2001). This protection from the oxidative stress of UV-visible radiation therefore reduces the energetic costs associated with repairing cell apparatus through further protein synthesis (Roy 2000). Xanthophyll cycling involves a number of photoprotective pigments including alloxanthin, antheraxanthin diadinoxanthin, diatoxanthin, violaxanthin, zeaxanthin and β-

carotene of which some are specific to certain taxonomic groups (Table.1.2), with each pigment having a corresponding absorption spectrum, which modifies the shape of the *in vivo* absorption spectrum of marine phytoplankton $a_{ph}(\lambda)$.

As the intracellular concentration of photosynthetic and photoprotective pigments for specific taxa will vary between regions, seasons and water column depth due to acclimation to the underwater light field and physicochemical environment, it is important to establish the effects of this localized photoacclimation when estimating spectral properties of phytoplankton populations. Furthermore, the synthesis of MAAs and photoprotective carotenoids (PPCs) and cell repair requires ample nitrogen stocks for the requisite enzymes and resulting synthesised proteins themselves; nitrogen limitation can therefore considerably reduce cells' capacities to adapt, affecting their absorption properties and photosynthetic efficiencies (Litchman et al. 2002). In the context of temperate shelf seas, this means that those communities restricted to the surface layer by strong stratification (which is more likely to be nutrient deplete), may have limited photoacclimation potential compared to communities at the subsurface chlorophyll maximum (SCM)(Hickman et al. 2012).

As phytoplankton cells are typically suspended in a turbulent medium, those in the surface mixed layer may be exposed to highly variable irradiances and must consequently optimise photosynthetic efficiency while avoiding photodamage at high irradiances (Falkowski et al. 1993; Geider et al. 1997; Moore et al. 2006; Raven 1980). This physiological optimisation can be inferred by the light saturation parameter E_k. Calculated by dividing P_m^B by α^B, the light saturation parameter E_k is a useful indicator of the irradiance level at which the phytoplankton population is acclimated. For example, cells present at the SCM may have E_k values of 15 to 50 µE m^{-2} s^{-1}, while surface communities may have values exceeding 200 µE m^{-2} s^{-1} (Morán and Estrada 2001).

Though algal cells have the capacity to photoacclimate over daily timescales by altering the number of photochemical reaction centres, the ratio of accessory pigments and the concentration of photochemical coenzymes, when phytoplankton are periodically exposed to high (supraoptimal) irradiances over short timescales, these photoacclimatory responses may not be sufficiently rapid to achieve optimal photosynthetic performance (Olaizola et al. 1994). In these cases, photosynthetic rates are depressed as a result of the cells reducing their photosynthetic efficiency by quenching absorbed light energy (Horton et al. 1996; Müller et al. 2001) resulting in the release of excess light energy through non-photochemical reactions in order to protect the reaction centre of photosystem II (RCII). In extreme cases photo-oxidative damage to the cell's photosynthetic apparatus may occur, particularly when intense UV radiation is present in surface waters (Cullen et al. 1992b; Falkowski et al. 1993; Powles 1984). The reduction in photosynthetic activity attributable to supra-optimal irradiances is termed photoinhibition (Platt et al. 1980b), denoted by the parameter β^B.

In the context of size-fractionated measurements of the *PE* parameters, it might be expected that smaller cells such as picoeukaryotes and cyanobacteria might be more sensitive to photo-oxidative stress than larger cells which have many magnitudes greater surface-area-to-volume ratios and different pigmentation (Key et al. 2010) (Raven 1998) and reduced pigment packaging (Duysens 1956). However, the complexity of variable cell photochemical pathways and ability to acclimate quickly to high visible and UV radiation across phytoplankton taxa means that phytoplankton cell size is not necessarily a good indicator of sensitivity to photoinhibition among larger, diverse eukaryotic cells (Laurion and Vincent 1998).

1.4.3 Influence of underwater light field on phytoplankton absorption

Chlorophyll-specific phytoplankton absorption at specific wavelengths is therefore determined by the relative concentrations of photosynthetic and photoprotective pigments with respect to chlorophyll-a, and the effect of any pigment packaging (self-shading) within cells (Kirk 1975). As such, phytoplankton absorption spectra can be reconstructed from the sum of the absorption coefficients of individual pigments (Bidigare et al. 1990) The measurement of pigment concentrations by HPLC (Abaychi and Riley 1979; Mantoura and Llewellyn 1983) therefore provides a means not only to discern the gross community structure (Mackey et al. 1996; Schlüter et al. 2000; Vidussi et al. 2001), but also the chromatic adaptation of natural phytoplankton assemblages to the intensity and spectral quality of the underwater light field and nutrient stress (Alipanah et al. 2015; Geider et al. 1998; Goericke and Montoya 1998; Henriksen et al. 2002; Rodriguez et al. 2006). However, differences in the absorption spectra of individual phytoplankton taxa are sufficiently large for changes in community composition to produce a greater spectral response than acclimation and stress effects within a population of phytoplankton (Ciotti et al. 2002; Ferreira et al. 2013; Nair et al. 2008).

Although variability in the sum of accessory pigments to chlorophyll-a concentration within species is small (Rodriguez et al. 2006), and thus chlorophyll-specific absorption values of pigments can be considered stable, cellular packaging effects can introduce a significant degree of variability in measured absorption, particularly in larger nanophytoplankton and microphytoplankton cells (Lohrenz et al. 2003). Reconstruction of unpackaged phytoplankton absorption spectra using pigment-specific absorption coefficients is therefore

susceptible to biases with cell size: a concentration of photosynthetic pigments in a high-light adapted picoeukaryote of cell diameter ~5 µm will be unlikely to contribute to the total phytoplankton absorption in the same manner as if the same concentration of pigments were within a low-light adapted diatom with cell diameter ~200 µm. Information on community structure from microscopy and/or flow cytometry is therefore necessary to examine the relative importance of pigment composition and cell size (packaging) in governing the differences in spectral shape and magnitude between reconstructed and measured $a_{ph}(\lambda)$ values. Even with combined datasets of phytoplankton taxonomy and photosynthetic and photo-protective pigments, it is not possible to decompose the total reconstructed spectrum into smaller classifications e.g. taxonomic group, phytoplankton size when the community is mixed, as the majority of pigments are common to a number of phytoplankton taxa, and may common to be different cell size ranges (Coupel et al. 2015).

Size-fractionation of phytoplankton absorption spectra provides an alternative method of estimating the contribution of size classes to total phytoplankton absorption a_{ph} (m^{-1}) is assumed to be an additive quantity of all cells within a community. The chlorophyll-specific absorption properties (a^*_{ph}) of individual species under various light and nutrient regimes can be quantified from culture experiments (Finkel and Irwin 2001; Fujiki and Taguchi 2002; Greg Mitchell and Kiefer 1988; Sathyendranath et al. 1987). *In situ* data from natural populations can also provide information on group-specific absorption properties where a single species, size class or functional group dominate phytoplankton biomass (Bricaud et al. 1995; Ciotti et al. 2002; Uitz et al. 2008). These measurements are useful for isolating the differences in a^*_{ph} spectra between phytoplankton groups due to their pigmentation and cell size, allowing generalisations to be made on their optical properties for use in spectral models of light penetration, primary productivity (Claustre et al. 2005; Uitz et al. 2010) and

water leaving radiances (Bracher et al. 2009; Cleveland 1995; Hirata et al. 2008; Roy et al. 2011).

However, these measured spectra of cultures and single-species-dominated blooms are not necessarily representative of natural populations within a mixed community growing within a light field influenced by other water constituents and vertical mixing. Photoacclimation state of these communities will likely be different to steady state communities, or to those populations within vertically segregated communities (Hickman et al. 2009; Moore et al. 2006). As many of these considerations apply to temperate shelf seas, using assumed values for phytoplankton absorption coefficient may lead to biases in efforts to model photophysiology, primary production and water optics, especially if values for individual taxa or size classes are taken from different experiments or field campaigns.

Photosynthetic rates (moles of carbon fixed per unit time) are determined by instantaneous light intensity (µE or moles of photons m^2 s^{-1}) and spectral quality, but also by the light history experienced by a phytoplankton community. This is to say that photoacclimatory responses of cells that are exposed to consistent light levels may differ from those experiencing variable light conditions (MacIntyre et al. 2000; Moore et al. 2006), for example, if being subjected to turbulent mixing or when exhibiting motile behaviour within the water column. In many cases, the mixing regime influences the structure of the phytoplankton community when certain photoacclimatory responses (particularly photoprotection) are selected for (Arrigo et al. 2010). In addition, when mixing rates exceed the acclimation plasticity of the phytoplankton, regional primary production may be depressed as cells cannot easily adapt to high variability in light intensity over short timescales (Moore et al. 2003).

1.5 The underwater light field of shelf seas

In most open-ocean regions, the primary attenuator of photosynthetically-active radiation (PAR) is seawater, which absorbs light most strongly in the red and near infrared (NIR) wavelengths. Measurements of the absorption spectrum of pure water, such as those made by Pope and Fry (1997) (Fig 1.2), provides the baseline absorption spectrum of pure water unmodified by dissolved and particulate compounds.

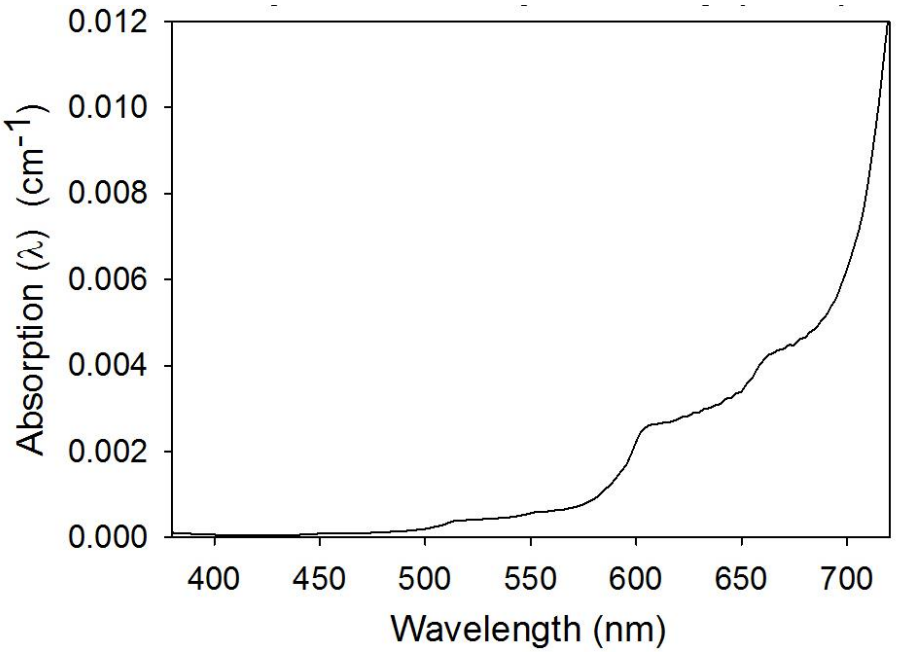


Fig 1.2 Absorption spectrum of visible wavelengths by pure water Pope and Fry (1997)

In open-ocean waters, variation in the vertical attenuation of light is principally caused by changes in phytoplankton biomass, and are commonly referred to as case 1 waters (Gordon and Clark 1980). The spectral diffuse attenuation coefficient $K_d(\lambda)$ is generally dominated by phytoplankton absorption (a_{ph}) between 440-700 nm and sometimes background concentrations of colour dissolved organic matter (CDOM) absorption (a_{CDOM}) between 400-440nm (Nelson and Siegel 2013), with changes in phytoplankton community structure (size and pigment complement) and photoacclimatory status (intracellular pigment

concentration) affecting the magnitude and shape of $a_{ph}(\lambda)$ (Barlow et al. 2017; Bricaud et al. 2004). In the most open-ocean regions under stable nutrient levels, photoacclimatory responses are driven by mixing regime and phytoplankton biomass – with the light field at a specific depths being determined by the pathlength through the water column and the spectral attenuation of the water and overlying phytoplankton. The same processes are present in coastal and shelf seas (Hickman et al. 2009; Moore et al. 2006; Stæhr et al. 2002), however greater seasonal variability and the influence of other optical constituents on the underwater light field require greater consideration.

The relative contribution of CDOM to total light absorption is often greater than that of phytoplankton in coastal and productive shelf regions, particularly when phytoplankton biomass is low, such as in winter months (Babin et al. 2003; Barnes et al. 2014). Both allocthanous inputs of organic compounds, such as low molecular weight humic and fluvic acids from terrestrial sources and the breakdown of carbon from new and secondary production by the microbial cycling of labile dissolved organic compounds may allow CDOM concentrations to dominate absorption in the blue region of the spectrum (Steinberg et al. 2004). As phytoplankton absorb most strongly in the blue wavelengths, even small concentrations of CDOM are problematic for when making estimates of phytoplankton biomass from satellite data. Chlorophyll retrieval algorithms use a limited number of wavebands from which the contributions of phytoplankton and CDOM to remotely-sensed reflectances may be difficult to distinguish (Siegel et al. 2005).

Case 2 waters are defined as regions where the optical properties of the water column are generally more strongly influenced by the presence of non-algal substances (i.e. CDOM and suspended terrigenous particles) than phytoplankton (Dubinsky and Stambler 2009; Tian et al. 2009). As CDOM absorbs most strongly in the blue region of the visible spectrum where

phytoplankton absorption is highest, high concentrations of CDOM will not only reduce the intensity of photosynthetically-useable radiation, but also alter its spectral quality such that the irradiance at depth is shifted towards the region of the visible spectrum where the cells absorb weakest. However, as CDOM absorbs strongly in the UVA and UVB – wavelengths which inhibit photosynthesis and cause oxidative stress to phytoplankton cells (Lesser 1996), (Cullen et al. 1992a) – CDOM can also protect the cells from photodamage (Arrigo and Brown 1996). Increased CDOM, therefore, promotes acclimation responses toward the synthesis of photosynthetic pigments and the reduction of the relative absorption by photoprotective pigments.

Another important component of the light absorption budget in natural waters is the concentration and spectral properties of suspended particles or total suspended matter (TSM). Inorganic TSM (mineral particles) cause scattering and backscattering of incident and diffuse sunlight through the water column, generally reducing irradiance levels, while organic TSM absorbs light, attenuating irradiance through the water column. Though heightened levels of TSM may be indicative of increased inorganic nutrient fluxes from riverine plumes or resuspension and transport of marine sediments, possibly supporting increased primary production when considered in isolation (Schallenberg and Burns 2004; Wisniewski 1993), particles suspended in the water column may affect light transmission to phytoplankton, thus constraining photosynthetic rates (Millie et al. 2003; Retamal et al. 2008; Tilstone et al. 2005).

CDOM and TSM are present in irregular concentrations in shallow shelf seas and therefore their influence on the light field may vary from insignificant to dominating the attenuation of PAR (case 2 conditions) particularly during the winter months after the thermocline breaks down. The sampling of phytoplankton *PE* parameters and absorption spectra presented in this study was conducted during the spring-summer in the Celtic Sea and

Western English Channel, as these periods see the bulk of annual phytoplankton production and biomass. These sampling periods are known to be during case 1 conditions (Groom et al. 2009; Tilstone et al. 2012), when phytoplankton are the principal determinants of non-water optics in the water column. I do not use CDOM and TSM spectra in the modelling of primary production at my sampling sites, assuming case 1 conditions during these periods. It would of course be beneficial to incorporate these data as they may still be present in small concentrations during spring-summer, but sampling CDOM and TSM absorption and scattering characteristics at multiple depths in addition to phytoplankton measurements is not feasible for this project without compromising the number of depths or size fractions sampled.

1.6 Modelling primary production in shelf seas

1.6.1 PP as a key environmental indicator

Due to the high rates of primary production common to many shelf seas, and their economic importance and sensitivity to transient and long-term anthropogenic perturbations (Gowen et al. 2002; McQuatters-Gollop et al. 2007; Ridgway and Shimmield 2002; Yunev et al. 2007), *in-situ* and remotely-sensed observations of primary production for these regions are of considerable value to marine managers and policy makers. Some examples of the importance of monitoring phytoplankton production include marine primary production being considered an essential climate variable by the United Nations framework convention of climate change (UNFCCC) and that monitoring of plankton and eutrophication is mandated by the European Union on members by the marine strategy framework directive (MSFD). The increasing interest of governments and marine conservationists in monitoring

coastal and shelf seas is reflective of these areas being most strongly impacted by human activity (Hallegraeff 2010; Levin et al. 2015).

1.6.2 Estimating PP simple functions to complex spectral models

Models of primary production range from simple functions of observable phytoplankton biomass (Smith et al. 1982) to more complex models which integrate production through the water column using biomass profiles, spectral light fields and photosynthetic parameters (Kyewalyanga et al. 1992; Longhurst et al. 1995; Morel 1991; Sathyendranath and Platt 1989; Sathyendranath et al. 1989; Tilstone et al. 2003). Although estimates of primary production using fully-spectral (photosynthesis and light) models may not necessarily produce estimates significantly different to broadband models (Carr et al. 2006), they incorporate information of the spectral quality of light field which influences the spectrally-dependent photosynthetic parameter α^B, also referred to as the light-limited photosynthetic rate. This can be important in regions where the vertical attenuation and spectral distribution of the underwater light field may be governed by optical constituents other than marine phytoplankton (e.g. CDOM and TSM).

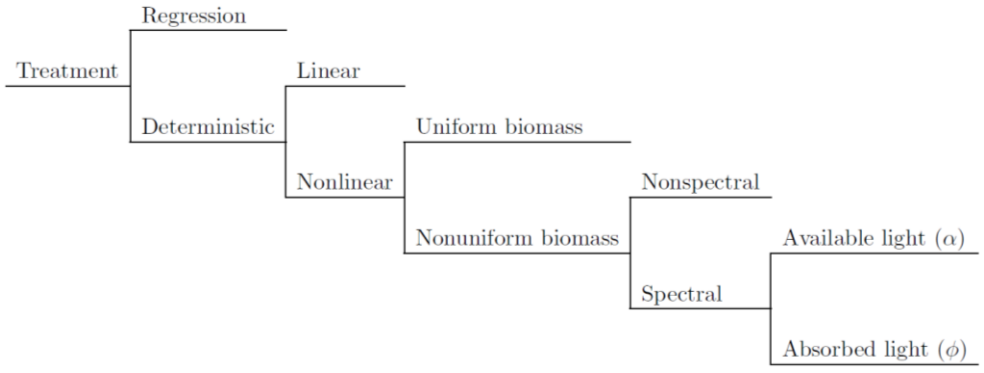


Fig 1.3 The hierarchy of approaches in modelling *in situ* PP from the most simplistic using assumed relationships with other variables (top left) to most complex (bottom right) (Platt and Sathyendranath 2009).

Fig 1.3 illustrates how primary production models can increase in complexity through incorporating additional spectral ($E(\lambda)$, $\alpha(\lambda)$) and vertical (biomass profile) resolution. Increased model complexity does not necessarily increase accuracy, but does allow for a more realistic representation of the growth environment. As shelf seas are highly dynamic in terms of hydrography, inherent optical properties (IOPs), phytoplankton abundance and species composition (Tilstone et al. 2005), using more complex models that account for regional differences in optical water types is desirable where observations exist to inform model parameterisation.

1.7 Estimating PP from satellite observations

The advent of ocean-colour radiometry from satellite-borne sensors, beginning with the ”proof of concept” Coastal Zone Colour Scanner instrument, launched in 1978, has allowed researchers to observe hydrodynamic and biological phenomena at synoptic scales and with regularity not previously possible with *in situ* sampling methods (Anding and Kauth 1970; Hamme et al. 2010; O'Reilly et al. 1998; Prabhakara et al. 1974; Reul et al. 2014; Ruf et al. 2016; Scales et al. 2014; Smith and Baker 1978; Thakur et al. 2018; Thomas et al. 1983). With an ever-increasing number of *in situ* water and phytoplankton optical measurements being available to calibrate and validate chlorophyll retrieval algorithms, improved estimates of phytoplankton biomass can be obtained from satellite ocean-colour imagery (Agirbas et al. 2015; Bailey and Werdell 2006; Brewin et al. 2015; Brewin et al. 2016; O’Reilly et al. 2000; Racault et al. 2017; Roy et al. 2017; Werdell and Bailey 2005). Ocean-colour sensors mounted on spacecraft only receive reflectance at a limited number of wavebands within the visible domain, and the signal is heavily weighted to the uppermost part of the ocean (Gordon et al. 1975). It is therefore recommended that bio-optical algorithms suited to the region of study are used to produce estimates of phytoplankton

biomass and derived variables from ocean colour data (Brewin et al. 2017b; Lutz et al. 2009; Tilstone et al. 2009; Uitz et al. 2012). Chlorophyll-based algorithms should also be validated as extensively as possible and the error characterised to define the limits of their applicability in terms of region (Brewin et al. 2017a; Jackson et al. 2017) and optical water type (Nechad et al. 2015; Qin et al. 2017; Tilstone et al. 2017).

1.7.1 Incorporating PE parameters in satellite models of PP

The distribution, abundance and biodiversity of phytoplankton in shelf seas is influenced by a great many physicochemical and biological factors, meaning modelling phytoplankton dynamics based on a few satellite-observable variables is non-trivial. Large datasets of *in situ* observations are required to calibrate and validate algorithms for photosynthetic parameters assignment and subsequent primary production computation. The *PE* parameters are often assigned using single or multiple physical variables such as depth, mixed layer depth, temperature or light availability following empirical relationships (Behrenfeld and Falkowski 1997; Bouman et al. 2005; Gallegos et al. 1983; Morel et al. 1996). Given that each of these variables will have a different deterministic effect on photosynthetic performance with respect to other co-variables, it follows that different empirical relationships may perform better under different environmental scenarios, an important consideration in highly seasonal temperate shelf seas and in the context of climate change. Despite the limitations of using statistical relationships in models of primary production, given sufficient calibration and validation using *in situ* data, establishing such relationships with remotely-sensed observables - such as sea surface temperature or total chlorophyll concentration -allow us to extrapolate experimentally-derived *PE* parameters over time and space (Barnes et al. 2014; Behrenfeld and Falkowski 1997; Longhurst et al. 1995; Saux Picart et al. 2014; Uitz et al. 2012).

There are many existing algorithms which use spectral radiometry data to estimate the concentration and distribution of surface chlorophyll from space, with some algorithms estimating the community size structure of phytoplankton (Uitz et al. 2008). In order to convert these maps of estimated biomass to computed fields of primary production for different size classes requires information on the variability in photosynthetic response of each fraction to different environmental conditions. It is understood that the cell structure of the phytoplankton community is a key determinant of phytoplankton growth rates and photosynthetic performance and thus we would expect the relationship of these parameters with environmental variables to vary across the size classes (Robinson et al. 2018). However, the measured and modelled values of light-limited and light-saturated photosynthetic rates of individual size fractions varies widely in the literature, conceivably due to differences in optical water types, nutrient supply and phytoplankton taxonomic composition between sampling locations (Barnes et al. 2014; Bouman et al. 2005; Kameda and Ishizaka 2005; Segura et al. 2013; Uitz et al. 2008). As the majority of existing studies of phytoplankton photophysiology are performed by measuring the whole community, most often in open-ocean waters, there is a urgent need to collect *in situ* measurements of the *PE* parameters of different phytoplankton size fractions in order to characterise any regional and seasonal changes in photo-physiology given the various hydrographic phenomena which can strongly influence phytoplankton dynamics within the UK shelf seas (Green et al. 2008; Hickman et al. 2009; Hickman et al. 2012; Moore et al. 2006).

1.8 Thesis objectives

This study seeks to investigate whether current remote sensing algorithms can be used to accurately capture the dynamics of size-fractionated phytoplankton primary production in

UK Shelf Seas, and to explore whether the parameterisation of both the photophysiology and the vertical distribution of different size classes may be improved.

There are several primary production models that incorporate photosynthetic rates (P_m^B and α^B) for the three main phytoplankton size classes (Brewin et al. 2017b; Uitz et al. 2008). However, despite using large datasets for calibration, there are no extant models explicitly tuned for shelf-sea applications, despite the importance of these regions in global ocean biogeochemistry and the cycling and storage of carbon. As discussed herein, there are considerable hydrodynamic, optical and ecological differences between open-ocean and temperate shelf seas – further modified by seasonality. Thus the development of extrapolation protocols for photosynthetic parameters in the size-class PP models of Uitz et al. (2008) and of Brewin et al. (2017b) should be carefully considered.

The thesis objectives are:

1. To determine how size-fractionated phytoplankton biomass, photosynthetic rates, absorption spectra and primary production vary across the UK Shelf
2. To investigate whether various of abiotic variables have a deterministic effect on the photophysiology and size structure of shelf sea phytoplankton communities
3. To examine how light absorption properties differ between the phytoplankton size fractions and establish the best method of estimating the *in vivo* absorption spectra in shelf-seas necessary for spectral models of primary production.
4. To test whether existing satellite models of size fractionated primary production for open ocean regions are accurate when applied in UK Shelf Seas
5. To produce a means of estimating S-F PP of UK shelf seas from satellite data

In order to validate estimates of photosynthetic parameters, $a_{ph}(\lambda)$ and primary production for the three phytoplankton size classes (micro-, nano- and picophytoplankton), size-

fractionated measurements were made during two research cruises to the Celtic Sea, and bi-weekly sampling through spring-summer at fixed time-series station L4 of the Western English Channel Observatory (WCO). These measurements and the environmental factors govern their spatial and temporal variability from coastal to shelf edge waters are the foundation of Chapter 2. The bio-optical dataset establishes the importance of cell size as a factor controlling the variability in the *PE* parameters and phytoplankton absorption coefficients used in PP models and how the physicochemical environment of shelf seas influences the variability of these bio-optical parameters. Daily integrated water-column primary production is estimated using the size- fractionated measurements in order to examine the seasonal cycle in photosynthetic activity for each size class, and allow comparison with previous studies.

In Chapter 3, I seek to develop an approach of assigning a spectral shape and magnitude for $a_{ph}(\lambda)$ in the absence of *in situ* data for shelf seas. The method utilizes information on the absorptive characteristics from natural assemblages, as opposed to using culture values, or estimates from dominant blooms (Ciotti et al. 2002; Seppälä et al. 2005; Uitz et al. 2008; Varunan and Shanmugam 2015) (Nair et al. 2008). Measurements of the spectral shape of $a_{ph}(\lambda)$ is necessary to for the correction of the photosynthetic parameter α^B, which is spectrally-dependent and thus sensitive to the spectral quality of the emission spectra of the light source used during *PE* experiments (Kyewalyanga et al. 1997b). Due to the sparsity of size-fractionated measurements of $a_{ph}(\lambda)$, three different methods of estimating $a_{ph}(\lambda)$ for the three phytoplankton size classes are compared with measured values. The modelled $a_{ph}(\lambda)$ values are then used to 1) correct values of α^B for the light source and 2) determine the spectral distribution of the underwater light field using a radiative transfer model.

Differences in estimates of water-column primary production for using each set of size-class spectra are examined and discussed.

Chapter 4 uses the shelf-sea measurements to regionally tune an existing algorithm of size-fractionated primary production, which is then combined with composite chlorophyll imagery to estimate monthly primary production in UK Shelf Seas. These estimates are compared with the original model parameterised using open-ocean data and a climatology of monthly primary production derived from in situ measurements to identify the relative performance of each model, how the model may be improved with respect to the chlorophyll profile through the euphotic zone.

2 Variability of size-fractionated photophysiology and primary production in UK shelf seas

2.1 Introduction

The level of primary production found in many temperate shelf seas sustains a great diversity of marine species in high abundances and as photosynthesising microalgae and cyanobacteria form the base of most pelagic food webs, shifts in their abundances, species composition and phenology can have a strong bottom-up effect on the higher trophic levels (Frederiksen et al. 2006) and thus fishery yield and sustainability (Blanchard et al. 2012{Chassot, 2010 #519; Kiørboe 1993a; Platt et al. 2003).

2.1.1 Heterogeneity of shelf seas

The productivity of shelf seas can often be attributed to physical forcing which promotes enhanced nutrient fluxes to euphotic waters through a number of processes including,

advective or estuarine input (Springer and McRoy 1993; Wasmund et al. 2001), seasonal temperature, salinity and eddy-driven stratification (Mahadevan et al. 2012), tidal mixing (Green et al. 2008; Sharples et al. 2001a) and the formation of various frontal features (Acha et al. 2004; Holligan 1981). The mixing regime strongly influences nutrient and light availability and hence phytoplankton community structure and photoacclimatory state (Hickman et al. 2009; Maguer et al. 2015; Moore et al. 2006). Photoacclimatory changes can be observed in the variability in biomass-specific photosynthetic rates and light absorption spectra (Table.1.2) between populations exposed to different physiochemical conditions. The effects of individual and multiple abiotic variables (nutrients, temperature, light) on the expressed photophysiology of individual species has been extensively studied in controlled experiments (Flameling and Kromkamp 1997; Karentz et al. 1991; Moisan and Mitchell 1999; Moore and Chisholm 1999; Petrou et al. 2012; Sosik and Mitchell 1994), and within natural communities of various regions (Bouman et al. 2005; Bouman et al. 2010; Helbling et al. 2001; Lohrenz et al. 1999; Marañón and Holligan 1999; Moore et al. 2006). Although phytoplankton are able to acclimate to their environment, differences in the physiological response between phytoplankton species means that in many cases, specific species or functional groups tend to dominate under certain conditions (Bode and Fernandez 1992; Chisholm 1992; Irwin et al. 2006; Kiørboe 1993a; Uitz et al. 2006). For example, large diatoms typically flourish in well-mixed eutrophic regions; while cyanobacteria and picoeukaryotes are more dominant the deep chlorophyll maxima of the oligotrophic gyres where light is severely limiting (Chisholm 1992; Marañón et al. 2001; Marañón et al. 2009; Margalef 1978). The spatiotemporal variability of shelf sea hydrography means that distinct assemblages of phytoplankton can be observed between proximal regions when strong physical forcing separates water masses or impacts surface mixed layer depth or nutrient input (Holligan 1981; Siemering et al. 2016).

In coastal regions surrounding larger estuaries, in addition to higher allocthanous nutrient loading, suspended particulates (TSM) and coloured dissolved organic material (CDOM) also impact phytoplankton through modification of the light field both by changing the spectral quality of downwelling light (CDOM absorbing most strongly at blue wavelengths), and by impacting light transmission due to the backscattering of incident sunlight by non-algal particles (Kirk 1994). High concentrations of CDOM and TSM dramatically alters the spectral quality of the underwater light field and attenuates blue light so rapidly as to limit photosynthesis in otherwise nutrient-replete waters The optical complexity of shelf seas therefore complicates efforts to produce generalised models of marine primary production, particularly for individual size fractions, which are known to have different physiological responses to physical and bio-optical drivers of acclimation. Another complication is the widespread occurrence of a sub-surface chlorophyll maximum (SCM) which is situated around the seasonal thermocline/nutricline. Studies have shown that a significant proportion of primary production during the stratified period occurs in the SCM (Hickman et al. 2012; Siswanto et al. 2005; Weston et al. 2005), though this important feature cannot be detected using ocean-colour satellites. As water-leaving radiances are heavily weighted towards the sea surface, ocean-colour data of surface chlorophyll concentrations may not be reliable indicator of the depth or intensity of the SCM and the integrated concentration of pigment biomass through the euphotic zone more generally (Gordon and McCluney 1975). The variability of IOPs in shelf seas drives changes in the euphotic light field between mixed, spring bloom and stratified conditions contributing to the vertical distribution of phytoplankton biomass and community structure (Flameling and Kromkamp 1997; Hickman et al. 2009; Klausmeier and Litchman 2001; Moore et al. 2006; Pingree et al. 1978; Sharples et al. 2001a; Sharples et al. 2001b). This variability presents an obstacle to reliably

estimating primary production in these regions using generalised models (An and Son 2010; Forget et al. 2007).

2.1.2 Modelling of primary production

Light-based bio-optical models of PP use input variables of chlorophyll concentration and photosynthetically available radiation (PAR – light intensity in the visible domain (400-700 nm)), and photophysiological parameters (which describe the response of phytoplankton to light in terms of carbon fixation per unit chlorophyll) in order to calculate carbon fixation rate per unit volume of seawater, usually expressed as daily rates integrated through the euphotic zone (mg C m^{-2} d^{-1}). Bio-optical models of primary production are often employed when attempting to estimate primary production over synoptic scales using these two variables (chlorophyll and light) as they can be estimated remotely using satellite chlorophyll products and radiative transfer models (Fig 2.1). Hydrodynamic and biogecohemical models, such as ERSEM (Butenschön et al. 2016), differ from the bio-optical models employed in this study by including many more dynamic variables and parameters e.g. nutrient concentrations, mixing period and grazing rates. This enables predictive estimates of primary production informed by the combined interactions of an ensemble of variables specific to a region of interest. However, although these models may use chlorophyll and PAR observations to set initial conditions, assumptions must be made when generating PP estimates for other biogeochemical variables for which satellite observations are not available. Bio-optical models are therefore the principal method to estimate primary production at synoptic scales using real observations, with assumptions made about the photophysiology of phytoplankton informed by *in situ* measurements.

In order to measure the photophysiological parameters of phytoplankton, carbon fixation is measured by the uptake of stable isotope ^{13}C (Furuya et al. 1998; Hama et al. 1983), or more

commonly, radioisotope ^{14}C (Eppley and Sloan 1965; Jassby and Platt 1976) at a range of irradiances. By dividing the amount of ^{13}C or ^{14}C uptake at each light level by the chlorophyll concentration of the phytoplankton community at the sampling depth (total or individual size fractions), chlorophyll-specific rates can be estimated across the light gradient. Experimental light levels of these photosynthesis-irradiance incubations capture the natural range of irradiances within the photic zone, from the surface to the depth at which light is diminished to less than 1% its surface value.

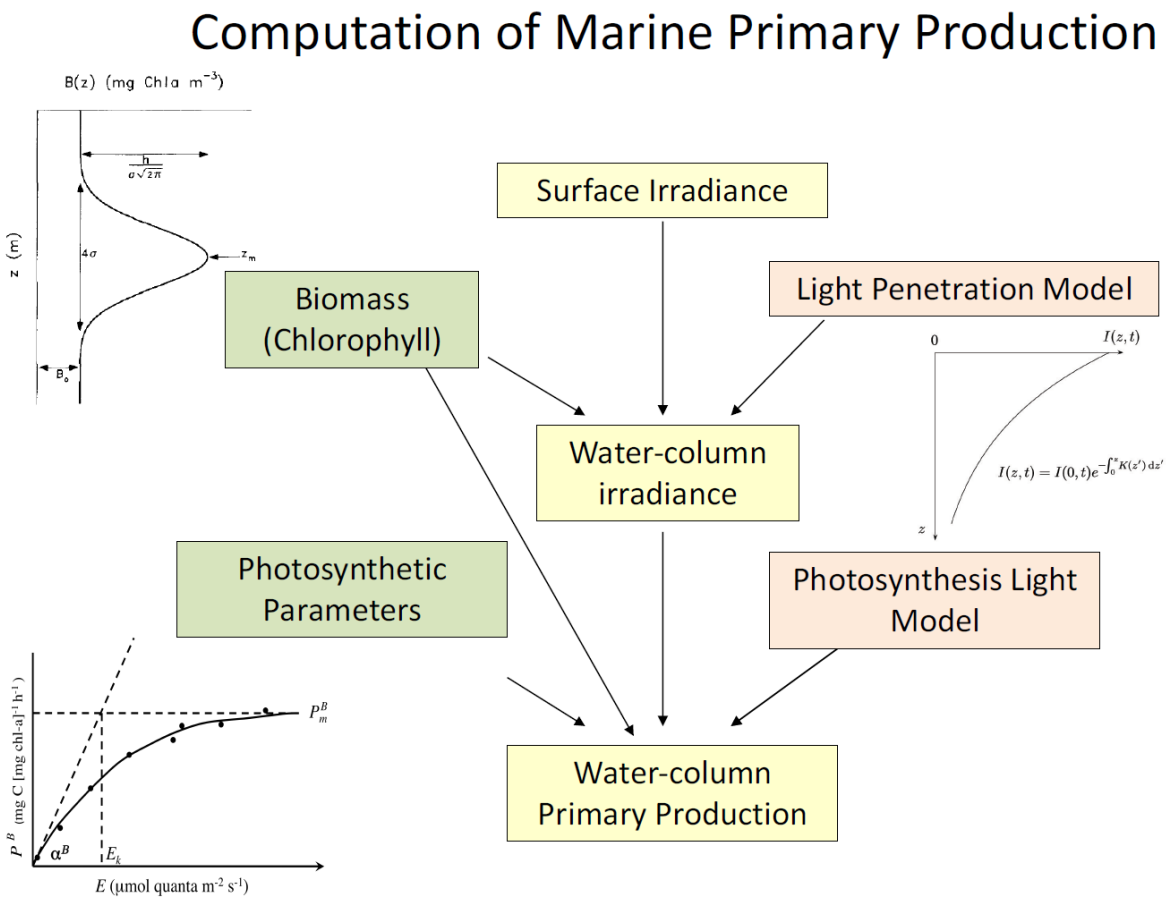


Fig 2.1 schematic of the variables and parameters required to estimate primary production using measurements of photosynthesis-irradiance (*PE*) parameters (Figs 1.1, 2.2)

When plotted against irradiance (*E*), a non-linear function (typically that of Jassby and Platt (1976) or (Platt et al. 1980a) which accounts for photoinhibition at high irradiances) is fitted to the data to derive *PE* parameters (Fig 2.2). The function and parameter values can then

be used with measured or modelled chlorophyll concentration and underwater light field to estimate PP (eq 2.2).

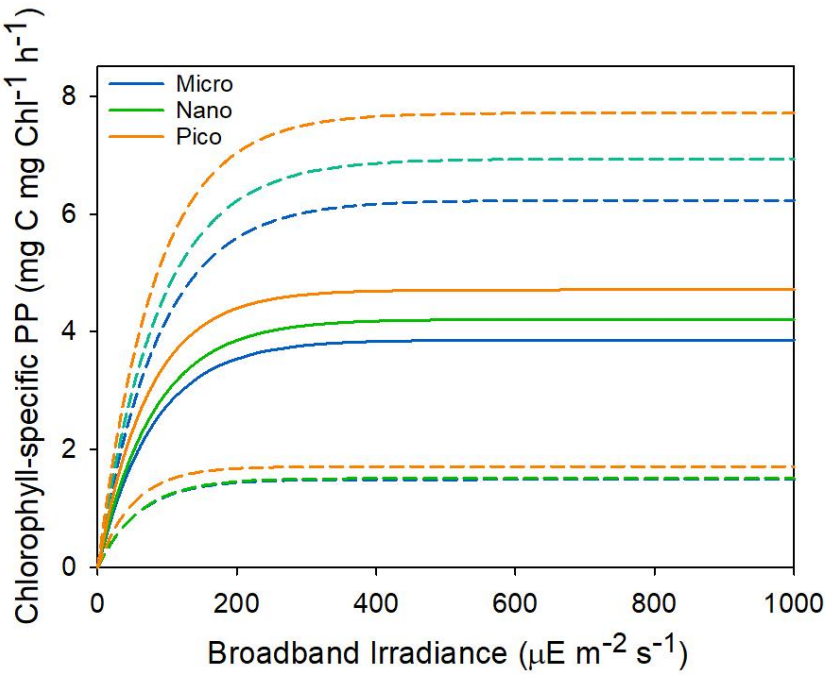


Fig 2.2 Average Photosynthesis-irradiance (PE) curves for different phytoplankton size fractions (solid lines) with upper and lower standard deviation bounds (dashed lines) using the equation of Platt et al. (1981) fitted to observations from station L4 (2014 & 2015) .

In addition to *PE* incubations, measurements of the phytoplankton light absorption spectrum ($a_{ph}(\lambda)$) is required to correct the spectrally-dependent photosynthetic parameter α^B for the spectrum of the artificial light source, and allow for the calculation of the quantum yield of carbon fixation φ_{max} . Measured chlorophyll-specific total light absorption (a^*_{ph}) varies with changes in phytoplankton taxonomy, cell size and photoacclimation state (the intracellular processes as the phytoplankton optimise their photosynthetic response to their physio- chemical conditions). Cells adapted to low light at greater depths may exhibit increased a^*_{ph} coupled with changes in the shape of the $a_{ph}(\lambda)$ due to the synthesis of accessory pigments to allow more efficient photosynthesis when exposed to low irradiances and of specific spectral distributions (Lewis et al. 1985b). Cells adapted to high irradiance

conditions may produce higher concentrations of photo-protective carotenoids, which in some cases may surpass chlorophyll-a as the predominant phytoplankton pigments, potentially lowering the quantum yield for photosynthesis as the conversion of absorbed light to fixed carbon is reduced. (Barlow et al. 2007; Dubinsky and Stambler 2009; Hoepffner and Sathyendranath 1991; MacIntyre et al. 2002b). In larger eukaryotic cells such as diatoms and dinoflagellates, chloroplasts within a single cell may shade each other from incident light, significantly reducing their chlorophyll-specific photosynthetic efficiency, a phenomenon called pigment packaging (Duyens 1956; Kirk 1975). The considerable variety in phytoplankton cell size is therefore reflected by differences in their specific absorption properties (Marañón et al. 2009; Nair et al. 2008), in addition to those due to acclimation to physical conditions (Bricaud et al. 1995; Ciotti et al. 2002; Henriksen et al. 2002; Hickman et al. 2009; Mitchell and Kiefer 1988; Vidussi et al. 2001).

Despite the differences in specific absorption observed between taxonomic groups, there remains a paucity of measurements of size-fractionated $a_{ph}^{*}$from natural populations, with some estimates being based on the dominant size fractions of total community measurements of a_{ph}^{*} (Ciotti et al. 2002), or using phytoplankton cultures to measure the absorption spectra of isolated species (Bricaud et al. 1995; Johnsen et al. 1994; Morel et al. 1993). Physical fractionation of the community in order to make measurements of a_{ph}^{*} for distinct size classes – as is pursued in this study – is rare (Seppälä et al. 2005), and relies on sufficient phytoplankton biomass in each individual fraction to provide reliable size-fractionated specific absorption measurements. Given the generally mesotrophic to eutrophic status of the UK shelf seas, physically fractionated measurements were attempted to elucidate the differences in absorption properties between phytoplankton size classes, and combined with size-fractionated *PE* parameters to calculate PP, with the aim to provide more representative estimates PP for the three phytoplankton size classes.

Measured and modelled values of light-limited and light-saturated photosynthetic rates of individual size fractions vary widely in the literature, conceivably due to differences in the optical characteristics, nutrient availability and taxonomic composition between sampling locations (Barnes et al. 2014; Bouman et al. 2005; Kameda and Ishizaka 2005; Segura et al. 2013; Uitz et al. 2008). Microphytoplankton are considered to have the highest maximum photosynthetic rates of any size fraction when grown under optimal light and nutrient conditions and tend to dominate under bloom conditions, while nanophytoplankton are considered to be globally ubiquitous and outside of the spring bloom period are responsible for the majority of annual primary production in many open ocean and shelf seas (Cermeno et al. 2005; Cermeño et al. 2005; Key et al. 2010; Marañón 2007; Uitz et al. 2008).. Picophytoplankton are generally considered a minor component of annual PP in shelf seas (Joint et al. 1986), given that the supply of macronutrients in shelf seas is often high enough that the competitive advantage of small cell size under nutrient-limited conditions is rarely beneficial. Nevertheless, a number of studies have shown that smaller size fractions may have higher photosynthetic rates than larger cells in shelf systems (Joint and Pomroy 1986; Morán and Scharek 2015; Platt et al. 1983; Stuart et al. 2000) and that these smaller cells are responsible for a significant proportion of annual PP (Chen 2000; Morán 2007).

2.1.3 Importance of photophysiological measurements for satellite models of PP

Although phytoplankton chlorophyll concentration can be estimated with reasonable accuracy from satellite observation of water leaving spectral radiances (due to the characteristic absorptive properties of phytoplankton) (Brewin et al. 2015; Nechad et al. 2015), the photosynthetic response of phytoplankton cannot be directly estimated by remote sensing. Thus the *PE* parameters are often assigned based on empirical relationships with

respect to single or combinations of physical variables such as depth, mixed layer depth, temperature or light availability (Behrenfeld and Falkowski 1997; Bouman et al. 2005; Gallegos et al. 1983; Morel et al. 1996). Yet it can be argued that generalised relationships between the *PE* parameters and abiotic variables are likely to be highly seasonal in temperate shelf seas. Despite these limitations, the collection of datasets from varied oceanographic conditions over many years combined with a more comprehensive and mechanistic understanding of the role of abiotic factors on phytoplankton physiology should allow such relationships to be established with remotely-sensed observables such as sea surface temperature or total chlorophyll concentration – allowing for the estimation of PP to be extended across the space and time for which there are satellite observations (Barnes et al. 2014; Behrenfeld and Falkowski 1997; Longhurst et al. 1995; Saux Picart et al. 2014; Uitz et al. 2012).

2.1.4 Objectives of this chapter

An extensive dataset of chlorophyll, *PE* parameters and phytoplankton light absorption spectra within three size classes was collected during two research cruises to the Celtic Sea and two spring-summer sampling seasons at two sites of the Western English Channel Observatory (WCO). These data were used to establish the patterns of size-fractionated *PE* parameters of this region and pursue the following objectives:

1. To investigate the variability of size-fractionated *PE* parameters in UK shelf seas
2. Establish patterns in seasonal and regional variability in size-specific primary production in the Western English Channel and Celtic Sea.
3. Comapre estimates of primary production made using new *in situ* measurements compare to previous studies of UK and other shelf seas.

2.2 Methods

2.2.1 Study area and sampling

At the WCO, water samples were collected on board RV *Plymouth Quest* from timeseries stations L4 and E1 between March-July 2014 and March-November 2015 (Fig 2.3). Vertical profiles of temperature, salinity, fluorescence and PAR were measured by SeaBird SBE19+ SECAT CTD, Chelsea MINITracka II fluorometer and 2-pi PAR sensor mounted on a CTD rosette frame. At L4, sampling depths were 0, 10, 25 and 50m, and at E1 were 0, 10, 30 and 60m. Water samples were transported in insulated blacked-out carboys to Plymouth Marine Laboratory and experiments were conducted within 2 to 5 hours of sample collection. In addition to the 2014-2015 data, a historical dataset sampled between 2009-2011 was included in the analyses of seasonal patterns (Table 2.1). Samples were also taken during two cruises to the Celtic Sea during August 2014 (DY026) and April 2015 (DY029) on board RRS *Discovery*, where up to four sampling depths were chosen with respect to profiles of temperature, salinity, density, fluorescence and PAR data obtained from CTD casts. The rosette system was equipped with the following sensors: SeaBird SBE9+ (temperature, salinity, density), Chelsea Aquatracka MKIII fluorometer (in vivo chlorophyll fluorescence) and Biospherical QCP Cosine PAR (irradiance).

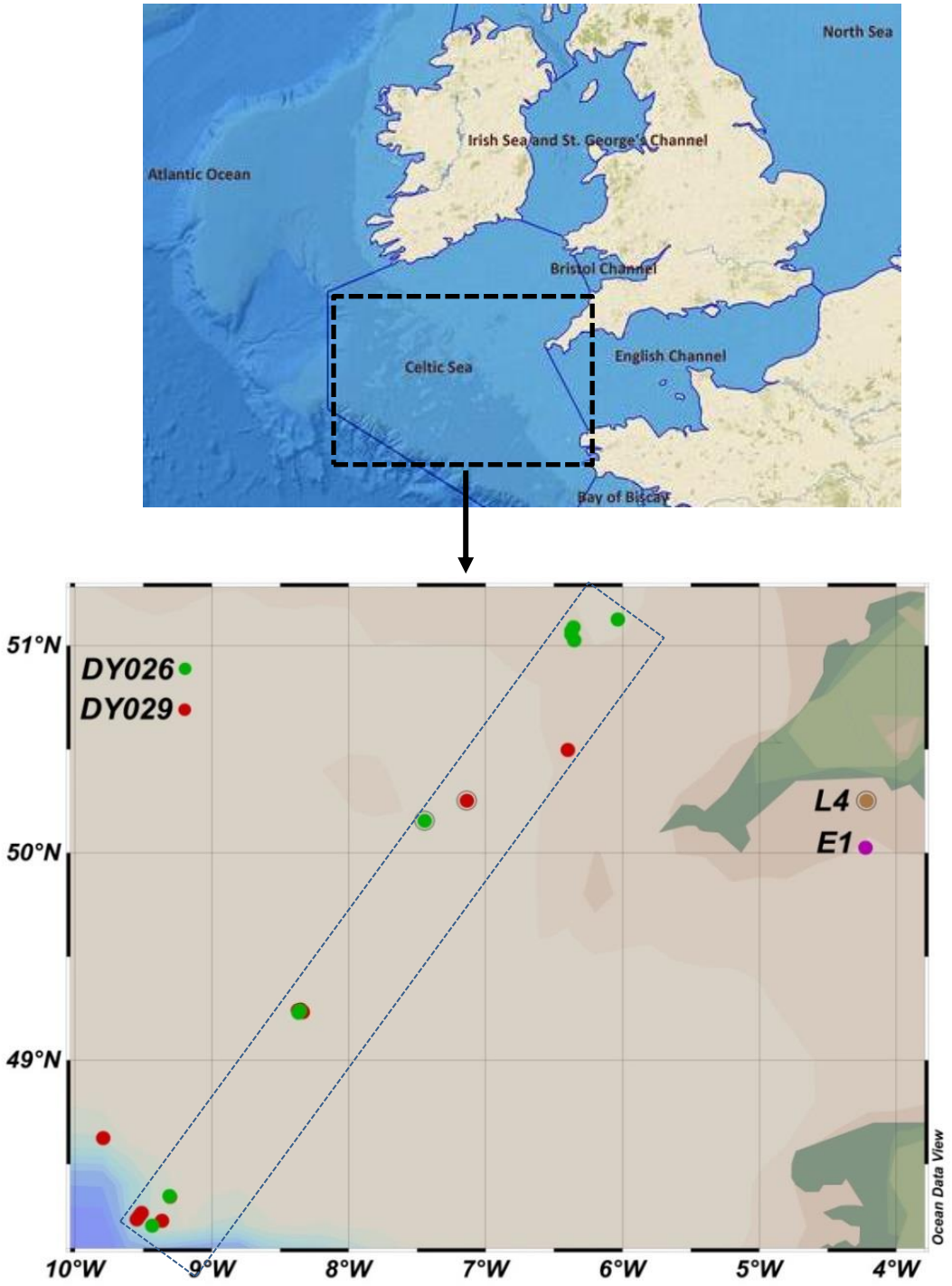


Fig 2.3(a) Sampling sites of L4, E1 and stations sampled during cruises in the Celtic Sea during Spring (DY029) and Summer (DY026). The box shows stations included in a cross-shelf transect.

Table 2.1 Sampling periods for station L4 with number of days sampled within each year. 2014, 2015 were sampled during this study, 2009-2011* are part of a historic dataset (Barnes et al. 2015)

Year	Sampling periods	Days Sampled
2009*	March - May, August, September	8
2010*	April, May, August, September	8
2011*	March, April	5
2014	March - July	15
2015	March, May - June, August, September, November	15

2.2.2 Size-fractionated chlorophyll–a concentrations

Chlorophyll concentration is used as the proxy for phytoplankton biomass with photosynthetic and absorption parameters being normalised to these values. Measurements of size-fractionated chlorophyll are therefore essential to begin to investigate patterns in phytoplankton the biomass, PE parameters and PP of individual fractions.

For all measurements of S-F chlorophyll in WCO and Celtic Sea datasets the phytoplankton community was split into three size fractions: microphytoplankton (>20 µm), nanophytoplankton (2.0-20 µm) and picophytoplankton (<2.0 µm). For each sample depth, triplicate 200 ml samples of seawater were filtered through a Sartorius sequential filtration system onto 47 mm track-etch polycarbonate filters (DHI) at pore sizes corresponding to phytoplankton size fractions (20 µm, 2.0 µm and 0.2 µm). Each filter was then stored at -18°C for 18 hours in 10 ml 90% acetone (VWR) to extract chlorophyll-a following Welschmeyer (1994). Extractions were then placed in glass vials and chlorophyll fluorescence measured using a Turner Designs Trilogy fluorometer calibrated with a Chl-a extract (Sigma). For Celtic Sea samples, a solid standard (Turner Designs) was used daily to check for instrument drift and calibrate subsequent measurements.

2.2.3 Size-fractionated phytoplankton and particulate absorption spectra (PABS)

For each sample depth during Celtic Sea cruises, 0.7-1.5 l of seawater was filtered onto a 25 mm GF/F (Whatman) (effective pore size 0.7 µm). After filtration, samples were flash frozen in liquid nitrogen and stored at -80°C for later analysis. These filters were used to determine the total phytoplankton absorption ($a_{ph_{total}}(\lambda)$); further samples were taken using the same seawater pre-filtered at 20 µm (nano + picophytoplankton) and 2.0 µm (picophytoplankton) to allow the contribution of each size fraction to total measured phytoplankton chlorophyll concentration and absorption to be quantified. For WCO samples, only measurements of total population (on GF/F) were taken as part of the WCO time series.

Phytoplankton absorption samples for both cruises and WCO sites were run to determine total particulate absorbance ($a_{PART}(\lambda)$) and absorbance of non-algal particles ($a_{NAP}(\lambda)$) using the quantitative filter-pad technique method of Kishino et al. (1985) Kishino et al. (1985). Methanol solvent was used to remove pigments from phytoplankton cells in order to measure $a_{NAP}(\lambda)$. Phytoplankton absorption $a_{ph}(\lambda)$ was determined for each sample by subtracting $a_{NAP}(\lambda)$ from $a_{PART}(\lambda)$ at each wavelength between 400 and 700 nm. Samples were run on a Lambda 800 UV/VIS spectrophotometer (Perkin Elmer) calibrated with optical density filters at 5 wavelengths in the visible domain (440, 465, 546, 590, 635nm) (Hellma Worldwide). Phytoplankton absorption $a_{ph}(\lambda)$ was determined for each sample by subtracting $a_{NAP}(\lambda)$ from $a_{PART}(\lambda)$ at each wavelength between 400 and 700 nm.

The absorption spectra of each size class were determined from pre-filtered samples as follows:

$$a_{ph_{micro}}(\lambda) = a_{ph_{total}}(\lambda) - a_{ph_{nano+pico}}(\lambda) \quad (2.1)$$

$$a_{ph_{nano}}(\lambda) = a_{ph_{micro}}(\lambda) - a_{ph_{pico}}(\lambda) \quad (2.2)$$

where $a_{ph_{micro}}$ is the absorption of microphytoplankton after subtracting the absorption of cells retained after pre filtration at 20 µm ($a_{ph_{nano+pico}}$) from the non-fractionated total absorption ($a_{ph_{total}}$). $a_{ph_{nano}}$ is the absorption of nanophytoplankton after subtracting the absorption of picophytoplankton cells retained after 2.0 µm filtration ($a_{ph_{pico}}$) from $a_{ph_{micro}}$.

2.2.4 Size-fractionated PE and photo-physiological parameters

Photosynthesis-irradiance (*PE*) curves were measured following the method of Tilstone et al. (2003). For each depth, 15 clear polycarbonate bottles containing 70 ml seawater were spiked with 5 – 10 µCi of ^{14}C-labelled $NaHCO_3$ (Perkin Elmer), administered as a 0.5-1.0 ml solution of autoclaved, 0.2 µm filtered sea water. Bottles were incubated in a linear photosynthetron and maintained at ambient temperature. Maximum irradiance on sampling days was measured using an above-water PAR sensor (Skye Instruments) and the maximum incubator light level in the incubator was set accordingly. High-output white LEDs were used for the majority of sampling days, when maximum irradiance was <1900 µE m^{-2} s^{-1} due to their superior spectral quality and low heat output compared to incandescent bulbs. However, for summer sampling days with higher incident light levels, 50 W halogen bulbs were used due to their higher emission. The light intensity along the length of the incubator was measured by measuring the irradiance at each bottle position using a portable PAR sensor (Skye Instruments). One bottle was occluded with neutral density filter to ensure low irradiance and another was blacked out to correct for dark uptake of carbon.

Following the 1.5-hour incubation, each bottle was filtered through sequential 47 mm polycarbonate filters (20 µm, 2.0 µm and 0.2 µm pore sizes) in the same manner as the chlorophyll samples. Each sample filter was then fumed for 15 hours in 37% HCl to remove residual inorganic carbon before being placed in 6 ml vials with 4 ml scintillation cocktail (Meridian Biotech). After 24 hours in cocktail, samples were run on a liquid scintillation counter (Tricarb - Perkin Elmer) to determine beta particle emission. External ^{14}C standards (Perkin Elmer) were used to correct for quenching following the dual channel ratio method in order to generate ^{14}C disintegrations per minute (DPM). Chlorophyll-specific photosynthesis-irradiance data were subsequently fitted to the function of Platt et al (1980) in SigmaPlot (Systat) using non-linear least squares regression. Curves with $R^2 \geq 0.95$ were used to determine the *PE* curve parameters P_m^B, α^B and β^B.

2.2.5 Spectral correction of light-limited photosynthesis

To correct the measurements of the spectrally-dependent parameters α^B and E_K', emission spectra for each light source (LED or 50W halogen bulbs) were measured by HyperSAS radiometer (Satlantic) at 1.5 nm resolution. These spectra were linearly interpolated to 1 nm resolution. The spectral correction factor X was calculated following the method of Kyewalyanga et al. (1997a)

$$X = \frac{\bar{a}_{ph}}{\bar{a}_t}, \tag{2.3}$$

where the unweighted mean absorption spectrum ($\bar{a}_{ph}$) is determined by

$$\bar{a}_{ph} = \frac{\int_{400}^{700} a_{ph}(\lambda) d\lambda}{\int_{400}^{700} d\lambda}, \tag{2.4}$$

and $\bar{a}_T$ which accounts for the spectral quality of the incubation light source is computed as

$$\bar{a}_T = \frac{\int_{400}^{700} a_{ph}(\lambda) E_T(\lambda) d\lambda}{\int_{400}^{700} E_T(\lambda) d\lambda}. \quad (2.5)$$

Where $E_T(\lambda)$ Is the incident lamp irradiance at wavelength (λ). P_m^B is not spectrally corrected as this parameter represents light-saturated photosynthesis and is not considered spectrally dependent (Kyewalyanga et al. 1997a; Pickett and Myers 1966).

2.2.6 Estimates of daily depth-integrated primary production

Following the approach of Smyth et al. (2005), meteorological data were obtained from the National Centre for Environmental Prediction (NCEP) and Earth-Probe Total Ozone Mapping Spectrometer data (EPTOMS and cloud cover data were obtained from the European Centre for Medium range Weather Forecasting (ECMWF). These datasets were used with a modified version of the Gregg and Carder (1990) radiative transfer model to estimate spectral irradiance at the sea-surface. Through computing the downwelling spectral irradiance ($E_d(\lambda)$) using *in situ* measurements of a_{ph} to calculate the spectral diffuse attenuation coefficient $K_d(\lambda)$. Simulated light fields of E_{PUR} at time *t* and depth *z* were generated for each sampling station and combined with profiles of size-fractionated measurements of phytoplankton biomass (B) and PE parameters (P_m^B, α^B, β^B and a_{ph}^*) to calculate daily integrated (mg C m^{-2} d^{-1}) and volumetric (mg C m^{-3} d^{-1}) primary production using the equation of Tilstone et al. (2003):

$$P = \int_{Z=0}^{Z=1\%} \int_{t=0}^{24} B\,(z) P_m^B(z) \left[1 - \exp\left(\frac{-E_{PUR}(t,z)}{E_{K(PUR)}(z)}\right)\right] dz.dt \quad (2.6)$$

where PP denotes the daily integrated primary production (mg C m^{-2} d^{-1}), B is the chlorophyll concentration (mg m^{-3}) and E_{PUR} denotes the irradiance of phytoplankton-useable radiation (PUR) (µE m^{-2} s^{-1}). Primary production was integrated at 1 m depth resolution (dz) (from the surface ($z = 0$) to the euphotic depth ($z = 1\%E(0)$)) and over 1-hour intervals (dt) for each size class, and the total phytoplankton community. Profiles of

$B(z)$, $P_m^B(z)$ and $E_{K(PUR)}(z)$ were estimated from linear interpolation of measured values. Both daily depth-integrated primary production (mg C m^{-2} d^{-1}) and volumetric primary production (mg C m^{-3} d^{-1}) at discrete 1 m intervals were computed from the surface to the euphotic depth for each size class. For most stations, the estimates of the euphotic depth generated by the model (defined here as the depth at which PAR is 1% of its surface value) were in good agreement with euphotic depth estimated from PAR data collected using CTD-mounted sensors. For stations where the euphotic depth was overestimated by the model, primary production was integrated to the euphotic depth measured from PAR sensors. In addition, where the sum of the primary production of the individual size fractions exceeded the productivity of the total phytoplankton community, size-fractionated values were corrected by multiplying each fraction's value by the quotient of total community PP with respect to summed S-F PP (eq 2.7).

$$PP_{mc} = PP_m \left(\frac{PP_{total}}{PP_{sum}}\right) \tag{2.7}$$

where PP_{mc} is the corrected PP for microphytoplankton fraction, PP_m is the uncorrected PP for microphytoplankton fraction, PP_{total} is the modelled total PP using community photosynthetic parameters, and $PP_{sum}$is the sum of all size fractionated PP measurements.

2.2.7 Phytoplankton taxonomy

In addition to the general physiological response of phytoplankton to nutrient and light availability, the measured photosynthetic properties of individual size fractions varies depending on taxonomic composition (Fragoso et al. 2017; Hickman et al. 2009). As a result, information on the dominant functional types within samples is important to contextualise differences in photophysiology beyond the influence of abiotic variables. Therefore, different methods were used to assess the taxonomic composition of each sample.

2.2.7.1 Light microscopy

Water samples taken from the same CTD rosette casts as those used for chlorophyll measurements and *PE* experiments were used to quantify the taxonomic composition of the phytoplankton community. These samples were taken as core measurements of the Western English Channel time series, and for the spring 2015 Celtic Sea cruise. Water samples were transferred to 250 ml glass amber sample jars containing acid Lugol's iodine (2% final concentration). Preserved samples were stored in cool, dark conditions until return to Plymouth Marine Laboratory. Prior to analysis, samples were acclimated to room temperature for >7 days and gently homogenised before 100 mL sub-samples were settled for >48 hours using Hydro-Bios settling chambers. Samples were analysed by Claire Widdicombe (PML) following the British Standard (BS EN 15204:2006).

Where possible, all cells >15 µm were identified to species level. Mean cell measurements were used to calculate cell biovolume, assuming appropriate geometric shapes (Olenina et al. 2006). Cell counts of species were generalised into diatom, dinoflagellate, coccolithophorid and phytoflagellate functional groups. Cell biovolume was estimated assuming appropriate geometric shapes (Olenina et al. 2006).. As cell size varies considerably between taxa, and cell counts therefore being a poor indication of relative biomass, carbon conversions (pg C $cell^{-1}$) were applied at the lowest taxon level possible (usually individual species) using the equations of Menden-Deuer and Lessard (2000) to estimate the total cellular carbon masses of each functional group.

2.2.7.2 Flow cytometry

As picophytoplankton and smaller nanophytoplankon cells are generally too small to identify and quantify accurately using light microscopy, a Becton Dickinson FACSort™ flow cytometer was used to enumerate photosynthetic prokaryotes (typically

Synechococcus), nanoplankton (grouped into cryptophytes, coccolithophores, small dinoflagellates and other nanoeukaryotes), and picoeukaryotes for L4 and the spring Celtic Sea cruise samples (Tarran et al. 2006). Cellular carbon values were subsequently generated using the conversion values of Booth (1988).

2.2.7.3 Statistical Analysis

Principal Component Analysis (PCA) was conducted to assess the variability of PE parameters, taxon-specific carbon concentration and abiotic parameters, with the aim to ascertain any relationships between *PE* parameters and environmental variables and dominance of specific taxonomic groups. Following the PCA, relationships between selected variables were further investigated through regression using quadratic functions to fit modelled relationships for a range of the observed variables. In addition, multiple stepwise linear regression was used to investigate variability among variables.

2.3 Results

2.3.1 Seasonal variability at WCO and Celtic Sea – stratification and nutrients

As previously described, phytoplankton photophysiology and PP is driven by changes in the physical environment and as temperate shelf seas undergo substantial seasonal changes in hydrography, nutrient concentrations and irradiance levels, it is necessary to understand how this variability may affect the phytoplankton community across the shelf regions that form the study region of this thesis.

Stations L4, E1 and CCS followed a typical temperate shelf sea seasonal pattern, characterised by a mixed water column through winter, followed by seasonal stratification beginning in the late spring/ early summer after which surface mixed layer nutrient concentrations quickly decrease (Figs 2.4-2.6 (Pingree et al. 1976).

By late summer, nutrient pools began to increase below the thermocline, with surface waters again being replenished after winter mixing. Peak irradiances are seen during the summer months and euphotic depths range between ~15-50 m, though typically fall between 22 and 28 m during post-bloom summer stratification. The hydrography of station L4 is additionally influenced by the river Tamar, and to a lesser extent the Plym and Yealm rivers, whereby periods of intense rainfall may affect water column stability and temporarily replenish nutrient pools (Fig 2.6).

Fig 2.5 illustrates the high degree of seasonality in macronutrient concentrations exhibited by stations L4 and E1, with concentrations at each site falling below the limit of detection in surface waters during summer stratification, with the nutricline extending as deep as 50 m for nitrate at L4. Nitrate and silicate concentrations were typically lower at the E1 than at

L4, while phosphate concentrations were broadly similar. Concentrations below the thermocline were replenished earlier for silicate than nitrate and phosphate, and to a much greater degree (relative to maximum concentrations) at E1 than L4. Nitrate stocks at L4 were generally replenished above 3 μM only after the breakdown of the thermocline in late October, while the concentrations were present at E1 from early August.

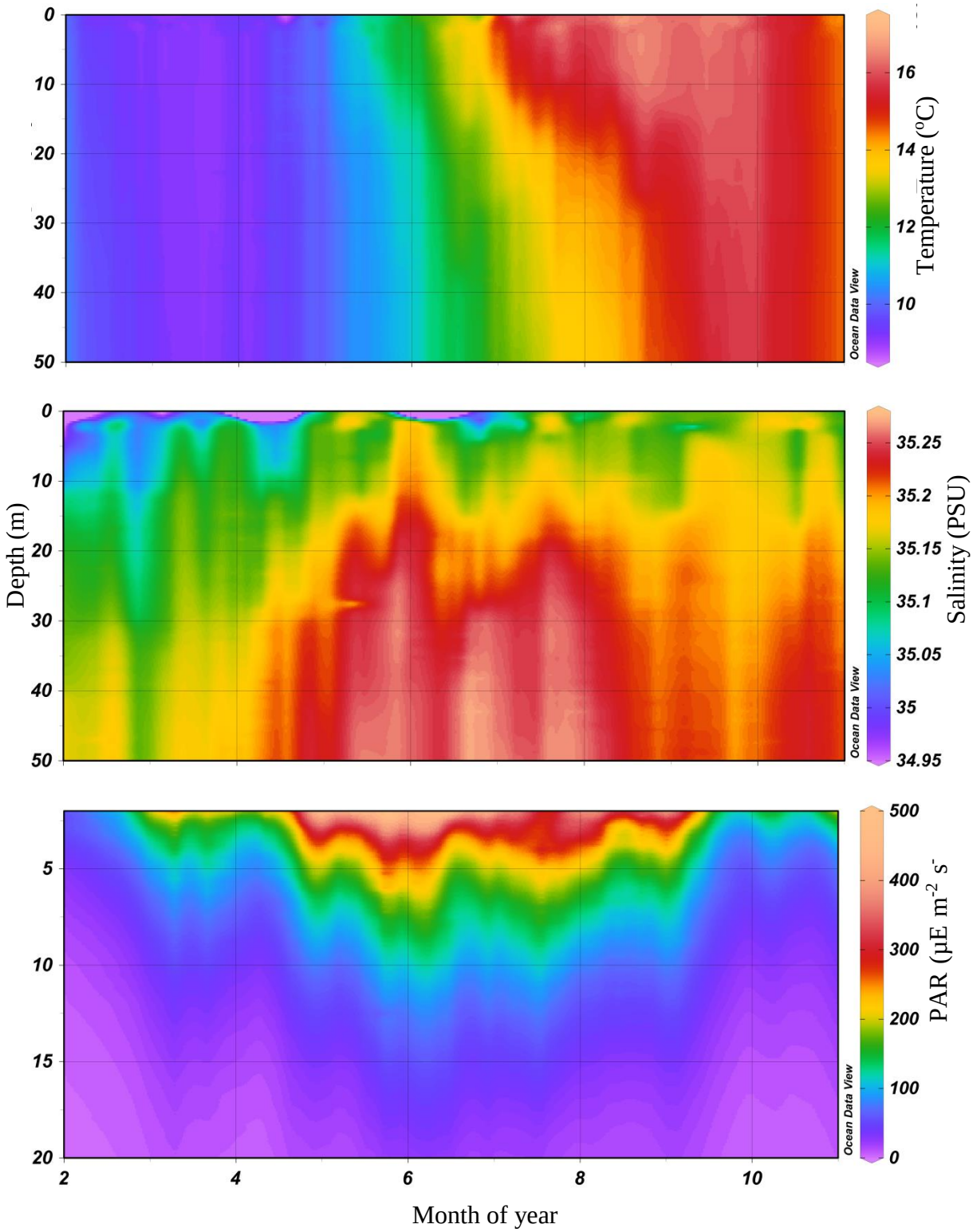


Fig 2.4 Climatological time series of temperature, salinity and PAR for station L4 Feb-Nov from 2009-2016 to indicate average seasonal changes in physical parameters at the shelf site using weekly CTD cast data.

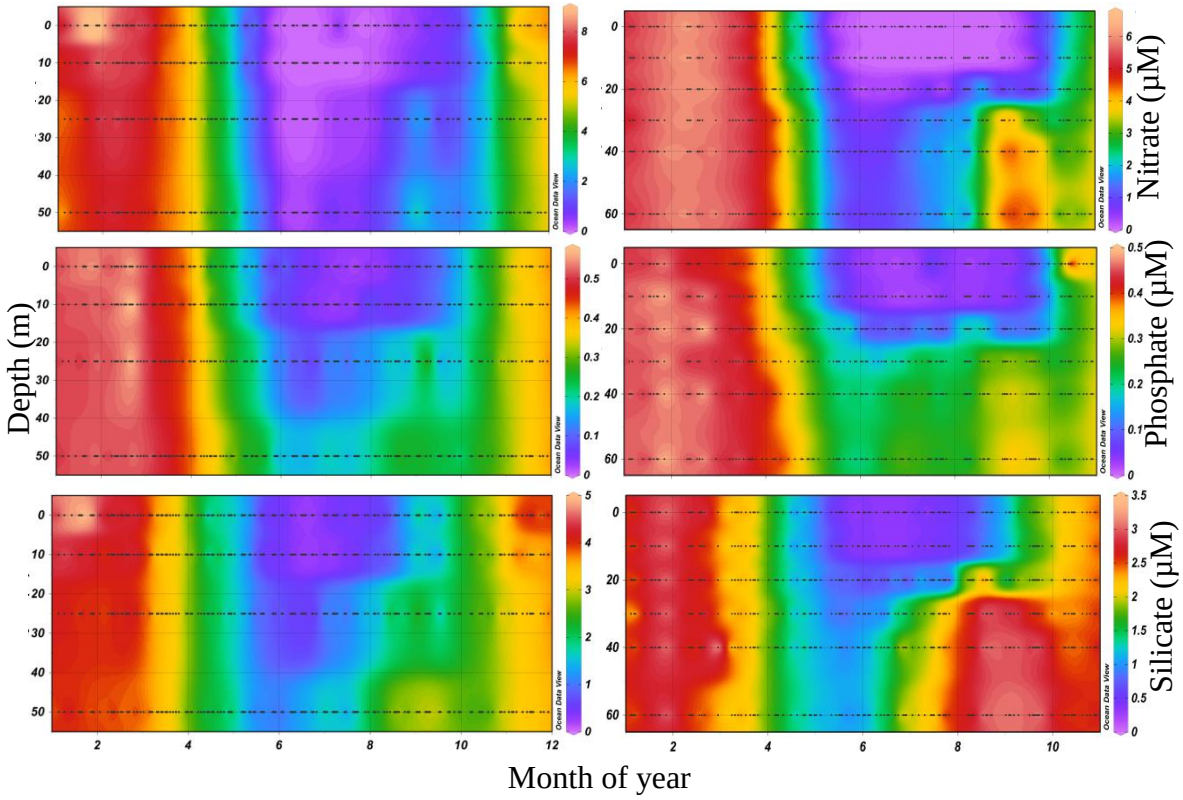


Fig 2.5 Climatological annual patterns of macronutrient concentrations (µM) for station L4 (left pane) and E1 (right pane) using data from 2009-2016 NB different scales at each site.

When compared to the western English Channel sites of E1 and L4, seasonal dynamics at on-shelf stations within the Celtic Sea follow a similar pattern. Though considerably fewer samples were taken from the Celtic Sea during 2014, the nutrient profiles showed well mixed pre-bloom conditions during March with high concentrations throughout all sampling depths, followed by summer stratified conditions during July with depleted nutrient pools from the surface to around 20 m depth at the Celtic Deep, and 45 m at Central Celtic Sea site. Following a long period of stratification until mid-November 2014, both sites were subject to deep winter mixing and the consequent replenishment of surface nutrient pools by late November. Data were collected more frequently during 2015, with the rapid drawdown of nutrients in euphotic waters being captured during the April 2015 Celtic Sea cruise: nitrate, silicate and phosphate concentrations were reduced to trace quantities at the Celtic Deep by the beginning of May; the Central Celtic Sea site showed a similar pattern except for silicate where stocks were reduced to intermediate levels (~1.7µM). Sampling

during July to August 2015 captured the typical summer stratified period with depleted surface nutrient pools separated from underlying nutrient-rich bottom water by a strong thermocline.

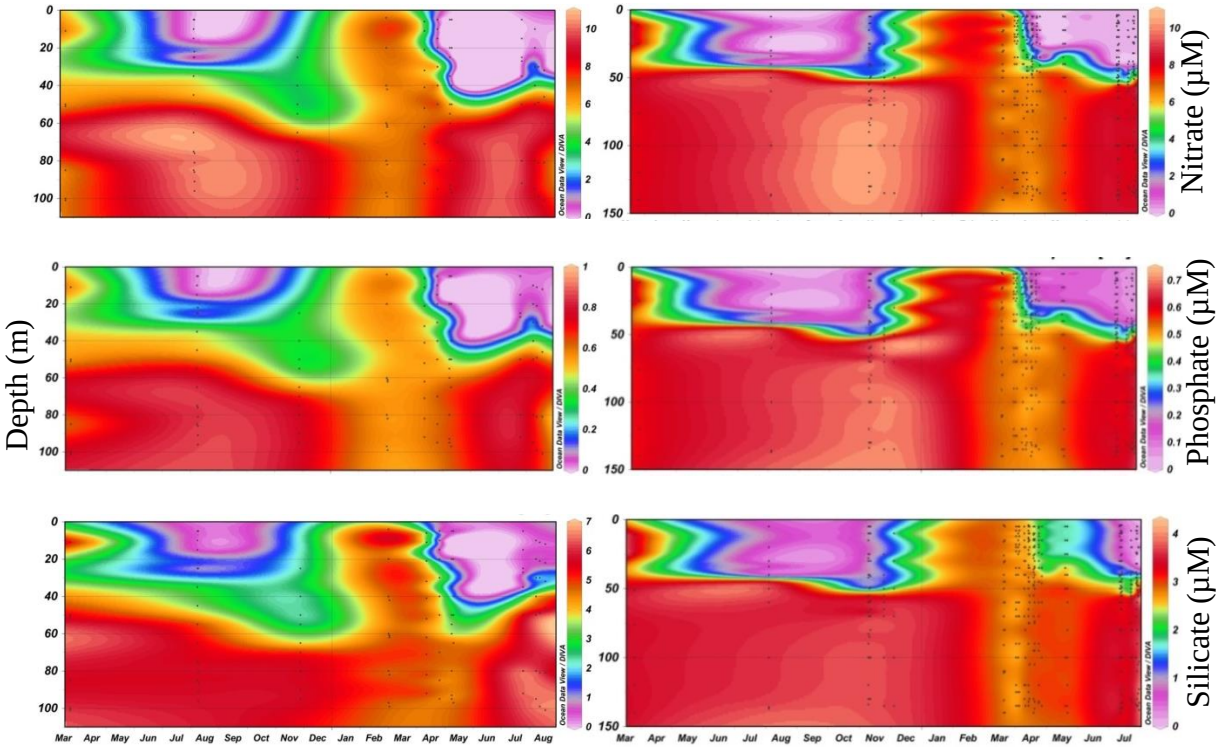


Fig 2.6 Macronutrient concentrations March 2014 - August 2015 for Celtic Deep station (left pane) (51.137 °N, -6.567 °E) and March 2014 - July 2015 for Central Celtic Sea station (CCS) (right pane) (49.280 °N, -8.367 °E).

2.3.2 Seasonal variability at WCO – phytoplankton biomass and taxonomy

The seasonality of hydrography and nutrient concentrations outlined in the preceding section will influence the community structure and photosynthetic activity of the phytoplankton at those responsive sites. By taking measurements of size-fractionated chlorophyll and phytoplankton taxonomy in addition it is possible to identify any effects of the physical environment on the phytoplankton dynamics observed at WCO sites and during the Celtic Sea Spring bloom of 2015.

Chlorophyll concentration at L4 varied throughout the year in relation to the seasonal cycles in water column structure and nutrient supply (Fig 2.3, 2.4, 2.6). Phytoplankton biomass (using chlorophyll as a proxy) peaked in April/May, when nutrient pools had begun to be reduced from their pre-bloom maxima. Microphytoplankton chlorophyll peaked first, across all depths (due to the mixed water column), usually consistent with a diatom bloom and hence the drawdown of silicate preceded other nutrients (Fig 2.4). Nano- and picophytoplankton biomass peaked in May when chlorophyll concentrations appear to increase with depth for nanophytoplankton and are similarly highest at 50 m for picophytoplankton, but with shallower depths having similar concentrations (~0.17 mg m^{-3}). Nano- and picophytoplankton chlorophyll concentrations decreased substantially during June-July, as did microphytoplankton chlorophyll in the surface mixed layer (0, 10m), though microphytoplankton biomass below the thermocline (25, 50m) also remained high during this period, which may be consistent with peak dinoflagellate abundance (Fig 2.8)

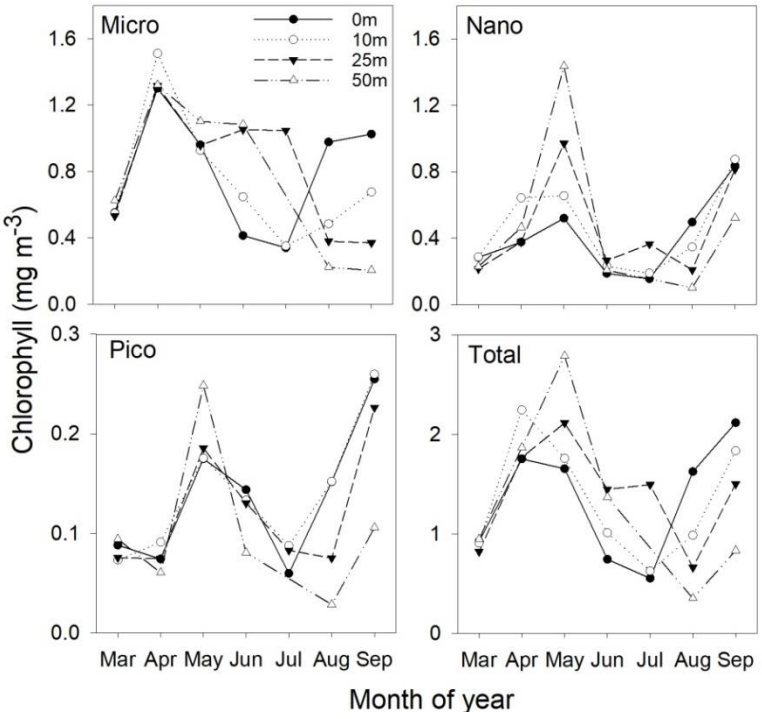


Fig 2.7 Mean monthly total and size-fractionated chlorophyll concentrations at L4 during 2009-2015.

Season variability in the abundances of individual groups were observed at station L4 at 10m (Fig 2.8a). Diatom abundance peaked in May and to a lesser degree in September, while dinoflagellates had the greatest abundance in July, dominating the microphytoplankton fraction. Phytoflagellate carbon was generally highest during May, consistent with the peak in nanophytoplankton chlorophyll (Fig 2.7) decreasing substantially by June as with diatoms, before a more gradual decrease through the autumn. A large summer bloom of *Karenia mikimotoi* during late August to early September 2009 (Fig 2.8b). The bloom of this species dominated the monthly mean chlorophyll and carbon concentrations for that month (as shown by the large decrease in carbon concentration when these species were removed from the dataset Fig 2.8a). These data were removed as the effect of one transient bloom profundoundly changes the seasonal dyanamics in taxonomy even when presented within a climatology of monthly averages from multiple years. The inclusion of data sampled during the *Karenia mikimotoi* bloom therefore produces a climatology that is not representative of an "average" year.

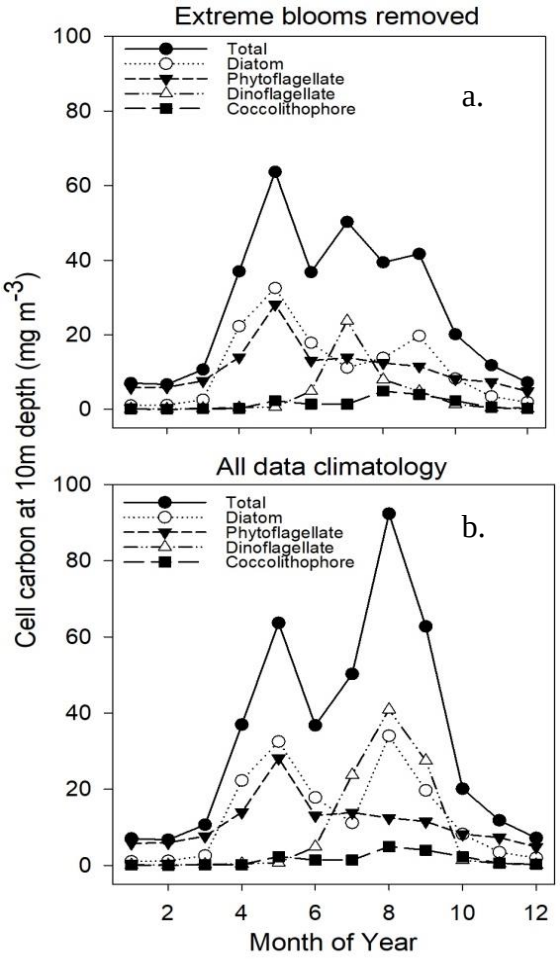


Fig 2.8 Mean monthly phytoplankton carbon concentration at L4 by functional type Estimated using light microscopy cell count data from 2009-2016. Panel a. is presented with extreme summer bloom events removed; panel b. includes these data to show the considerable difference in the annual pattern of phytoplankton biomass

Coccolithophores were a less significant component of the L4 phytoplankton community in terms of cellular carbon, (these carbon conversions do not include shed liths), though did show a greater mean abundance in August and September.

Averaging the cell-carbon concentration of micro- and nanophytoplankton taxonomic groups sampled from 10 m at station L4, season differences in the abundances of individual groups can be observed (Fig 2.7). Diatom abundance peaked in May and to a lesser degree in September, while dinoflagellates had the greatest abundance in July, dominating the microphytoplankton fraction. Phytoflagellate carbon was generally highest during May, consistent with the peak in nanophytoplankton chlorophyll (Fig 2.7) decreasing substantially by June as with diatoms, before a more gradual decrease through the autumn. Coccolithophores were a less significant component of the L4 phytoplankton community in terms of cellular carbon, (these carbon conversions do not include shed liths), though did show a greater mean abundance in August and September. Panel b. of Fig 2.8 shows the difference in the mean monthly averages when measurements made during a large summer bloom of *Karenia mikimotoi* during late August to early September 2009 were included in the dataset.

2.3.5 Seasonal variability at WCO – size-fractionated PE parameters

As phytoplankton adapt their photosynthetic acitivity to within the constraints of the physical environment, the seaasonal changes in thelf sea hydrography and nutrient concentrations presented in section 2.3.1 may force changes in the values of PE parameters measured throughout the growing season. Furthermore, Given the different patterns in the peak abbundances of different phytoplankton taxa observed in Fig 2.8, the PE parameters of different size fractions may also follow disticnt patterns.

When mean climatologies of P_m^B and α^B values are produced for station L4, patterns in the valyes of both parameters can be observed (Fig 2.9), However,given the variability of these measurements (evident in Fig 2.11), the seasonal differences in microphytoplankton and picophytoplankton mean P_m^B and α^B values are insignificant. Mean surface values of P_m^B values for nanophytoplankton do appear to show a trend of increasing substantially from April to May. Overall, PE parameter values tend to be lower preceeding the spring bloom and in late summer, while Picophytoplankton P_m^B values appear to decrease throughout the growing season.

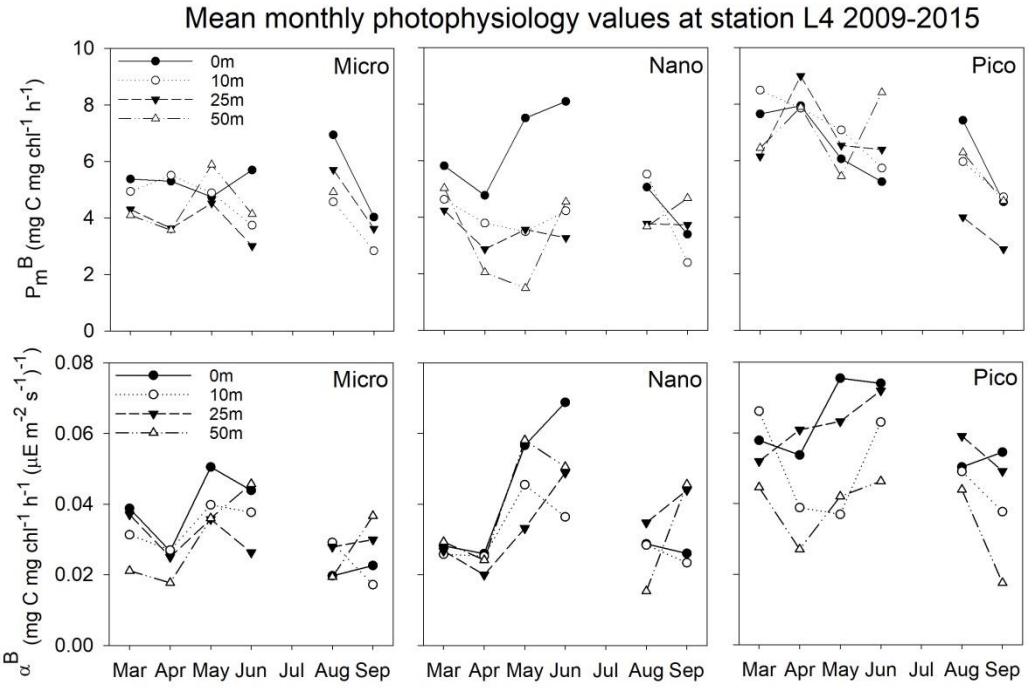


Fig 2.9 Climatologies of monthly mean P_m^B and α^B values of micro, nano and picophytoplankton measured at station L4 2009-2015. Gap for July is due to too few measurements to calculate average.

2.3.3 The Celtic Sea spring bloom – Stratification, biomass and taxonomy

Although data taken during the August and April cruises were restricted to sampling only two months of the year, by using measurements conducted during the 2015 spring bloom it

is possible to see some of the similarities and differences in phytoplankton dynamics between this open shelf site (Central Celtic Sea) and the coastal L4 site

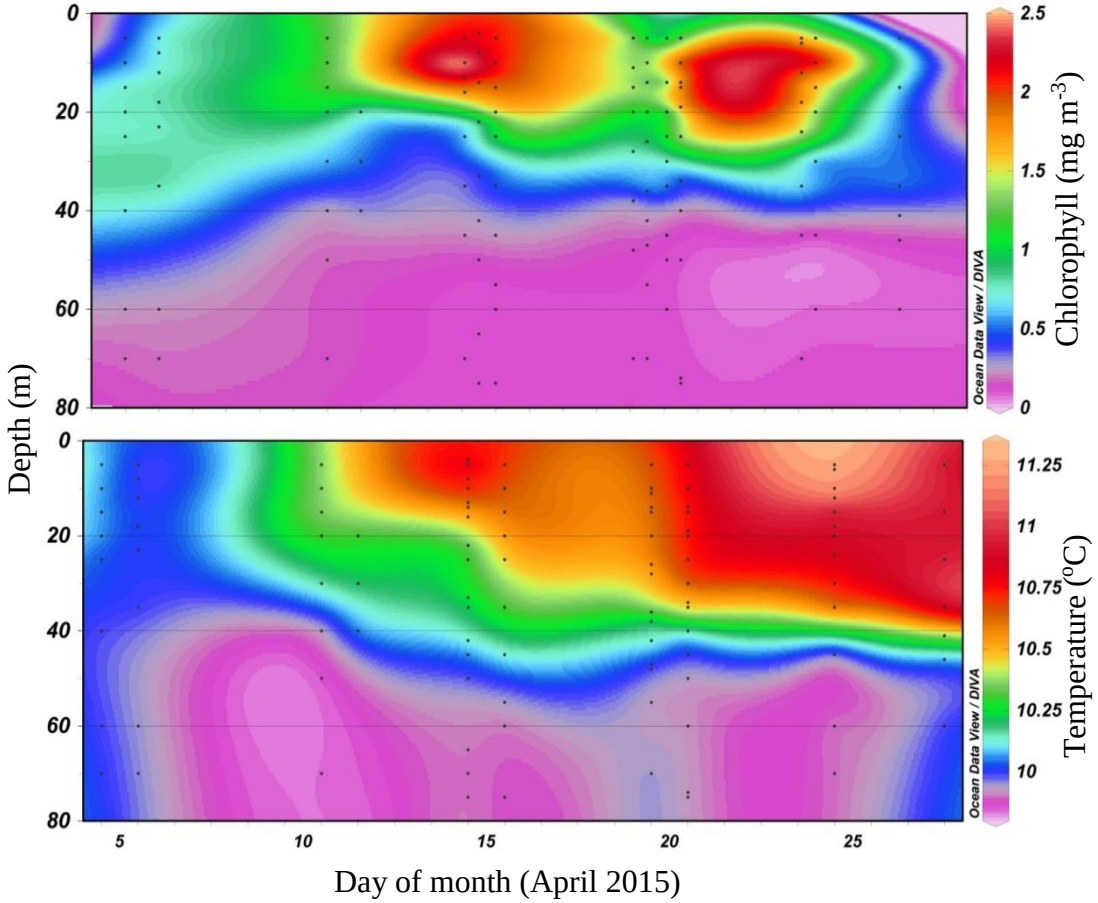


Fig 2.10 Time series of total chlorophyll concentration and water temperature at the Central Celtic Sea during April 2015, showing the development of the thermocline and transition into stratified conditions.

Fig 2.10 shows the onset of the spring bloom at the Central Celtic Sea, with a gradual increase in chlorophyll within the surface mixed layer followed by a more rapid increase in phytoplankton biomass once stratification became sufficient to restrict populations to the higher irradiance and nutrient-replete surface waters (April 14th). At the beginning of April the temperature gradient in the upper 80 m of the water column was ~0.1 °C, at its highest the gradient was ~1.8 °C. The bloom measured at the Central Celtic Sea during April 2015 was not persistent. The reduced insolation and increased wind stress diminished the strength

of initial stratification. Chlorophyll concentrations in this period decreased before increasing again as stratification strengthened around the 20th April.

Fig 2.11 provides information on the taxonomic composition of the spring bloom at the Central Celtic Sea during 2015 which was initiated 4-6th April by a smaller bloom of mixed taxonomic composition, with diatoms at the surface, dinoflagellates at the surface and 18-24 m, and phytoflagellates throughout the euphotic zone. Peak chlorophyll concentration was reached around the 15th April between 4-16m where both dinoflagellate (*Ceratum* and *Gymnodiniales*) and phytoflagellate concentrations were consistently high, with diatoms being abundant at 12m (~1.8 g C m^{-3}). Despite diatom biomass peaking at 3.5-10 g C m^{-3} on 25th April (a mono-specific bloom of *Rhizosolenia hebetata*), chlorophyll concentrations were no higher than the combined flagellate bloom, which had a carbon concentration an order of magnitude lower. It could therefore be assumed the chlorophyll-to-carbon ratio is much greater for the larger diatom species.

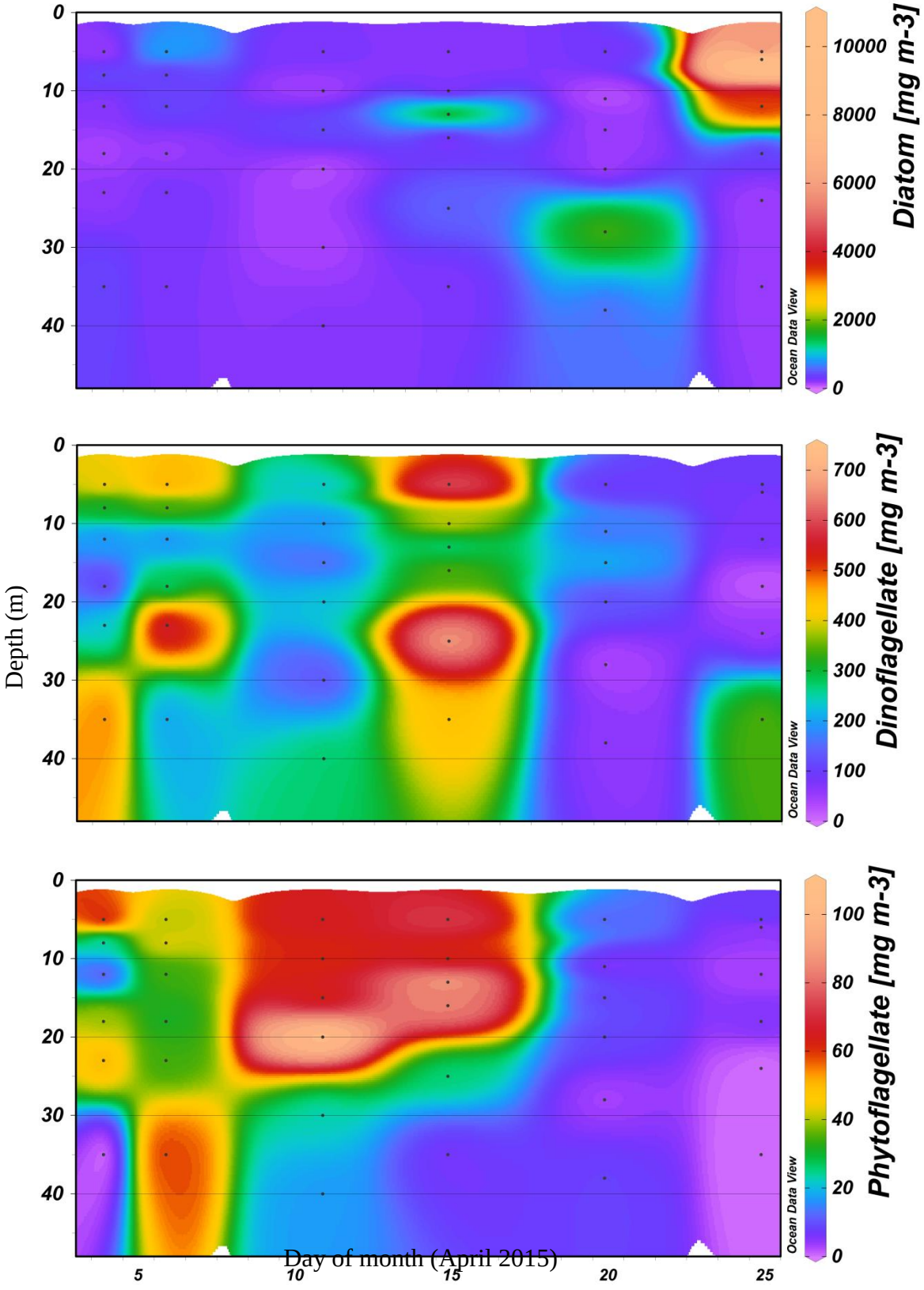


Fig 2.11 Time series of cellular carbon concentrations at the Central Celtic Sea during April 2015, showing the variability in the taxonomic composition of the phytoplankton community as the spring bloom progressed (see Fig 2.9).

2.3.4 Seasonal variability in the Celtic Sea – size-fractionated chlorophyll

As Celtic Sea samples were collected over two cruises in August 2014 and April 2015 it is not possible to examine seasonality in size-fractionated chlorophyll concentrationsthrough the water column for Celtic Sea sites in the same way as WCO sites. Comparison is therefore between spring bloom and stratified summer communities, with focus on the absolute concentrations and vertical distribution of S-F chlorophyll.

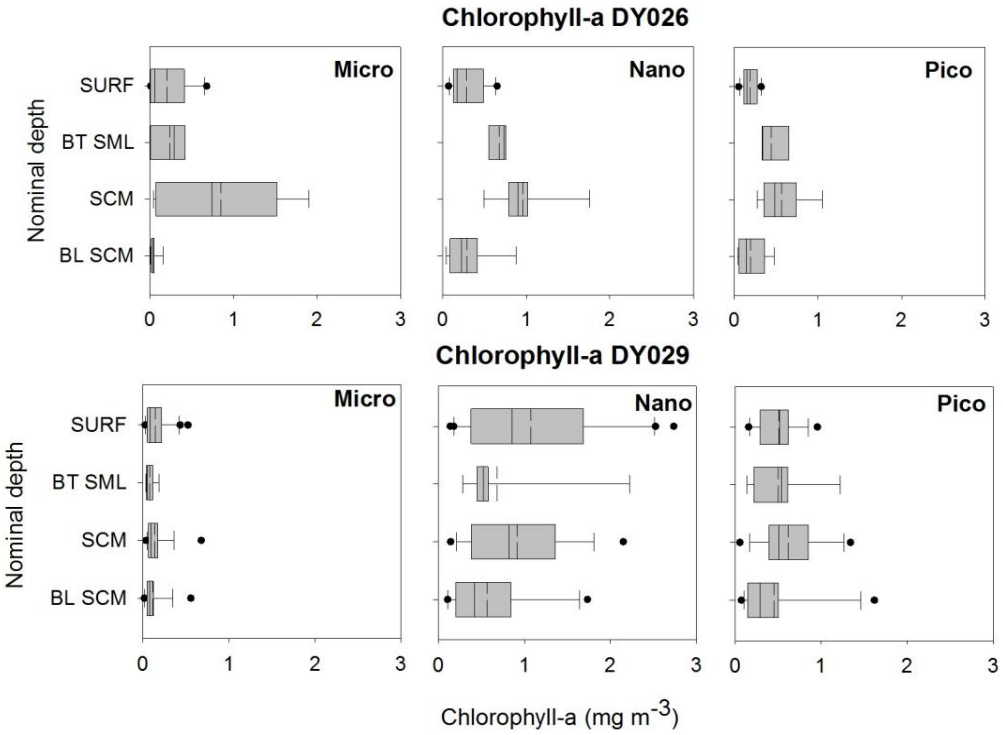


Fig 2.12 Mean values of chlorophyll concentrations at nominal depths during the August 2014 cruise (DY026) top pane, and April 2015 cruise (DY029) bottom pane. Nominal depths: SURF = surface water (typically 0-6m), BT SML = Bottom of surface mixed layer, SCM = sub-surface chlorophyll maximum (present under stratified conditions), BL SCM = below the SCM. Box plots show mean (solid bar), median (dashed bar), interquartile ranges (boxes), maximum non-outlier values and outliers.

As cruise sampling depths were chosen following biomass (fluorometric), seawater density and PAR profiles, samples were subsequently grouped into nominal depth intervals in order to aid comparisons in phytoplankton biomass between stations with respect to water column

structure and light environment: surface (SURF), bottom of surface mixed layer (BT SML), subsurface chlorophyll maximum (SCM) and below the subsurface chlorophyll maximum (BL SCM). This grouping allows comparison between sampling sites and cruises where sampling depths and vertical hydrography may be dissimilar. During the April 2015 cruise at the first few stations preceding the spring bloom the water column was mixed or inconsistently stratified (high variability in CTD profile data), and therefore nominal depths of SURF and BT SML only were used.

During the summer Celtic Sea cruise, a strong subsurface chlorophyll maximum was present across all shelf stations; maximum mean chlorophyll concentrations were therefore highest at the SCM for all size classes (average mean values of 0.85, 0.96 and 0.57 mg m^{-3} for micro-, nano- and picophytoplankton fractions respectively). All size classes exhibited highest variability in biomass at the SCM, with either micro- or nanophytoplankton being dominant. Picophytoplankton chlorophyll concentrations were moderate at most stations, showing less variability than the larger size classes between stations.

Chlorophyll concentrations for microphytoplankton were relatively uniform throughout the surface mixed layer, whereas nano- and picophytoplankton concentrations were significantly higher at the bottom of the surface mixed layer than at the surface. Chlorophyll concentration for the microphytoplankton fraction was consistently lowest below the SCM (average mean <0.05 mg m^{-3}), while nano- and picophytoplankton concentrations below the SCM were similar to surface samples.

During the spring Celtic Sea cruise, microphytoplankton were typically present at low concentrations in the form of large diatoms (e.g *Coscinodiscus wailesii, Rhizosolenia hebetata* (Fig 2.11). This was surprising for a temperate shelf-sea spring bloom, where microphytoplankton, typically diatoms, often initially dominate the spring bloom, followed

by a shift towards nanophytoplankton-dominated communities with the occurrence of *Phaeocystis* blooms (Holligan et al. 1984; Reid et al. 1990; Weeks et al. 1993). However, despite the low microphytoplankton biomass observed during the spring, chlorophyll concentrations reached bloom level (up to 7 mg m^{-3}) from the combined smaller (< 20 μm) size fractions. Preceding the formation of the permanent thermocline, maximum chlorophyll concentrations were either at the surface or just below (6-10 m), with a SCM only observed when thermal stratification was maintained over day-night cycles (fig 2.10). A combination of changing hydrography under conditions of weak, transient stratification of the water column, spatial variability in SML depth between stations, and differences in the timing of the onset of stratification in different regions led to enhanced variability in the distribution of phytoplankton biomass during the dynamic spring bloom period. This can be observed for every size fraction and nominal depth (Fig 2.12) with the exception of the microphytoplankton within the SCM, which increased during August 2014 resulting in greater variability between stations compared to the consistently low values of April 2015.

The high degree of variability in S-F chlorophyll concentrations (B_i) within each nominal depth interval during April 2015 reflects the poor correlation between the vertical distribution of biomass and hydrographic gradients (e.g. mixed layer depth) when generalised across the Celtic Sea during the spring bloom, wheras this effect is obvious during the August 2014 cruise (Fig 2.12). Mean B_i values were highest in the surface for micro- and nanophytoplankton fractions and at the SCM for picophytoplankton. Mean surface values during April 2015 were higher for nano- and picophytoplankton than during August 2014, while mean SCM values were similar, though with greater variability. Microphytoplankton chlorophyll during April 2015 was lower than during August 2014 at all nominal depths except below the SCM.

2.3.5 Seasonal variability in the Celtic Sea - size-fractionated phytoplankton light absorption spectra

As this chapter seeks to examine and where possible, quantify the differences between the photophysiologies of individual size fractions and the variability of these various parameters, size fractionated measurements of absorption were attempted. This approach to determining the absorption spectra of different sizes of phytoplankton is not common in previous literature and no attempts to conduct these measurements for shelf sea communities are known to the author. Size-fractionated measurements of a_{ph}were therefore taken in an effort to inform the spectral correction of α^B and calculation of $\varphi_{max}$for each fraction, rather than using measurements of the whole community.

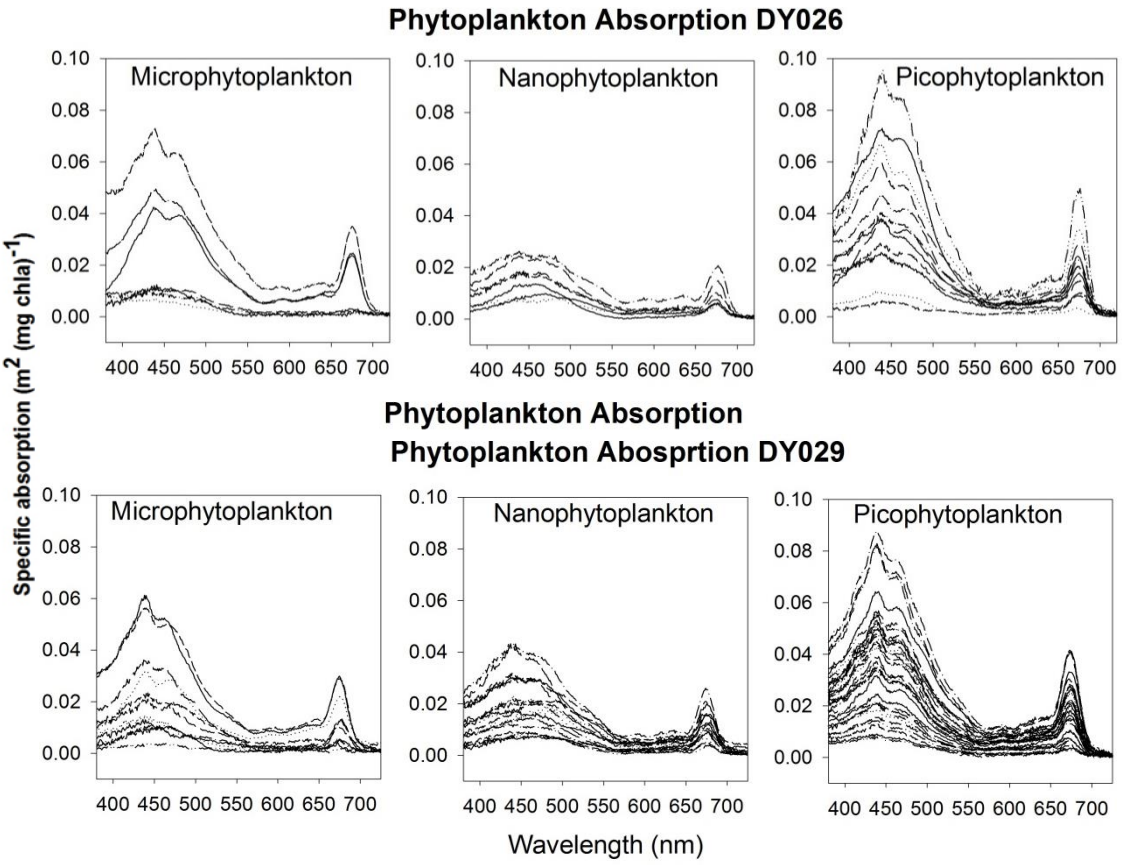


Fig 2.13 Chlorophyll-normalized size-fractionated phytoplankton light absorption spectra (a^*_{ph}) measured from Celtic Sea samples taken during August 2014(DY026) and April 2015 (DY029).

Size-fractionated absorption spectra were measured during Celtic Sea cruises DY026 (summer) and DY029 (spring), revealing differences in the chlorophyll-normalised (specific) absorption spectra for each size class. Picophytoplankton were observed as having the highest specific absorption values with nanophytoplankton the lowest. However, as microphytoplankton biomass was generally low at stations sampled during the cruises (save for a limited number of samples within the SCM during the summer) microphytoplankton absorption spectra were of poorer quality than the other size fractions. The variability in magnitude and shape and seemingly erroneously high values with respect to previous literature means many of these microphytoplankton spectra were considered to be unrepresentative. As the calculation of microphytoplankton absorption is taken from the difference between total and <20 µm (equation 2.1), and microphytoplankton biomass is generally very low relative to nano- and picophytoplankton fractions, variability in <20 µm absorption may be greater than the signal of microphytoplankton absorption given the low biomass and lower specific absorption of microphytoplankton. Indeed, small levels of noise in the signal of < 20 µm absorption could be seen very strongly in resultant microphytoplankton spectra. Furthermore, when microphytoplankton chlorophyll is low, small inaccuracies in measured chlorophyll values can produce unrealistic specific absorption spectra for microphytoplankton. The limited number of reliable microphytoplankton spectra owing to the low microphytoplankton biomass is a potential problem for spectral primary production and calculation of spectrally-corrected light-limited photosynthetic rates and parameters derived from spectral measurements.

2.3.6 Variability with depth – size-fractionated PE parameters at L4, E1 and the Celtic Sea

The climatology presented in Fig 2.8 shows the typical seasonal changes in *PE* parameters at station L4 at a number of depths, made possible by the inclusion of historical datasets (2009-2011). However, to apply models of phytoplankton PP over a broader hydrographic region, it is necessary to test the regional variation in the *PE* parameters and how the vary with depth. Therefore, the seasonally-averaged and depth-resolved PE parameters for the WCO are compared to those for the Celtic Sea (Fig 2.14) that shows the depth-dependent variation in size-fractionated mean P_m^B values at both discrete (L4 & E1) and nominal depths (Celtic Sea cruises).

In the L4 dataset, mean P_m^B was highest at the sea surface across all size fractions (Fig 2.13). The mean values increased with decreasing cell size: picophytoplankton had the highest rates and microphytoplankton the lowest at the surface in both years. In general, mean values between 10 - 50 m depths changes little for each size fraction, given the considerable variability for each size fraction in both years. However, there are some observable patterns in these mean rates: in 2014, nano- and picophytoplankton exhibited a similar pattern in mean P_m^B with each sample depth, decreasing substantially from 0 - 10 m and slightly from 10 - 25 m. Microphytoplankton show an minimum in mean P_m^B at 10 m increasing with depth at 25 m and again at 50 m. Picophytoplankton P_m^B values display a slightly different relationship with depth, with a more pronounced reduction in P_m^B from 10 to 25 m.

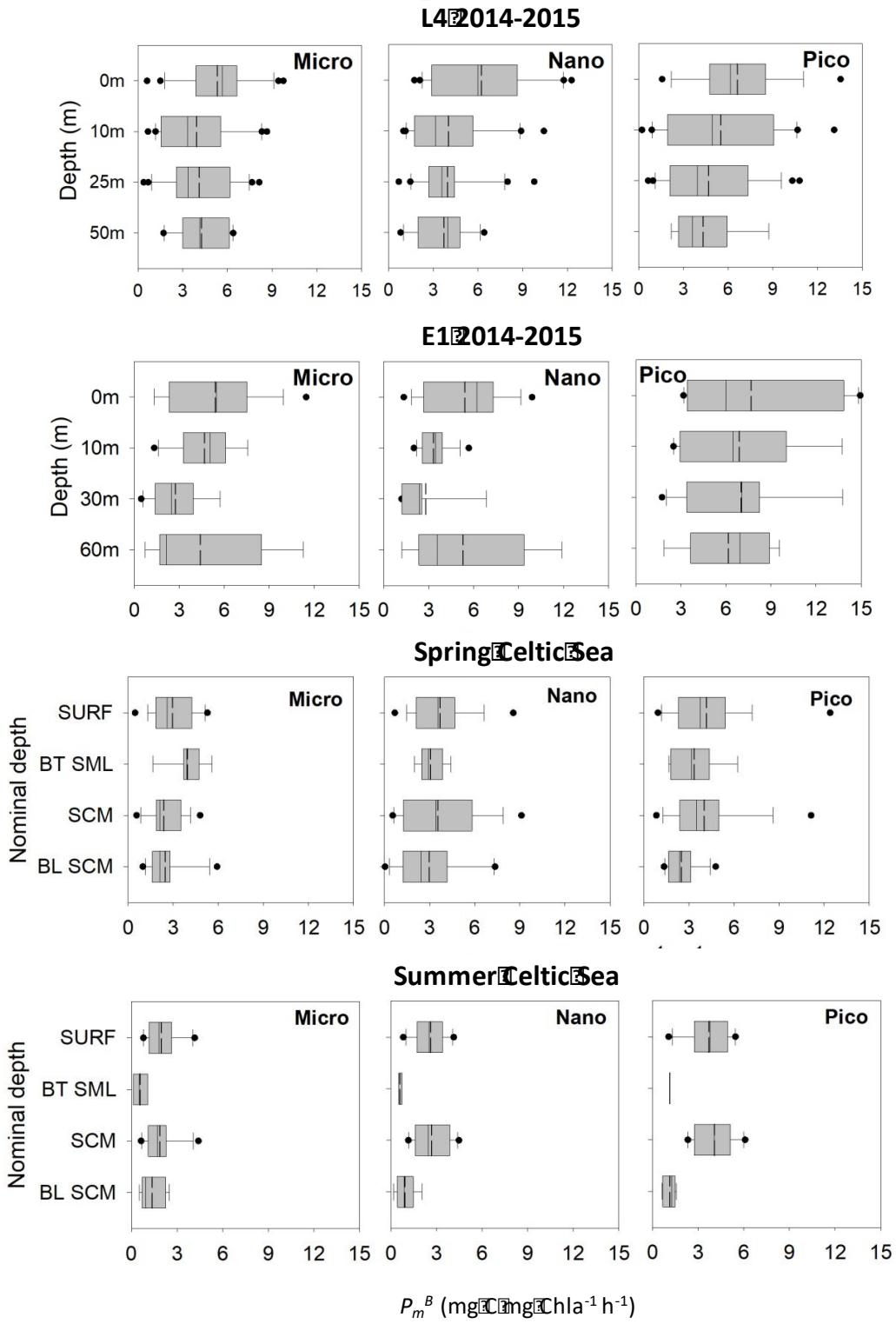


Fig 2.14 Boxplots of size-fractionated measurements of P_m^B at each sampling depth taken during 2014 and 2015 at stations L4 & E1, and at each nominal depth during Celtic Sea cruises consistent with chlorophyll samples (Fig 2.12). Boxplots contain all L4 and E1 data and cruise data (2014 – 2015).

As with L4, peak mean values of light-saturated photosynthetic rates were observed in E1 surface samples, though differences between surface values and other depths were only observed for nanophytoplankton. Mean P_m^B values for micro- and nanophytoplankton were typically lower than observed at L4, particularly at deeper sampling stations of 30 m and 60 m for microphytoplankton. Picophytoplankton mean P_m^B values were relatively similar with depth, but displayed high variability given the smaller sample size. L4 and E1 had relatively similar picophytoplankton P_m^B values, while micro- and nanophytoplankon light saturated photosynthetic rates were generally lower at E1 (Fig 2.14).

On both Celtic Sea cruises mean P_m^B values were highest in the surface and at the SCM for all size classes, with the exception of microphytoplankton sampled at the bottom of the surface mixed layer during April 2015), with lower maximum rates at the bottom of the surface mixed layer and below the SCM. This follows a similar pattern to that observed in the mean chlorophyll data, with differences in P_m^B values between nominal depths being markedly different during August 2014, when the water column was strongly stratified, resulting in lower P_m^B values at the bottom of the SML and below the SCM. Picophytoplankton generally have the highest mean P_m^B values, followed by nano- and then microphytoplankton.

Variability in P_m^B is higher during the spring, possibly due to more heterogeneous hydrography than in the summer, and rapid drawdown of nutrients in the surface mixed layer (Figs 2.6, 2.10). The size class with the lowest observed variability during April 2015 is the microphytoplankon which also constitute the lowest biomass. Variability in P_m^B is similar in pattern and magnitude for all size fractions during the summer, though again with the exception of microphytoplankton at the bottom of the surface mixed layer. Variability is much lower during the summer and could be explained by weather conditions and

hydrography being considerably less variable, and therefore physio-chemical differences between nominal depths at different sampling stations were less pronounced than during the evolution of stratification and rapid nutrient drawdown of the spring bloom.

Light-limited photosynthetic rates (α^B) measured at L4 during 2014 and 2015 showed a similar vertical pattern across all size classes, whereby mean values decreased from the surface to 10 m (Fig 2.15). Differences in the α^B values at 25 and 50 m are evident between years, with data from 2015 giving higher mean values than both 10 and 25 m, and surface values for micro- and picophytoplankton. Mean values for α^B typically follow the observed pattern of P_m^B insofar as picophytoplankton generally exhibit highest values, consistent with the climatologies of Fig 2.9. Values of α^B measured at station E1 were only slightly lower than those measured at L4 (see Table 2.2). For all size classes, values of α^B were highest, and most variable at 10 m. Micro- and picophytoplankton mean α^B values were similar between 30 and 60 m whereas the average α^B value for nanophytoplankton had its minimum value at 30 m.

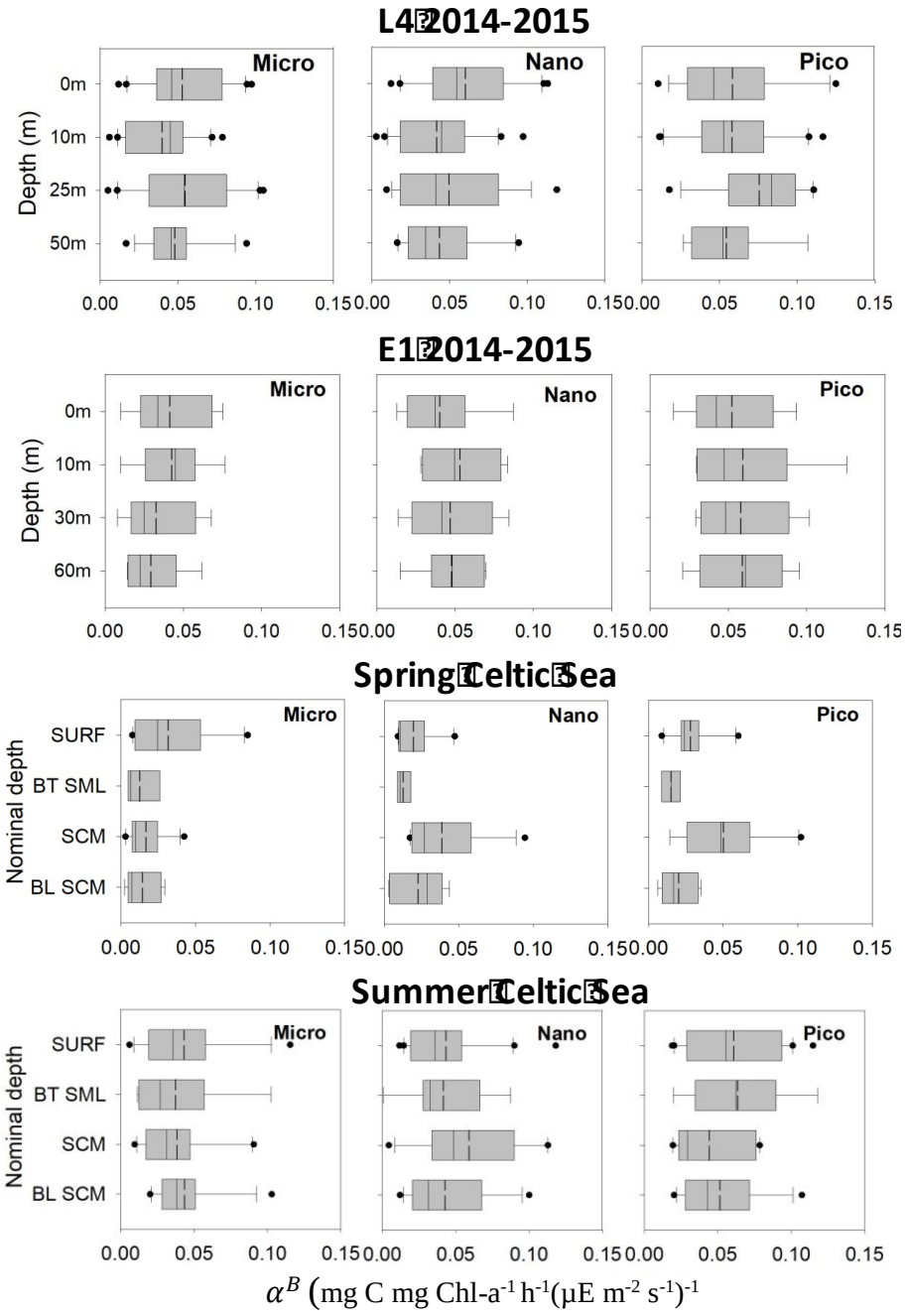


Fig 2.14 Boxplots of size-fractionated measurements α^B at each sampling depth taken during 2014 and 2015 at Western English Channel stations L4 & E1, and at each nominal depth during Celtic Sea cruises.

Mean α^B values for the summer followed a similar pattern to that observed for P_m^B for pico- and microphytoplankton with higher values at the surface and SCM. Nanophytoplankon appear to have exhibited similar mean rates at the surface and below the SCM, though the median value below the SCM was higher than 75% of surface observations. Values are generally lower and less variable for the summer samples compared with the spring. Mean

α^B values for the spring were similar across nominal depths, but exhibited high variability, as observed with chlorophyll and P_m^B datasets. For the spring, mean α^B is constant across all nominal depths for micro- and nanophytoplankton except at the SCM where nanophytoplankton had higher mean values. Mean values for picophytoplankton were less consistent between the surface and bottom of the surface mixed layer while the SCM and BL SCM depths exhibited lower α^B values. Low α^B values at the surface can be explained by the community having adequate PAR levels and, for most of April, adequate nutrients, reducing the requirement for light efficiency. At the bottom of surface mixed layer samples had increased α^B values relative to surface samples; it can be assumed that this is a product of acclimation to lower PAR levels than surface communities whilst still having access to adequate nutrients for most of the spring bloom period. SCM communities would be expected to have greater α^B values given they exist in a compromise between light and nutrients, driving them to be efficient photosythesisers with limited PAR, as in summer conditions. However, the spring and summer SCM communities sampled on the cruises have similar αB values and therefore BT SML communities having higher α^B may be due to the short-lived period of high nutrient, moderate light conditions at the beginning of the spring bloom before these communities become nutrient depleted.

Table 2.2 Size-fractionated chlorophyll concentrations (B) and photo-physiological parameter values with ± one standard deviation measured at the WCO sites. (sf) = size-fractionated and (t) = total community measurements for historical data.

L4 2014 - 2015	Total	Micro	Nano	Pico	n
B	1.39 ± 0.99	0.75 ± 0.65	0.48 ± 0.60	0.16 ± 0.14	95
P_m^B	4.86 ± 2.53	3.86 ± 2.37	4.21 ± 2.72	4.71 ± 3.0	88
α^B	0.054 ± 0.023	0.048 ±0.023	0.052 ± 0.027	0.064 ± 0.030	88
E_k	92.3 ± 53.6	90.6 ± 53.9	79.4 ± 42.9	74.7 ± 40.7	88
E1 2014 - 2015	**Total**	**Micro**	**Nano**	**Pico**	**n**
B	0.40 ± 0.43	0.32 ± 0.24	0.14 ± 0.09	0.86 ± 0.57	33
P_m^B	4.17 ± 2.36	3.64 ± 2.16	3.79 ± 2.41	6.0 ± 3.23	33
α^B	0.047 ± 0.023	0.042 ± 0.026	0.045 ± 0.025	0.058 ± 0.028	33
E_k	91.9 ± 41.9	94.0 ± 62.48	90.6 ± 35.1	91.7 ± 62.9	33
L4 2009 - 2011	**Total**	**Micro**	**Nano**	**Pico**	**n**
B	1.06 ± 1.36	1.09 ± 1.26	0.38 ± 0.36	0.08 ± 0.06	85 (sf) 341 (t)
P_m^B	4.16 ± 2.27	4.73 ± 2.94	5.94 ± 6.41	9.87 ± 6.17	85 (sf) 341 (t)
α^B	0.014 ± 0.01	0.015 ± 0.009	0.019 ± 0.016	0.044 ± 0.035	85 (sf) 341 (t)
E_k	382.9 ± 243.3	408.8 ± 301.1	335.7 ± 260.3	314.7 ± 247.4	85 (sf) 341 (t)

Table 2.2 details the differences in chlorophyll concentration and *PE* parameters measured during this study and from the historical dataset used to produce climatologies of *PE* parameters (Fig 2.8), and test the relationship of abiotic and taxonomic variables with these parameters (Fig 2.15, 2.16, Tables 2.5, 2.6). It can be seen that mean values of P_m^B and α^B are highest for picophytoplankton and lowest for microphytoplankton. Values of E_K measured 2009-2011 are higher than measured in this study owing to the higher P_m^B and lower α^B values reported by Barnes et al. (2015). This dataset was subject to the same QC of values measured I this study, however, so a number of questionably high P_m^B and α^B values were removed that were present in the original analyses of Barnes et al. (2015).

2.3.7 Statistical analyses

The preceding sections have provided detail on the variability of abiotic variables and the S-F biomass and photophysiology, and taxonomic composition of the phytoplankton communities of the Western English Channel and Celtic Sea. As different physiochemical variable may affect size classes or taxonomic groups of phytoplankton to a different degree, multivariate statistics were employed to elucidate any potential relationships between abiotic and biotic parameters and variables by using Principal Component Analysis (PCA).

2.3.7.1 Principal component analyses (PCA)

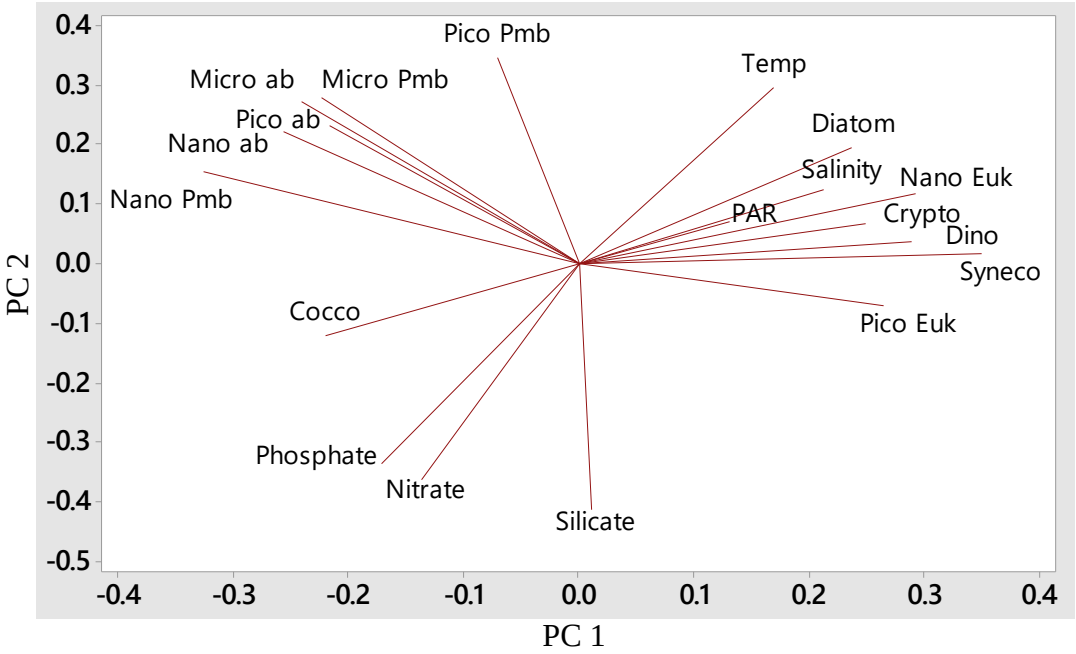


Fig 2.16 Principal components loading plot for abiotic variables, taxon-specific cell carbon concentrations and photosynthetic parameters for L4 and April 2015 Celtic Sea cruise data (no cell carbon data available for August 2014 cruise). Pmb and ab denote P_m^B and α^Brespectively.

A multivariate analysis by means of PCA was conducted on all coincident datasets of taxon-specific cell carbon, photo-physiology and abiotic parameters to ascertain any relationships between *PE* parameters and environmental co-variables. Four components were considered significant with Eigenvalues over 1.0, with the first two components accounting for 63% of the total variability in the mixed dataset from L4 and DY029 where cell carbon, photo-

physiology and abiotic variables were available. PC1 separates phytoplankton taxa carbon counts into essentially coccolithophores (negative loading) and the other taxa plus temperature, salinity and PAR (positive loading). *PE* parameters appear to be associated with both PC1 (negatively) and PC2 (positively) to a similar degree, with picophytoplankton P_m^B values being an outlier, with only slight (-0.07) negative loading with respect to PC1. Nutrients have strong negative loading with PC2 and with nitrate and phosphate have also having negative loading with PC1. Silicate had a very slight positive loading with PC1 (0.01) and the greatest loading with respect to PC2 of any variable or parameter (-0.41).

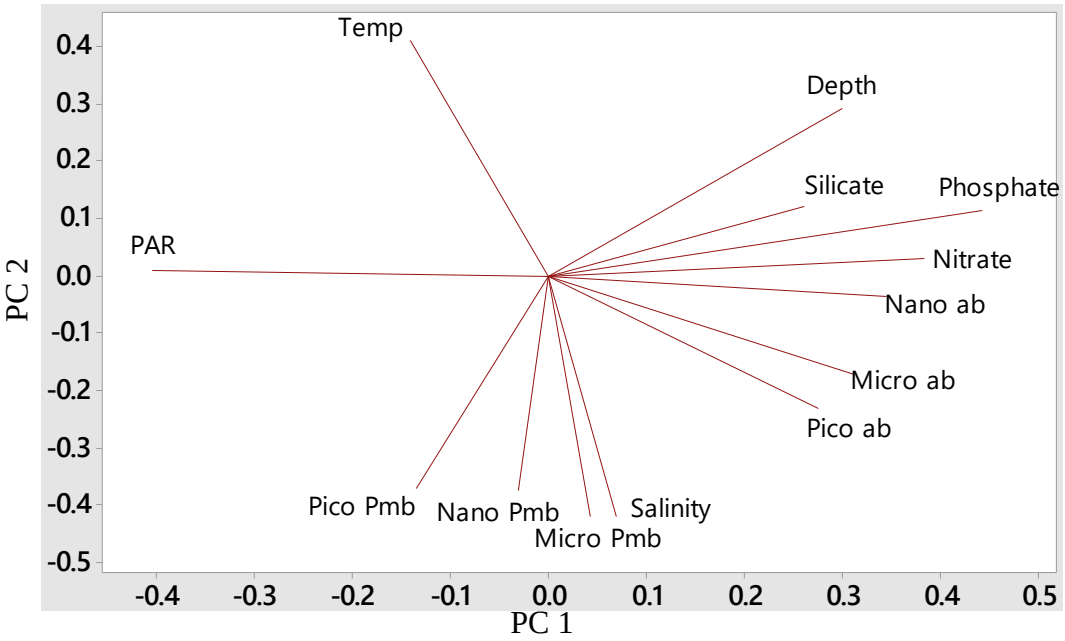


Fig 2.17 Principal components loading plot for abiotic variables and photosynthetic parameters for L4 and Celtic Sea data. Pmb and ab denote P_m^B and α^B respectively

An analysis of abiotic variables produced for significant components with eigenvalues greater than 1.0. The first 2 components of the analysis accounted for 48% of the variability in abiotic variables with PC1 having strong positive loading from phosphate (0.44), nitrate (0.38) and nanophytoplankton α^B (0.35) and negative loading from PAR (-0.40). All nutrients, α^B and depth were positively loaded with respect to PC1. Though nutrient levels were consistently higher at greater depth, this was only observed for α^B values at 25m (L4)

and at the SCM (DY026) (Fig. 15), therefore PC1 is likely to be related to light intensity more strongly than depth given the limited loading of PAR with PC2 (0.01) and its string negative loading with PC1. PC2 separates maximum photosynthetic rates (0.42, -0.38, -0.37 for micro-, nano- and picophytoplankton respectively) and salinity (-0.42) and temperature (0.41).

2.3.7.1 Relationships of photophysiological parameters with physical variables

Phytoplankton PE parameters have been observed to be closely correlated or constrained by environmental conditions, to the extent that in some situations, certain variables such as temperature and light may be used to predict values of P_m^B and α^B (Bouman et al. 2005; Bouman et al. 2010; Geider et al. 1997; Harrison and Platt 1980; Kulk et al. 2012; Robinson et al. 2018; Xie et al. 2015). Despite the obvious variability in these measurements of shelf-sea size-fractionated photophysiology (Figs 2.13-2.15, Table 2.2) it is therefore worthwhile to establish whether physical variables show any predictive power for PE parameters as these relationships can be used to inform the parameterisation of PP models.(Field et al. 1998; Geider et al. 1998).Following the PCA, relationships of P_m^B and α^B with temperature, salinity and downwelling PAR were investigated though regression using quadratic functions to fit modelled relationships across the range of variable and parameter values observed in the L4 and cruise datasets (Table 2.3).

Table 2.3. Results of quadratic regression fit between physical variables (Temperature, Salinity and Photosynthetically Available Radiation) and *PE* parameters P_m^B and α^B for L4 data (2009-2015) and both Celtic Sea cruises showing p value, F value and degrees of freedom (DF).

	P_m^B			α^B		
Temp.	p	F	DF	p	F	DF
Micro	0.2	1.62	224	0.017	4.18	213
Nano	0.28	1.27	220	0	9.75	210
Pico	0.05	3.05	206	0.012	4.52	198
Salinity						
Micro	0.001	7.11	220	0.003	5.91	209
Nano	0.465	0.77	215	0	21.55	206
Pico	0	8.75	201	0	36.91	195
PAR						
Micro	0.204	1.61	162	0.432	0.84	154
Nano	0.834	0.18	157	0.034	3.47	155
Pico	0.592	0.53	149	0.116	2.18	146

Temperature and salinity were significantly correlated with α^B for all size fractions, with PAR also showing a significant relationship with α^B for the picophytoplankton fraction. P_m^B values showed no significant correlation with PAR for any size fraction, In addition, multiple stepwise linear regression was used to investigate how much variability in the size-fractionated values of P_m^B and α^B could be explained by these abiotic variables (Table 2.4). Temperature and salinity were significant predictors of micro and picpophytoplankton P_m^B, though with low coefficients of determination. No variable was a significant predictor of nanophytoplankton P_m^B at the 5% level. Salinity was a significant predictor of α^B for each size class, with higher coefficients of determination for nano- and picophytoplankton than microphytoplankton. Depth-specific PAR was a significant predictor of nanophytoplankton α^B, which temperature was not a significant predictor for any size fraction at the 5% level.

Table 2.4 Results of multiple stepwise linear regression between all physical variables and PE parameters P_m^B and α^B for L4 data (2009-2015) and both Celtic Sea cruises showing coefficient of determination (r^2) correlation coefficients and associated standard error (SE), p value, F value and degrees of freedom (DF).

P_m^B			
Micro	Coefficients ± SE	F	p
r^2=9.87, DF = 145			
Temperature	-0.166 ± 0.075	4.88	0.029
Salinity	-3.017 ± 0.974	9.6	0.002
Salinity	-1.58 ± 1.15	1.89	0.171
Pico			
r^2=15.9, DF = 135			
Temperature	-0.389 ± 0.119	10.71	0.001
Salinity	-5.85 ± 1.59	13.47	0.000
α^B			
Micro	Coefficients ± SE	F	p
r^2=12.57, DF = 137			
Temperature	0.0012 ± 7.85x10^{-4}	2.35	0.128
Salinity	0.0091 ± 0.0099	17.95	0.000
Nano			
r^2=28.19, DF = 137			
Salinity	0.08 ± 0.0116	26.49	0.000
PAR	-3.6x10^{-5} ± 1.5x10^{-5}	48.09	0.018
Pico			
r^2=32.5, DF = 129			
Salinity	-0.994 ± 0.0127	61.63	0.000

2.3.8 Variability in modelled size-fractionated primary production

By collecting size-fractionated measurements of phytoplankton chlorophyll concentrations (B_i), photosynthetic parameters (P_m^B and α^B) which describe the fixation of carbon per unit irradiance, and cellular spectral light absorption properties per unit chlorophyll (a_{ph}^*), it is possible to estimate carbon fixation at a given level of phytoplankton-useable irradiance (E_{PUR}) (eq 2.6). Such estimates, when integrated through the euophotc zone allow comparison of the productivity of different size fractions are each sampling date and station,

and may be considered representative when information of the daily irradiance levels are used to generate the water column light field (section 2.2.6).

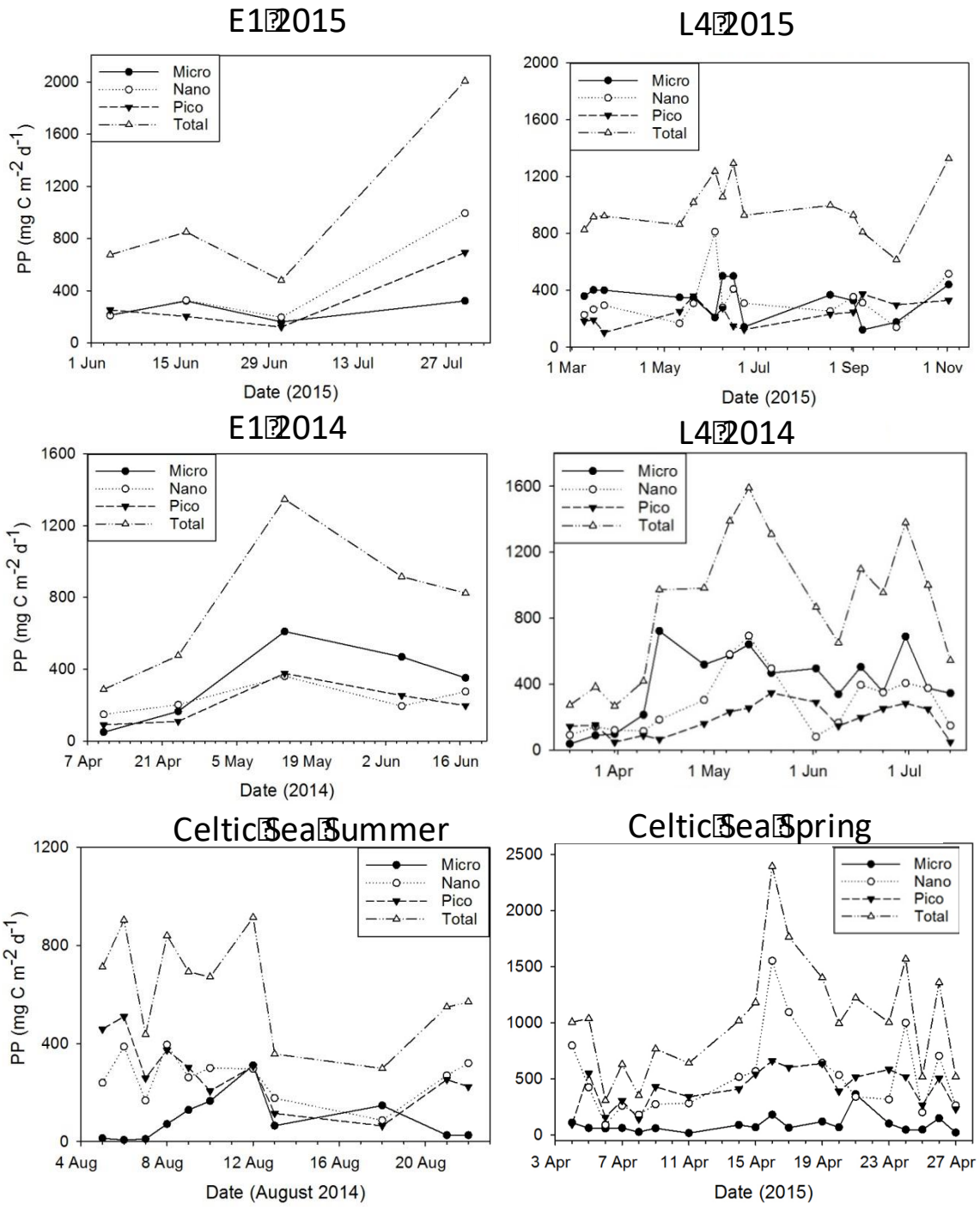


Fig 2.18. Time series of size-fractionated primary production using *in situ* measurements of biomass and the *PE* parameters with the primary production model of Tilstone et al. (2003).

Measurements of size-fractionated chlorophyll PE parameters and absorption spectra taken at WCO stations and Celtic Sea sites allowed the estimation of S-F PP using the model of Tilstone et al. (2003). These estimates give an indication of the differences in PP at each site at different times of the year for each size fraction, and provides insight into the differences between the primary production dynamics of each location.

The greatest value for integrated production was observed between 16 and 17th April when chlorophyll values were consistently between 2.0 and 3.1 mg m^{-3} in the surface mixed layer, with high surface irradiances. Lower maximum productivity rates for the Celtic Sea were observed in August 2014. Sampling at station L4 did not continue into the early autumn bloom of 2014 but was observed in 2015 where the succession of micro-, nano- and then picophytoplankton was observed, before a larger bloom of micro- and nanophytoplankton in early November (chlorophyll values of 2.81 mg m^{-3} at 0 m and 2.40 mg m^{-3} at 10 m). This period also saw a sustained level of picophytoplankton production 350 - 380 mg C m^{-2} d^{-1} due to high densities of active *Synechococcus* and picoeukaryotes. A large bloom of *Noctiluca scintilans* occurred in September 2015, though this heterotrophic species does not feature in estimates of photosynthetic production.

At station L4 in 2014, variability was highest for micro followed by nanophytoplankton, with the inverse true for 2015. In both years picophytoplankton primary production was less variable than larger fractions and generally accounted for the lowest component of the primary production due to its lower biomass, never being responsible for >0.4 g C m^{-2} d^{-1}. 2014 at L4 saw the typical microphytoplankton-dominated spring bloom associated with a coastal temperate shelf sea, and though the cruise sampling during April meant this period is missed in 2015, a later period of the bloom is captured with increased nanophytoplankton production, as seen April to June 2014.

Station E1 was sampled less frequently and as a consequence has lower resolution of changes in size-fractionated primary production. However, two distinct periods of enhanced production are observed in May 2014 predominantly due to microphytoplankton, and 30th July 2015 which was predominantly due to nanophytoplankton with a significant contribution by picophytoplankton. The sample of July 30th 2015 does appear erroneously high for mid-summer, however, P_m^B and α^B values were moderate for all size classes respectively, chlorophyll values were moderate at 0.9 mg m^{-3} at 0m, 2.2 mg m^{-3} at 10 m, and surface irradiances were especially high, with values of 800 µE m^{-1} s^{-2} at 2 m and 300 µE m^{-1} s^{-2} at 8 m. Cruise DY026 sampled the strongly-stratified Celtic Sea in August 2014, though despite lower nutrient levels in the surface mixed layer, high PAR levels (~2000 - 2300 µE m^{-2} s^{-1}) at the surface) coupled with a substantial subsurface chlorophyll maximum sustained high production levels. Peaks in production were generally associated with microphytoplankton, specifically large dinoflagellates within the SCM. The stations with the lowest microphytoplankton production were typically off-shelf or shelf break stations where nano- and picophytoplankton were responsible for the majority of production. Productivity of each size class was generally more strongly coupled at on-shelf sites than off-shelf sites.

DY029 sampled the onset of stratification and spring bloom during April 2015. Though there is considerable patchiness in the bloom characteristics of the Celtic Sea, most sites sampled during bloom conditions showed a dominance of nanophytoplankton, converse to the expected spring diatom blooms associated with temperate shelf seas. Though large centric diatoms such as *Coscinodiscus* were observed, microphytoplankton biomass was consistently low, producing > 0.5 g C m^{-2} d^{-1} at only 2 stations. Picophytoplankton chlorophyll concentration sampled during the Celtic Sea cruise of April 2015 was consistently high relative to concentrations found in L4samples and the August 2014 Celtic

Sea summer cruise, with high densities of picoeukaryotes and *Synechococcus* at later stations. A large coccolithophore bloom was observed at one mid-shelf station, though this did not correspond to a peak in PP.

Though the PP estimates presented in this chapter are high for an open shelf sea when compared with previous studies (Table 2.6), these high productivity rates are reflected in the high chlorophyll concentrations which often fell between 4 and 9 mg m^{-3}. Overall, these estimates indicate a productive shelf sea environment with considerable spatial and temporal heterogeneity in primary production – quite dissimilar to most open-ocean regions which are often used to tune global models of phytoplankton dynamics.

2.7 Discussion

2.7.1 Differences in photo-physiology between size fractions in shelf seas

The results of *in situ* measurements of phytoplankton photophysiology indicate that micro- and nanophytoplankton P_m^B and α^B values are broadly similar with average nanophytoplankton values being higher, while the values of picophytoplankton are significantly higher than the values of the larger fractions (Fig 2.2, Table 2.5).

These observations of photosynthetic rates with phytoplankton size are consistent with previous studies in UK shelf seas (Table 2.5), with similar relationships of *PE* parameters with size observed in other regions (Malone and Neale 1981) .

In addition to photosynthetic rates of phytoplankton, the differences in specific absorption spectra indicated that picophytoplankton are more efficient absorbers of visible light per mg of chlorophyll (Fig 2.15). This result is consistent with previous studies of culture and

natural populations, whereby increasing cell size results in decreased efficiency of light absorption, a product of cell pigment suite and the packaging of photosynthetic and photoprotective pigments within the cell (Bricaud et al. 2004; Ciotti et al. 2002; Devred et al. 2006; Duysens 1956; Fujiki and Taguchi 2002).

Table 2.5 Mean size-fractionated photo-physiological parameters measured bring this study and other shelf sea studies. Range of values indicated in parentheses (min - max), (NA) denotes data not reported by Segura et al (2013).

Reference	**Region**	**Pore Size (µm)**	**P_m^B (mg C mg Chl-a^{-1} h^{-1})**	**α^B (mg C mg Chl-a^{-1} h^{-1}(µE m^{-2} s^{-1})$^{-1}$)**	**E_k (µE m^{-2} s^{-1})**
This study n=120	Western English Channel	Micro >20	3.92 (0.42 – 13.24)	0.054 (0.007 – 0.180)	110 (15.8 – 395)
		Nano 2 – 20	4.35 (0.69 – 12.28)	0.055 (0.006 – 0.188)	103 (16.2 – 310)
		Pico 0.2 - 2	5.13 (0.23 – 13.85)	0.072 (0.01 – 0.192)	106 (26.4 – 511)
This Study n=83	Celtic Sea	Micro >20	2.51 (0.37 – 6.64)	0.036 (0.004 - 0.106)	90.5 (22.8- 367)
		Nano 2 – 20	3.00 (0.03 – 9.11)	0.0407 (0.0007 – 0.136)	91.8 (20.1 – 315)
		Pico 0.2 - 2	3.69 (0.61 – 13.14)	0.0495 (0.008 – 0.207)	92.8 (31.8 – 246.1)
deMadariaga and Joint (1994) n=11	Celtic Sea	Micro >5	3.44 (1.75 – 8.26)	0.013 (0.007 – 0.033)	257 (195 – 390)
		Nano 1 – 5	4.10 (1.80 – 9.58)	0.024 (0.009 – 0.043)	184 (103 – 300)
		Pico 0.2 – 1	8.49 (3.84 – 17.22)	0.219 (0.044 – 0.68)	105 (19 - 236)
Barnes et al (2014) n=87	Western English Channel	Micro >10	4.15 (1.06 - 17.38)	0.015 (0.002-0.049)	332 (84-2186)
		Nano 2 – 10	4.10 (0.44 – 26.10)	0.019 (0.001 – 0.092)	259 (44 – 1569)
		Pico 0.2 - 2	8.09 (1.66 – 24.55)	0.044 (0.004 – 0.223)	278 (13 – 1163)
Segura et al. (2013) n=70	Argentine Sea	Micro >5	3.17 (NA)	0.15 (NA)	(NA)
		Nano+ Pico <5	2.40 (NA)	0.19 (NA)	
Moran & Sharek (2015) n=11	Bay of Biscay	Nano+Micro >2	3.62 (1.98-5.60)	0.024 (0.003 - 0.026)	179 (98 – 291)
		Pico 0.2 - 2	5.41 (0.88-7.17)	0.031 (0.002 – 0.052	282 (104 – 572)

Table 2.5 shows a number of previous measurements of size-fractionated *PE* parameters from shelf regions alongside the measurements of this study. Great variability is evident in α^B values and to a lesser extent P_m^B in each of these shelf regions. Values for 2014-2015 sit within previous measurements, though average α^B values for micro- and nanophytoplankton are higher than each previous dataset other than Segura et al. (2013). P_m^B values for the Celtic Sea and WCO follow a similar pattern as observed by de Madariaga and Joint (1994), with picophytoplankton having the highest P_m^B values by a significant margin and microphytoplankton having the lowest values.

Average light saturation parameter (E_k) values measured during 2014-2015 at the WCO and in the Celtic Sea exhibited little variation between sizes, with Celtic Sea values typically ~12% higher. There is considerable variability in E_k values for each individual fraction such that no significant difference is observed between size fractions in the individual 2014 - 2015 and combined datasets (Table 2.5). The average values of E_k from this study (2014-2015) were lower than other previous measurements; maximum values were consistent with de Madariaga and Joint (1994) and Morán and Scharek (2015) but lower than Barnes et al. (2014) (Table 2.5). The difference in E_k values measured at L4 between the 2009-2011 and 2014-2015 datasets is principally due to higher α^B values measured during 2014-2015 and to some extent lower P_m^B values for picophytoplankton (Table 2.2).

2.7.2 Seasonal and regional variability in phytoplankton biomass and photo-physiology

Average P_m^B and α^B values and chlorophyll concentrations were higher for all fractions in the Western Channel than measured in the Celtic Sea (Table 2.5, Fig 2.14, 2.15), consistent with higher nutrient loads (Fig 2.4, 2.5). Interannual variability in chlorophyll concentration was greater at station L4 where spring bloom peak values varied between ~3.8 – 11 mg m^{-3}

and often exhibited secondary peaks later in spring or in late summer, whereas at the central Celtic Sea values varied between 1.5 – 3 mg m^{-3}, with less pronounced late summer/autumn blooms and more regular timing of peak chlorophyll biomass between years (Fig 2.19). For Celtic Sea data, significant differences in photophysiology between nominal depths were only observed for nano- and picophytoplankton during the summer at the SCM with respect to the surface mixed layer (Figs 2.14, 2.15).

The results of the principal components analysis (PCA) (Fig 2.16, 2.17) indicates a negative relationship between α^B and PAR as might be expected as α^B values are affected by photoacclimation processes, however this relationship was only significant for nanophytoplankton (Tables 2.3, 2.4). Instead, salinity is the physical variable which best explains variability in α^B, despite the PCA indicating that salinity was more strongly associated with P_m^B. This result may be due to two factors. Measured α^B and P_m^B values were highest at L4, moderate at E1 and lowest in the Celtic Sea, i.e. increasing with decreasing salinity at more coastal sites. Salinity is indeed negatively associated with P_m^B for all size fractions, and α^B for nano- and picophytoplankton, but regression coefficients are positive for microphytoplankton α^B (Table 2.4). Therefore the variation in P_m^B and α^B explained by salinity may relate to the vertical distribution of the community: whether measurements are from the surface mixed layer or below. This relationship would link with observations of *PE* parameters from the summer Celtic Sea cruise which show differences with nominal depths under a stratified water column, most strongly for P_m^B (Figs 2.14, 2.15). However, *PE* parameters do not appear to diverge by depth with respect to mixed or stratified conditions at L4 when comparing hydrography and climatologies of P_m^B and α^B (Figs 2.4, 2.5, 2.9). The covariance of salinity and photophysiology may therefore be both due to location e.g. low salinities at L4 consistent with eutrophic nutrient pools, high salinities in Celtic Sea with deeper, light-limited communities. Temperature was negatively associated with P_m^B for all

size fractions, significant to the 5% level for micro and picophytoplankton (Table 2.4), though this relationship is weak for all fractions, and is contrary to a number of previous studies showing positive correlation of P_m^B with temperature (Bouman et al. 2005; Harding Jr et al. 1986; Jassby and Platt 1976; Robinson et al. 2018; Xie et al. 2015). As this analysis incorporates data from two distinct shelf regions, differences in the covariance of nutrients, *PUR* and mixed layer depth, community structure of size fractions with the same temperatures at each site may weaken the relationships between *PE* parameters and temperature due to the influence of other variables. The influence of light environment, nutrient availability, temperature and mixing regime on photoacclimaton and photophysiology are not easily deconvolved in this dataset. In addition to the physicochemical and biotic variables used in this study, photophysiology and primary production may also be influenced by other variables distinct WCO and Celtic Sea datasets such as periodic iron stress in summer (Behrenfeld and Milligan 2013; Birchill et al. 2017), estuarine influence at coastal sites or differences in grazing and viral dynamics (Payet and Suttle 2008; Suttle and Chan 1994).

Though problematic, this situation is not unexpected given the evident variability in phytoplankton population dynamics and photophysiology. Even with a comparatively large dataset, the heterogeneous nature of the shelf sites sampled in this study means that considerable natural variation in observed biotic variables and parameters is to be expected, and thus larger datasets using the same methods and covering similar regions are required to constrain sources of variability in photosynthetic parameters over annual, rather than experimental timescales and at a number of spatial scales where datasets are large enough to allow general patterns to be established on smaller scales.

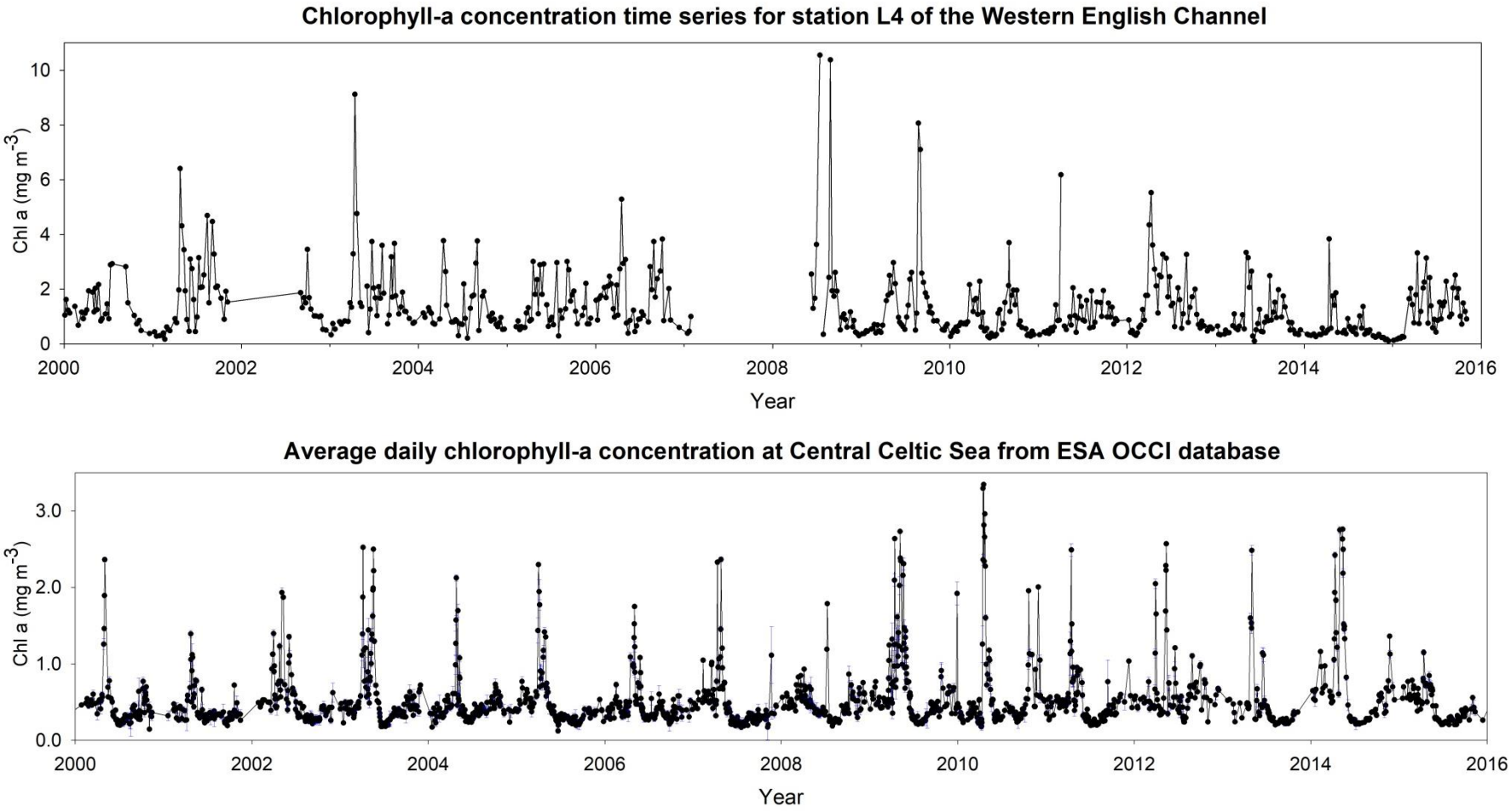


Fig 2.19 16 year time series of surface chlorophyll-a concentration measured at station L4 and from ESA OCCI v3.1 chlorophyll product (http://www.esa-oceancolour-cci.org/)

2.7.3 Seasonal and regional variability in Biomass and Primary production

The estimates of total daily integrated primary production obtained here are in agreement with those of previous studies in analogous shelf seas and exhibit significant variability with distinct maxima in productivity corresponding to phytoplankton blooms (Table 2.6) (Barnes et al. 2015; Hickman et al. 2012; Joint et al. 1986; Joint and Pomroy 1993; Joint et al. 2001; Robinson et al. 2009).

Table 2.6 Measurements of daily integrated primary production from previous studies in UK shelf seas.

Study	Location	Season	PP (mg C m^{-2} d^{-1})
Joint et al 1986	Celtic Sea	Summer	279 - 994
Joint & Pomroy 1993	Southern North Sea	All	<75 - >2400
Joint et al 2001	Goban Spur	Summer	456 – 1015
Robinson et al 2009	Celtic Sea	Summer	216 – 3372
Hickman et al 2012	Celtic Sea	Summer	174 – 386
Barnes et al 2015	Western Channel 2009 -2011	Spring Summer	103 - 1189 302 - 1816
This Study	Celtic Sea	Spring Summer	517 -2540 298 - 914
This Study	Western Channel 2014 -2015	Spring Summer	272 – 1589 542 - 1378

Microphytoplankton (diatoms) were observed to dominate spring bloom primary production during 2014 at L4 and E1 and from 10 - 23rd March and 20th May - 21st June 2015 at L4 excepting one sampling station where nanophytoplankton dominated production. Modelled microphytoplankton PP peaked at 74.3% of total during the spring bloom (Table 2.7).

Microphytoplankon production at L4 and E1 in March to June/July 2012 is consistent with the trend in diatom abundance observed by Widdicombe et al. (2010) in the western English Channel**.** As phytoflagellates are present in high abundances throughout the spring-summer period, nanophytoplankon primary production could be expected to have consistent background rate between bloom peaks when compared with microphytoplankton, indeed table 2.7 shows that the average contribution of nanophytoplankton to total PP is consistent between 2014 and 2015 (32.4% and 32.8% respectively). Compared with the estimates of Barnes et al. (2015), using and absorption-based model, with microphytoplankton accounting for 52% of PP, the values reported in table 2.7 show a reduced dominance of PP by microphytoplankton. Though 2015 PP values may have an anomalously low average microphytoplankton contribution to PP due to no sampling during April, it may be assumed to be a typical year with a bloom of *P. globosa* and *P. pouchetii* and smaller diatoms following high densities of larger diatoms (*C. walessii*) was sampled in March. Diatoms were the dominant phytoplankton taxon until June, consistent with the time series of Widdicombe et al. (2010). It could therefore be assumed that patterns in S-F PP of 2015 are typical, and that values measured for April would show increased micro PP from larger diatoms as they were restricted to surface waters and higher irradiances, with subsequent increased nanophytoplankton primary production whilst *Phaeocystis* was present.

Table.2.7 The contribution of individual size fractions to total community primary production at station L4 and Celtic Sea, expressed as percentage contribution.

L4 2014 PP	Micro	Nano	Pico
Average %	44.6	32.4	23.0
Min %	13.8	9.3	6.7
Max %	74.3	45.4	52.7
Std Dev	14.3	9.1	11.1
L4 2015 PP	**Micro**	**Nano**	**Pico**
Average %	33.8	32.8	25.5
Min %	15.1	19.5	11.2
Max %	47.4	65.7	48.5
Std Dev	10.5	10.7	11.1
DY029 PP	**Micro**	**Nano**	**Pico**
Average %	8.2	48.8	43.1
Min %	3.1	35.1	10.9
Max %	14.1	76.9	59.2
Std Dev	5.0	12.0	12.0
DY026 PP	**Micro**	**Nano**	**Pico**
Average %	16.2	44.3	44.4
Min %	0.75	29.1	21.5
Max %	49.4	58.3	64.4
Std Dev	15.2	9.6	13.2

Perhaps the most notable observation of the relative contribution of each size fraction to total PP is that picophytoplankton account for a quarter of PP through spring-summer, and may even dominate community primary production on occasion. This result appears contrary to previous observations and models which estimate primary production in eutrophic shelf regions as being dominated by microphytoplankton (Uitz et al, 2010) with picophytoplankton being responsible for comparatively little primary production and only dominating in warmer and nutrient-poor regions typical of more oligotrophic environments (Agawin et al. 2000; Iriarte and Purdie 1994; Marañón et al. 2001; Ning et al. 2000; Rousseaux and Gregg 2013). Some more recent studies have indicated that picophytoplankton may contribute a more significant proportion of phytoplankton biomass and primary production in estuarine, coastal and shelf regions at mid to high latitudes (Bonato et al. 2016; Gall and Zeldis 2011; Gaulke et al. 2010; Retamal et al. 2008; Tremblay et al. 2009). The high picophytoplankton primary production during stratified periods may be attributed to the efficiency of picophytoplankton in using diapycnal fluxes at the SCM owing to their small cell size and chlorophyll-specific photosynthetic efficiency (Falkowski et al. 1998). In the case of Celtic Sea samples, diapycnal nutrient fluxes into the surface mixed layer can be regionally heightened by internal tides and rough bathymetry, particularly near the shelf break (Green

et al. 2008; Hickman et al. 2012; Palmer et al. 2015; Sharples et al. 2009; Tweddle et al. 2013).

With picophytoplankton accounting for an average of 43% of primary production in the Celtic Sea during the spring bloom period, the lack of microphytoplankton biomass at sampled stations could be assumed to be the reason for smaller fractions being preponderant in subsequent PP estimates. While previous measurements of PP and community structure in the Celtic Sea indicate that the canonical pattern of microphytoplankton dominating the bloom is generally observed in this region (Dixon et al. 2006; Joint et al. 1986), picophytoplankton and small nanophytoplankton have been measured as being dominant producers in pre-bloom communities in the NE Atlantic (Joint et al. 1993) Celtic Sea (Rees et al. 1999) and coastal shelf regions (Kahru and No¨mmann 1990; Morán 2007). The biomass of nano- and picophytoplankton preceding and throughout the spring bloom is therefore presumably sufficient to exhaust stocks of nitrate and phosphate in the surface mixed layer (Fig 2.4, 2.5). The lack of active diatom biomass may be evidenced by the moderate concentrations of silicate at the Central Celtic Sea as late as May (Fig 2.6), however the low concentrations at the Celtic Deep (Fig 2.6 indicate that diatoms may have regional variation in productivity consistent with physical variability and not captured during repeat transects.

Compared to global or open-ocean observations and models of size-fractionated primary production (Brewin et al. 2017b; Huot et al. 2013; Li et al. 2011; Morán et al. 2004; Uitz et al. 2008) this study indicates a converse trend in UK shelf waters, with *PE* parameters of picophytoplankton exhibiting significantly higher rates than larger fractions (Table 2.7). This has implications for modelling primary production and biogeochemistry in these regions. Increased picophytoplankton production relative to other classes means that carbon fixed in photosynthesis will be likely to have a different fate than microphytoplankton.

Within the context of the biological carbon pump (Falkowski et al. 1998) picophytoplanton cell carbon is more likely to be recycled through protist grazing and respiration than exported as zooplankton faecal matter or as aggregates of cell fragments as is the case for microphytoplankton (Burd and Jackson 2009; Falkowski et al. 1988; Giering et al. 2016; Henson et al. 2012), potentially sustaining nutrients pools and thus phytoplankton and heterotrophic bacteria through the recycling of nutrients (Azam et al. 1983; Malone et al. 1986).

Measurements of the *PE* parameters for the micro- and nanophytoplankton size fractions in UK Shelf seas are consistent with other shelf-sea and open-ocean environments (Table 2.7) (Uitz et al. 2008), suggesting these values are robust across a range of environmental settings. Targeted investigations on seasonal and vertical variability may be beneficial to refine estimates of size-fractionated PP. The *PE* parameters obtained in the UK Shelf Seas for the picophytoplankton size fraction differ substantially with previous open ocean studies, with shelf communities having much higher values of P_m^B and α^B(Table 2.5) (Brewin et al. 2017b; Uitz et al. 2008), which could reflect the physiological differences between the taxonomically diverse picoeukaryote and *Synechococcus* lineages that reside in shelf regions and the various *Prochlorococcus* ecotypes that dominate in the oligotrophic open ocean (Moore et al. 1998). One could argue that picophytoplankton is the phytoplankton size class which exhibits the largest variation in terms of its ecophysiology and taxonomy. Although the link between photosynthetic performance and picophytoplankton taxa are well established in subtropical gyres where these cells dominate, this study shows that there is also a growing need to understand picophytoplankton photophysiology in shelf sea and coastal environments. Studies which combine measurements of photosynthetic performance with detailed taxonomic information using molecular approaches (Rodríguez et al. 2005;

Schaum et al. 2013) could be of great benefit to our understanding and modelling of primary production in UK Shelf Seas.

The differences in photophysiology with generalised cell sizes are sensitive to bias with respect to the taxonomic composition of the phytoplankton community. For example, the pigmentation suite and the degree of pigment packaging, and therefore absorption spectrum, can vary substantially within a size class if the species composition changes (Ciotti et al. 2002), particularly for picophytoplankton where some taxa may synthesise high concentrations of various phycobiliproteins (Stuart et al. 1998). One example of this variability is the spring bloom of DY029, where a bloom of diatoms contained as much chlorophyll as a mixed community of dinoflagellates and phytoflagellates despite this bloom having an order of magnitude lower carbon biomass (Figs 2.10, 2.11). Measurements of the total community and size-fractionated photophysiology should therefore be accompanied by information on the community taxonomic composition and preferably pigmentation, to inform the interpretation of parameter values with respect to cellular physiology, pigmentation and photoacclimation (Cermeño et al. 2005; Falkowski et al. 1993; Fishwick et al. 2006; Marañón 2007).

2.8 Conclusions

The *PE* parameters of micro-, nano- and picophytoplankton are highly variable in UK Shelf Seas and this is reflected in their integrated rates of primary production. In this study, coastal WCO sites were characterised by higher chlorophyll concentrations and productivity rates which coincides with enhanced nutrient availability. The effect of individual physico-chemical variables on the *PE* parameters could not be easily distinguished using simple correlation or multivariate analyses for the UK Shelf Sea dataset. To estimate size-fractionated photophysiological parameters with respect to ocean observables (SST, salinity, daily PAR) two approaches may be used: to conduct a greater number of *in situ* observations for each size fraction that covers a wide range of oceanographic conditions, or use a much more extensive shelf-sea dataset with *PE* data from the entire phytoplankton community and information on single and combined variable effects taken from controlled phytoplankton culture studies (Fujiki and Taguchi 2002; Sathyendranath et al. 1987). The measurements presented in this chapter indicate that picophytoplankton values of α^B, P_m^B and a_{ph}^* were significantly higher than for larger size fractions and consequently fixed more carbon per unit chlorophyll and up to 64% of daily integrated PP.

The absorption data collected in this study revealed that picophytoplankton can absorb more photosynthetically-active radiation per chlorophyll molecule than larger cells, consistent with previous bio-optical studies (Fig 3.14). Microphytoplankton specific-absorption coefficients were highly variable (a_{ph}^* (443) ranged from < 0.002 - 0.07 m^2 (mg Chl-a^{-1})), which may be attributed to methodological difficulties in separating microphytoplankton absorption from total absorption when microphytoplankton biomass was low, with most reliable spectral data coming from the SCM, skewing the values towards these spectrally-diverse optical niches (Stomp et al. 2004). Nanophytoplankton chlorophyll-specific

absorption was less variable, with this intermediate fraction having lower absorption than picophytoplankton. Quantifying the differences in chlorophyll-specific absorption between size classes and throughout the water column is important for correctly modelling marine primary production; photoacclimation states of phytoplankton can vary considerably with depth, and whilst measurements of pigmentation may elucidate how cells have acclimated to their light environment, they do not provide a reliable basis for estimating the absorption properties of phytoplankton. In addition to differences due to phytoplankton size structure, this study found physical variables, particularly salinity, to be strongly correlated with differences in values of α^B.

Observations of the PP of micro- and nanophytoplankton were more consistent with previous literature, showing little significant variation throughout the water column other than samples collected near the SCM during summer, which had higher PP rates than nutrient-limited surface communities, such that they contributed significantly to integrated production, even with much less ambient PAR. This observation of the importance of SCM communities in stratified shelf waters is consistent with those of Hickman et al. (2012) .Microphytoplankton PP dominated total production during the spring-summer months at L4 (reduced in 2015 due to the spring bloom not being extensively sampled), whereas nano- and picophytoplankton co-dominated during the same period during both Celtic Sea cruises. Whilst nanophytoplankton are often considered to be responsible for the bulk of yearly PP in many shelf and open ocean environments (Boney 1986; Froneman et al. 2001; Tilstone et al. 1999; Uitz et al. 2010; Uitz et al. 2012), in the Celtic Sea picophytoplankton exhibited similar and often higher levels of PP. These unexpected results are explained by the aforementioned higher photosynthetic rates and considerably higher chlorophyll-specific absorption of picophytoplankton, such that despite constituting 32 to 36 % of the chlorophyll concentration on average, they are responsible for 44 % of the primary production.

Using physical separation of the phytoplankton community when making photophysiological measurements, such as by pre-filtration, is beneficial to the parameterisation of spectral primary production models given the differences in specific absorption properties observed in this study and from previous measurements of cultures and mono-specific blooms. Of course, for most existing datasets, measured or derived size-fractionated absorption measurements are not available; taking these samples multiplies the effort required in measuring photophysiology, models of size-fractionated absorption are useful to fill data gaps and reduce biases in model output due to generalising absorption properties.

3 Estimating the light absorption properties of different size classes of phytoplankton for use in shelf sea primary production models

3.1 Introduction

Phytoplankton absorption properties are a key component of bio-optical models of primary production: used in combination with measurements of phytoplankton photosynthetic response and biomass (chlorophyll concentration), they allow the estimation of carbon fixation per mg of chlorophyll per unit time (mg C mg Chl^{-1} h^{-1}) under a measured or modelled light field. Information on the spectral shape of phytoplankton light absorption is also necessary to correct values of α^B for the emission spectrum of the artificial light source (e.g. halogen lamps or LEDs) used in *PE* experiments (Chapter 1, Equation 2). In addition to the importance of the spectral shape of phytoplankton absorption, the magnitude of chlorophyll-specific absorption (a^*_{ph}) is required to calculate the maximum quantum yield of photosynthesis (φ_{max}). Quantification of magnitude and shape of $a^*_{ph}(\lambda)$ is also required to estimate the attenuation of downwelling spectral irradiance ($E(\lambda)$), known as K_d (m^{-1}), which is a function of phytoplankton absorption.

As the spectral shape and magnitudes of a^*_{ph} may vary between taxa, depths, regions and seasons (Fig 2.13), it is necessary to capture this variability to ensure accurate calculation of α^B and φ_{max} when modelling primary production using spectrally-resolved models that allow for regional differences in optical properties (Sathyendranath, Platt et al. 1989, Antoine and Morel 1996, Kyewalyanga, Platt et al. 1997, Tilstone, Figueiras et al. 2003). Although some sources of variability have been extensively investigated using measurements of total community absorption properties with respect to physical variables

and general community structure (Mitchell and Kiefer 1988, Bricaud, Babin et al. 1995, Ciotti, Lewis et al. 2002, Bouman, Platt et al. 2003, Uitz, Huot et al. 2008, Organelli, Nuccio et al. 2017). The time-consuming nature of separating the phytoplankton community biomass into size fractions using sequential vacuum filtration, size-fractionated measurements of a^*_{ph} are scarce. The absence of coincident measurements of size-fractionated $a_{ph}(\lambda)$ means that applying a spectral correction to size fractionated α^B values must be accomplished by either using estimated values or the measured phytoplankton absorption spectrum for the entire phytoplankton community ($a_{ph_{total}}(\lambda)$).

Size fractionated values of $a^*_{ph}(\lambda)$ can be derived from $a_{ph_{total}}(\lambda)$ if the average $a^*_{ph}(\lambda)$ for each size class is estimated. Typically such estimates are based on measurements of $a^*_{ph_{total}}(\lambda)$ when a specific size fraction dominates cell biomass. By adopting this approach, a^*_{ph} is assumed to be constant within a given size class: no allowance is made for changes in the shape and magnitude of $a^*_{ph}(\lambda)$ caused by variation in photoacclimatory state or shifts in taxonomic composition within each size class. This approach may lead to errors in derived α^B and φ_{max} values, particularly in regions which undergo significant seasonal shifts in hydrography and community structure as would be expected in the temperate shelf sea region of this study. A number of methods for estimating phytoplankton light absorption by different size fractions have been developed which approach the problem of estimating this important parameter in different ways. Although this study is not an exhaustive test of existing methods, a variety of approaches are tested and their accuracy in estimating *in situ* absorption is discussed.

3.1.1 Estimating size-fractionated light absorption from total measurements using diagnostic pigments

3.1.1 Estimating size-fractionated light absorption from phytoplankton pigments

To address the impact of variations in the underwater light field on the absorptive characteristics of different size fractions, Uitz et al (2008) used a large dataset (n= 2807) of phytoplankton pigments to infer community structure and size spectrum with coincident $a_{ph}(\lambda)$ measurements covering a range of open-ocean trophic conditions. Non-fractionated measurements of $a_{ph}(\lambda)$ were used to produce estimates of $a^*_{ph}(\lambda)$ for micro-, nano- and picophytoplankton size fractions using estimated size-fractionated chlorophyll from the concentration of diagnostic pigments (Vidussi et al. 2001) (Table 1.1). Mean surface size-fractionated $a^*_{ph}(\lambda)$ values were then used with corresponding slope values of the linear relationship between size-fractionated $a_{ph}(\lambda)$ and z/z_{eu} (hereafter ζ) at respective wavelengths to produce values of size-fractionated $a^*_{ph}(\lambda)$ at depth . The resultant changes in size-fractionated a^*_{ph} following relationships with respect to their position within the light field incorporates the effect of photoacclimation for each size fraction.

The measurements used in the Uitz, Huot et al. (2008) study were taken from mid-to-low latitude regions of the Atlantic, Pacific and Mediterranean and were predominantly collected from oligotrophic Case 1 oceanic waters. Yet these estimates of $a^*_{ph}(\lambda)$ have been used to produce global maps of size-fractionated primary production, covering a range of diverse water types, including oligotrophic, mesotrophic, and eutrophic regions including shelf and

coastal systems (Uitz et al. 2010). The relationship between a_{ph}^{*} and ζ requires rigorous validation in these diverse water types, especially in productive, nutrient-rich waters such as temperate shelf seas, since these regions may have a different and distinctive range in IOPs than is typical of oceanic waters (Platt and Sathyendranath 1988, Falkowski, Barber et al. 1998, Garaba, Voß et al. 2014, Mitchell and Cunningham 2015).

3.1.2 Estimating size-fractionated light absorption using pigment reconstruction

Photosynthetic and photoprotective pigments are present in varying concentrations within phytoplankton cells, with some pigments being almost exclusive to certain taxa such that they can be considered markers of community structure (e.g. peridinin in dinoflagellates, fucoxanthin in diatoms) (Vidussi et al. 2001). If the phytoplankton light absorption spectrum is not known, it can be reconstructed knowing *in situ* pigment concentrations along with the light absorption properties of individual pigments, which can be assumed to be fixed (a process known as 'pigment reconstruction') (Bidigare et al. 1990). Pigment reconstruction provides a means with which to estimate phytoplankton absorption in a consistent manner across any region where the information on the entire pigment complement is known. Where this method becomes problematic is allowing for the so-called packaging effect of pigments within the cell, and the interactions of accessory pigments which may augment the specific absorption of other pigments (in terms of spectral shape and magnitude) beyond simply their additive absorption (Duysens 1956). Through measures of phytoplankton absorption and pigment concentration the differences between packaged and unpackaged absorption spectra

can be investigated, but converting pigment-derived spectra to packaged values requires assumptions on cell geometry and photoacclimation (Morel and Bricaud 1981).

3.1.3 Estimating size-fractionated light absorption from ocean colour remote sensing data

With enough spectral resolution (sensor band number and width) remote sensing reflectance spectra (R_{rs}) contain information on the absorption properties of phytoplankton communities when biomass is high enough to provide sufficient signal to noise ratio. Phytoplankton functional types have been resolved by all ocean colour sensors, including CZCS (Blondeau-Patissier et al. 2014; Merico et al. 2003) but methods to discriminate multiple functional types began with SeaWifS (Ahn and Shanmugam 2006; Sathyendranath et al. 2004; Subramaniam et al. 2001). To produce contemporary products of phytoplankton functional type distributions, datasets from a number of operational satellite sensors can be used: MODIS-Aqua and Terra, OCM-2, OLCI and VIIRS (SNPP and JPSS-1).

In case 1 regions, where the optical signal covaries with Chl-a, it is possible to separate differences in taxonomy by assessing the spectral shape of the reflectance spectrum (Alvain et al. 2008) though the limited spectral resolution of most extant geosynchrous ocean-colour sensors makes differentiation of smaller variations(such as those reported by Ciotti et al (2002)) difficult to detect with confidence. Satellite observations of total phytoplankton absorption and chlorophyll biomass at the sea surface can be used to generate size-fractionated a_{ph} using a fixed $a^*_{ph}(\lambda)$ for each size class and empirical relationships of total and size-fractionated chlorophyll concentration (Brewin et al. 2011). In addition, Hirata, Aiken et al. (2008) used the spectral slope of remote sensing reflectances (after inversion to obtain absorption) $R_{rs}(443)/R_{rs}(510)$ and peak blue absorption $R_{rs}(443)$ to classify the dominant phytoplankton size class in natural communities (which is easier to quantify from

R_{rs} as most sensors cover these wavelengths for the production of chlorophyll products than more subtle changes in shape). However, much of the previous work on linking $R_{rs}(\lambda)$ with estimates of phytoplankton community structure and $a_{ph}(\lambda)$ has been focussed on open-ocean areas, and little work has been conducted in shelf and coastal regions One exception is the phytoplankton light absorption spectra derived by Varunan and Shanmugam (2015), who combined surface chlorophyll concentration estimates and spectral reflectances to provide size–fractionated estimates of $a_{ph}(\lambda)$, validated in productive oceanic (Arabian Sea, Gulf of Oman), shelf (Persian Gulf) and turbid coastal regions (Chennai, Point Calimere delta).

3.1.4 Estimating size-fractionated light absorption from dominant taxa

As the vast majority of measurements of phytoplankton absorption are made by concentrating marine particles onto glass fibre (GF/F) filters before being analysed by spectrophotometry (Kishino, Takahashi et al. 1985, Tassan and Ferrari 1995, Röttgers and Gehnke 2012), most historical datasets consist of absorption coefficients for the total phytoplankton community, $a_{ph_{total}}(\lambda)$. Where ancillary information on the phytoplankton taxonomy or size distribution is present, it is sometimes possible to deconvolve the absorption characteristics of individual sub-groups from the total community, where their biomass forms a significant part of the total phytoplankton standing stock at that sample depth. Although size-fractionation is increasingly common in measurements of chlorophyll concentration and photosynthesis-irradiance (*PE*) parameters, the most common means to determine dominant taxa are through the cell counts (microscopy or flow cytometry) as with Ciotti, Lewis et al. (2002), or phytoplankton diagnostic pigment analysis (Vidussi, Claustre

et al. 2001, Uitz, Huot et al. 2008) where specific pigments are indicative of phytoplankton functional groups.

Ciotti et al (2002) found that by classifying the phytoplankton community to one of four dominant size classes, more than 80% of the variance in $a_{ph}(\lambda)$ could be explained by cell size. Differences in spectral shape between size-classes could then be quantified by comparing normalised spectra of each of 16 sub-groups. Ultimately this allows the estimation of surface $a^*_{ph}(\lambda)$ for a range of size classes, with modification for the dominant taxon in each class. Although this approach of estimating size-class specific absorption properties does not include changes in photoacclimation state due to environmental forcing, changes in pigmentation, cell size and packaging effect are incorporated by the taxonomy and cell size groupings.

3.1.5 Measuring size-fractionated light absorption *in vivo*

By physically separating the phytoplankton community into individual size fractions by filtration before measuring their absorptive properties, it is possible to acquire absorption spectra for each size class within natural communities. Given the considerable differences in chlorophyll-specific absorption spectra measured from water samples dominated by small or large cells (Ciotti et al. 2002; Devred et al. 2006) even small changes in the relative abundances of the smallest or largest phytoplankton species within a mixed community may introduce a source of uncertainty as generalisations of the absorption properties of the dominant taxon may be substantially different when accompanied by mostly smaller or mostly larger cells, particularly if the species had extremely high or low specific absorption, or distinct pigmentation (Claustre et al. 2004; Ferreira et al. 2013; Fishwick et al. 2006; Lohrenz et al. 2003). Filtration allows the effects of cellular acclimation and changes in size

structure to be separated. This method provides important insight on how the absorption properties of individual size classes vary under different hydrographic conditions.

3.1.6 Objectives

There are a number of data gaps in the measurements of size-fractionated absorption taken during this study from the Celtic Sea and Western English Channel following quality control and due to the practical constraints of sampling and analysis of S-F measurements. In this chapter I aim to test a number of existing models of total and size-fractionated phytoplankton absorption in order to establish whether modelled spectra are sufficiently representative of shelf sea communities to fill gaps in measured datasets and provide photosynthetic parameters necessary in modelling PP.

This overall aim will be achieved through the following analyses:

1. Examine the viability of measured S-F and total a^*_{ph} spectra within and between fractions
2. Compare the differences in magnitude and spectral shape of $a^*_{ph}(\lambda)$ between measured values and four methods of estimating $a^*_{ph}(\lambda)$
3. By using modelled spectra in the primary production model of Tilstone et al (2005), test the effects of different spectra on estimates of integrated and depth-specific primary production.

3.2 Methods

3.2.1 Study area and sampling

For the WCO, water samples of size-fractionated fluorometric chlorophyll, $a_{ph_{total}}(\lambda)$, and phytoplankton accessory pigment concentrations were collected on board RV *Plymouth Quest* from the Western Channel Observatory (WCO) at station L4 at 0, 10, 25, and 50 m between March - July 2014 and March - November 2015 (Fig 2.3). Size-fractionated fluorometric chlorophyll and phytoplankton absorption spectra measurements were also taken from the Celtic Sea during August 2014 (DY026) and April 2015 (DY029) on board RRS *Discovery*, where up to four sampling depths were chosen based on CTD profiles of temperature, density, chlorophyll fluorescence and PAR.

At the WCO station L4, temperature, salinity, fluorescence and PAR were measured using a SeaBird SBE19+ SECAT CTD, Chelsea MINITracka II fluorometer and a 2-pi PAR sensor. During Celtic Sea cruises the same measurements were made by SeaBird SBE9+, Chelsea Aquatracka MKIII fluorometer and Biospherical QCP Cosine PAR sensor. For WCO samples, water samples were transported in insulated blacked-out carboys to Plymouth Marine Laboratory for analysis, whereas Celtic Sea water samples were processed immediately on board the research vessel.

3.2.2 Size-fractionated chlorophyll–a concentrations and phytoplankton light absorption

For each Chlorophyll sample, triplicate 200 ml samples of seawater were filtered through a Sartorius sequential filtration system onto 20 µm, 2.0 µm and 0.2 µm pore size 47 mm track-

etch polycarbonate filters (DHI). Each filter was then stored at -18°C for 18 hours in 10 ml 90% acetone (VWR) to extract chlorophyll-a as per Welschmeyer (1994). Extractions were then placed in glass vials and chlorophyll fluorescence measured using a Turner Designs Trilogy fluorometer calibrated with a chlorophyll-a spinach standard (Sigma). For Celtic Sea samples, a solid standard (Turner Designs) was used daily to check for instrument drift and calibrate subsequent measurements.

Phytoplankton absorption samples for both Celtic Sea cruises and the L4 time series were run to determine total particulate absorption coefficients ($a_{PART}(\lambda)$) and absorption due to non-algal particles ($a_{NAP}(\lambda)$) using the quantitative filter pad technique method of Kishino, Takahashi et al. (1985), using methanol solvent to extract phytoplankton pigments. All absorption samples were run on a Lambda 800 UV/VIS spectrophotometer (Perkin Elmer) calibrated with optical density filters at 5 wavelengths in the visible domain (440, 465, 546, 590, and 635 nm) (Hellma Worldwide). Phytoplankton absorption $a_{ph}(\lambda)$ was determined for each sample by substracting absorption of non-algal particles following methanol extraction ($a_{NAP}(\lambda)$) from the absorption of all particulates ($a_{PART}(\lambda)$) at each integer wavelength between 400 and 700 nm.

As the absorption properties of particulate material concentrated on filters will have a different optical density than in suspension within a volume of water (the pathlength amplification effect)(Mitchell 1990; Nelson et al. 1998) a correction is applied to measurements to ensure they reflect the absorption of particulate material in the water column. The measurements of this study use the method of Arbones et al. (1996), which show good performance when tested with 9 phytoplankton genera, to correct filter pad measurements of phytoplankton absorption.

Light absorption by microphytoplankton ($a_{ph_{micro}}(\lambda)$) was calculated by subtracting the absorption coefficients of samples pre-filtered through a 20 µm pore size, 47 mm diameter track-etched polycarbonate filter (DHI) from the total phytoplankton absorption spectra $a_{ph_{total}}(\lambda)$; absorption due to the presence of nanophytoplankton ($a_{ph_{nano}}(\lambda)$) was calculated by subtracting absorption measured samples filtered through a 20 µm filter from absorption that was filtered through a 2.0 µm filter (which represents picophytoplankton absorption ($a_{ph_{pico}}(\lambda)$) (equations 2.1, 2.2). Resulting spectra were quality controlled by only retaining spectra that had low noise, with no erroneous spikes, and that when normalised to chlorophyll ($a^*_{ph}(\lambda)$) that values were realistic. $a^*_{ph}(443)$ values of >0.08 m^{-1} for microphytoplankton and for nanophytoplankton and >0.1 m^{-1} for picophytoplankton were treated as being erroneous and those spectra discarded.

3.2.3 Estimation of size-fractionated light absorption from phytoplankton pigments (Uitz et al 2008)

The size-fractionated surface values of a^*_{ph} reported by Uitz et al. (2008) are presented with corresponding slope values which quantify how $a^*_{ph_i}(\lambda)$ values change through the water column with ζ for each size fraction. PAR (Z_{eu}) and CTD profiles (z) measured during both Celtic Sea cruises and WCO stations can therefore be used to calculate $a^*_{ph}(\lambda)$ spectra for each size class using the Uitz et al. (2008) model.

3.2.4 Estimation of light absorption by pigment reconstruction (Bidigare et al 1990)

Phytoplankton pigment concentrations measured using samples taken from a time series collected at station L4 (see Fig 2.3) were used to produce the total reconstructed absorption

spectra ($a_{rec}(\lambda)$) following the method of Bidigare, Ondrusek et al. (1990). The pigment groups used in the reconstruction method are chlorophylls a, b and c1+2, photoprotective carotenoids and photosynthetic cartenoids (PPC and PSC, respectively) (Fig 3.1). Values of unpackaged pigment-specific absorption coefficients ($a_i^*(\lambda)$) were scaled to values of *in situ* pigment concentrations (C_i) measured by high performance liquid chromatography (HPLC) and the summed to reconstruct the total unpackaged *in vivo* absorption spectrum ($a_{rec}(\lambda)$) (Equation 3.1):

$$a_{rec}(\lambda) = \sum a_i^*(\lambda) C_i, \tag{3.1}$$

where a_i^* is the specific absorption coefficient of pigment i at wavelength λ multiplied by its concentration C_i.

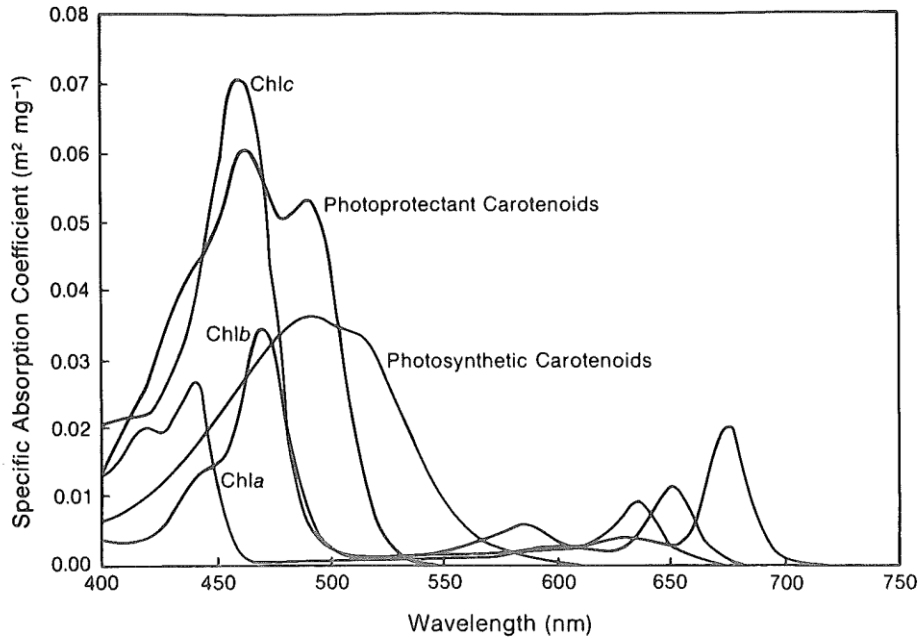


Fig 3.1 Specific absorption coefficients of phytoplankton pigments by Bidigare et al (1990) showing chlorophylls a, b and c, and the photoprotective and photosynthetic carotenoids.

For each reconstructed total absorption spectrum using the L4 pigment data ($a_{rec_{total}}(\lambda)$), measured s-f chlorophyll concentrations were used with the average values of $a_{ph}^*(\lambda)$ (taken from cruise samples) was used to calculate $a_{ph}^*(\lambda)$ for the nano and picophytoplankton size fractions. The spectra of Ciotti et al. (2002) were used for microphytoplankton due to the

lack of reliable measurements of microphytoplankton $a^*_{ph}(\lambda)$ in this study. The average $a^*_{ph}(\lambda)$ for the three size classes were then summed to give $a_{ph_{total}}(\lambda)$, the absorption spectra for the total phytoplankton assemblage.

For each sample and each wavelength, the percent contribution of each size fraction to measured $a_{ph_{total}}(\lambda)$ was calculated using S-F chlorophyll measurements and $a^*_{ph}(\lambda)$ spectra for each size class. This percentage value for each fraction was then used to re-scale the pigment-reconstructed value of $a_{rec_{total}}(\lambda)$ into estimates for microphytoplankton ($a_{ph_{micro}}(\lambda)$), nanophytoplankton ($a_{ph_{nano}}(\lambda)$) and picophytoplankton ($a_{ph_{pico}}(\lambda)$).This method uses a fixed value for $a^*_{ph}(\lambda)$ for each size fraction, which is representative of the average difference in spectral shapes between the size fractions.

$$(a_{ph_i}(\lambda)) = C_i(a^*_{ph_i}(\lambda)) \tag{3.2}$$

$$(a_{ph_{total}}(\lambda) = \sum(a_{ph_i}(\lambda)) \tag{3.3}$$

$$a_{ph_{ip}}(\lambda) = \left(\frac{a_{ph_i}(\lambda)}{a_{ph_{total}}(\lambda)}\right)100 \tag{3.4}$$

$$a_{rec_i}(\lambda) = (a_{rec_{total}}(\lambda))(a_{ph_{ip}}(\lambda)) \tag{3.5}$$

Where $a_{ph_{ip}}(\lambda)$ is the absorption of size fraction i at wavelengthλ, as a percentage of the total phytoplankton absorption, $C_i$is the chlorophyll concentration of size fraction i, $a^*_{ph_i}(\lambda)$ is the chlorophyll-specific absorption of size fraction i. The contribution of a size fraction to total absorption at a specific wavelength is given by $a_{ph_{ip}}(\lambda)$ which allows estimation of pigment-reconstructed size-fractionated absorption $a_{rec_i}(\lambda)$ from pigment-reconstructed total absorption $a_{rec_{total}}(\lambda)$.

3.2.5 Estimation of light absorption using ocean colour remote sensing data (Varunan and Shanmugam 2015)

The Varunan and Shanmugam (2015) method also makes use of a set of fixed $a^*_{ph}(\lambda)$ values for the three size classes to estimate $a_{ph}(\lambda)$. Estimates of the chlorophyll concentrations of each size class were derived from remote sensing reflectance

$$B_{(P)} = B^*_{(P)}[1 - \exp\left(-B^2\left(\max\left(R_{rs}(678), R_{rs}(748)\right)\right)\right)]^{S^P} \quad (3.6)$$

$$B_{(N)} = B^*_{(N)}[1 - \exp\left(-B^2\left(\max\left(R_{rs}(678), R_{rs}(748)\right)\right)\right)]^{S^N} \quad (3.7)$$

where B represents the chlorophyll concentration, B^* the concentration coefficients of individual size fractions as a proportion of total chlorophyll (B) , and S denotes the slopes values (the exponential increase in $B_{(P)}$ and $B_{(N)}$ with increasing B), with the subscripts P and N denoting to pico- and nanophytoplankton size fractions, respectively. Size-class specific $B^*$and S values were derived through regression analysis of the NOMAD dataset against *in situ* measurements of phytoplankton pigments used to produce size-fractionated chlorophyll estimates following Vidussi et al. (2001). The chlorophyll concentration of the microphytoplankton fraction (B_M) was calculated as the difference between the total chlorophyll-a concentration and the concentrations of the pico- and nanophytoplantkon fractions as follows:

$$B_{(M)} = B - \left(B_{(P)} + B_{(N)}\right) \quad (3.8)$$

R_{rs}(678) and R_{rs}(748) are incorporated into the equation of Varunan and Shanmugam (2015) to give more accurate estimates of pico- and nanoplankton chlorophyll concentration. Here, however, as chlorophyll for each size fraction was measured, the concentrations were multiplied by the average specific absorption values for each size class between 400 and 683

nm derived by Varunan and Shanmugam (2015), as shown in Table 2.5. The calculation of total and size-fractionated $a_{ph}(\lambda)$ is shown in equations 3.9-3.12.

$$a_{ph_{(M)}}(\lambda) = a^*_{ph_{(M)}}(\lambda)B_{(M)} \tag{3.9}$$

$$a_{ph_{(N)}}(\lambda) = a^*_{ph_{(N)}}B_{(N)} \tag{3.10}$$

$$a_{ph_{(P)}}(\lambda) = a^*_{ph_{(P)}}B_{(P)} \tag{3.11}$$

$$a_{ph_{total}}(\lambda) = a_{ph_{(M)}}(\lambda) + a_{ph_{(N)}}(\lambda) + a_{ph_{(P)}}(\lambda) \tag{3.12}$$

Where subscripts M, N and P denote micro- nano and picophytoplankton respectively.

The Varunan and Shanmugam (2015) dataset supplements a sample of NOMAD v1.3 data – from predominantly clear to semi-turbid waters – with a smaller dataset of measurements from turbid and productive coastal and lagoon waters, which may be better suited to estimating phytoplankton *in vivo* absorption spectra for the optically-complex WCO samples, despite these additional measurements being taken from a tropical latitude (10-12^{O}N).

3.2.6 Estimation of light absorption from dominant taxa (Ciotti et al 2002)

Ciotti et al (2002) used size-fractionated measurements of chlorophyll, combined with phytoplankton taxonomy and phytoplankton absorption data taken from the Bering Sea, Bedford Basin and Oregon coast to parameterise a taxon and cell size-based model of phytoplankton absorption. Phytoplankton communities were first classified according to dominant fraction (in terms of size-fractionated chlorophyll content), and then the dominant taxa within that fraction were characterised using light microscopy or flow cytometry into 1 of 16 groups. The shape of $a_{ph}(\lambda)$ was examined by normalising each spectrum to the

average phytoplankton absorption between 400 and 700 nm. Differences in spectral shapes of $a_{ph}(\lambda)$ were observed as the dominant size fraction within the phytoplankton community changed. In addition, there were small differences in spectral shape within size fractions because of changes in taxonomy. Average values for four size classes (micro-, nano-, ultra- and picophytoplantkon) were presented in their study, given that only minor changes in spectral shapes were observed for taxonomic groupings within size-fractions. To estimate size-fractionated absorption spectra using this method, taxonomic data gained from light microscopy were used to identify the closest match to one of 16 communities with the distinct spectra presented by Ciotti et al. (2002) for each measured size fraction (micro-, nano- and picophytoplantkon). To calculate $a^*_{ph}(\lambda)$, the basis vector tables (minimum and maximum $a^*_{ph}(\lambda)$ values) of the microphytoplankton ($a^*_{ph_{(M)}}(\lambda)$) and picophytoplankton ($a^*_{ph_{(P)}}(\lambda)$) spectra of Ciotti et al. (2002) were used with size parameters for different phytoplankton communities to scale $a^*_{ph}(\lambda)$ with respect to $a^*_{ph_{(M)}}(\lambda)$ and $a^*_{ph_{(P)}}(\lambda)$ using equation 3.13 (Ciotti et al. 2002) .

$$a_{ph_{total}}(\lambda) = \left[F_{\langle s \rangle} \cdot \bar{a}_{ph_{(P)}}(\lambda)\right] + \left[(1 - F_{\langle s \rangle}) \cdot \bar{a}_{ph_{(M)}}(\lambda)\right] \quad (3.13)$$

where $\bar{a}_{ph_{(P)}}(\lambda)$ and $\bar{a}_{ph_{(M)}}(\lambda)$ are the basis vectors (average-normalised $a^*_{ph}(\lambda)$ spectra of smallest and largest cells), $F_{\langle s \rangle}$is a size factor for each of 16 communities which ranges from 0 (dominated by microphytoplankton) to 1 (dominated by *Prochlorococcus*).

3.2.7 Comparisons of PP estimates using modelled and measured $a_{ph}(\lambda)$

Phytoplankton absorption spectra are used to correct α^B for the emission spectra of the light source (Kyewalyanga, Platt et al. 1997) and the subsequent calculation of the maximum

quantum yield of carbon fixation ($\varphi_{max,}$ mol of carbon fixed (mol of quanta absorbed)$^{-1}$), which was then calculated following Babin, Morel et al. (1996):

$$\varphi_{max} = \frac{\alpha^B}{12000\ \bar{a}^*} \tag{3.14}$$

where α^B is the spectrally-corrected light-limited photosynthetic rate, 12000 is the molecular weight of carbon and $\bar{a}^*$ is the spectrally-averaged, chlorophyll-specific absorption coefficient for that size fraction (Babin, Morel et al. 1996).

As some models use a single total absorption spectrum for all size classes, they produce a the same spectral correction constant X (equation 2.2) for a given light source and thus according to equation 3.14 estimates of $\varphi_{max,}$ for a specific size class are determined solely by the broadband α^B measurement (assuming same incubation light source), and thus using a single spectrum for all classes may producer errors in S-F α^B and φ_{max} values.

The spectral radiative transfer equations of Gregg and Carder (1990) were used to compute the irradiance field just below the sea surface at 5nm resolution between 350 to 700 nm at 30 minute intervals.

To calculate integrated, water-column primary production, the model of Tilstone et al. (2005) was used in the same manner as in Chapter 2 (section 2.16)

$$PP_{(z,t)} = \int_{Z=0}^{Zeu=1\%} \int_{T=0}^{24} Chla(z) P_m^B(z) \left[1 - \exp\left(\frac{-E_{PUR}(z,t)}{E_{k_{PUR}}(z)}\right)\right] dz\ dt \tag{3.15}$$

where $PP_{(z,t)}$ denotes the daily, integrated primary production (mg C m^{-2} d^{-1}). E_{PUR} denotes the irradiance of phytoplankton-useable radiation (PUR) (µE m^{-2} s^{-1}). Chlorophyll-specific carbon fixation was integrated at 1 m depth resolution (dz) (from the surface ($z = 0$) to the euphotic depth ($z_{eu} = 1\%$) and over 1 hour intervals (dt) for both each size class, and the

total phytoplankton community. Both daily depth-integrated primary production (mg C m^{-2} d^{-1}) and volumetric primary production (mg C m^{-3} d^{-1}) at discrete 1 m intervals were computed from the surface to the euphotic depth for each size class to calculate integrated, water-column primary production, the model of Tilstone et al. (2005) was used in the same manner as in chapter 2 (section 2.2.6)

$$PP_{(z,t)} = \int_{Z=0}^{Zeu=1\%} \int_{T=0}^{24} B(z) P_m^B(z) \left[1 - \exp\left(\frac{-E_{PUR}(z,t)}{E_{k_{PUR}}(z)}\right)\right] dz\, dt \qquad (3.15)$$

where $PP_{(z,t)}$ denotes the daily, integrated primary production (mg C m^{-2} d^{-1}). E_{PUR} denotes the irradiance of phytoplankton-useable radiation (PUR) (µE m^{-2} s^{-1}). Chlorophyll-specific carbon fixation was integrated at 1 m depth resolution (dz) (from the surface ($z = 0$) to the euphotic depth ($z_{eu} = 1\%$) and over 1 hour intervals (dt) for both each size class, and the total phytoplankton community. Both daily depth-integrated primary production (mg C m^{-2} d^{-1}) and volumetric primary production (mg C m^{-3} d^{-1}) at discrete 1 m intervals were computed from the surface to the euphotic depth for each size class.

3.3 Results

3.3.1 Measured total and chlorophyll-specific phytoplankton absorption

Total phytoplankton absorption spectra ($a_{ph}(\lambda)$) measured during the August 2014 cruise exhibited less variability than in the April 2015 cruise (with the exception of two high chlorophyll SCM stations of August). Total chlorophyll concentration was generally less

variable during August 2014 whereas the onset of the spring bloom during April 2015 exhibited greater variation in phytoplankton biomass between samples (Fig 3.2, 3.3). CTD profile data from the two cruises showed that the depth of the mixed layer was highly variable during April 2015 with the evolution of mixed to stratified conditions during the cruise. This contributed to high variability in $a_{ph}(\lambda)$ as a result of differences in photoacclimation status of phytoplankton between sampling stations. Micro- and nano-phytoplankton exhibit similar bulk absorption spectra for both seasons in the Celtic Sea, whereas pico-phytoplankton absorption spectra are more variable, with the highest values of any of the size fractions. The high absorption coefficients for the pico-phytoplankton fraction are a function of both a higher chlorophyll-specific absorption coefficient (Fig .3), and their high relative chlorophyll concentrations at some stations (Fig 2.11)

The magnitude of chlorophyll-specific phytoplankton absorption coefficients $(a_{ph}^{*}(\lambda))$ for the nano- and pico-phytoplankton were consistent with previous studies (Ciotti et al. 2002; Devred et al. 2006; Lohrenz et al. 2003). Picophytoplankton had the highest chlorophyll-specific absorption coefficients during both the spring and summer cruises. Nanophytoplankton generally had lower chlorophyll-specific absorption coefficients, with only three spectra with peak values greater than 0.05 m^2 $(mg\ Chl)^{-1}$

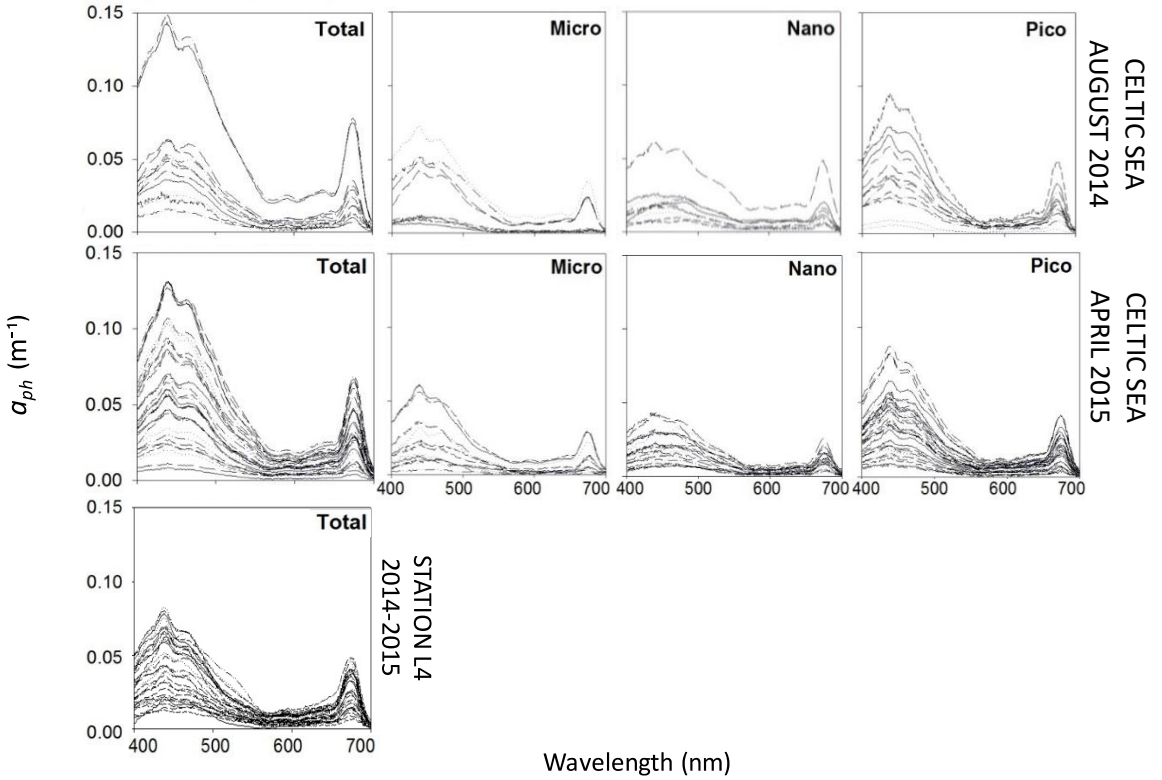


Fig 3.2 Total and size-fractionated absorption spectra measured during August 2014 (top row) and April 2015 (middle row) in the Celtic Sea and total absorption spectra measured at station L4 2014-2015 (bottom row)

. Most of the data from the microphytoplankton size fraction has to be excluded owing to unrealistically high chlorophyll-specific absorption coefficients in many samples, thus only a few, noisy microphytoplankton absorption spectra were retained after the quality control procedure. Microphytoplankton biomass was typically very low throughout both spring and summer Celtic Sea cruises (Fig 2.11, Table 3.1). This may have arisen from small measurement inaccuracies of chlorophyll concentrations and/or phytoplankton absorption were likely to produce erroneous phytoplankton absorption coefficients when normalised to chlorophyll concentration.

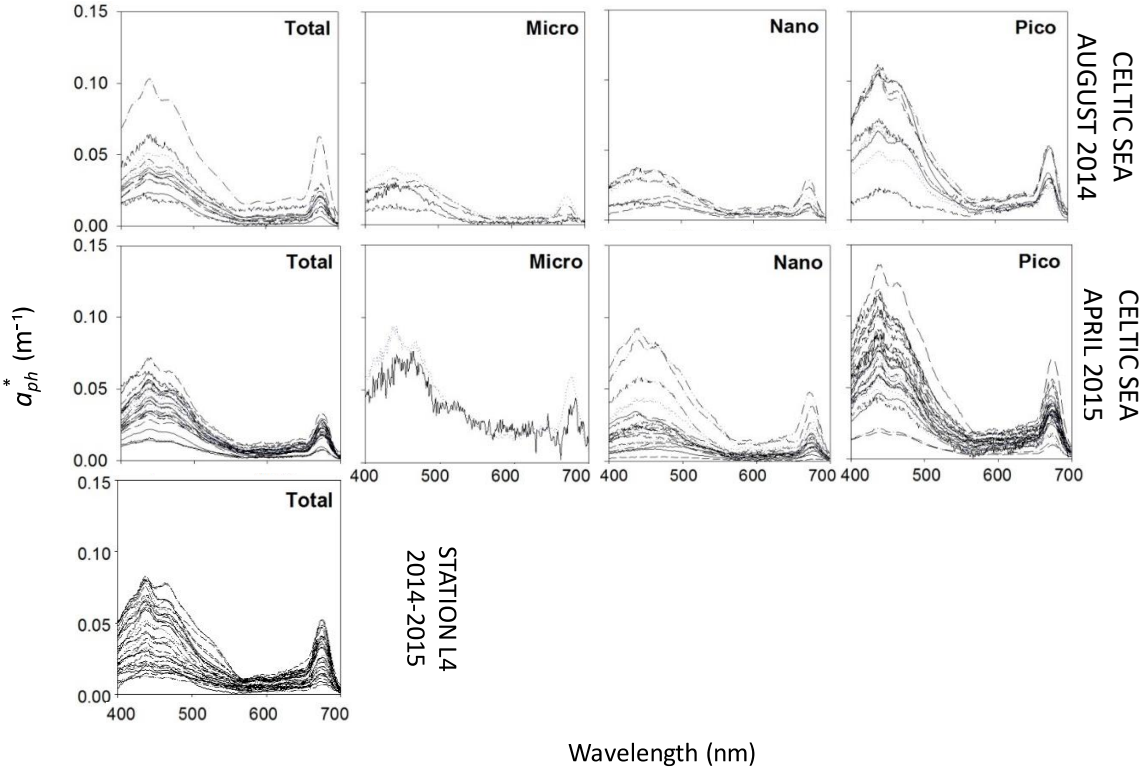


Fig 3.3 Total and size-fractionated chlorophyll-specific absorption spectra measured during August 2014 (top row) and April 2015 (middle row) in the Celtic Sea and total absorption spectra measured at station L4 2014-2015 (bottom row).

Table 3.1 Median size fractionated chlorophyll values measured during Celtic Sea cruises.

Size Class	August 2014 Median chlorophyll (mg m^{-3})	April 2015 Median chlorophyll (mg m^{-3})
Total	1.04	1.23
Micro	0.095	0.08
Nano	0.5	0.55
Pico	0.275	0.45

As microphytoplankton chlorophyll concentration (B_m) was low in both cruise datasets, even slight variability in B between water subsamples used for the determination of $a_{ph_{total}}(\lambda)$ and $a_{ph_{micro}}(\lambda)$ may have resulted in erroneously low value of $a_{ph_{micro}}(\lambda)$. For example, if the 20 µm pre-filtered sample contained a similar concentration of chlorophyll to the total (not pre-filtered) sample, then the product of total absorption

coefficient minus the absorption coefficient for the <20 µm size fraction would not produce a reliable spectrum for microphytoplankton.

Only two noisy spectra were retained from the spring cruise and in both cases microphytoplankton biomass was particularly low with respect to the sum of the other size fractions (Table 3.1). This paucity of reliable microphytoplankton-specific absorption data is problematic for spectral correction of light-limited photosynthetic rates measured from photosynthesis-irradiance experiments, and subsequent calculation of water-column primary production.

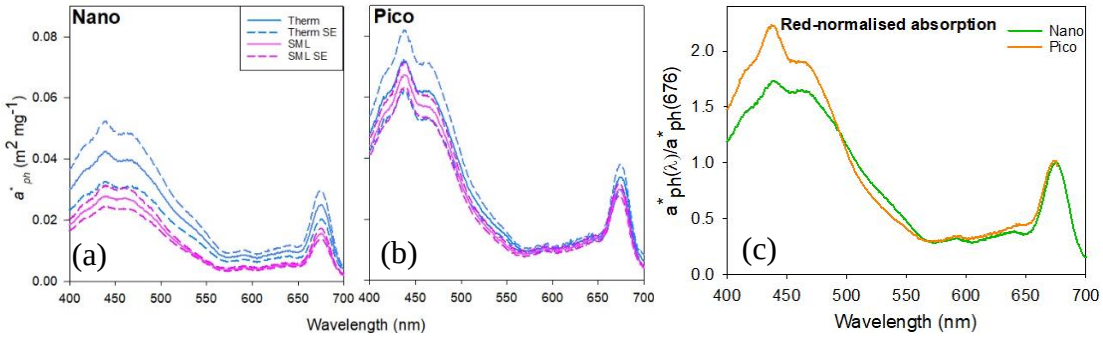


Fig 3.4 Average chlorophyll-specific absorption spectra measured in the Celtic Sea during August 2014 and April 2015 for nano- (a) and picophytoplankton (b) populations within the surface mixed layer (SML) and below the thermocline (Therm) (solid lines) with standard error of the mean plotted to indicate variability within each sub group (SML SE) (Therm SE). Microphytoplankton spectra are excluded due to poor data quality (Fig 3.3). Plot (c) shows the chlorophyll-specific absorption of nanophytoplankton (Green) and picophytoplankton (Orange) normalised to 676nm to show differences in specific absorption across wavelengths more clearly.

Mean nano- and picophytoplankton a^*_{ph} spectra from the Celtic Sea cruises are given in (Fig 3.4) It was not possible to derive a mean spectrum for microphytoplankton due to the small sample size and low biomass. The average a^*_{ph} spectra of nano and picophytoplankton are consistent with previous studies – picophytoplankton having the highest chlorophyll-specific absorption between 400-700nm and nanophytoplankton having lower values (Fig 3.14). To assess vertical differences caused by photoacclimation, mean absorption spectra were separated into two groups: those within the surface mixed layer and those at or below

the thermocline by using CTD density profiles. By separating the measured spectra into communities experiencing high irradiances periodically and those experiencing lower irradiances deeper in the water column, the impact of photoacclimation on the chlorophyll-specific absorption of each size class could be investigated. As there were too few microphytoplankton spectra to perform a meaningful comparison, only nano- and picophytoplankton spectra are reported. Fig 3.4 shows that for picophytoplankton, there were no significant differences in mean specific absorption spectra between surface mixed layer and below surface mixed layer communities – the standard error for both mean spectra overlaps over all wavelengths. For nanophytoplankton, there were differences between surface mixed layer samples and those taken from below the thermocline. For nanophytoplankton, surface samples exhibited significantly lower absorption, particularly between 500-550 nm and around the red absorption peak of chlorophyll-a. Both size classes exhibit greater variability for at/below the thermocline than within the surface mixed layer.

In addition to plotting average spectra for above and below the thermocline, values of a^*_{ph}(443) were plotted against ζ to allow comparison with the study of Uitz et al. (2008) (Fig 3.5).

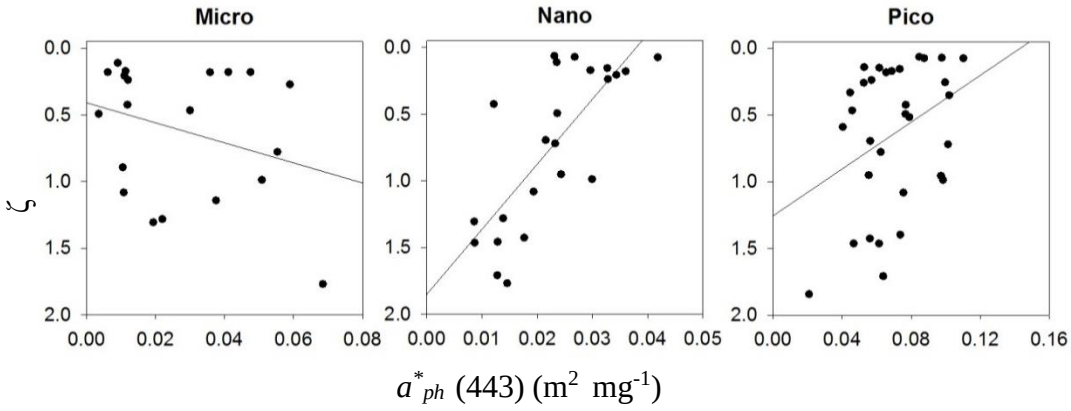


Fig 3.5 a^*_{ph}(443) values of different size fractions measured during the April 2015 (DY029) Celtic Sea cruise plotted against ζ (dimensionless depth) consistent with the model of Uitz et al (2008).

As the dataset of measured a^*_{ph} values is small and covers only two months of the year, establishing a relationship between specific absorption and ζ for the Celtic Sea samples is

perhaps beyond the scope of this incipient S-F dataset. However, there is a general negative relationship between nano- and picophytoplankton a^*_{ph}(443) with increasing ζ, similar to the study of Uitz et al. (2008) and the relationships presented in chapter 4 for P^B_m and α^B (Fig 4.3). However, the smaller dataset for microphytoplankton, which contains many erroneously high values and noisy spectra, exhibits no discernible trend.

By calculating the mean values of $a^*_{ph}(\lambda)$ for nano- and picophytoplankton, it is thereafter possible to produce estimates of $a_{ph}(\lambda)$ by simply multiplying a^*_{ph} by size fractionated chlorophyll. However, given the low number of microphytoplankton spectra, another parameterisation for the specific absorption spectrum of this size class must be used. Therefore, in this study, the spectra of Ciotti et al (2002) for diatom- and dinoflagellate-dominated communities from mid to high latitude shelf and coastal seas were chosen, and taxonomic data taken at L4 and during the April 2015 cruise were used to decide which of the two microphytoplankton spectra would be used (although differences in $a^*_{ph}(\lambda)$ are minor between diatoms and dinoflagellates (Fig 3.13)). The limited number of microscopic cell counts from the August Celtic Sea cruise indicated that within the subsurface chlorophyll maximum the bulk of microphytoplankton biomass consisted of naked dinoflagellates, so this spectrum was used as a more appropriate representation of this size class.

These measurements phytoplankton absorption were used to correct light-limted photosynthetic rates for the spectrum of the light source and the corrected α^B values where then used the calculate maximum quantum yield of carbon fixation for the phytoplankton communtity at L4 (section 2.2.5). As size-fractionated measurements were not taken for station L4 and are not reported within the literature, calculating absorption spectra and spectrally-dependent parameters for each size fraction requires using average specific

absorption coefficents (this study) (Ciotti et al. 2002; Devred et al. 2006; Varunan and Shanmugam 2015), or modelled values with respect to another observed variable (Uitz et al. 2008). The following results comprise an analysis of some of these approaches, with comparisons to *in situ* measurements where available.

3.3.2 The model of Uitz et al (2008): scaling size-fractionated values of $a^*_{ph}(\lambda)$ with ζ

Phytoplankton absorption spectra derived from the Uitz et al (2008) model exhibit increasing specific absorption with decreasing size, which is consistent with most models of size-fractionated a^*_{ph} as well as optical theory (Morel and Bricaud 1981) (Fig 3.13). As the values of a^*_{ph} at each wavelength change following the relationship with ζ, erroneous absorption spectra are produced when of $a^*_{ph}(\lambda)$ is estimated for ζ values greater than 1.5. Although such high values ζ of were not encountered in the open ocean study of Uitz et al (2008), samples in the Celtic Sea cruise were collected with reference to the shape of the chlorophyll fluorescence profile instead of light attenuation (i.e. the depth at which a percentage of surface irradiance reached a specific value) and consequently there were occasions when samples were collected below the depth of 1% surface irradiance. This was a frequent occurrence during the August 2014 cruise, where strong stratification resulted in the formation of a pronounced sub-surface chlorophyll maximum which was sometimes accompanied by smaller and shaper chlorophyll peaks at low irradiances (<1% surface value) near the nutricline. In these instances, ζ could be greater than 2.0, where $a^*_{ph}(\lambda)$ estimates from the Uitz et al (2008) values are not applicable and thus yield erroneous values, particularly in the region of the red chlorophyll peak of the picophytoplankton, although anomalous values are also visible in the blue region for both micro- and picophytoplankton.

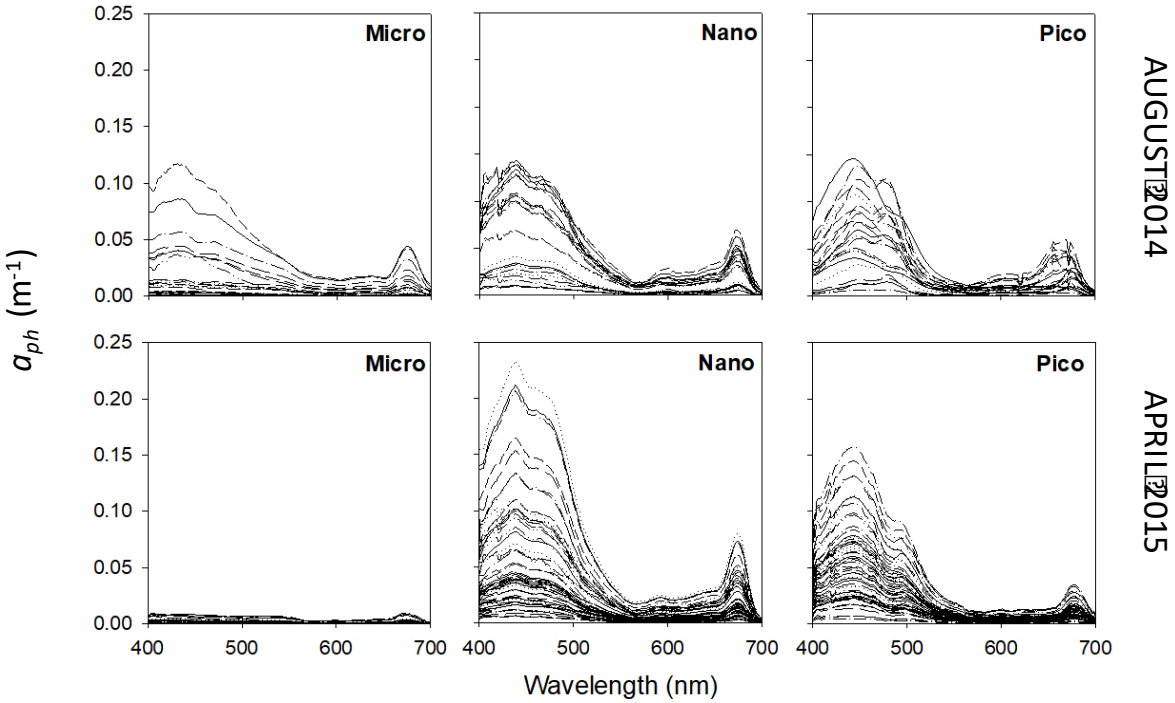


Fig 3.6 Size-fractionated $a_{ph}(\lambda)$ calculated for August 2014 (top row) and April 2015 (bottom row) Celtic Sea cruises using the approach of Uitz et al (2008) and *in situ* measurements of S-F chlorophyll concentration.

The chlorophyll-specific absorption of nanophytoplankton seems less affected at extreme values of ζ, but the magnitude of peak $a^*_{ph}(443)$ is high at 0.09 m^2 mg Chl-a^{-1} , with a considerable number of estimated nanophytoplankton spectra exhibiting markedly higher a^*_{ph} than the majority of measured spectra from August and April cruises.

3.3.3 Modelled phytoplankton absorption spectra using the pigment reconstruction method (Bidigare et al. 1990)

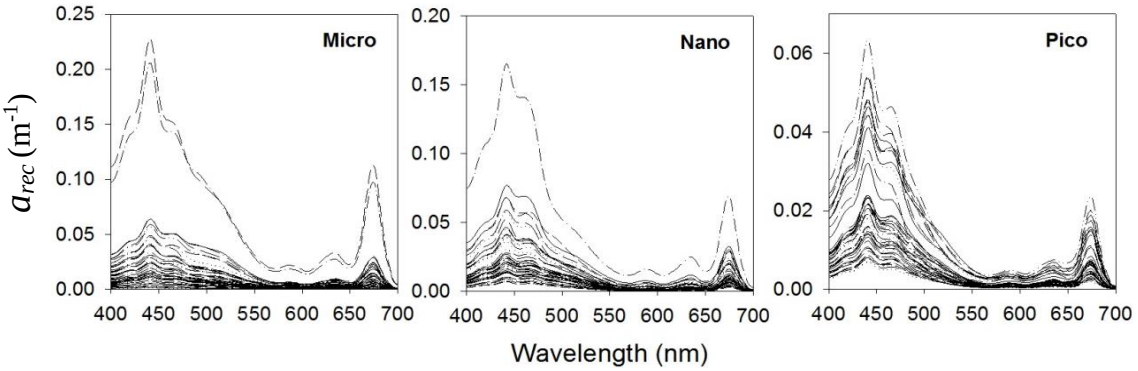


Fig 3.7 Phytoplankton absorption spectra calculated using the pigment reconstruction technique of Bidigare et al (1990) with phytoplankton pigment concentrations from station L4.

For some high-chlorophyll samples, $a_{rec}(\lambda)$ estimates using the pigment reconstruction method were sometimes much higher than those observed from *in vivo* absorption measurements (Fig 3.2).

As size-fractionated pigment samples were unavailable, analysis of measured spectra and pigment-reconstructed spectra is limited to total $a_{ph}(\lambda)$. No total $a^*_{ph}(\lambda)$ above 0.08 m^{-1} was observed, whereas both micro- and nanophytoplankton had $a_{rec}(\lambda)$ higher values, highlighting the significance of pigment packaging to chlorophyll-specific absorption. For most samples, $a_{rec}(\lambda)$ coefficients were higher at both 443 and 665 nm by a considerable margin, with an average difference between measured and reconstructed of $a_{ph}(443)$ of 0.038 m^{-1} (Fig 3.8b). These larger discrepancies between measured and reconstructed spectra were reduced when outliers were removed (Fig 3.8c).

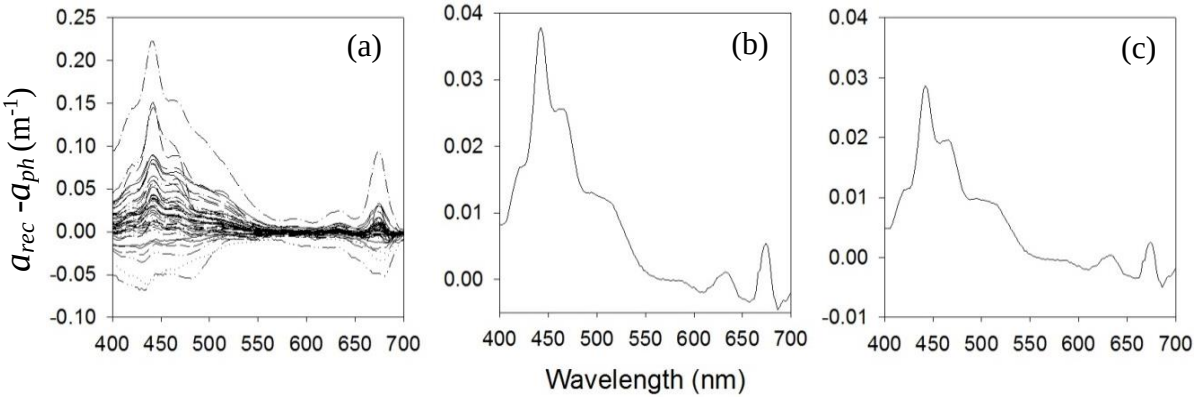


Fig 3.8 (a) Difference between total phytoplankton absorption spectra ($a_{rec}(\lambda)$) and measured $a_{ph}(\lambda)$ values for station L4 from the same depths; (b) the average difference between of $a_{rec}(\lambda)$ and $a_{ph}(\lambda)$ (c) The average difference between $a_{rec}(\lambda)$ and $a_{ph}(\lambda)$ when outliers of high-chlorophyll monospecific blooms are removed. Negative values are produced when measured $a_{ph}(\lambda)$ is greater than reconstructed $a_{rec}(\lambda)$.

These outliers were caused by HPLC-determined chlorophyll concentrations being significantly higher than those that were determined fluorometrically for size-fractionated chlorophyll measurements. However, there was still a significant overestimate of absorption

by reconstructed spectra in the blue part of the spectrum after this correction. Towards the red end of the spectrum, overestimates are only significant between 660 and 678 nm, with small underestimates of absorption at other wavelengths in this region (Fig 3.8c).

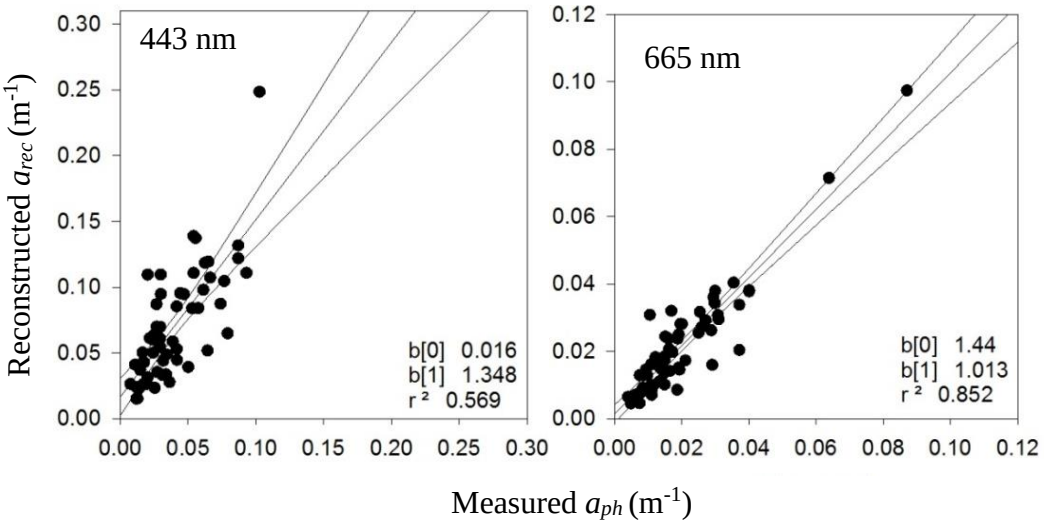


Fig 3.9 Linear regression of phytoplankton absorption at 443 nm (a) and 665 nm (b) for measured (a_{ph}) and pigment-reconstructed (a_{rec}) absorption spectra for coincident samples depths at station L4

This tendency for $a_{rec}(\lambda)$ to be markedly higher measured than a_{ph} in the blue part of the spectrum can be observed in the regression plots of coincident pigment and a_{ph} samples collected at L4 from 2014-2015 (Fig 3.9): $a_{rec}(443)$ values are on average 35% higher than $a_{ph}(443)$ values. This is not observed at the red peak, where the agreement is good and the offset between $a_{rec}(665)$ and $a_{ph}(665)$ is not significant, with an average difference of <1.5%. However, there is a large difference in the spectral shapes between measured and pigment-reconstructed values apparent in the spectral shapes, with reconstructed spectra having a much steeper spectral slope from peak values (443-400nm) which contrasts markedly with the flatter and smoother shape of the measured spectra, where the packaged pigment suite is coupled within protein complexes in the light harvesting apparatus of the cell (Johnsen and Sakshaug 2007; Johnsen et al. 1994).

In order to use reconstructed spectra to estimate the phytoplankton absorption spectra where only pigment data are available spectrally-averaged values were calculated between 400 and 700 nm. The resulting mean absorption coefficients derived from both reconstructed and measured spectra were then compared using linear regression.

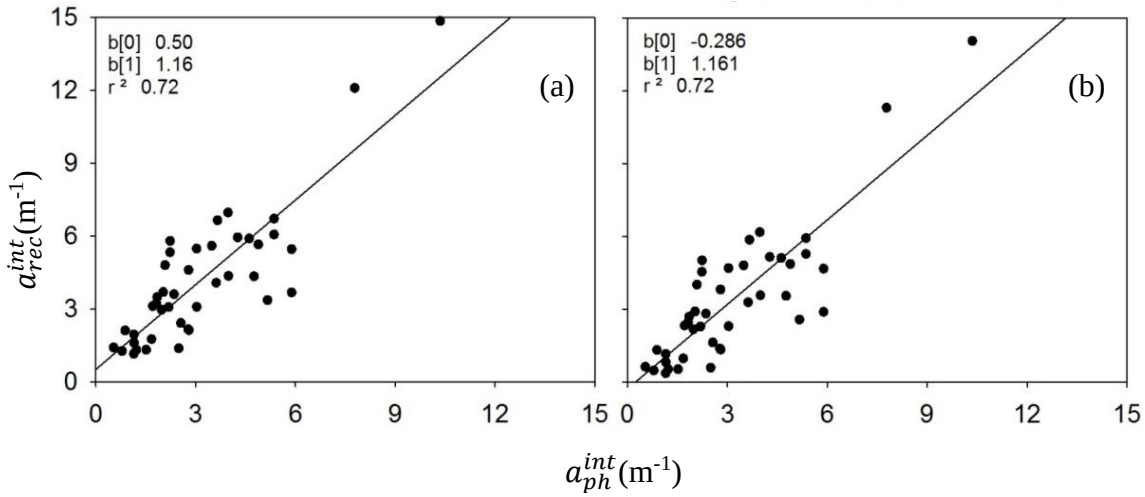


Fig 3.10 Linear regression of the integrated absorption coefficient of phytoplankton computed from measured (a_{ph}^{int}) and pigment-reconstructed (a_{rec}^{int}) spectra for station L4 (a). Plot (b) shows the change in regression statistics when the mean overestimation of $a_{ph}(\lambda)$ (Fig 3.9c) is applied to $a_{rec}(\lambda)$ to correct reconstructed values.

Integrated absorption coefficients showed good agreement (r2 = 0.72)(Fig 3.10), with reconstructed spectra being slightly higher, though there is a high degree of scatter and in some cases differences of a factor of 2 were observed. Correcting for the overestimation of $a_{ph}(\lambda)$ by the pigment reconstruction by subtracting the average difference between $a_{ph}(\lambda)$ and $a_{rec}(\lambda)$ at each wavelength had a negligible effect on the relationship between reconstructed and measured values. As this is a fixed correction value, only the y intercept changes; there is now a slight underestimation of the measured spectrum of around half the magnitude of the previous positive intercept (-0.286 compared with 0.50 m^{-1}). This result suggests that measured and pigment-reconstructed spectra would result in a similar vertical attenuation coefficient of PAR, since the difference in spectral shapes were eliminated when

integrated over the visible domain. Thus, the pigment reconstructed spectra may be suitable for broadband PP models, which are not impacted by strong differences in spectral shape.

3.3.5 Size-fractionated light absorption using ocean-colour remote-sensing data (Varunan & Shanmugam 2015)

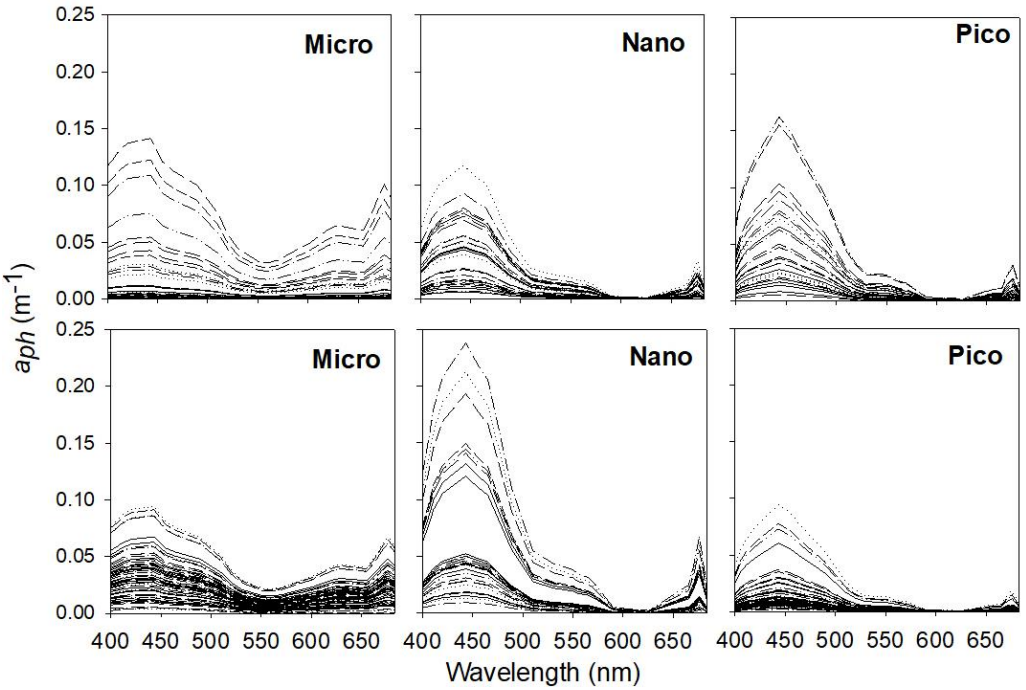


Fig 3.11 Phytoplankton absorption spectra reconstructed using the Varunan & Shanmugam (2015) method using size-fractionated chlorophyll data from two Celtic Sea cruises (August 2014 cruise top row, April 2015 cruise bottom row)

The model of Varunan and Shanmugam (2015) was used to calculate absorption spectra for each class from ocean-colour remote-sensing data and compared to measured values during spring and summer Celtic Sea cruises. As model specific absorption values $a^*_{vs}(\lambda)$were fixed, variability in $a_{ph}(\lambda)$ was determined only by S-F chlorophyll concentration. Fig 3.13 shows how $a^*_{vs}(\lambda)$ differs from other models

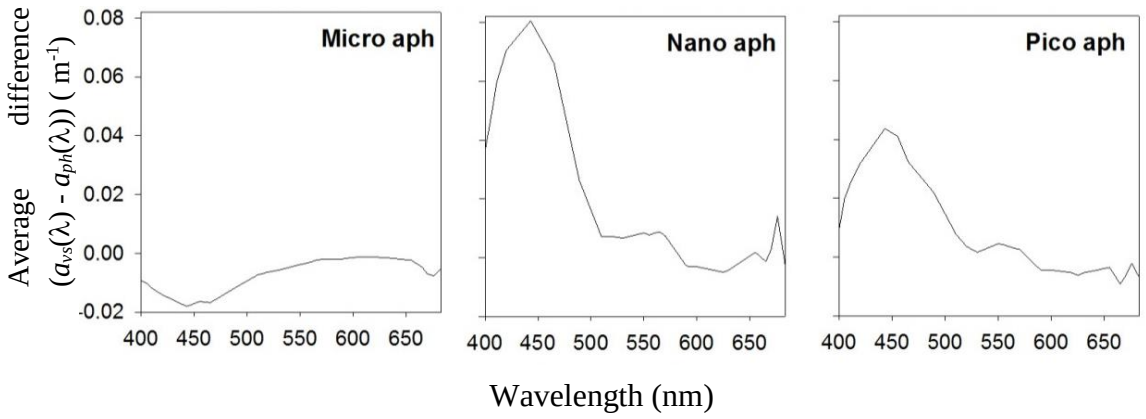


Fig 3.12 Spectra of the average (mean) difference between phytoplankton absorption estimated using the values of Varunan & Shanmugam (2015) ($a_{vs}(\lambda)$) and the values measured during both Celtic Sea cruises ($a_{ph}(\lambda)$).

When comparing differences between $a_{ph}(\lambda)$ and estimated $a_{vs}(\lambda)$, both nano- and picophytoplankton size classes are overestimated by the model. In contrast, microphytoplankton $a_{vs}(\lambda)$ is generally underestimated, particularly in the blue part of the spectrum.

3.3.6 Comparison between models of $a^*_{ph}(\lambda)$

There is considerable variability in the size-fractionated $a^*_{ph}(\lambda)$ derived from the Ciotti et al (2002), Uitz et al (2008), Brewin et al (2011) and Varunan & Shanmugam (2015) methods (Figure 3.14). The $a^*_{ph}(\lambda)$ estimates of Varunan and Shanmugam (2015) were consistently higher. The microphytoplankton spectra for diatom and dinoflagellate communities of Ciotti et al. (2002) were similar in magnitude and spectral shape, whilst the spectra of Varunan and Shanmugam (2015) and Uitz et al. (2008) had consistently higher values, particularly at the red chlorophyll absorption peak and between 460 -570 nm; the blue absorption peak was

therefore flattened in relation to the other spectra. For the Uitz et al. (2008) method, where specific absorption scales with ζ, microphytoplankton a^*_{ph} increased with increasing values of ζ, while the inverse was true of the smaller size fractions (Fig 3.3).

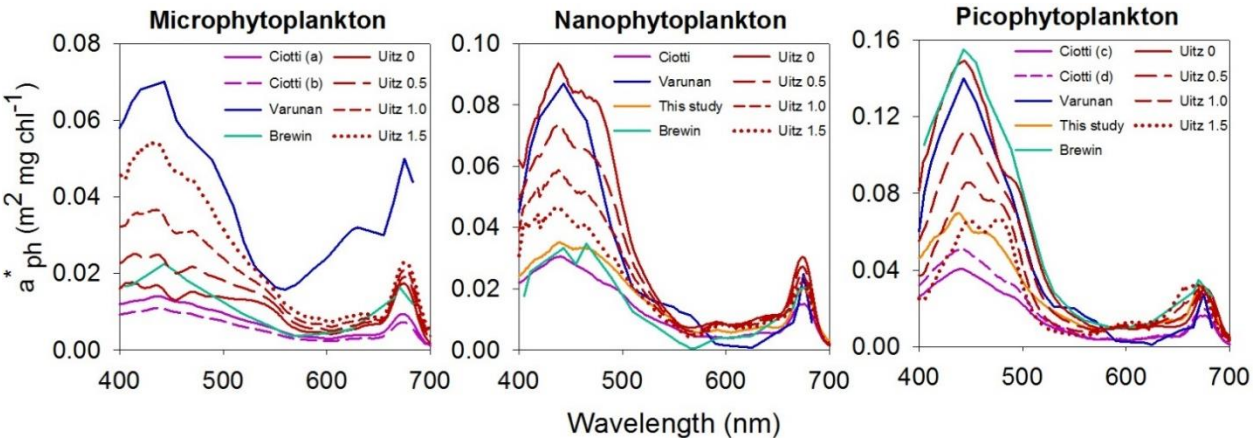


Fig 3.13 Chlorophyll-specific absorption coefficient spectra from the models of Ciotti et al (2002), Uitz et al (2008), Brewin et al (2011), Varunan & Shanmugam (2015) and measured values from this study (nano- and picophytoplankton only). Ciotti spectra: (a) diatom (b) dinoflagellate (c) Picoeukaryote (d) *Synechococcus.* Uitz spectra partitioned by sample depth divided by euphotic depth (ζ = 0, 0.5, 1.0, 1.5).

Nanophytoplankton spectra showed substantial differences between the values of the Varunan and Shanmugam (2015) and the surface values of Uitz et al. (2008), with peak values >0.08, while the average spectra from the Celtic Sea dataset were a factor of 2 lower in the blue wavelengths. Though the overall spectrum for nanophytoplankton $a^*_{ph}(\lambda)$ measured during this study correspond closely to the spectra of nanoflagellates derived via the method of Ciotti et al. (2002), the spectral shapes in the blue were distinct, with measured spectra from the Celtic Sea being higher between 450-570 nm. The nanophytoplankton $a^*_{ph}(\lambda)$ values of Varunan and Shanmugam (2015) were the closest to the measured nanophytoplankton $a^*_{ph}(\lambda)$ around the peaks of absorption in the blue (400-470 nm) and red wavelengths (655-680 nm) in terms of magnitude (Fig 3.14). However, the lower spectral resolution of the values derived following Varunan and Shanmugam (2015) (20 individual wavelengths), and reduced specific absorption values between 470-600 nm, mean the

spectral shape was generally less representative of the measured spectra than the model of Ciotti et al. (2002).

Picophytoplankton $a_{ph}^{*}(\lambda)$ values were markedly split between the higher surface values of Uitz et al. (2008); Varunan and Shanmugam (2015) and , and the lower values of Ciotti et al. (2002) and average measured values of this study. However, there was a greater difference in the magnitude of picophytoplankton $a_{ph}^{*}(\lambda)$ between measured values and those of the model of Ciotti et al. (2002) than for nanophytoplankton.

Between 400-570 nm the spectra Brewin et al. (2011); Uitz et al. (2008); Varunan and Shanmugam (2015) were similar (where Uitz et al (2008) model ζ values used to scale $a_{ph}^{*}(\lambda)$ were <0.5), with small differences in blue to green spectral slope being due to the higher spectral resolution of the model of Uitz et al. (2008). Between 580-660nm, the specific absorption values of the model of Varunan and Shanmugam (2015) are lower compared to the other models, but are similar to spectra from the models of Ciotti et al. (2002). In this region of the spectrum, the average spectrum from measured values, and the models of Uitz et al. (2008) and are similar. There was a pronounced shift in spectral shape with increasing ζ values for the Uitz et al. (2008) model, with increased absorption in the blue-green wavelengths with respect to the blue peak and substantial depression in specific absorption between 400-520nm generally. This may be due to the fact that both of these models are based on samples from open ocean communities where picophytoplankton biomass could be assumed to be prokaryote-dominated, specifically *Prochlorococcus*. This species was not found in high abundance in measured Celtic Sea samples which were a mixture of picoeukaryotes and *Synechococcus*, and the two selected picophytoplankton spectra from Ciotti et al (2002) corresponded to these groups, not *Prochlorococcus.*

This species was not found in high abundance in measured Celtic Sea samples which were a mixture of picoeukaryotes and *Synechococcus*, and the two selected picophytoplankton spectra from Ciotti et al (2002) corresponded to these groups, not *Prochlorococcus.*

When comparing the red peak of chlorophyll absorption, the values appear to be more consistent with decreasing size, such that there were considerable differences in the blue peak to red peak absorption ratio between models, particularly for the picophytoplankton fraction where the models of Uitz et al. (2008) and Brewin et al. (2011) had specific absorption values at the blue chlorophyll peak as high as double that of the observed averages of this study, but consistent values at the red chlorophyll peak. There is the possibility that databases containing measurements from low latitude oligotrophic regions may contain a greater number of high-light acclimated samples, where increased cellular concentrations of photo-protective carotenoids may increase chlorophyll-specific absorption between 450-500 nm absorption substantially (Barlow et al. 2002; Lutz et al. 2001). Without corresponding pigment data from the Celtic Sea absorption samples, it is not possible to directly test whether the large differences chlorophyll-specific absorption coefficients in the blue part of spectrum between models were due to a higher proportion of high-light photoacclimation responses in their respective datasets (including higher proportion of photo protective carotenoids) in the open-ocean datasets used to develop the models.

3.4 How do modelled phytoplankton absorption spectra affect estimates of primary production in shelf seas?

Following the analysis of the absorption spectra to determine the utility of modelled spectra for filling data gaps of the measured spectra from *in situ* sampling efforts, modelled spectra

were used in the calculation of PP following the method described in section 2.2.6 to investigate the differences in output when using different spectra and values of spectrally-corrected α^B and φ_{max}.

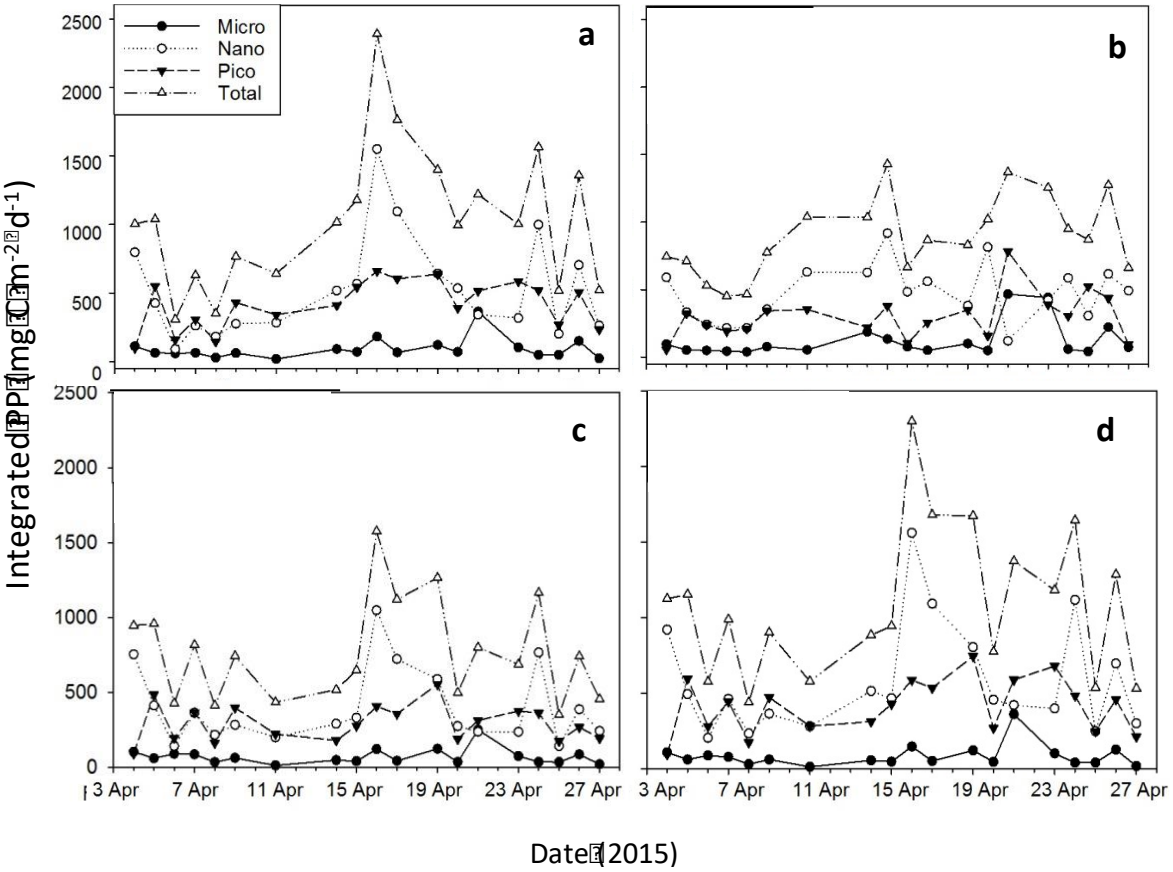


Fig 3.14 Daily integrated primary production estimated for the April 2015 Celtic Sea cruise using the $a_{ph}(\lambda)$ from (a) measurements of *in vivo* absorption (b) the Uitz et al (2008) model, (c) the Ciotti et al (2002) model and (d) the Varunan & Shanmugam (2015) to calculate α^B and φ_{max}.

For the April 2015 cruise, mean size-fractionated $a^*_{ph}(\lambda)$ measurements for nano- and picophytoplankton were used to calculate primary production at each station (Fig 3.14) following the same procedure as 2.2.6 (Fig 2.17). These estimates were compared against model estimates using $a_{ph}(\lambda)$ calculated using the method of Uitz et al (2008), Ciotti et al (2002) and Varunan & Shanmugam (2015).

Linear regression of total and S-F PP estimates using measured and modelled spectra are presented in tables 3.2 and 3.3. When compared against the primary production values modelled using measured values of a_{ph} spectra to spectrally correct α^B, both sets of model values appear to correlate well. Running integrated production using values calculated using the Varunan & Shanmugam (2015) model values appears to give estimates close to measured spectra (Fig 3.15 a), whereas the Ciotti et al (2002) values appear lower (Fig 3.15 b).

Table 3.2 Summary of regressions of PP estimates when α^B is corrected for the spectrum of the lamp using different modelled a_{ph}spectra against PP estimated using measured spectra.

Size Class	Ciotti et al (2002)		Var. & Sham. (2015)		Pigments		Uitz et al (2008)	
	R^2	slope	R^2	slope	R^2	slope	R^2	slope
Total	0.75	0.56	0.9	0.90	0.6	0.9	0.08	0.13
Micro	0.87	0.65	0.96	0.96	0.53	1.0	0.52	1.17
Nano	0.88	0.64	0.96	0.96	0.51	0.69	0.16	0.13
Pico	0.62	0.55	0.80	0.93	0.44	0.89	0.11	0.32

Despite the shape and magnitudes of the a^*_{ph} spectra of Varunan & Shanmugam (2015) being quite different from measured spectra (Fig 3.13), PP estimates using these spectra are much closer to estimates using measured spectra than those obtained from other models (Table 3.2).

Table 3.3 Summary of PP regressions when modelled a_{ph} values are used with measured α^B values.

Size Class	Ciotti et al (2002)		Var. & Sham.(2015)		Uitz et al (2008)	
	R^2	slope	R^2	slope	R^2	slope
Total	0.78	0.54	0.88	0.90	0.94	1.11
Micro	0.66	0.41	0.70	0.96	0.77	0.98
Nano	0.89	0.75	0.88	0.96	0.83	1.26
Pico	0.46	0.46	0.66	0.93	0.78	0.85

Total primary production was also calculated using modelled a_{ph} spectra with α^B values corrected by measured spectra in order to establish whether PP estimates are more sensitive to the correction of α^B, or absorption and attenuation of light (Table 3.3). Daily integrated PP was overestimated by ~11% using the spectra from the model of Uitz et al (2008), underestimated by 10% when using the spectra of Varunan & Shanmugam (2015) and underestimated by 56% using the spectra of Ciotti et al (2002). Water-column primary production estimates for each size class exhibit more variability than total community estimates; microphytoplankton and picophytoplankton PP is best estimated using the spectra of Uitz et al (2008) and nanophytoplankton by Varunan & Shanmugam (2015). Overall the most accurate a_{ph} model in terms of estimates of integrated PP was that of Varunan and Shanmugam (2015).

As $a^*_{ph}(\lambda)$ defines the absorption of visible light for a given concentration of chlorophyll, differences in the magnitudes of $a^*_{ph}(\lambda)$ of each model used in the integrated PP model estimates presented in table 3.3 may lead to variability in light attenuation and therefore PP(z). Figure 3.16 shows the variability in this vertical distribution of PP(z) for each model with respect to when using measured spectra.

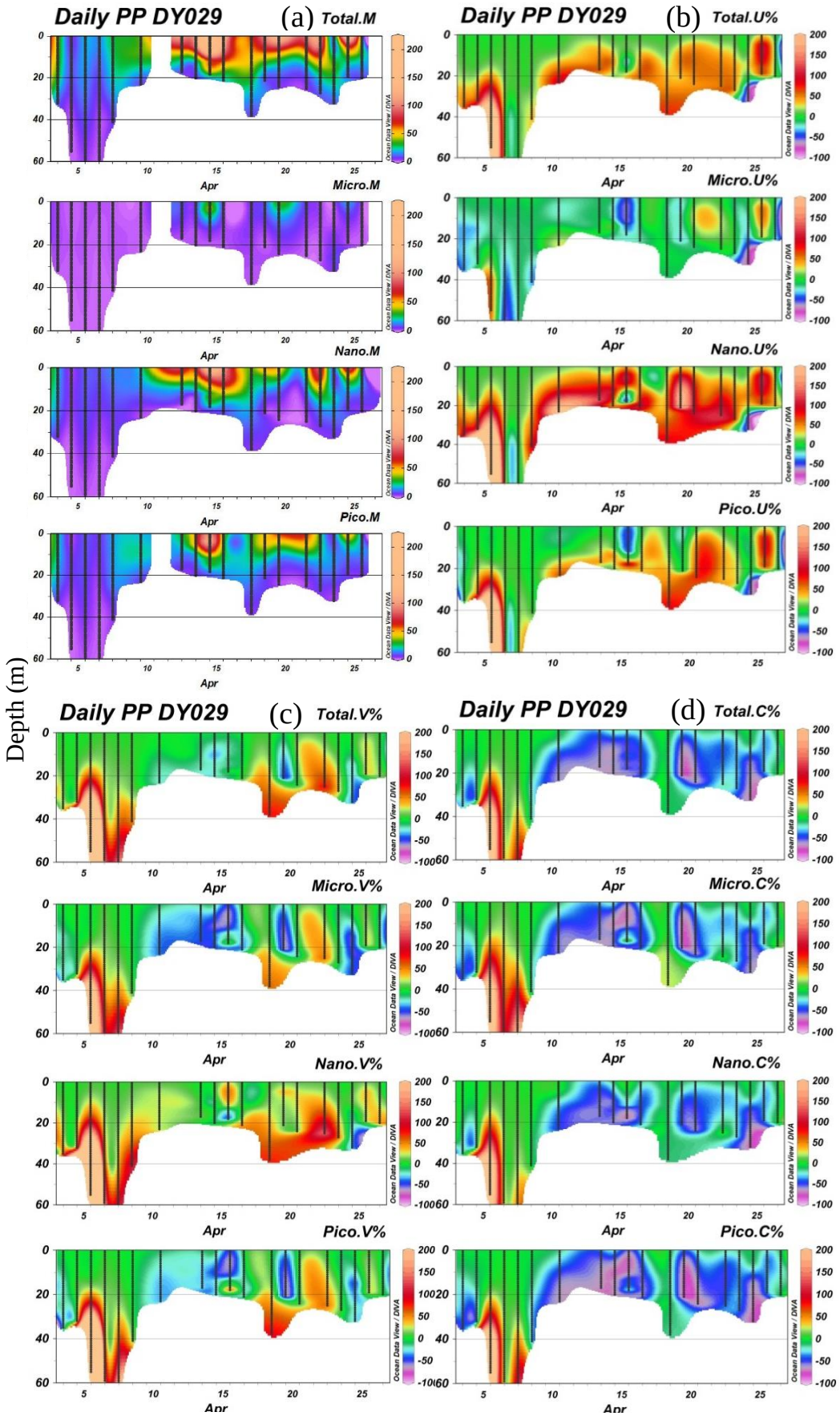

Daily PP DY029
(a) Total.M
Daily PP DY029
(b) Total.U%
Micro.M
Micro.U%
Nano.M
Nano.U%
Pico.M
Pico.U%
Daily PP DY029
(c) Total.V%
Daily PP DY029
(d) Total.C%
Micro.V%
Micro.C%
Nano.V%
Nano.C%
Pico.V%
Pico.C%
Depth (m)
Day of month (April 2015)

Fig 3.15 (Preceding page) Plot of modelled volumetric primary production (mg C m^{-3} d^{-1}) using (a) measured spectra during April 2015 (DY029) with corresponding plots for the models of (b) Uitz et al (2008), (c) Varunan & Shanmugam (2015) and (d) Ciotti et al (2002) showing the percentage difference in modelled volumetric primary production using modelled versus measured phytoplankton absorption spectra.

Fig 3.15 (b) shows that for microphytoplankton, the Uitz et al (2008) generally performs well across the range of sites and depths, with fewer overestimations than the smaller size fractions. Some stations have consistent underestimates through the water column (15th, 20th April 2015, both at 49.241°N, -8.372°W), while only one station showed a consistent overestimate of 20-40% on the 25th April 2015.

The depth-specific PP model output ($PP(z)$) using a_{vs} values of Varunan & Shanmugam (2015) (Fig 3.15 (c)) shows a general underestimation of total PP across most depths, though some stations had overestimated PP at the SCM compared with measured spectra PP estimates ((Fig 3.15 (a)). However, as the overestimation using a_{vs} spectra is generally at the SCM and therefore low irradiances, it does not influence depth-integrated estimates to the same extent as the overestimation at the surface as with the Uitz et al. (2008) spectra, or underestimation at the surface using the Ciotti et al. (2002) spectra.

3.5 Discussion

3.5.1 How well do modelled size-fractionated specific absorption coefficients match measured spectra?

The initial aim of this chapter is to establish how well a number of existing models of phytoplankton absorption for different size classes perform when compared to measured spectra. The results showed that no method of estimating size-fractionated absorption closely resembled the *in situ* measurements of $a_{ph}^{*}(\lambda)$ when considering both magnitude and shape. It is widely accepted that chlorophyll-specific absorption is inversely correlated with cell size, (Ciotti, Lewis et al. 2002, Bricaud, Claustre et al. 2004, Devred, Sathyendranath et al. 2006, Uitz, Huot et al. 2008, Brewin, Devred et al. 2011, Ferreira, Stramski et al. 2013) and was observed in the size-fractionated data taken in the Celtic Sea where picophytoplankton had higher specific absorption coefficients than nanophytoplankton (Fig 3.4). Measurements of $a_{ph}^{*}(\lambda)$ for the nano- and picophytoplankton classes showed considerable variability (Fig 3.3). While a_{ph}^{*} is influenced by cell size, is also a function of the photoacclimatory responses of these cells to hydrographic conditions: mixing dynamics (mixing period and vertical extent), may cause strong fluctuations in the exposure of cells to visible and UV radiation and can also influence nutrient supply. The availability of light and nutrients are primary factors governing changes in the intracellular concentration of pigments, which is a primary determinant of *in vivo* specific absorption (Cermeño et al. 2005; Fujiki and Taguchi 2002; Key et al. 2010; Poulton et al. 2006).

Measurements of $a_{ph}^{*}(\lambda)$ at station L4 during 2014 and 2015 (Fig 3.2) showed a high degree of variability in both shape and magnitude, reflecting the large fluctuations in phytoplankton biomass and community structure at this site throughout the two sampling periods. Specific

taxa can periodically dominate the plankton biomass at station L4 during blooms, most typically within the micro- and nanophytoplankton fractions, and these successional changes in species composition is reflected in the chlorophyll-specific absorption spectra of the total phytoplankton community ($a^*_{ph_{total}}(\lambda)$) (Fig 3): blooms of larger cells such as *Coscinodiscus* and *Chaeotoceros* exhibit different absorptive characteristics (spectral shape and degree of pigment packaging) to nanoplankton cells such as *Phaeocystis*, and the background mixed nano- and picoeukaryote communities found at the site (Widdicombe et al. 2010). Changes in size distribution of the community within the three fractions may also be an important factor governing the observed variability in $a^*_{ph}(\lambda)$ (Ciotti et al, 2002). Fig 3.4 illustrates the marked differences in a^*_{ph} between nano and picophytoplankton measured in the Celtic Sea**.**

Estimates of a_{ph} spectra using fixed chlorophyll-specific absorption coefficients (Varunan & Shanmugam 2015) and from pigment reconstruction (Bidigare et al. 1990), may only be compared against averaged measured spectra, as the spectral shape of $a^*_{ph}(\lambda)$ does not change as a function of chlorophyll biomass in these models and is only modified by variations in pigment composition. In the case of the Varunan & Shanmugam (2015) method, where chlorophyll-specific absorption coefficients remain constant for a given size class and are assumed not to change as a function of the growth environment, estimated absorption coefficients have been shown to be markedly higher than mean observed values by a factor of 2 (this study), 1.75 (Brewin, Devred et al. 2011) and 2.3 (Bricaud, Babin et al. 1995). These results indicate that the Varunan & Shanmugam (2015) approach of estimating chorophyll-specific absorption coefficients and resulting spectra for the three phytoplankton size classes are poorly suited to estimating the absorption properties of phytoplankton in UK shelf seas, at least in terms of the magnitude of $a^*_{ph}(\lambda)$. The model of Uitz, Huot et al. (2008)

provides a more realistic approach for estimating the chlorophyll-specific absorption as it represents the vertical changes in the photoacclimatory status of cells in response to changing light levels. However, although $a^*_{ph}(\lambda)$ changes with ζ, the estimated coefficients are still typically greater than measured spectra for nano- and picophytoplankton at ζ values of 1.5 (Fig 3.13). Despite this, slope values used to describe the vertical changes in $a^*_{ph}(\lambda)$ with respect to ζ (Fig 3.3) may be tuned using *in situ* data for a region of interest. Fig 3.5 suggests there is a correlation between chlorophyll-specific absorption and ζ in the Celtic Sea for nanophytoplankton and possibly picophytoplankton, although the number of observations is insufficient to establish a robust relationship. Further investigation of this approach is warranted using more extensive datasets, perhaps initially using conventional measurements of $a^*_{ph_{total}}(\lambda)$ rather than size-fractionation data as they are more commonly measured.

As mentioned in section 2.2.3, size-fractionated measurements of phytoplankton absorption by physical separation of natural shelf sea communities have not been reported in the literature to date, hence the attempt to fill this data gap in this thesis. The measurements presented here support the relationships of cell size and a^*_{ph} presented by previous modelling studies based on optical theory and provide a basis for future measurements. As this nascent dataset of size fractionated absorption is small compared to the extant datasets of $a_{ph_{total}}(\lambda)$, the ability to produce robust empirical relationships with other physicochemical variables is limited. However, given the observed relationships between a^*_{ph} with ζ for nano- and picophytoplankton in this small dataset, additional sampling, particularly under microphytoplankton-dominated conditions, may allow researchers to further develop and refine existing methods used to estimate the shape and magnitude of $a^*_{ph}(\lambda)$ for shelf seas .

As $z_{eu}$is influenced by IOPs other than phytoplankton absorption, it would be prudent to make contemporaneous measurements of CDOM, TSM and particle backscattering alongside measurements of a_{ph}^{*} to contextualise differences in the relationships of a_{ph}^{*} with ζ across a range of case 1 to case 2 environments. Combined datasets of this type exist for the purposes of calibration and validation of ocean-colour remote sensing algorithms, but investigating the mechanistic links between IOPs and the absorptive properties of phytoplankton size classes would benefit efforts to model PP in optically complex waters.

Diagnostic pigments have been used to as indicators of phytoplankton size structure (Vidussi, Claustre et al. 2001) and to apportion community photo-physiological properties to individual size classes. Using unpackaged pigment-specific absorption coefficients, datasets of phytoplankton accessory pigments can be of further value in allowing the estimation of phytoplankton absorption spectra based that capture changes in pigment composition (Bidigare, Ondrusek et al. 1990) rather than using a fixed $a_{ph}^{*}(\lambda)$ for each size class. Plots comparing measured and reconstructed spectra (Fig 3.12) showed that the spectral shapes generated by the pigment reconstruction approach were inconsistent with measured values, with the blue peak of absorption being much narrower than is observed in natural samples. This shape can be attributed to soluble pigments *in vitro* not being subject to packaging as in living cells (Duysens 1956), therefore, the contributions of chlorophyll c, zeaxanthin and β-carotene, which absorb strongly in the blue are more prominent in pigment reconstructions than in measured spectra**.** Absorption coefficients were also higher and over a narrow band of wavelengths around the red peak of the reconstructed spectra than was observed with measured spectra. Overall, using unpackaged pigment specific absorption coefficients produced considerable anomalies in reconstructed spectra versus measured spectra (Fig 3.13), though spectrally-integrated total absorption showed reasonable agreement (Fig 3.14).

3.5.3 To what extent do differences in modelled phytoplankton absorption spectra influence calculated size-fractionated primary productivity?

There is considerable natural variability in phytoplankton specific absorption spectra between samples and individual size classes. This natural variability is common to each size class and therefore the total community (Fig 3.4, Fig 3.8), and alongside variability in chlorophyll concentration, contributes to variability in observed $a_{ph}(\lambda)$ (Fig 3.3, Fig 3.8). Phytoplankton absorption spectra generated using models from previous studies mirrored this variability. All models addressed in this chapter exhibit differences between the absorption properties of each size class with specific absorption coefficient increasing with decreasing cell size. However, some models were able to capture variability within size classes due to taxonomic changes within size classes (Ciotti, Lewis et al. 2002) and photoacclimatory changes in pigment compositon and packaging as a function of optical depth (Uitz, Huot et al. 2008

The relevance of these differences in phytoplankton absorption properties to the estimation of primary production comes in to the spectral correction of the photosynthetic parameter α^B and the modelling of downwelling photosynthetically-usable radiation at specific depths. The measured emission spectrum of the incubation light source and the phytoplankton absorption spectrum can be used to correct α^B to the solar spectrum. As the spectra of some models used in this chapter are fixed, the *X* value is constant for a given size fraction. As can be seen from Fig 3.13, despite considerable deviations in both shape and magnitude from measured *in situ* a^*_{ph} reasonable estimates of integrated? PP are obtained – the productivity rates of Varunan & Shanmugam (2015) are close to those using spectra with much lower chlorophyll-specific absorption coefficients. Therefore discrepencies between

modelled and measured PP is likely due to the spectral shape, since the magnitudes of the spectra are normalised to average absorption 400-700nm) in the calculation of the correction factor *X*. In other words, a greater mismatch between the shape of the lamp emission spectrum and phytoplankton absorption spectrum will likely influence α^B more than differences in the magnitude of $a^*_{ph}(\lambda)$ (equation 2.5).

Despite having markedly higher $a^*_{ph}(\lambda)$, the models of Varunan and Shanmugam (2015) and Uitz, Huot et al. (2008) showed good agreement with PP estimated using measured spectra, in particular for the nano- and picophytoplankton fractions (Fig 3.13). This may be explained by increased light attenuation caused by the higher chlorophyll-specific absorption coefficients, resulting in light becoming limiting deeper in thte water column where a large fraction of the phytoplankton biomass is located (e.g. SCM of during the August 2014). Though integrated values of primary production estimated by the two models were often quite close to those using measured spectra (Fig 17), profiles of carbon fixation differed. PP(z) was overestimated deeper in the water column both in the vicinity of the SCM and towards the bottom of the euphotic zone (Fig 3.15). Note that the impact of the choice of absorption spectra on PP(z) at the surface is minimal due to the presence of saturating light conditions under which the maximum rate of photosynthesis (P^B_m) operates. Since light attenuation ($K_d(\lambda)$) is governed by the absorption of the entire phytoplankton community, accurate estimates of $a^*_{ph_{total}}(\lambda)$ is more critical for modelling the underwater light field. The high specific absorption values of Varunan and Shanmugam (2015) led to only a slight underestimation in PP(z) at depth when compared to the Uitz, Huot et al. (2008) model since light was attenuated more quickly. The results presented in Fig 3.15 shows that none of the model runs using estimated values of $a^*_{ph}(\lambda)$ captured the vertical structure of PP well. PP estimates using the Uitz, Huot et al. (2008) spectra tended to overestimate PP, the Ciotti,

Lewis et al (2002) spectra led primarily to an underestimation of PP, whereas model runs using Varunan and Shanmugam (2015) size class spectra both over- and underestimated PP. This modelling exercise offer an important context to estimates of integrated daily PP (Tables 3.2, 3.3, Fig 3.15), as the accuracy of $PP(z)$ at specific depths is key to the utility of models of PP to investigations of wider biogeochemistry.

3.8 Conclusions

This study provides a novel dataset of *in situ* size-fractionated phytoplankton absorption measurements from a variety of stations across a temperate shelf sea during spring bloom and strongly-stratified (boreal) summer conditions. The relationship of chlorophyll-specific absorption spectra with phytoplankton cell size is consistent with the findings of previous studies using different methods both from samples taken from a variety of oceanographic regions and from phytoplankton cultures (Sathyendranath, Lazzara et al. 1987, Ciotti, Lewis et al. 2002, Fujiki and Taguchi 2002, Nair, Sathyendranath et al. 2008, Uitz, Huot et al. 2008, Mao, Stuart et al. 2010)(Ciotti et al., 2002; Fujiki & Taguchi, 2002; Mao et al., 2010; Nair et al., 2008; Sathyendranath, Lazzara, & Prieur, 1987; Uitz et al., 2008). However this dataset also revealed considerable variation in the spectral shapes and magnitudes of absorption within the three phytoplankton size fractions fig 3.13. Picophytoplankton spectra in particular showed a marked difference of some models and the samples taken in the Celtic Sea, most likely due to differences in prevalence of *Prochlorococcus* in datasets that include open ocean observations, with associated high absorption at blue wavelengths in surface picophytoplankton communities due to photoprotective pigments. The picophytoplankton $a^*_{ph}(\lambda)$ values presented by Ciotti et al (2002) for *Synechococcus* and picoeukayotes are much closer in magnitude to the Celtic Sea measurements of this study, suggesting that

picophytoplankton absorption should perhaps be separated based on whether *Prochlorococcus* is the dominant phytoplankter.

Despite these differences, when measured $a^*_{ph}(\lambda)$ values were replaced with estimated $a^*_{ph}(\lambda)$ values from Uitz et al. (2008) and Varunan and Shanmugam (2015) to compute water column PP using a spectrally-resolved model, the impact on estimates of integrated PP was small, although differences in the shape of the PP(z) profile was pronounced at some stations. Deviations in PP estimates at depth were likely caused by errors in $a^*_{ph}(\lambda)$ and consequently $K_d(\lambda)$ leading to anomalies in the modelled underwater light field.

The shortcomings of using modelled $a^*_{ph}(\lambda)$ values highlights the need to collect further measurements of S-F absorption in order to increase the accuracy and utility of model outputs from S-F PP models in temperate shelf and other regions.

Although the nascent global dataset of measured size-fractionated spectra is small, the addition of further measurements from future field campaigns will produce more reliable estimates of size-fractionated $a^*_{ph}(\lambda)$ through the water column in different regions, and may allow the development of more accurate models of phytoplankton absorption useful for other applications in the fields of marine bio-optics and remote sensing.

Calculating average spectra measured in the region of study allows the spectral correction of PE incubation α^B measurements where S-F measurements of absorption are missing, or of questionable accuracy, although this approach may have limitations if applied in regions that have large differences in $a^*_{ph}(\lambda)$ spectral shape within size fractions e.g. high light/ low light ecotypes of same taxon. To account for this, nano and picophytoplankton communities were separated by surface and thermocline sub groups and small differences in the magnitude but not spectral shape were observed for $a^*_{ph}(\lambda)$ in the Celtic Sea, meaning *X*

values should not be substantially different between surface and SCM communities. In addition, model spectra may augment datasets where insufficient *in situ* measurements are available to generate representative spectra for a specific size class. By employing these approaches a greater number of S-F α^B values can therefore be used with confidence to tune a new remote sensing primary production model specific to UK shelf seas in the following chapter.

4 Estimates of size-fractionated primary production from satellite

4.1 Introduction

4.1.1 Previous efforts to estimate S-F PP

Phytoplankton size classes and functional types have been incorporated into ecosystem and biogeochemical models for some time (Aumont et al. 2003; Baretta-Bekker et al. 1997; Moloney and Field 1991; Moore et al. 2001; Van den Berg et al. 1996). By including information on the photosynthetic properties of individual phytoplankton groups, models of phytoplankton primary production can partition total carbon fixation to size classes or functional types of interest. These models can subsequently be used to estimate the cycling of carbon and nutrients with respect to the considerable variability in group-specific rates, elemental stoichiometry and importance to grazers (Arrigo 2004; Finkel et al. 2009; Hessen et al. 2002; Poulton et al. 2017). Measuring primary production *in situ* at synoptic scales is not feasible and therefore relationships of phytoplankton photosynthetic activity with respect to light intensity and other variables such as temperature are often used with measurements or estimates of chlorophyll concentrations to estimate carbon fixation over a range of scales. However, despite *in situ* measurements of phytoplankton optics and size-fractionated (S-F) photo physiology being available from culture and field experiments, alongside increasingly well-validated satellite chlorophyll products, producing reliable estimates of integrated S-F primary production from satellite data remains problematic. Efforts to produce regional and global estimates of primary production using satellite data must combine accurate estimates of their respective biomasses (chlorophyll concentrations) with estimates of photosynthetic parameters for each size class, specifically light saturated

(P_m^B) and light-limited (α^B) photosynthetic rates. As relative biomasses and photo-physiologies of phytoplankton size fractions vary considerably throughout the oceans, with respect to hydrography, irradiance and biogeochemistry (Banse 1976; Bricaud et al. 2004; Kulk et al. 2012; Marañón et al. 2001; Mino et al. 2013; Moore et al. 2006),and cannot be measured from satellite, generalisations must be made when parameterising these components of primary production models.

4.1.2 Estimating phytoplankton size distribution from satellite

Total chlorophyll-a concentration in phytoplankton, used as an index of phytoplankton biomass, is typically estimated from the spectral shape of water leaving radiance at the satellite sensor after atmospheric correction, normally using a blue-green band ratio (outside of extreme case 2 waters) with specific coefficients for each sensor to ensure consistent estimates against a common validation dataset (Werdell and Bailey 2005). As successive ocean colour sensors have increased the spectral resolution of ocean colour observations (Blondeau-Patissier et al. 2014), algorithms to identify specific phytoplankton functional types from their optical properties have been proposed (Alvain et al. 2005; Astoreca et al. 2008; Nair et al. 2008), increasing the value of remote sensing products for researchers, environmental and public health agencies and marine businesses (Carvalho et al. 2010; Kurekin et al. 2014; Lubac et al. 2008). However, despite these advances in identifying phytoplankton types or cell sizes that dominate specific blooms, the complex optics of some marine regions means that although some phytoplankton groups – such as cyanobacteria and coccolithophores – are more easily detected (Kutser 2009), other groups can be more difficult to identify (Hunter et al. 2008). Identifying specific taxa is particularly difficult if sensor spectral resolution is too low, or bandwidths are too wide to capture small differences in water leaving radiances (indicative of changes to phytoplankton absorption spectral

shapes). Hyperspectral platforms are a promising means of overcoming some of the difficulties in identifying phytoplankton functional types from satellite (Uitz et al. 2015; Xi et al. 2015) and will support continued improvements in estimates of IOPS, particularly in case 2 regions (Guanter et al. 2015; Sathyendranath et al. 2017; Wolanin et al. 2016). Enabling the discrimination of phytoplankton taxa using reflectance data by making use of subtle differences in spectral absorption increases the usefulness of ocean colour data in wider biogeochemical and ecological research and monitoring (Mouw et al. 2017; Organelli et al. 2017; Vandermeulen et al. 2017). However, hyperspectral ocean colour sensor datasets are not as extensive as for multispectral platforms, which offer a wealth of observations over many decades from CZCS to modern sensors such as OLCI and VIIRS.

Despite the significant gap in the ocean colour "record" between 1986-1997 between CZCS and SeaWIFS, there is a broken time series of satellite chlorophyll measurements of nearly 40 years which is of great benefit in the study of climate change impacts of phytoplankton phenology and distribution, if not biomass and short term or regional dynamics (Racault et al. 2014). Since 1997, successive ocean colour missions have overlapped, allowing cross-calibration of their respective sensors and the production of merged datasets of various products, including chlorophyll. The use of these merged products allows quantitative analysis of regional, seasonal and interannual variability, as well as investigation of the effects of specific climate oscillations such as El Niño on phytoplankton dynamics.

In this chapter, I take the measured hydrographic and photophysiological parameters including the spectrally corrected S-F light-limited photosynthetic rates (see Chapter 1 and 2) and attempt to make estimates of primary production over an annual cycle in the UK Shelf Seas, through tuning an existing ocean-colour based primary production model (Brewin, Tilstone, et al. 2017). Initially I aimed to establish the performance of this model for estimating size-fractionated primary production from remote sensing data in UK shelf seas.

Initially developed using *in situ* measurements from the Atlantic Ocean (Brewin et al. 2017b), here I tune the model to the UK Shelf seas. Measurements from the Celtic Sea and Western English Channel were used to test the representativeness of this model's parameterisation and subsequent output and thereafter re-tune the model to the region of interest. I investigate the differences in PP estimates of different size fractions and their seasonal variability from both the original and regionally-tuned model and discuss potential sources of error due to the hydrographic and biological differences across the UK shelf and between shelf and open ocean waters.

4.2 Methods

4.2.1 Estimating primary production using the available light model of Brewin et al (2017)

In order to generate estimates of size-fractionated primary production over the NW European shelf seas, the model of Brewin et al. (2017b) (eq.1) was used in the calculation of daily integrated primary production, expressed in units of g C m^{-2} d^{-1}. This model was chosen for two reasons

1. It is parameterised using measurements of size-fractionated chlorophyll and photophysiology conducted using the same methodology as samples of this study.

2. Samples are taken from the Atlantic, including many North Atlantic data, the adjoining open-ocean region to the Celtic Sea and English Channel which were the sampling locations of this study.

The measurement datasets, parameters and equations used to run this model and the various changes made to re-tune to a shelf sea dataset are outlined below. This is achieved by changing parameter values to match shelf sea measurements and recalculating regression coefficients of photophysiology and biomass with depth and light.

$$PP = \int_{t=0}^{D} \int_{z=0}^{1.5Z_{eu}} \sum_{i=1}^{3} B_i(z) P_{m,i}^{B}(z) \left[1 - \exp\left(-\frac{\alpha_i^B(z)E(z,t)}{P_{m,i}^{B}(z)}\right)\right] dz\, dt \qquad (4.1)$$

Equation 4.1 The formulation of the model of daily primary production used in this study. Parameterised through the euphotic zone using photosynthetic parameters and available light (Platt et al. 1980b), with depth-resolved estimates of community size structure, chlorophyll biomass and irradiance (Brewin et al. 2017b).

Where D is day length, $Z_{eu}$is euphotic depth (depth of 1% of surface photosynthetically available radiation (PAR)), z is depth, t is time. Subscript i denotes size fraction e.g. micro (>20µm), nano (2-20µm), pico (<2µm) used with respect to light-saturated ($P_{m,i}^{B}$) and light-limited (α_i^B) photosynthetic rate values and chlorophyll biomass (B_i). These size ranges are consistent with the model of Uitz et al. (2008) and differ from the model of Brewin et al. (2017b) which defines microphytoplankton as >10µm due to the limited concentrations of cells above 20µm in Atlantic waters.

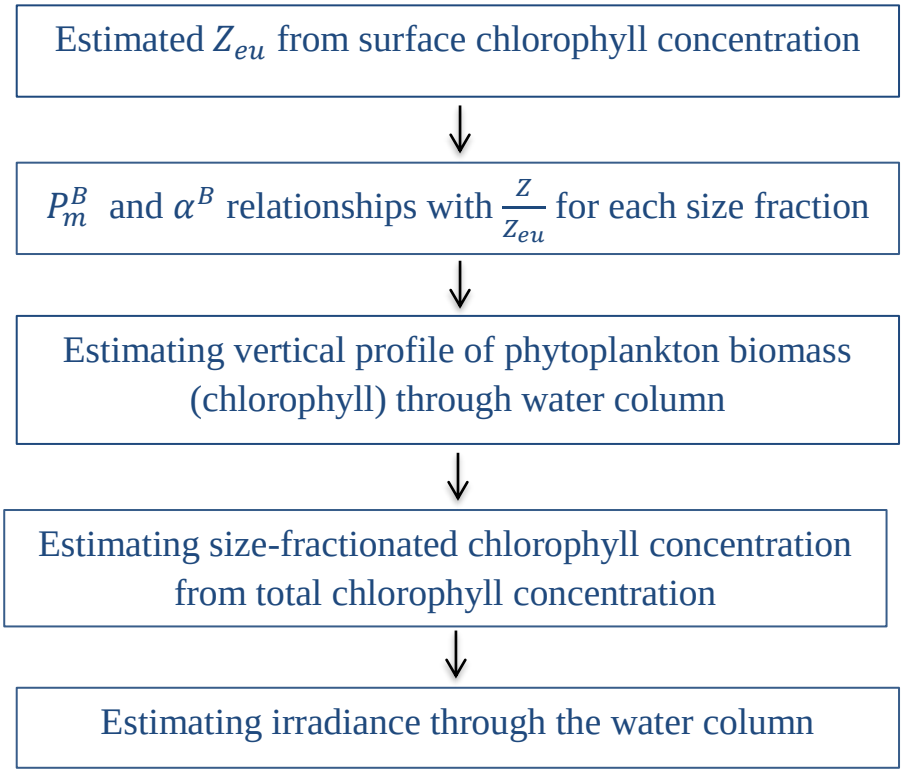


Fig 4.1 (Preceding page) Variables and parameters required to calculate size-fractionated primary production using the model of Brewin et al (2017)

4.2.2 Euphotic Depth

CTD rosette-mounted downwelling PAR sensors (Biospherical Cosine 2-pi sensor) were used at WCO sampling stations and both Celtic Sea cruises to estimate euphotic depth (Z_{eu}) as the depth at which downwelling PAR was 1% of surface irradiance. Values of $\frac{Z}{Z_{eu}}$ could then be generated for each sample depth for phytoplankton photophysiology and chlorophyll concentration. In addition, measured Z_{eu} and surface chlorophyll concentrations were used to test whether Z_{eu} can be estimated accurately from satellite observations of chlorophyll concentration in the UK shelf. This comparison included data from previous cruises to the Celtic Sea and Irish Sea (JR98, CD173) (Hickman et al. 2009; Hickman et al. 2012) which were plotted together with measurements of this study against the equation of Morel et al. (2007), modified by Brewin et al. (2017b) who used a dataset of Atlantic Ocean measurements to produce new coefficient values was plotted (equation 2) (Fig 4.5).

$$Z_{eu} = 10^{[q_a + q_b \log_{10}(B_s) + q_c \log_{10}(B_s)^2 + q_d \log_{10}(B_s)^3]} \quad (4.2)$$

Equation 4.2 Calculation of euphotic depth (Z_{eu}) from surface chlorophyll concentration (B_s) (Brewin et al. 2017b)

4.2.3 Vertical variability in chlorophyll-a concentration

Vertical biomass profiles were calculated as shifted Gaussian distributions normalised to surface chlorophyll concentrations following Brewin et al. (2017b) (parameter *B* in equation 4.3), such that ocean colour surface chlorophyll data could be used to parameterise the vertical distribution of phytoplankton chlorophyll concentration. In order to test the accuracy of this method for determining *B*, *in situ* data of chlorophyll concentration (at > 4 depths to

produce interpolated profiles), mixed layer depth (Z_m) and euphotic depth (Z_{eu}) were taken to compare with the existing parameterisation and allow re-tuning to shelf waters.

$$B^{B_s}(\zeta) = 1 - S^{B_s}\zeta + B_m^{B_s} exp\{-[(\zeta - \zeta_m)/\sigma]^2\} \quad (4.3)$$

Equation 4.3 Calculation of the vertical distribution of phytoplankton biomass (chlorophyll concentration) with respect to surface chlorophyll (B^{B_s}) (Brewin et al. 2017b)

Where B^{B_s} is the chlorophyll concentration profile normalised to surface concentration at dimensionless depth, ζ, S^{B_s} is the background linear decrease of $B^{B_s}$with increasing ζ, $B_m^{B_s}$ is the maximum chlorophyll concentration, ζ_m is the dimensionless depth at which $B_m^{B_s}$ occurs and σ is the width (in terms of ζ) of the $B_m^{B_s}$ peak biomass.

4.2.4 Photophysiological parameters

To model primary production (Equation 4.2) requires a description of how P_m^B and α^B change with depth, in order to calculate rates of carbon fixation for a given irradiance (E) and chlorophyll concentration at any specific depth $B(z)$.The methods used to sample S-F chlorophyll, photosynthetic rates P_m^B and α^B, euphotic depths and dimensionless depth ζ during this study are detailed in chapter 1.

As these photosynthetic parameters exhibit regional and vertical variability (see chapter 1) and cannot be observed remotely in the way that chlorophyll or PAR can, I modelled P_m^B and α^B as a function of dimensionless depth (ζ) by retuning the model of Brewin et al. (2017) (adapted from Uitz et al. (2008), using size-fractionated measurements made in the Celtic Sea and Western English Channel. I compared my results with the original parametrisation of Uitz et al. (2008), and the Atlantic parameterisation by Brewin et al. (2017b) (Fig 4.4). Table 1 shows the mean surface values and their respective slopes with ζ for the original Atlantic parameterisation of the Brewin et al (2017) model, and when retuned using the

values measured during this study, indicating the much greater differences in light-limited photosynthetic rates (α^B) than light-saturated rates (P_m^B).

Table 4.1. Average surface values of α^B and P_m^B and their slope values S^{Bs} and S^{α_s} with respect to dimensionless depth ζ for UK shelf data (this study) and under the original parameterisation using Atlantic data Brewin et al. (2017b).

Parameter	Size Class	UK Shelf Model	Atlantic Model	Shelf Values % of North Atlantic Values
$P_m^{B_s}$	Micro	4.27 (±0.25)	6.05 (±0.98)	70.6
	Nano	4.43 (±0.28)	5.13 (±0.94)	86.4
	Pico	5.51 (±0.30)	3.46 (±0.80)	159.2
α^{B_s}	Micro	0.047 (±0.027)	0.016 (±0.004)	293.8
	Nano	0.050 (±0.032)	0.014 (±0.003)	357.1
	Pico	0.062 (±0.031)	0.011 (±0.001)	563.6
S^P	Micro	0.49 (±0.34)	0.35 (±0.27)	140.0
	Nano	0.38 (±0.32)	0.59 (±0.29)	64.4
	Pico	0.45 (±0.28)	0.68 (±0.31)	66.2
S^{α_s}	Micro	0.51 (±0.32)	−0.07 (±0.30)	−728.6
	Nano	0.25 (±0.29)	−0.12 (±0.23)	−208.3
	Pico	0.30 (±0.29)	−0.32 (±0.17)	−93.75

4.2.5 Irradiance

Irradiance values (PAR) used in the estimation of PP are required by equation 4.1 through the euphotic zone and at hourly intervals (*t*) over day length *(D)* (hours). The estimation of downwelling irradiance using remote sensing data is summarised below, from just below surface values through the euphotic zone using relationships in attenuation with surface and sub-surface chlorophyll concentrations.

$$E(0-,t) = \frac{E_m(0-)\sin(\frac{\pi t}{D})}{3600} \quad (4.4)$$

Where $E(0-,t)$ is the hourly average irradiance just below the surface at time step *t*, $E_m(0-)$ is the maximum irradiance at midday just below the surface. Dividing by 3600 converts hours units of day length into seconds units common with PAR and α^B (µmol m^{-2} s^{-1}). For each hourly time step (*t*), changes with irradiance (*E*) with depth (*z*) are modelled with respect to diffuse attenuation of PAR.

$$E(z,t) = E(0-,t)\exp[-K(z)z] \quad (4.5)$$

Where $K(z)$ is the diffuse attenuation coefficient of PAR (K) at depth (z), which can vary with depth due to changes in water column optical properties. $K(z)$ is estimated at specific depths as a function of chlorophyll concentration $B(z)$ and background PAR attenuation K_c. To estimate $K(z)$, the average attenuation coefficient must be known, which is generated following equation (4.6)

$$K_{Zeu} = 4.6/Z_{eu} \quad (4.6)$$

Where and K_{Zeu} is the average attenuation coefficient through the euphotic zone derived from the estimated euphotic depth Z_{eu} using surface chlorophyll and equation (4.2) (Fig 4.5)

$$K(z) = \left[(K_{Zeu} - K_c)\left(\frac{B(z)}{1/N\sum_{j=1}^{N} Bj}\right)\right] + K_c \quad (4.7)$$

Where K_c denotes the background attenuation of PAR independent of phytoplankton biomass and depth – assumed to be due to pure water (Pope and Fry 1997) $1/N\sum_{j=1}^{N} Bj$ represents the average chlorophyll concentration through the biomass profile of $B(z)$.

4.2.6 Satellite datasets

The model of Brewin et al. (2017b) (equation 1) requires three satellite data values for each pixel in order to generate integrated size-fractionated primary production estimates: Surface chlorophyll concentration (B_s); estimates of photosynthetically available radiation (PAR); estimates of mixed layer depth (Z_m).

Estimates of B_s were taken from the Ocean-Colour Climate Change Initiative (Version 3.1, hhtp://www.oceancolour.org/), which is an error-characterised time series of merged ocean colour data from a number of satellite missions (SeaWiFS, MODIS Aqua, MERIS, VIIRS).

For estimates of PAR, MODIS-Aqua level-3 PAR data were extracted at 4x4km resolution for 2016 (https://modis.gsfc.nasa.gov/data/dataprod/ipar.php). Mixed layer depth values were estimated using monthly average climatological values from de Boyer Montégut et al. (2004) (http://www.ifremer.fr/cerweb/deboyer/mld/home.php).

4.3 Objectives

By estimating the vertical profile of phytoplankton biomass, daily broadband light environment and phytoplankton size distribution from surface chlorophyll, it is thereafter possible to generate primary production estimates for each size fraction from remote sensing chlorophyll datasets for our region of interest, using the photophysiology parameters and their relationships with ζ.

The following analysis investigates how well an existing model of S-F PP – which is tuned using Atlantic data taken using the same methods as this study – matches the observed relationships in photophysiology and primary production measured and estimated for the UK Shelf. Subsequently, a climatology of remote sensing chlorophyll data (monthly composites) will be used with both open Atlantic (Open Sat) and UK Shelf (Shelf Sat) model parameterisations to quantify the differences in S-F PP estimates between both models over an annual cycle in UK shelf waters.

4.4 Results

4.4.1 Modelling size-fractionated chlorophyll from total chlorophyll

To estimate size-fractionated chlorophyll from values of total chlorophyll through the water column, we adopted the model of Brewin et al. (2017a). This model estimates the

chlorophyll in three size classes as a continuous function of total chlorophyll. The model follows the work of Sathyendranath et al. (2001) and assumes as total chlorophyll concentration increases the community size structure changes from picophytoplankton dominated in low-chlorophyll regions such as the gyres to microphytoplankton dominated in high-chlorophyll regions such as temperate shelf seas or upwelling zones. Nano and picophytoplankton reach asymptotic chlorophyll concentration values (C_n^m, C_p^m), such that C_p does not increase above 0.13 mg m^{-3}, and C_n does not increase above 0.82 mg m^{-3}, beyond which additional chlorophyll is apportioned to microphytoplankton (Fig 4.2). Results indicate that microphytoplankton biomass follows the model as total chlorophyll increases, but nano and picophytoplankton data can extend beyond the asymptotic values at high total chlorophyll concentrations. The high degree of variability in relative contribution of each size class to total chlorophyll cross a range of values can also be seen as the scatter in the respective F_i values.

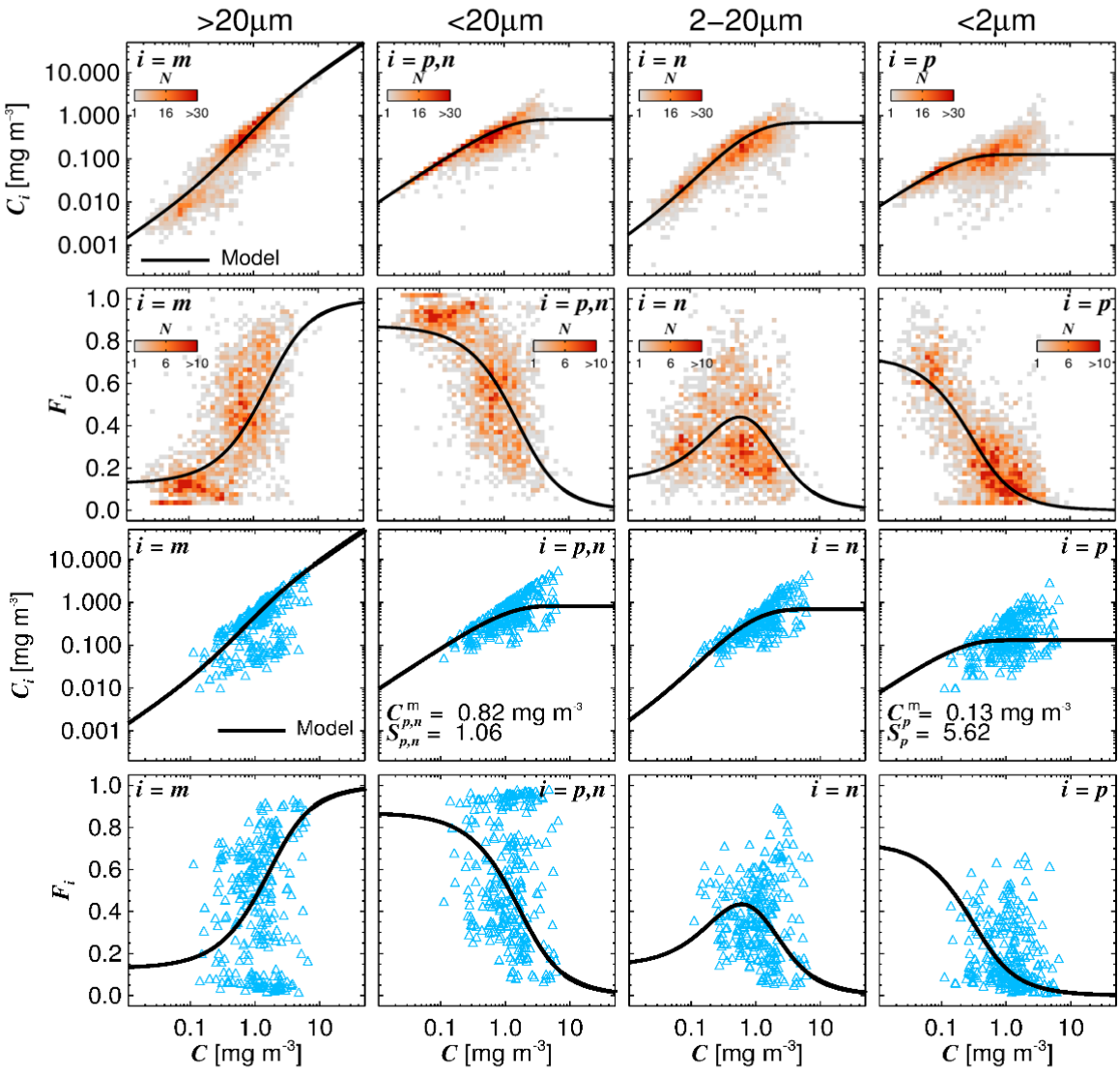


Fig 4.2 Brewin et al. (2017b) model of size-fractionated chlorophyll scaled to total chlorophyll concentration showing the original North Atlantic dataset (top, red panes) and model relationships overlaid with observed values taken from the Celtic Sea and Western English Channel during this study (bottom, blue panes). Size-fractionated chlorophyll concentrations C_i increase with total chlorophyll concentration C and the fractional contribution of individual size fractions F_i to total chlorophyll concentration are also shown.

A tuning of the model was attempted to Celtic Sea and Western English Channel data of size-fractionated and total chlorophyll concentrations, but model fit was not increased significantly, and thus the North Atlantic model parameterisation of Brewin et al. (2017a) was retained.

4.4.2 Comparison of measured and modelled photo-physiological parameters

Values of size-fractionated photo-physiological parameters with respect to the dimensionless depth ζ as used by Atlantic model of Brewin et al. (2017b) were tested with measured values from this study to identify whether either of these parameterisations was suitable for the UK shelf seas, and if not, whether a model could be tuned to different parameter values scaling with ζ .

Values of P_m^B and α^B were modelled at specific values of ζ by Brewin et al. (2017b); Uitz et al. (2008) using:

$$P_{m,i}^B = P_{m,i}^{B_s}\exp(-S_i^P\zeta) \quad (4.8)$$

$$\alpha_i^B = \alpha_i^{B_s}\exp(-S_i^\alpha\zeta) \quad (4.9)$$

Equations 4.8, 4.9 calculation of P_m^B and α^B at specific dimensionless depth ζ from mean surface values $P_{m,i}^{B_s}$ and $\alpha_i^{B_s}$ and respective slopes S_i^P and S_i^α (Brewin et al. 2017b)

Where $P_{m,i}^{B_s}$ and $\alpha_i^{B_s}$ are surface values when ζ~0, S_i^P and S_i^α are slope values quantifying the change in $P_{m,i}^B$ and α_i^B from surface values with respect to ζ.

Fig 4.3 shows the differences between the values of P_m^B and α^B estimated by both aforementioned models and a retuned model using the parameters that I derived for shelf waters. The model of Brewin et al. (2017b) is only used for comparison of the pico fraction due to differences in cell size ranges, as microphytoplankton are defined as being >10µm by Brewin, Tilstone, et al. (2017).

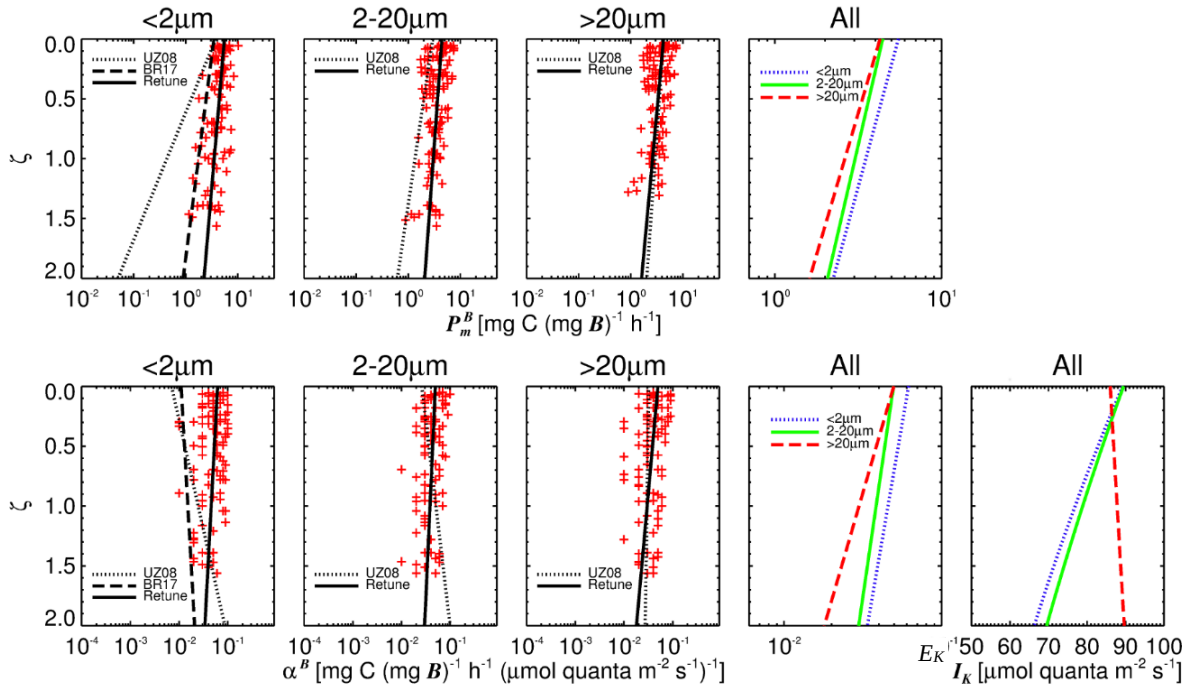


Fig 4.3 Relationship of P_m^B and α^B with respect to ζ for each size class using the retuned shelf model (black lines) with the models of Uitz et al. (2008) (dotted lines) and Brewin et al. (2017b) (dashed lines). Values for light saturation parameter E_k of retuned model in bottom right pane.

Measured values of P_m^B follow a similar trend with respect to ζ compared to other models (Fig 4.3). However, mean measured surface values of P_m^B and α^B were highest for pico and smallest for microphytoplankton, an opposite trend with cell size to the open ocean measurements used to parameterize the models of Uitz et al. (2008) and Brewin et al. (2017b). Picophytoplankton had significantly higher mean surface values than the larger fractions and followed a similar reduction with increasing ζ. However, given the considerable variability of parameter measurements for each size class, none of these slopes are significantly different from a vertically constant value.

When compared to the profiles of Uitz et al. (2008), differences in microphytoplankton photo physiology are less pronounced than for the smaller fractions, with similar mean surface values of $P_{m,i}^{B_s}$ and $\alpha_i^{B_s}$ and slopes S_i^P and S_i^α. Nano and pico fractions have greater $P_{m,i}^{B_s}$ and particularly $\alpha_i^{B_s}$ values when compared with the values of Uitz et al. (2008) and

Brewin et al. (2017b) (pico only). Pico values of S_i^P are closer to those reported by Brewin et al. (2017b) while the negative trend of picophytoplankton S_i^α values with ζ common to Uitz et al. (2008) and Brewin et al. (2017b) models is not observed in the measurements of this study. The light saturation parameter E_k calculated as $(\frac{P_m^B}{\alpha^B})$ follows a negative trend with ζ for pico and nano fractions – which were of similar magnitude – while a slight positive trend is observed for microphytoplankton, which have substantially greater values of E_k than smaller fractions at ζ >0.5.

4.4.3 Estimates of euphotic depth from surface chlorophyll

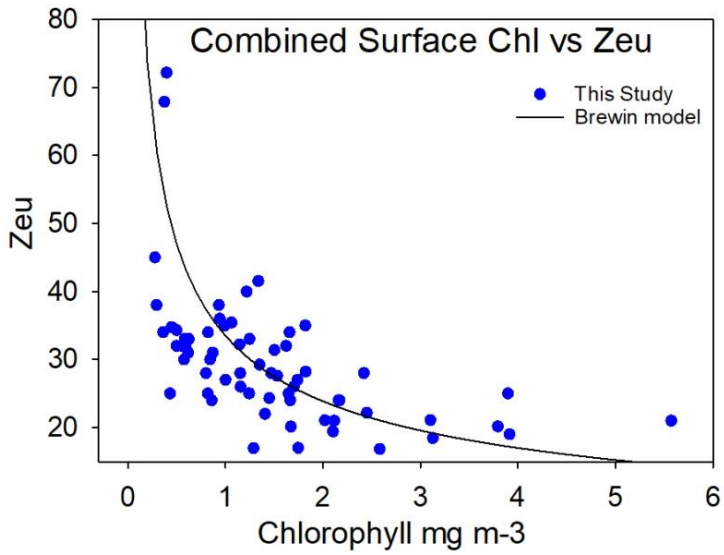


Fig 4.4 *In situ* measurements of surface chlorophyll and euphotic depth Z_{eu} measured in the Western English Channel and Celtic Sea during four separate cruises (DY026, DY029, JR98, CD173)(Hickman et al. 2009; Hickman et al. 2012). The model of Brewin et al. (2017b) (equation 4.3) is overlaid to indicate agreement with measured shelf sea data.

Fig 4.4 shows measured surface chlorophyll concentrations and euphotic depth from the western channel and the Celtic Sea. Observations were in good agreement with the re-tuned algorithm of Brewin et al. (2017b), though showing a considerable degree of variability at lower chlorophyll values (<0.7mg m^{-3}). With these results it is possible to use surface chlorophyll concentration to estimate euphotic depth with some confidence, although the

scatter may indicate that CDOM and TSM may not co-vary consistently with surface chlorophyll.

4.4.5 Vertical distribution of phytoplankton biomass

An accurate estimate of the distribution of phytoplankton biomass though the photic layer is required for accurate estimates of primary production in available light models as phytoplankton biomass is a key variable in light attenuation calculations as well as PP (equations 4.1, 4.2, 4.7).

As sub-surface chlorophyll maxima were common to both Western English Channel and Celtic Sea datasets, non-uniform profiles of biomass (chlorophyll concentration) were used.

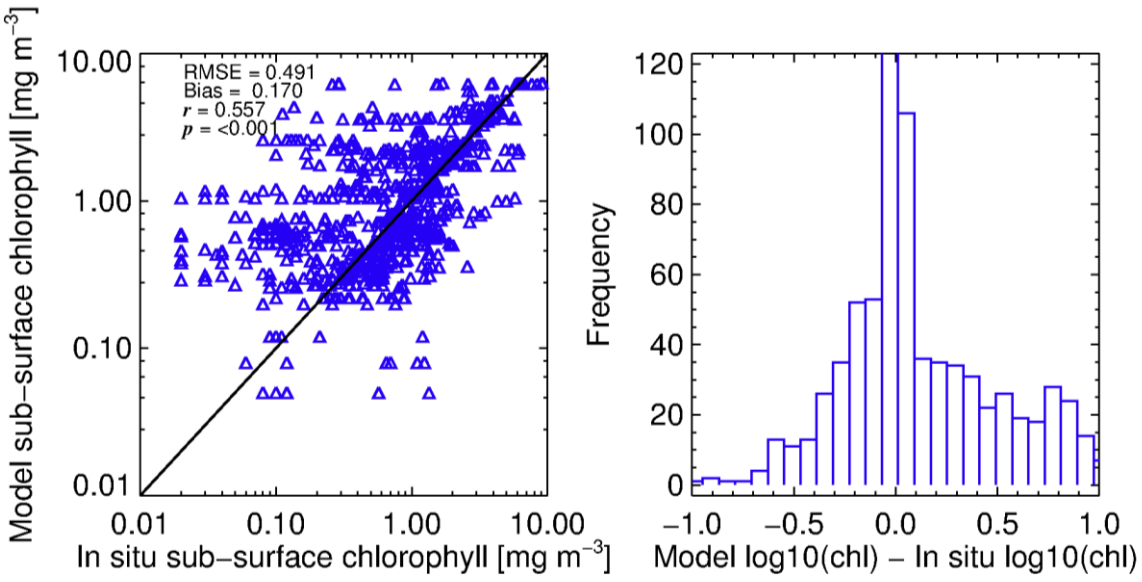


Fig 4.5 Modelled sub-surface chlorophyll calculated using equation 4.3 assuming a well-mixed water column vs profiles of *in situ* measurements of chlorophyll from UK shelf seas.

Fig 4.5 shows the non-uniform distribution of modelled to measured sub-surface chlorophyll when a vertically homogenous distribution of chlorophyll is assumed (i.e. mixed conditions). Although highly significant, the correlation is poor, with model chlorophyll values' invariance with depth represented by bands of values with respect to *in situ* profiles.

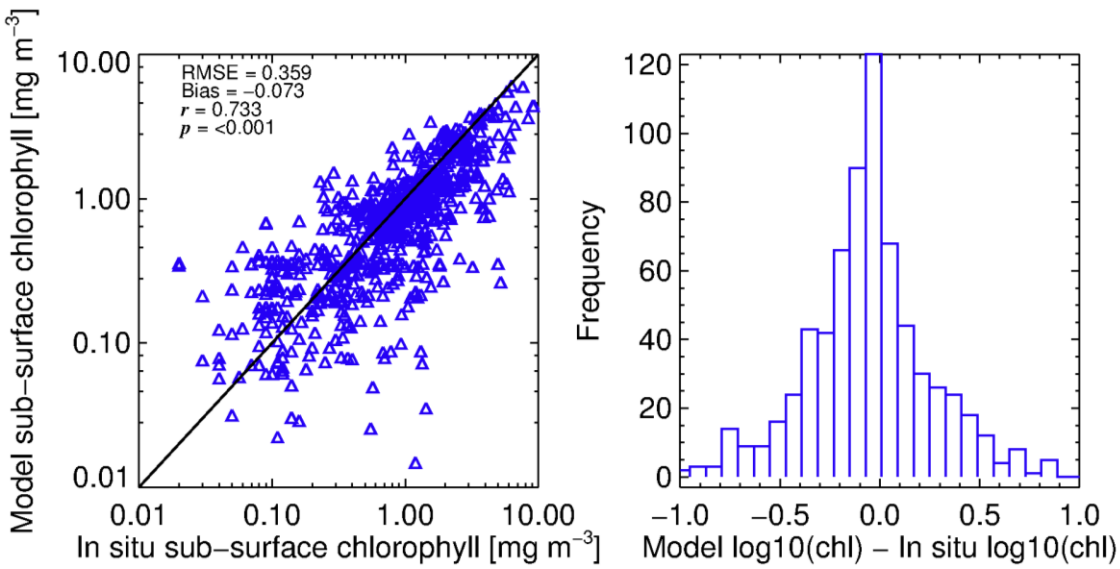


Fig 4.6 Modelled sub-surface chlorophyll calculated using equation 4.3 assuming a stratified water column vs profiles of *in situ* measurements of chlorophyll from UK shelf seas.

Fig 4.6 Shows the improvement in model skill when permanent stratification is assumed, with a Gaussian biomass distribution around a sub-surface maximum. The distribution of observed vs measured values plotted via regression is more normal, with reduced bias and RMSE compared to a uniform profile, indicating that this parameterisation is more representative for the Celtic Sea and Western English Channel sites.

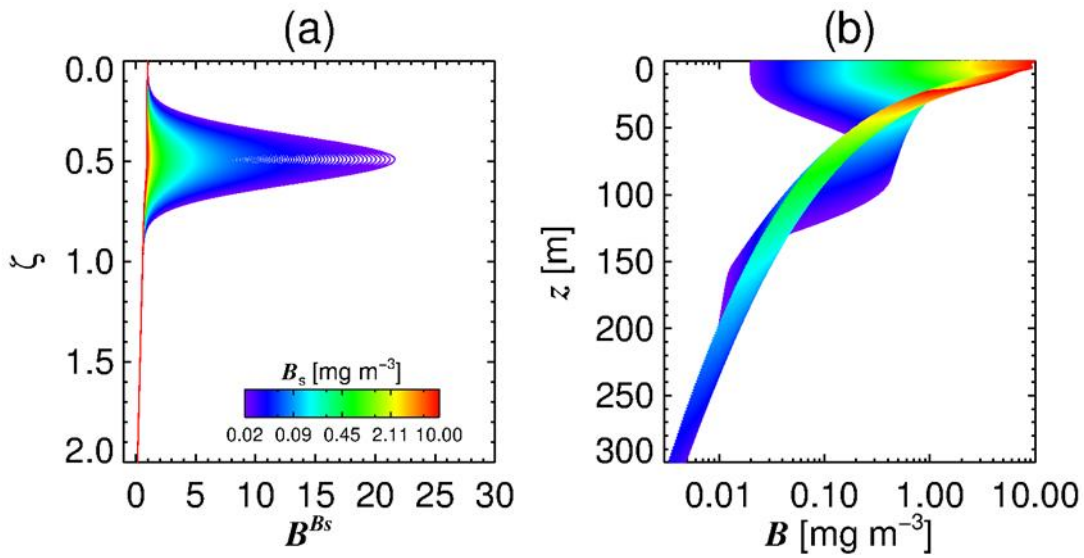
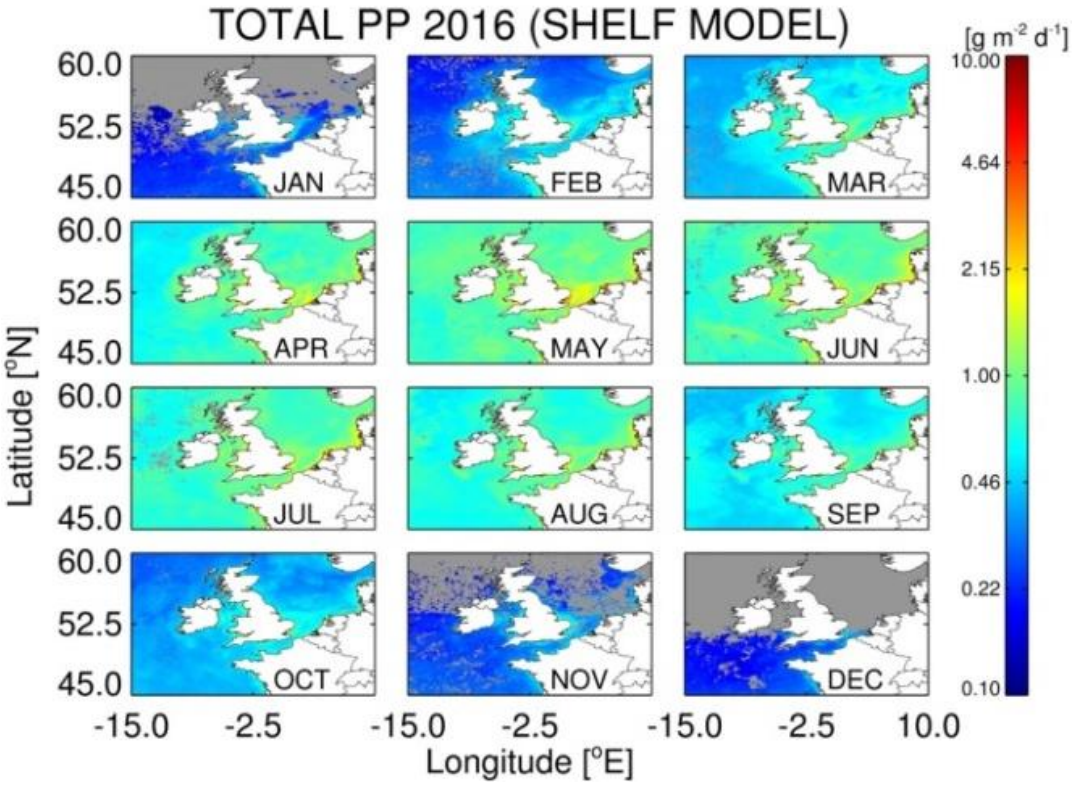


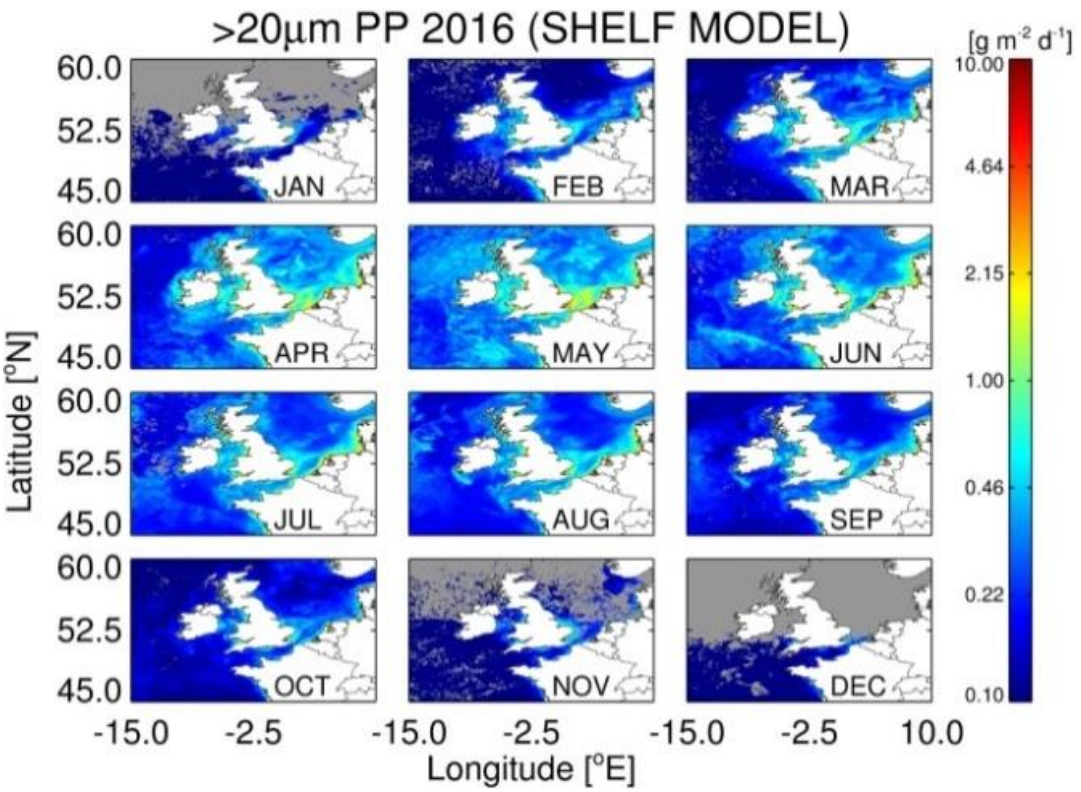
Fig 4.7 (a) shows the relative biomass (B^{Bs}) with respect to dimensionless depth (ζ) and surface chlorophyll concentration(B_s), and (b) the absolute concentration of chlorophyll at specific depths across a range of surface chlorophyll values.

Compared to the values reported by Brewin et al. (2017b), where the peak of phytoplankton biomass resides at between ζ =0.8-1.2, Fig 4.7 indicates that the shelf sea data used here produce a peak biomass at shallower depths within the photic zone.

4.4.6 Estimates of annual PP from ocean colour data

Using the original (Open Sat) and refined (Shelf Sat) algorithms, we estimate size-fractionated primary production using remote sensing chlorophyll and PAR products for 2016, meaning results are not biased toward the shelf dataset sampled during 2014-2015. Differences in model output was subsequently calculated as a positive or negative anomaly (figs 4.10 - 4.12), and subsequently compared with climatological means of monthly PP at the Western English Channel station L4, where a time series of total PP calculated using measured PE parameters was available (Chapter 1).


TOTAL PP 2016 (SHELF MODEL)
[g m-2 d-1]
10.00
4.64
2.15
1.00
0.46
0.22
0.10
JAN
FEB
MAR
APR
MAY
JUN
JUL
AUG
SEP
OCT
NOV
DEC
60.0
52.5
45.0
-15.0
-2.5
10.0
Latitude [°N]
Longitude [°E]


>20µm PP 2016 (SHELF MODEL)
[g m-2 d-1]
10.00
4.64
2.15
1.00
0.46
0.22
0.10
JAN
FEB
MAR
APR
MAY
JUN
JUL
AUG
SEP
OCT
NOV
DEC
60.0
52.5
45.0
-15.0
-2.5
10.0
Latitude [°N]
Longitude [°E]

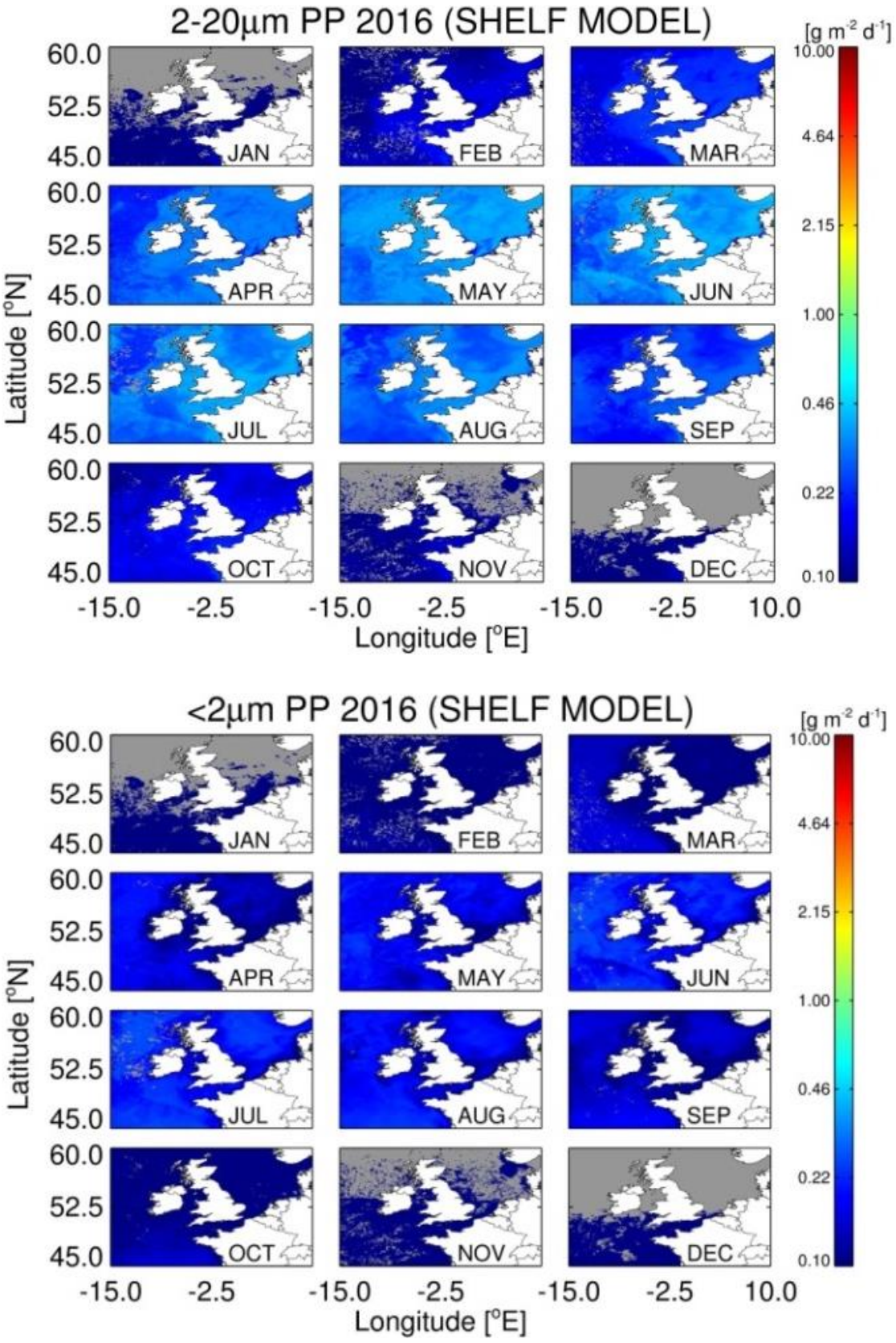


Fig 4.8 (Including panes on previous page) Estimates of total and size-fractionated PP using the retuned shelf model run with the monthly composites of ESA OC-CCI chlorophyll product data (Jackson et al. 2017) and NASA MODIS-Aqua PAR.

Total daily integrated primary production peaked in April, with open shelf regions having values of 0.6-1.7 g m^{-2} $d^{-1,}$ with the highest values of 4-6 g m^{-2} d^{-1} being found in areas with correspondingly high chlorophyll concentrations, principally estuarine regions such as the Thames estuary, The Wash, The Rhine Delta etc. As these high chlorophyll areas are modelled as being dominated by cells >20µm, PP is dominated by microphytoplankton.

Nanophytoplankton (2-20µm) PP is lower and more uniformly distributed than microphytoplankton with values of 0.3-0.5 g m^{-2} d^{-1} April – August, as under the model used, nanophytoplankton peak at around 40% of total chlorophyll concentration (Fig 4.2), and have similar photosynthetic rates to microphytoplankton (Table 4.1, Fig 4.3), therefore do not have the defined regional peaks and minima of PP as micro and picophytoplankton.

Picophytoplankton account for the lowest proportion of total PP, never exceeding 0.4 g m^{-2} d^{-1}. As they are the least abundant fraction at high chlorophyll concentrations, they follow an inverse pattern to microphytoplankton in the distribution of their maximal PP, with lower PP in coastal regions and often relatively higher PP in off-shelf areas.

4.4.7 Differences with open ocean parameterisation (Open Sat) of Brewin et al (2017) model

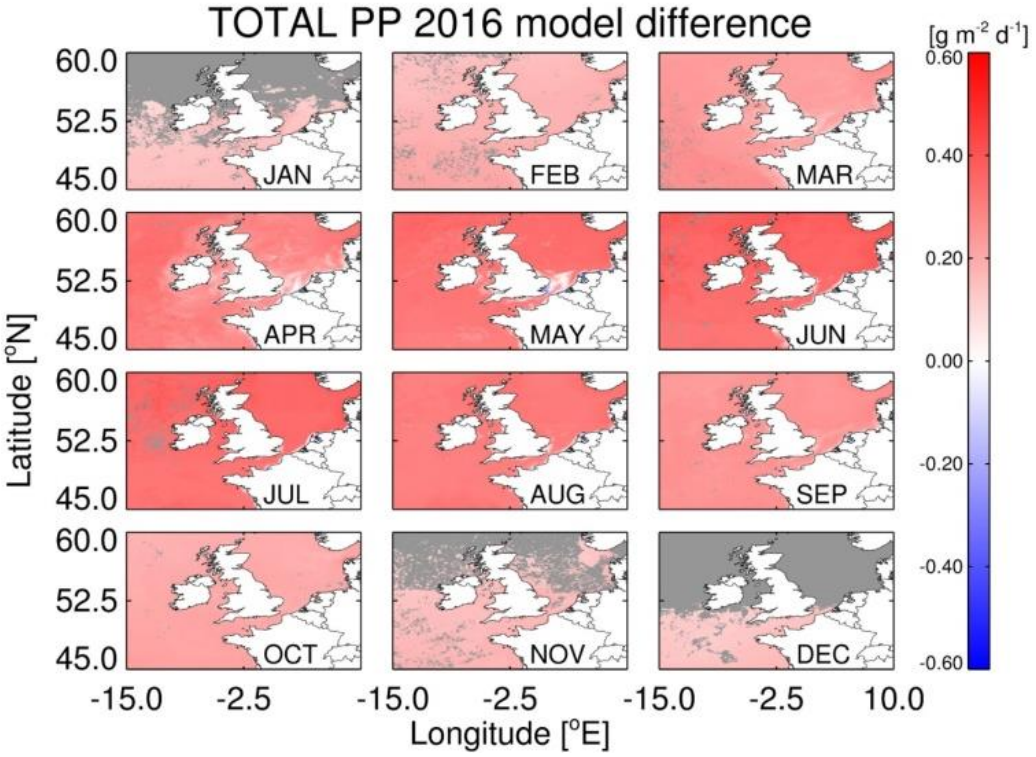


Fig 4.9 Calculated difference in monthly total PP using the retuned shelf model (Shelf Sat) (Fig 4.8) instead of the original North Atlantic model tune (Open Sat). Values are the absolute anomalies showing the increased estimates of PP using the Shelf Sat model.

Running primary production estimates with the shelf sea data tuned photophysiology and biomass profile equations produced an increase in total PP over the open ocean model of Brewin et al. (2017b) of 0.06 -0.5 g m^2 y^{-1}, with the greatest differences observed between May and July. The relative overestimation of the re-tuned model was lower in coastal regions, particularly around estuarine plumes, where total PP was highest.

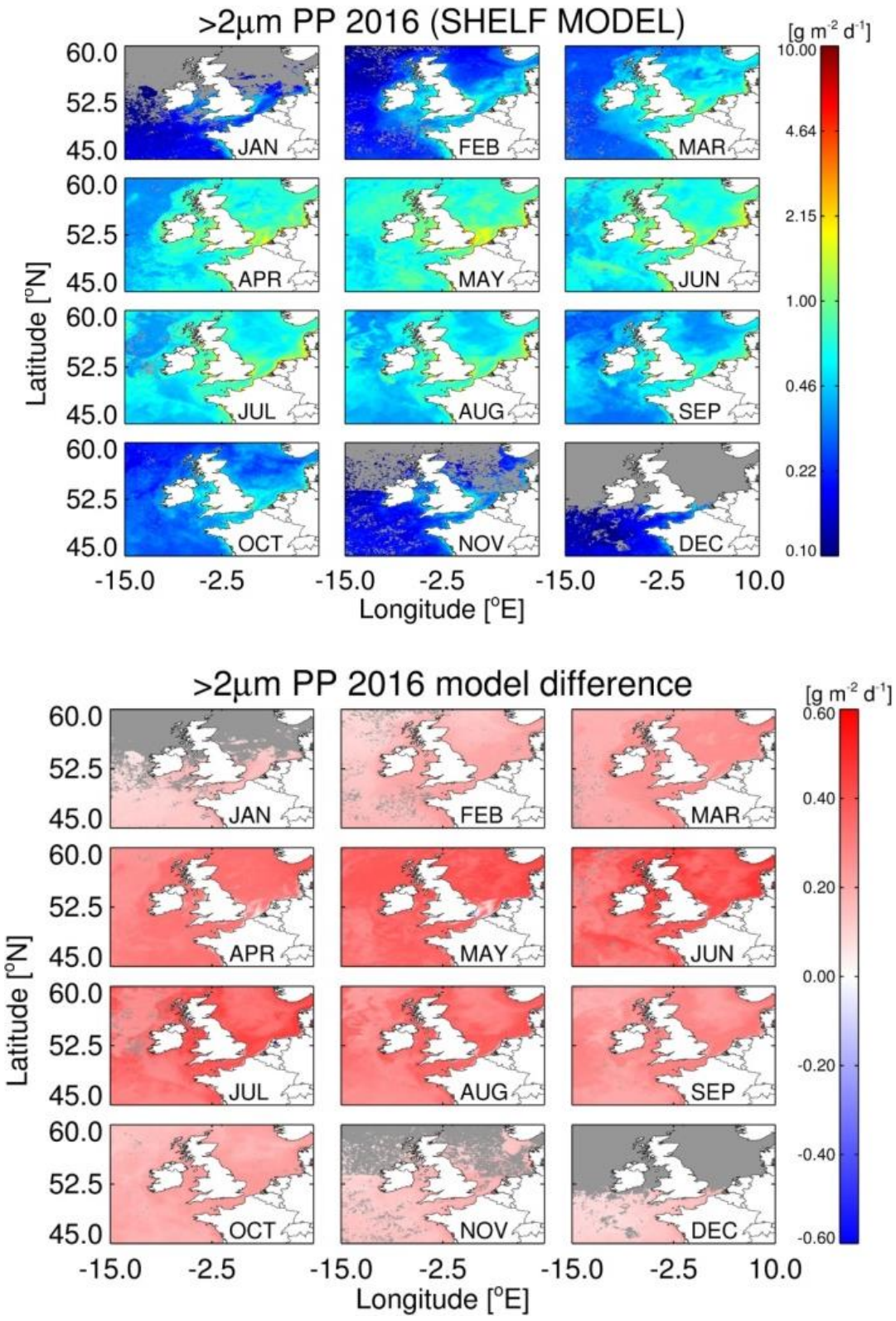


Fig 4.10 Estimates of monthly micro + nanophytoplankton PP using the Shelf Sat model (top panel) and the difference in micro + nanophytoplankton PP estimated by the Shelf Sat and Open Sat models (bottom panel) as in fig 4.9.

Combined estimates of micro and nanophytoplankton PP (which accounts for the difference in fractionation sizes between the two models) contributes the greatest proportion in the relative overestimation in total PP vs the model of Brewin et al. (2017b). Values were consistently higher across all months, with the most productive regions generally having the greatest levels of overestimation, consistent with the highest chlorophyll concentrations around coastal regions.

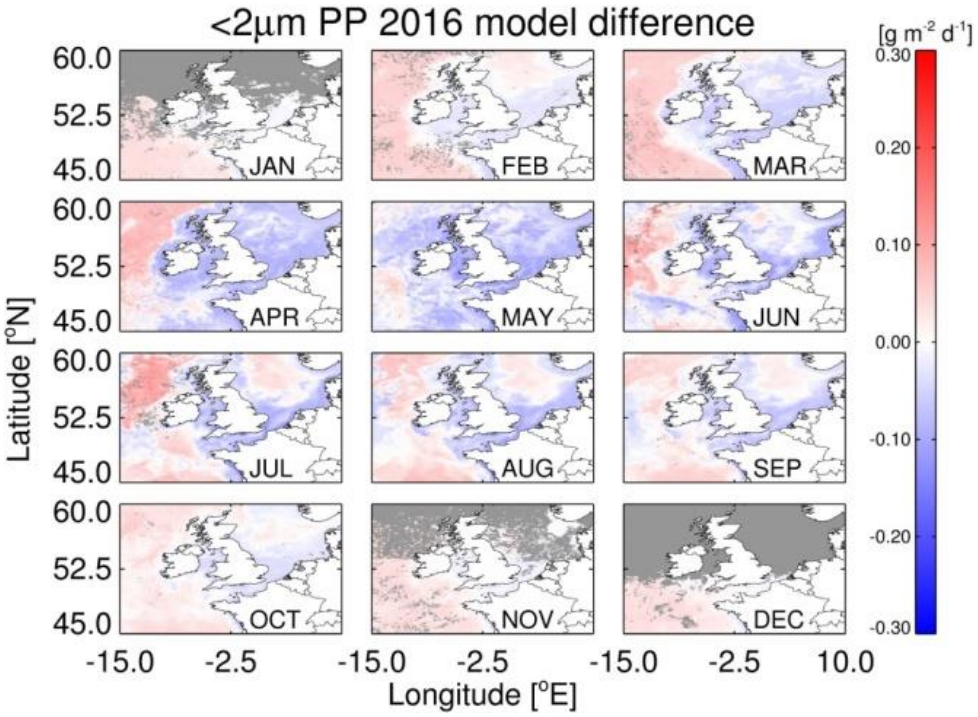


Fig 4.11 Differences in estimated monthly picophytoplankton PP between the Shelf Sat and Open Sat model tunes.

Picophytoplankton PP estimates had a more complex pattern in their differences between models; estimates using the re-tuned model were lower in regions of high total PP and higher in regions of low total PP (Atlantic waters and Northern North Sea) for most months.

4.4.8 Annual patterns of size-fractionated PP in UK shelf seas: estimates from satellite models compared with a bio-optical model using measured photophysiology.

As there is considerable variability in PE parameters measured at station L4 over weekly timescales with some months being sampled less frequently through the year (table 2), a climatology is used to give a generalised indication of seasonal patterns in PP, given the limited and variable dataset available to validate the two models. The climatology of primary production data from station L4 using average values for each month over 2009-2015 (reported in chapter 1) allows a comparison of how well the original and re-tuned models capture typical seasonal dynamics in total primary production at a station L4.

Table 4.2 Number of total daily PP estimates for Station L4 2009-2015 used in constructing the climatology presented in Fig 4.12

Month	*Jan*	*Feb*	*Mar*	*Apr*	*May*	*Jun*	*Jul*	*Aug*	*Sep*	*Oct*	*Nov*	*Dec*
PP values	3	7	19	17	15	15	10	10	15	8	6	8

Ocean Colour Climate Change Initiative (OCCCI: www.oceancolour.org) chlorophyll data were extracted for 2016 taking single and 3x3 pixel averages for station L4, ensuring results weren't biased by including pixels sampled during the study, annual trends were plotted for the original Open Sat model, the re-tuned Shelf Sat model, and the mean climatology of PP using average values calculated from measured parameters (see chapter 1). Two values of total PP were removed from the climatology for August as these were taken during an anomalously large *Karenia mikimotoi* bloom; however, these are included for size-fractionated climatologies for reference, and notated as "August QC" in the respective legends. 3x3 pixel averages were not substantially different to single match-up pixels (Fig 4.12) so were used as the values for model PP.

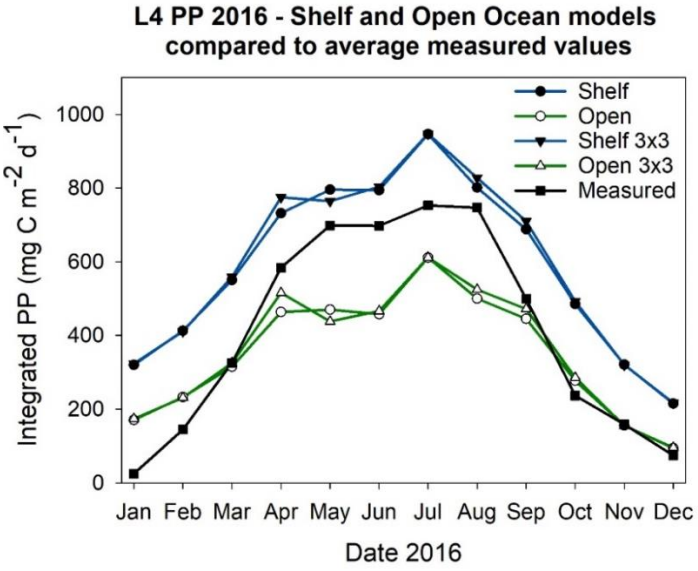


Fig 4.12 Monthly average total PP calculated using in situ data from station L4 2009-2015 (black line), with estimated PP from the Open sat tune (green) and Shelf sat tune (blue). Triangle symbols are 3x3 pixel averages and circles are single pixel covering station L4

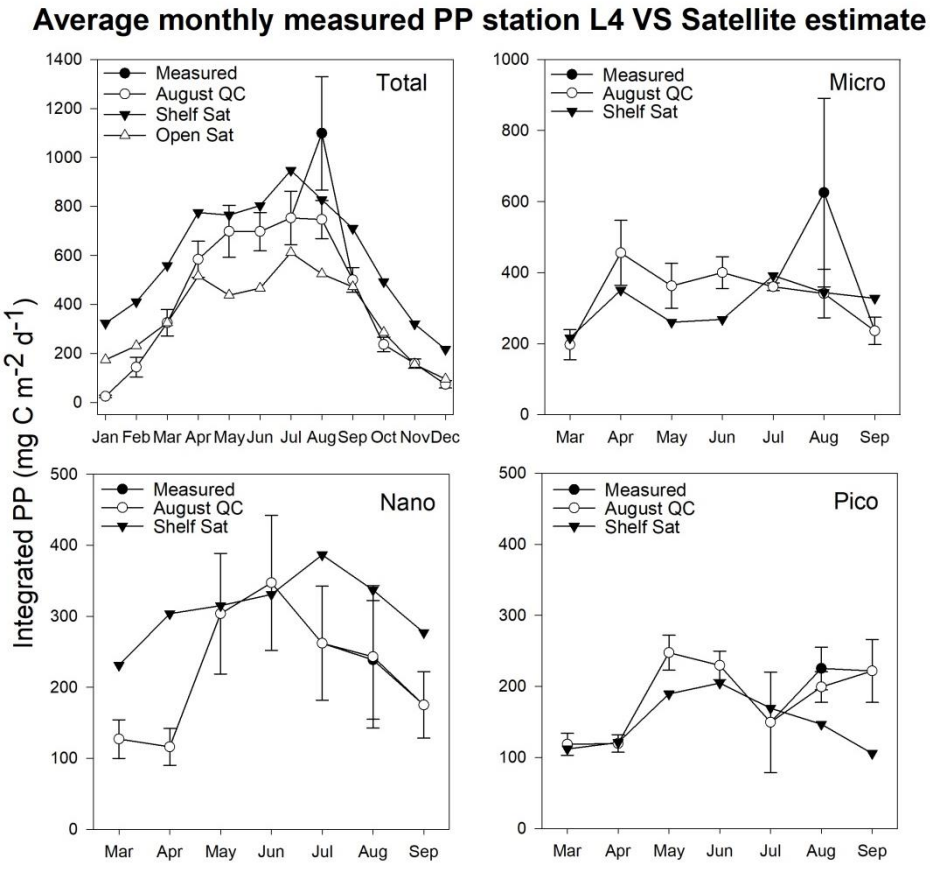


Fig 4.13 Climatological means of total and size-fractionated PP for station L4 2009-2015 with standard error plotted with estimates by the shelf tune (Shelf Sat) using chlorophyll imagery for 2016. Size-fractionated values are restricted to Mar-September to ensure sufficient data to calculate averages and standard error.

The retuned model (Shelf Sat) overestimates total PP with respect to the climatology of average calculated values across all months but most substantially at lower daily PP values from Oct-Mar. The original model (Open Sat) overestimates total PP in Jan-Feb, underestimates PP April to August and matches the climatology Sep-Dec. In terms of total PP, the original model therefore appears more accurate in periods of lower PP, while the retuned model performs better at high values in the spring-summer period, when most of the data of this study was measured.

Microphytoplankton PP estimates from the retuned model are underestimated in Apr-Jun and slightly overestimated in September, with values in Mar, Jul and Aug being within the interannual variability around the climatological mean. Nanophytoplankton PP had considerably higher interannual variability than other fractions, but modelled values only fell within the climatological variability in May-Jun, and greatly overestimating PP outside of these months. Picophytoplankton PP was estimated more accurately, but was under estimated in three months (May, Aug, Sep).

The average seasonal dynamics of PP was generally captured for total, micro and picophytoplankton (excepting Aug-Sept), with seemingly poorer performance for nanophytoplankton, though the greater variability of nanophytoplankton PP makes this difficult to say conclusively with one year of modelling.

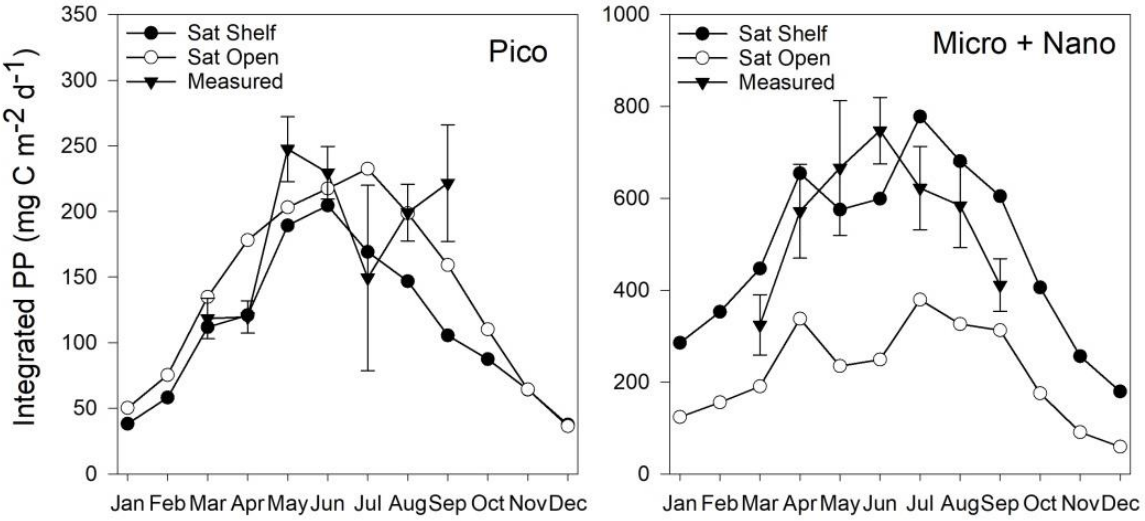


Fig 4.14 Climatological means of picophytoplankton and micro + nanophytoplankton PP for station L4 2009-2015 with standard error plotted with estimates by the shelf tune (Sat Shelf) and North Atlantic tune (Sat Open) using OC-CCI v3.1 chlorophyll imagery for 2016.

When comparing the original and retuned parameterisations against comparable size fractions (pico <2.0µm, micro + nano > 2.0µm) we see that the retuned shelf model captures the seasonal dynamics of picophytoplankton PP better between March-July, but with higher values, the Atlantic tuned returns values closer to the climatological means. Combined micro and nanophytoplankton production is generally better estimated by the shelf model, though is often overestimated outside of May and June. The Atlantic model consistently underestimates micro and nanophytoplankton PP.

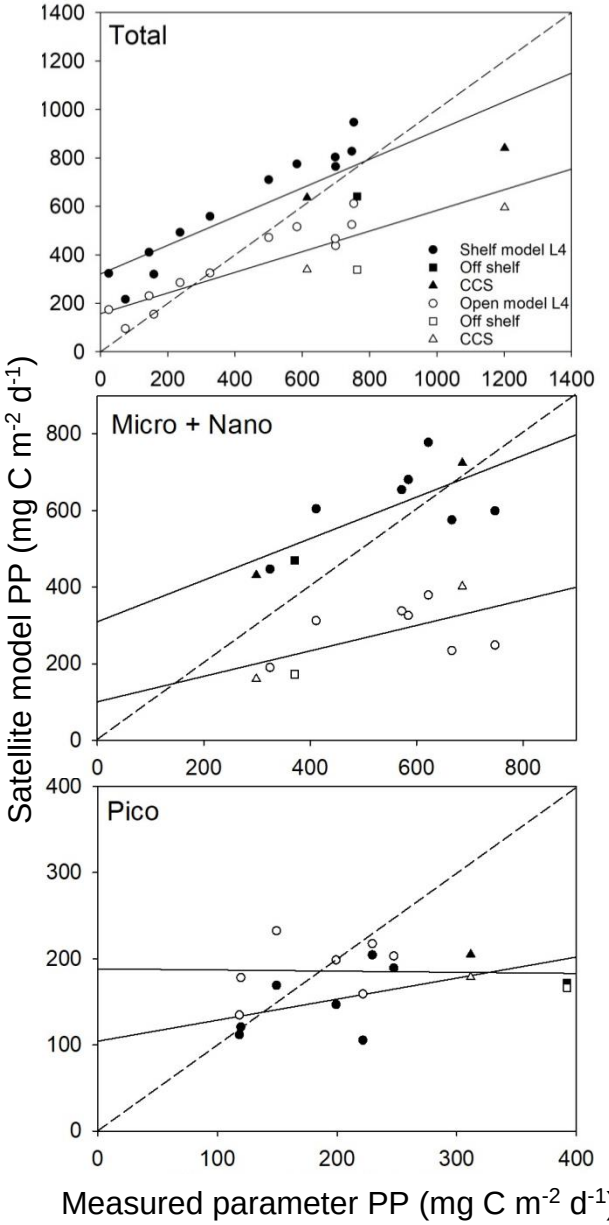


Fig 4.15. Linear regression of daily integrated PP from satellite models against calculated values for stations L4, Central Celtic Sea (CCS) off the Celtic Shelf (Off shelf). Values are climatological monthly averages for L4 and monthly averages for cruises DY026 and DY029 for Celtic Sea stations. Regression statistics in table 4.3.

Table 4.3 Regression statistics for Shelf sat and Open sat models using data from station L4, CCS and Off the shelf edge.

Modelled PP	r^2		Slope		Intercept	
	Shelf	Open	Shelf	Open	Shelf	Open
Total shelf	0.78	0.75	0.59	0.43	321	158
M,N shelf	0.56	0.39	0.54	0.33	309	101
Pico shelf	0.32	N/A	0.24	-0.01	104	188

Linear regression of mean daily integrated PP values at station L4 (50.25° N, -4.21° E), CCS (49.24° N, -8.36° E) and off shelf (48.62°N, -9.79°E) with modelled values from the Open Sat and Shelf Sat model tunes are presented above, providing further detail on the relative performance of each model across a range of mean monthly primary production values at different sites within the western English channel and Celtic Sea. Both models performed well for total PP, with the shelf model having a slightly higher coefficient of determination and slope closer to 1:1, but a considerable offset, consistently overestimating at low to moderate values (0-0.5 g m^{-2} d^{-1}). The Atlantic model has reduced slope and offset and therefore is more accurate at lower PP values but underestimates as PP increases above 0.5 g m^{-2} d^{-1}. The number of size-fractionated PP values is reduced compared to total but indicates that the shelf model generally performs better at estimating micro + nano PP, but is likely to overestimate PP at lower values (<0.25 g m^{-2} d^{-1}) which were not frequently encountered within this study. Picophytoplankton PP showed a weak correlation for the shelf model, with reduced range in PP vs calculated values and thus underestimates PP at >0.15 g m^{-2} d^{-1}. A more detailed analysis using daily match-ups with cruises and Western English Channel data may elucidate differences in PP between both models and estimates using *in vivo* PE parameters. There is considerable variability in Celtic Sea Primary production at the same sampling sites on sub-month time scales that is not captured in monthly averages and composites. In order to calibrate and validate the Shelf Sat model to the same degree as the Open sat model, more data from the shelf are needed, preferably sampled with match up satellite data of chlorophyll and PAR products.

4.5 Discussion

4.5.1 How accurate are satellite estimates of size-fractionated PP using a retuned model?

By retuning the model of Brewin et al. (2017b) using measurements made in UK shelf seas the overall accuracy of estimates of total and size-fractionated PP was generally increased, with the original model sometimes providing more accurate estimates at lower PP values (figs 4.12, 4.14), during periods of the year where no data was available when tuning the shelf model. There does appear to be considerable overestimation of PP by the retuned model from September to March with respect to the L4 climatology, and this can be seen in the composite imagery as reduced seasonal and regional variability versus what would be expected.

While the re-tuned model of size-fractionated primary production used in this analysis appears to replicate the trends of PP calculated from *in situ* data, there are many instances where there are large differences in the magnitude of primary production values, with nanophytoplankton PP being greatly overestimated outside of May and June for example (Fig 4.13). Furthermore, the original model appears to capture total PP more accurately outside of the spring-summer growing season indicating that some generalised modelled parameters may be less accurate at lower chlorophyll concentrations, or that periods of mixed water column dynamics are better parameterised by the original model which was tuned to Atlantic datasets, and switches from a non-uniform to uniform biomass profile when the mixed-layer depth is deeper than the euphotic depth. A sensitivity analysis of the model's PP output was conducted by Brewin et al. (2017b) using Monte Carlo simulations (200 iterations) on input variables (total surface chlorophyll, surface irradiance and mixed layer

depth) and model parameters. The sensitivity analysis of the model's input and parameters indicated that total PP, and the PP of all size fractions were particularly sensitive to S^{Bs} the background decrease of B^{Bs} with ζ, and q_a , q_b the empirical parameters used in the calculation of Z_{eu} from surface chlorophyll (Eq 4.3). Output PP values for nano and picophytoplankton were most sensitive to changes in asymptotic maximum chlorophyll ($B_1^m, B_{1,2}^m$) and scaling parameters with respect to total chlorophyll ($S_1, S_{1,2}$) in mesotrophic environments (chlorophyll = 0.2mg m^{-3}). From Fig 4.2, it is obvious that the *in situ* measurements of chlorophyll have a high degree of variability in relation to modelled asymptotic maximum chlorophyll values and the fractional contribution to total chlorophyll. There are a number of sampling stations within this study where nano- and occasionally picophytoplankton dominate S-F chlorophyll across a range of total concentrations, meaning PP may be incorrectly apportioned to microphytoplankton when total PP is > 1.0mg m^{-3}. Although there were periods in this study when high biomasses of nanophytoplankton were present and dominated PP, during the typical peaks of primary production of spring and late summer/autumn blooms of microphytoplankton occur, (Widdicombe et al. 2010; Wiltshire et al. 2008) such that PP should be correctly attributed to the largest cells.

In the original OpenSat model, in a well-mixed eutrophic environment (chlorophyll = 2.0mg m^{-3}), the model is generally less sensitive to individual parameters than lower chlorophyll regions (particularly for S^{Bs} as the water column is considered uniform), but the relative sensitivity to $\alpha_i^{B_s}$ is increased for all size fractions. Considered individually, the means by which these model parameters might be impacted in a highly seasonal, meso/eutrophic shelf sea may explain some sources of error and elucidate ways to improve the modelling of size-fractionated PP with refined models.

4.5.2 Photo physiological parameters and biomass distribution

Total and size-fractionated primary production estimates calculated by the model of Brewin et al. (2017b) for an open-ocean and shelf region are more sensitive to differences in α^{B_S} than $P_m^{B_S}$. The lower significance of P_m^B as a source of error in applying this modified open-ocean PP model is compounded by the small differences in values of P_m^B and S^{B_S} between the UK Shelf and Atlantic model tunes (Table 4.1). The accurate parameterisation of α^B is therefore of more consequence to estimates of PP, with substantial differences in α^{B_S} and S^{α_S} between each dataset (Table 4.1). A 3.5-4.3 increase in the average value of light-limited photosynthetic rate may seem questionable when maximum photosynthetic rates are broadly similar between both regions, however, values from previous studies in shelf regions range over an order of magnitude, from similar values to the Brewin et al. (2017b) surface averages to over double the UK shelf values measured as part of this study. (Barnes et al. 2015; de Madariaga and Joint 1994; Morán and Scharek 2015; Pemberton et al. 2004; Segura et al. 2013). These previous works highlight the high degree of variability of size-fractionated α^B values with changes in hydrography and community composition within individual size fractions, which cannot be easily accounted for in these generalised satellite models.

The effect of inaccurately parameterising α^B is highly dependent on the location of phytoplankton biomass within the euphotic layer; at lower irradiances the effect on integrated PP values may be insignificant. During bloom conditions (which feature prominently in this study) where biomass is typically near the surface following water column stabilisation or fresh nutrient input, poor generalised estimates of α^B will have a greater effect than for high biomasses at the SCM in summer, as PAR is typically much lower at those depths. As the Shelf Sat model calculates peak biomass under low-moderate

surface chlorophyll conditions (Fig 4.8) as being at half the euphotic depth (ζ=0.5) , higher α^B values measured in the UK Shelf will heighten the effect of the increased available irradiance (vs the original parameterisation of peak B^{B_S} being ζ=0.75-1.25). This situation may be the cause of overestimated PP for October-March, as under the better-performing stratified model of subsurface to surface chlorophyll, low surface values of chlorophyll (and thus deeper Z_{eu}) (Fig 4.5) may introduce a moderate biomass of phytoplankton (following the B^{B_S} curve (Fig 4.8)) to sufficient light for considerable photosynthetic activity given the high light-limited photosynthetic rates of all size classes.

4.5.3 Effect of hydrographic differences between open ocean and shelf seas on modelled PP

The sites where measurements were taken during this study ranged from shallow, coastal sites (55m) of the English Channel, the off-shore shelf of the Celtic Sea (100-140m) and its shelf break (200m) to the continental slope at the Celtic Margin (1500m). Whilst many of these areas may show similarities to the North Atlantic waters, being seasonally stratified with depleted surface nutrient pools (Birchill et al. 2017; Holligan and Groom 1986; Pemberton et al. 2004), mixing and nutrient dynamics are distinct. Outside of deep winter mixing vertical water transport in the North Atlantic is often through Ekman pumping and mesoscale eddies, with little diapycnal flux of nutrients (Martin and Richards 2001; McGillicuddy et al. 2003; Williams and Follows 1998), whereas dynamics are quite different on the NW European Shelf: nutrients may be supplied by advective, tidal, frontal and diapycnal means, with internal tides and wind stress modifying the supply of nutrients to the euphotic layer (Green et al. 2008; Holligan 1981; Palmer et al. 2012; Palmer et al. 2015; Pingree et al. 1982; Reul et al. 2006; Sharples and Tett 1994; Tweddle et al. 2013). There is therefore a potentially much greater variability in the vertical distribution, biomass,

community structure and size-fractionated photophysiology (and thus PP) with respect to the surface values of variables observable from satellite and their respective model parameters. For example, subsurface chlorophyll maxima in the Celtic Sea have been observed to have greater chlorophyll concentrations in regions with stronger tides (Pingree et al. 1982). However, given the difficulty in modelling variable sub-surface physical features in different regions with respect to those variables observable from satellite – with the associated added complexity and thus sources of error – using simpler, generalised models of sub-surface biomass distribution tuned to the hydrography of specific regions seems a reasonable path to pursue. The advent of combined passive ocean colour and active LIDAR sensor arrays will conceivably increase the accuracy of satellite estimates of the vertical distribution of phytoplankton (Hostetler et al. 2017; Hu et al. 2016; Schulien et al. 2017), partially removing the requirement to model biomass distribution. These new platforms will not provide time-series datasets useful for climate change investigation for a number of decades yet, meaning legacy models will still be necessary to model PP from historic ocean colour data, however, overlap between long-running missions such as MODIS will allow better cross-calibration and the validation of models and BioArgo float data with LIDAR measurements at scales not achievable with ship-based measurements.

4.5.4 Optics

The chlorophyll algorithm used in the OC-CCI v3.1 dataset is tuned to an optical classification, with output of various algorithms applied to imagery blended by a pixel's cumulative association to one of 14 optical types (rather than using defined regional boxes) (Jackson et al. 2017). While it should therefore provide reliable estimates of chlorophyll when other optical constituents are present, the effect of the variability in light attenuation

by CDOM and particulates with respect to surface chlorophyll is not considered in the modelling of Z_{eu}.

Although observed values of surface chlorophyll vs Z_{eu} show good overall agreement to the model being used (Fig 4.4), there is considerable scatter and evidence that the relationship between these two variables may be different across a shelf sea environment than in an oceanic region given the differences in hydrography and biogeochemistry (Nelson and Siegel 2013; Siegel et al. 2005). Concentrations of CDOM and non-algal particles are likely to be greater in temperate shelf seas than the open ocean, and may dominate the attenuation of downwelling irradiance (what has classically been termed "case-2" conditions) (Morel and Prieur 1977). As the UK shelf seas are highly heterogenous in their optical characteristics and may exhibit classical case 1 optics in deeper, off-shore areas, to more extreme case 2 waters around estuaries (Astoreca et al. 2009; Groom et al. 2009; Ioccg 2000; Kratzer et al. 2000; Tilstone et al. 2005), the inclusion of IOPs in the estimation of Z_{eu} may benefit the accuracy of the modelled light field from ocean colour data.

The available light PP model used here model is broadband – irradiances are expressed as values of the integrated flux of photons 400-700nm (μmol photons m^{-2} s^{-1}), and does not consider the spectral distribution of the light field and the variable specific absorption properties of phytoplankton. Although retuning this model is a theoretical exercise, using a number of in situ measurements to evaluate the suitability of a Atlantic-tuned size-fractionated PP model, an improved model would benefit from a consideration of the spectral absorption of different phytoplankton fractions and how spectra change with depth, for instance, as modelled by (Uitz et al. 2008), and the light attenuation due to phytoplankton CDOM and non-algal particles, allowing the calculation of PP which incorporates water spectral IOPs and photophysiology (Bricaud et al. 1995; Morel 1991)

4.6 Conclusions

Using photosynthetic parameters measured during my thesis, the size-fractionated primary production model of Brewin et al. (2017b) was tuned to operate in UK shelf waters. Satellite surface chlorophyll and PAR datasets, together with tuned *PE* and vertical biomass parameterisations, were used to compute primary production for the three phytoplankton size classes in UK shelf waters. The retuned model captured the seasonal patterns in S-F PP for micro- and picophytoplankton, and performed better, in general, than the original model of Brewin et al. (2017b) that was tuned to the open-ocean. However, the retuned model substantially overestimated nanophytoplankton PP outside of May-June. The shelf-sea pigment dataset also showed a significant degree of variability in the relative concentrations of Chl of three size fractions for a given total surface Chl concentration (Fig 4.2), suggesting the relationships used to partition total chlorophyll into the three size classes in the Brewin et al. (2017b) model may require further development for UK shelf waters.

Compared against a climatology of measured data at station L4, the retuned model performed better when phytoplankton biomass was high (April-August), but overestimated PP under conditions of low phytoplankton biomass. This overestimation is thought to be attributed in part to the sensitivity of primary production models to the parameterisation of the biomass profile. The parameterisation of biomass profile was tuned using data collected during Spring-Summer conditions primarily. The difficulty in producing a generalised model of the vertical distribution of phytoplankton within the euphotic water column in seasonally-stratified shelf seas was shown to be a potential source of error in integrated estimates of daily PP, especially outside of the spring bloom period. Establishing new relationships between surface chlorophyll and the vertical biomass profile for UK Shelf seas is worthy of further investigation using existing and future sampling platforms.

5 Conclusions and future directions

The overall aim of my thesis was to examine the accuracy of current models of size-fractionated primary production when applied in the temperate shelf seas surrounding the United Kingdom. As bio-optical models of primary production require an approach for assigning the size-fractionated *PE* parameters, these data alongside pigment and physico-chemical variables were collected during two cruises to the Celtic Sea and two sampling seasons at the Western English Channel Observatory which was augmented by historical data from 2009-2011.

5.1 Do Shelf Sea phytoplankton communities require separate parameterisation of photophysiology?

The analysis of the *PE* parameters in UK shelf systems presented in Chapter 2 indicates that size-fractionated values of P_m^B and α^B were lowest for microphytoplankton and highest for picophytoplankton, though differences in nano- and microphytoplankton values were not significant. This result is inconsistent with previous studies of open-ocean (Brewin et al. 2017b; Uitz et al. 2008) and shelf regions (table 2.7) and would suggest that increased P_m^B and α^B with decreasing cell size is a common relationship across many shelf sea systems systems. This pattern was also mirrored in the magnitudes of a_{ph}^* coefficients and is in agreement with the findings of previous studies which have estimated $a_{ph}^*(\lambda)$ through different techniques, adding to the knowledge of the relationship of cell size and $a_{ph}^*(\lambda)$(Brewin et al. 2011; Ciotti et al. 2002; Devred et al. 2006; Uitz et al. 2008; Varunan and Shanmugam 2015). Considerable differences in the magnitude of $a_{ph}^*(\lambda)$ values were found between different methods of estimating the phytoplankton absorption. In Chapter 3, modelled and measured values of $a_{ph}^*(\lambda)$ were used in a regionally-tuned primary production

model for the Celtic Sea. Changes in the vertical distribution of primary production highlighted how even with similar integrated PP values, changes in our assignment of $a^*_{ph}(\lambda)$ can modify the relative importance of the surface mixed layer and the SCM to integrated water column production. Modelled $a^*_{ph}(\lambda)$ were then used to identify how best to spectrally correct size-fractionated α^B when size-fractionated a^*_{ph} measurements are not available. My results show that the primary production model was more sensitive to the spectral correction of α^B than its influence of a^*_{ph} on light attenuation. When incorporated into the spectral PP model, the a^*_{ph} spectra of Uitz et al. (2008) was found to generate PP estimates that most closely resembled in situ measurements, but may be improved by tuning surface spectra and slope values using shelf sea data. However, to produce a robust set of regional parameters would require a significantly larger dataset of S-F $a^*_{ph}(\lambda)$ and therefore might be best achieved using historical total $a^*_{ph}(\lambda)$ measurements and coincident pigment or taxonomic data to classify sizes.

The modest vertical changes in $a^*_{ph}(\lambda)$ between surface and deeper samples, with picophytoplankton spectra showing no discernible difference, was surprising. Given the wealth of literature describing the effects of photoacclimation processes on phytoplankton pigmentation and absorption spectra with respect to water column hydrography (Hickman et al. 2009; MacIntyre et al. 2002a; Rodriguez et al. 2006; Stæhr et al. 2002), finding weak relationships between the absorptive properties of the various size fractions and both depth and ζ (Fig 3.5) was unexpected. The lack of observable vertical trends in $a^*_{ph}(\lambda)$ may be attributable to the high degree of variability in measured $a^*_{ph}(\lambda)$ for each size class, which is discussed in Chapter 3. Factors which possibly contribute to this variability include changes in the size class community structure (Ciotti et al. 2002), differences in mixed layer depth and mixing timescales between sampling stations, and uncoupling of nutrient supply

and daily irradiance possibly caused by episodic mixing events (Dubinsky and Stambler 2009; Flameling and Kromkamp 1997; Geider et al. 1997; MacIntyre et al. 2000; Moore et al. 2006; Stæhr et al. 2002; van de Poll et al. 2007). However, these sources of variability within size classes are likely to be small compared to differences between fractions (Lohrenz et al. 2003) and measurement error of the size-fractionated a_{ph}^{*} spectra method. As size-fractionated $a_{ph}(\lambda)$ were opportunistic measurements taken to compliment other size-fractionated parameters and total $a_{ph}(\lambda)$, there is certainly scope for improving the methodology to try to reduce any cross contamination due to filter clogging, or from residual water when using the same deposit. These measurements would have been complimented by a dataset of size-fractionated phytoplankton pigment concentrations, but these samples were compromised, and unfortunately not able to elucidate the degree of variability attributable to pigmentation suite, or validate pigment reconstructions of size-fractionated absorption. Future studies of S-F absorption would benefit from testing the pigment concentrations of individual size fractions in this manner as it would provide a validation of pigment-based size indices (Uitz et al. 2008; Vidussi et al. 2001) and contextualise differences between regions and depths due to changes in pigment ratios. It would be prudent to adopt other techniques for estimating size-fractionated absorption other than sequential filtration; one candidate would be the use of a long path length spectrophotometer (such as a SeaBird ACS) to measure absorption of cells in suspension after pre-filtration at a desired pore size, rather than using the quantitative filter pad method. This would remove some of the sources of error associated with the beta correction of cells concentrated onto a filter and retention of cells on GFF filters which have a nominal pore size (0.7 µm) greater than some species of picophytoplankton. Measurements taken after <0.2 µm filtration to separate phytoplankton absorption from seawater and with ultrapure water to separate absorption by dissolved compounds from water would provide useful CDOM spectra whilst following the

same operational method. The sensitivity of these instruments in measuring CDOM absorbance at values of 0.005 m^{-1} (Dall'Olmo et al. 2017) would suggest that even with the reduced phytoplankton biomass due to pre-filtration, this method may provide means to measure S-F a_{ph} at natural concentrations of phytoplankton in shelf seas *in situ,* with newer models offering increased spectral resolution (4nm) and more stable response across the visible spectrum (SeaBird Scientific.com). If modified to use a number of water sample inlets using different pore sizes, a single system could be used to make S-F measurements of surface waters at high frequency, generating more data and requiring less labour per sample than the method used in this study. Such flow-through systems may also be linked with other instruments such as fast repetition rate fluorometers which require only small samples to measure phytoplankton photophysiology (Silsbe et al. 2015) and may even be used to estimate photosynthetic parameters normally measured by PE incubations (Keys et al. 2017).

Values of P_m^B and α^B measured during this study were highly variable within fractions, across sampling regions, through the water column and at different times of the year. Most relationships of these parameters with other variables were unclear, due to the multivariate nature of cell acclimation to the physiochemical environment. However, values were found to have significant relationships with some individual variables: Salinity was a significant predictor of α^B for all size classes and both salinity and temperature were significant predictors of P_m^B for micro and picophytoplankton. Mean values for each size class were highest at the coastal WCO site (L4), moderate at the off-shore WCO site (E1) and lowest in the Celtic Sea, suggesting a pattern of decreasing photosynthetic rates from more eutrophic, estuarine-influenced coastal waters to more mesotrophic open-shelf and shelf-edge waters. This finding is not surprising when considering that the principal limits to phytoplankton photosynthesis are nutrient concentrations irradiance, degree of

photoinhibition and surface mixed layer dynamics and depth. With respect to each of these variables, coastal regions provide a more favourable environment for cells of each size class to acclimate to higher rates of photosynthesis than off-shore areas. The correlation of salinity and photosynthetic parameters may be a consequence of P_m^B and α^B being highest in coastal areas and lowest in the open shelf, as correlation is negative for P_m^B for each size fraction; however, α^B values correlate positively with salinity, suggesting that position with a stratified water column may be a controlling factor, rather than proximity to eutrophic coastal waters. A high degree of variability in parameter values was observed in P_m^B and α^B at specific and nominal depths as was the case with a_{ph}^* spectra, with patterns in parameters with depth only observable for stratified sampling periods (where vertical salinity gradients were strongest). Despite the high degree of variation when the whole dataset is considered together, both P_m^B and α^B follow trends with ζ as in the observations of Uitz et al. (2008) and Brewin et al. (2017b). This observation has allowed the values to be scaled to surface values through the water column following generalised relationships to other variables (surface chlorophyll concentration and PAR used to estimate Z_{eu}) and therefore be used to retune the satellite model of Brewin et al. (2017b). These relationships diverged from the open ocean datasets used for comparison, with the differences being greatest for picophytoplankton and smallest for microphytoplankton. This is perhaps due to the smaller functional diversity and photoacclimation potential within microphytoplankton taxa (principally diatoms and dinoflagellates) than picophytoplankton, where specialized ecotypes of *Prochlorococcus* common to the sub-tropic gyres will exhibit photophysiological traits not found among the mixed picoeukaryote and *Synechococcus* community of temperate shelf seas (Ciotti et al. 2002; Morel et al. 1993; Veldhuis et al. 2005). Smaller differences in microphytoplankton photophysiology is partially explained by the bloom dynamics of this size class; diatoms tend to bloom in a turbulent water column,

at lower temperatures whether in the early spring bloom of a shelf sea, or coastal upwelling of deep waters (Cloern 1996; Fasham et al. 1983; Kiørboe 1993b), while motile dinoflagellates have more regionally variable bloom dynamics, they are normally associated with post-spring bloom stratified conditions in shelf seas (Garcia-Soto and Pingree 2009; Pingree et al. 1978; Raine and McMahon 1998) and exhibit only minor differences in normalised absorption compared with diatoms (Ciotti et al. 2002; Lewis et al. 1985a).

Average picophytoplankton α^B values are close to an order of magnitude higher in the shelf data reported here compared to both open ocean models used in Chapter 4. This was surprising given that open ocean picophytoplankton ecotypes are generally considered to be more efficient absorbers of light than those common to coastal and shelf communities (Bricaud et al. 1995), with *Prochlorococcus* strains even attenuating more light through absorption than scattering, unique among phytoplankton (Morel et al. 1993). The profound difference in light-limited photosynthetic rates between these study regions may be explained by extreme photoadaptation and photoacclimation strategies between surface (high-light) and deep chlorophyll maximum (DCM) (low light) open ocean communities. Surface communities are limited by nutrient availability and the need to prioritise photoprotective pigmentation (Marra et al. 2000), depressing α^B and φ_{max} values, while DCM communities have ample nutrients to synthesise photosynthetic pigments to maximise photosynthetic efficiency at light-limited depths. This pattern in evident in the data of Uitz et al. (2008) and to a lesser extent by Brewin et al. (2017b), while the shelf data for pico and nanophytoplankton show an opposite and weaker trend with ζ , suggesting differences in photoacclimation and photosynthetic properties between surface and SCM communities in shelf seas is potentially much less acute. This result matches with previous studies of shelf sea photoacclimation and vertical distributions of phytoplankton communities, which show more gradual succession in phytoplankton communities through euphotic depths,

particularly around the SCM, rather than binary high-light and low-light communities (Hickman et al. 2009; Klausmeier and Litchman 2001; Moore et al. 2006; Suggett et al. 2009). These comparisons between this study (which forms one of the largest shelf sea datasets of size-fractionated photophysiology) with the extensively validated pigment-based model of (Uitz et al. 2008), and the large size-fractionated Atlantic dataset of Brewin et al. (2017b) presented in Chapter 4 indicates that picophytoplankton photophysiology is markedly different in shelf waters compared with the open ocean, and should be parameterised as such with bio-optical PP models to ensure more accurate estimates.

When considering the influence of natural variability in estimates of phytoplankton primary production, the photophysiology of phytoplankton is important, but is constrained by the rates of cellular biochemistry. Extreme photophysiology of shelf sea communities is most likely due to measurement error rather than adaptation (such as seen in sub-tropical gyre regions)(Zinser et al. 2007), and as such, variability in biomass is dominant control of differences in PP between locations and over time. For example, even a doubling of P_m^B will only have a significant effect at saturating irradiances i.e. boreal summer when stratified surface waters have low biomasses) and a doubling of α^B will have a minor to moderate effect on integrated PP due to the low irradiances at depth. Although the differences between open ocean and shelf sea communities' photophysiology presented in this thesis indicate that they should be considered separately, they are a second-order contributor to estimates of PP after the biomass profile. It is therefore necessary to consider the accuracy of bio-optical models of PP in estimating the chlorophyll concentration through the water column in addition to accurate parameterisation of phototphysiology before refined models can be claimed to be more representative – a non-trivial task considering the difficulties in estimating shelf sea vertical structure from satellite observations.

5.2 Estimating PP for the UK shelf – improvements in model performance and steps for improvement

The shelf tuned model (Shelf Sat) of size-fractionated primary production adapted from the existing open ocean model of Brewin et al. (2017b) (Open Sat) improves estimates of monthly PP from satellite when compared against averages estimated using *in vivo* data from station L4. However, the original model tune appears to perform better during periods of lower total productivity (< 0.5 g C m^{-2} d^{-1}). The parameterisation of the Shelf Sat model uses data focussed on the weeks preceding the spring bloom period through to the end of summer, with few samples taken during periods of low biomass, which may potentially bias the average values of photophysiology used in the retuned model if there are further seasonal differences to those detailed in chapter 1. Given more time, and potentially using a larger dataset, it would have been useful to compare the PP estimates of both models at a range of shelf sites, in a similar manner to station L4. It may be the case that with L4 being the most coastal station – and conceivably the site least well suited to the open ocean model – that the performance of the models diverges most substantially here.

Another potential source of the overestimation of PP is the use of a broadband model in waters which may periodically have more complex optics, not solely determined by the optical properties of phytoplankton and seawater. Increased densities of TSM or concentrations of CDOM will attenuate available light and therefore alter the euphotic depth and will alter the spectral quality of the euphotic light field. In these instances, satellite-estimated surface chlorophyll concentrations may not be an adequate predictor of the attenuation coefficient. As few samples within this dataset are taken between autumn to early spring it is difficult to test the z_{eu} to surface chlorophyll relationship (which seems to perform well for spring – summer data), a key component of the Brewin et al. (2017b) model and the retuned model presented here. A potential solution to this problem of

assuming a case 1 water column (Sathyendranath et al. 2001) is to use a more complicated algorithm to estimate the underwater light field, either by using satellite CDOM and TSM products in addition to surface chlorophyll to estimate broadband K_d values and thus estimate Z_{eu} based on other water IOPs which may be seasonally important (Chen et al. 2017; Mannino et al. 2008). A better, but significantly more computationally expensive method would be to incorporate $a_{ph}(\lambda)$ for each size class with water IOPs into a spectral available light model to more consistently and accurately constrain regional and seasonal variances in water optics on phytoplankton primary production (Siswanto et al. 2011; Smyth et al. 2005; Tilstone et al. 2005) . However, this would require spectra to be calculated for a number of parameters for each pixel and potentially vertically resolved for a_{ph}, which may require compromises in the spectral resolution of parameters or pixel size in order to be efficient, or the exploitation of parallel processing by GPU to accelerate pixel-by-pixel calculations. It is also possible that this added complexity may introduce its own sources of error, so testing with broadband models and assessing efficiency, accuracy against *in situ* data and reliability over a range of IOPs would be beneficial.

As the results of chapters 2 and 3 show, picophytoplankton have photophysiology distinct from larger size fractions, having significantly higher photosynthetic rates and chlorophyll-specific absorption coefficients in the visible domain. Owing to their measured greater photosynthetic efficiency in these temperate shelf sea sites, they can be responsible for a significant proportion of primary production even when they are not the dominant size fraction. That a greater proportion of primary production than previously assumed is attributable the smallest phytoplankton is an important consideration in efforts to model food webs and carbon cycling in these regions. Pathways of carbon fixed by diatoms and prokaryotes for example may be quite distinct – a greater proportion of picophytoplankton primary production would likely reduce carbon export and benthic-pelagic coupling of labile

carbon. This is however, difficult to quantify in dynamic regions where mixing profiles and grazing taxonomy will influence carbon cycling in addition to phytoplankton community structure. For instance, picophytoplankton carbon may reach the same fate as microphytoplankton if large metazoan zooplankton (such as copepods) feed on protozoan grazers, but if viral lysis is the chief cause of picophytoplankton mortality, then cellular carbon will most likely be used by heterotrophic bacteria within the microbial loop. Given the complexity of coupled hydrodynamic-biogeochemical models, reparametrising the photosynthetic activity of the phytoplankton community to reflect the results of this study may produce interesting differences in carbon and macro nutrient fluxes between different model components.

5.3 Improvements to estimates of the vertical distribution of phytoplankton

In addition to efforts to improve estimates of the pelagic light environment – a non-trivial task when constrained by using only variables observable from satellite – wider validation of the sub-surface vertical distribution of the phytoplankton community would be of great benefit to PP models. Chapters 2 and 3 discuss how temperate shelf seas exhibit a wide variety of hydrodynamic phenomena which affect distribution, community structure and photoacclimation of the phytoplankton and the importance of this to the parameterisation of primary production model. It is unsurprising therefore, that patterns in their vertical distribution might be less consistent than a model tuned with open ocean observations (Brewin et al. 2017b) as is seen in chapter 4. Measuring chlorophyll concentration at a number of depths is a common procedure on many oceanographic research cruises, such that there are large archived datasets available to investigate patterns in abundance relative to surface populations, but there are far fewer data which are part of bio-optical datasets taken

in shelf seas coincident with measurements of the light field and IOPs, which are necessary to reference the position of phytoplankton biomass within a specific light field rather than simply depth. Samples from specific depths require interpolation to produce profiles of biomass, which may be prone to overestimate where the SCM covers a restricted range (or thin layer) at the nutricline or small-scale density gradient (Durham and Stocker 2011; Sullivan et al. 2010), is not symmetrical due to scouring by turbulent water below the thermocline, or has variable position over short time scales due to a motile flagellate community often found in shelf seas, including during this study (Cullen et al. 1983; Sharples et al. 2001b).

Though platforms such as profiling floats and autonomous gliders can provide a means to assess the vertical distribution of phytoplankton biomass and generalised size distribution (through fluorescence and backscattering measurements) with respect to hydrography (Boss et al. 2008; Mignot et al. 2014) at greater resolution than water samples, and with greater frequency over greater areas than CTD-mounted profiling instruments, these profiles must be paired with accurate estimates of satellite-observable surface chlorophyll variables to allow any empirical relationships to be calculated. Although these active sensors can be calibrated using contemporary measurements at deployment, fluorometric estimation of chlorophyll is problematic, particularly in surface waters important to satellite observations due to non-photochemical quenching by phytoplankton and considerable variability in the ratio of fluorescence to chlorophyll concentration between phytoplankton communities (Xing et al. 2011). However, even with uncertainties in absolute chlorophyll concentrations, an increased number of shelf sea biomass profile measurements with CTD data and water optics (PAR or multispectral radiance) using gliders and profiling floats will help to constrain the sources of and spatial and temporal scales in the variability of biomass profiles within the euphotic zones of these regions (Erga et al. 2014; Palmer et al. 2015; Williams et

al. 2016). As mentioned in chapter 4, the advent of satellite LIDAR instruments for sub-surface studies of particle distributions will undoubtedly advance our understanding of the regional dynamics of phytoplankton biomass and size distribution in near-surface waters, and possibly and can be paired with ocean colour datasets to test relationships with chlorophyll and IOPs. Whilst *in situ* size-fractionated chlorophyll or diagnostic pigment measurements will be required to validate new algorithms for these applications, the step change in data volume and coverage afforded by these combined datasets should allow the creation on of new products for the community.

References

Abaychi, J., & Riley, J. (1979). The determination of phytoplankton pigments by high-performance liquid chromatography. *Analytica Chimica Acta, 107*, 1-11

Acha, E.M., Mianzan, H.W., Guerrero, R.A., Favero, M., & Bava, J. (2004). Marine fronts at the continental shelves of austral South America: Physical and ecological processes. *Journal of Marine Systems, 44*, 83-105

Agawin, N.S., Duarte, C.M., & Agustí, S. (2000). Nutrient and temperature control of the contribution of picoplankton to phytoplankton biomass and production. *Limnology and Oceanography, 45*, 591-600

Agirbas, E., Martinez-Vicente, V., Brewin, R.J., Racault, M.-F., Airs, R.L., & Llewellyn, C.A. (2015). Temporal changes in total and size-fractioned chlorophyll-a in surface waters of three provinces in the Atlantic Ocean (September to November) between 2003 and 2010. *Journal of Marine Systems, 150*, 56-65

Ahn, Y.-H., & Shanmugam, P. (2006). Detecting the red tide algal blooms from satellite ocean color observations in optically complex Northeast-Asia Coastal waters. *Remote Sensing of Environment, 103*, 419-437

Alipanah, L., Rohloff, J., Winge, P., Bones, A.M., & Brembu, T. (2015). Whole-cell response to nitrogen deprivation in the diatom Phaeodactylum tricornutum. *Journal of experimental botany, 66*, 6281-6296

Alvain, S., Moulin, C., Dandonneau, Y., & Bréon, F.-M. (2005). Remote sensing of phytoplankton groups in case 1 waters from global SeaWiFS imagery. *Deep Sea Research Part I: Oceanographic Research Papers, 52*, 1989-2004

Alvain, S., Moulin, C., Dandonneau, Y., & Loisel, H. (2008). Seasonal distribution and succession of dominant phytoplankton groups in the global ocean: A satellite view. *Global Biogeochemical Cycles, 22*

An, N.T., & Son, V.D. (2010). Primary production models and the problem of estimation of their parameters in various conditions of the water column. *Russian journal of marine biology, 36*, 139-146

Anding, D., & Kauth, R. (1970). Estimation of sea surface temperature from space. *Remote Sensing of Environment, 1*, 217-220

Arbones, B., Figueiras, F.G., & Zapata, M. (1996). *Determination of phytoplankton absorption coefficient in natural seawater samples: Evidence of a unique equation to correct the pathlength amplification on glass fiber filters*.

Arrigo, K.R. (2004). Marine microorganisms and global nutrient cycles. *Nature, 437*, 349

Arrigo, K.R., & Brown, C.W. (1996). Impact of chromophoric dissolved organic matter on UV inhibition of primary productivity in the sea

Arrigo, K.R., Mills, M.M., Kropuenske, L.R., van Dijken, G.L., Alderkamp, A.-C., & Robinson, D.H. (2010). Photophysiology in two major Southern Ocean phytoplankton taxa: photosynthesis and growth of Phaeocystis antarctica and Fragilariopsis cylindrus under different irradiance levels. *Integrative and comparative biology, 50*, 950-966

Astoreca, R., Rousseau, V., & Lancelot, C. (2009). Coloured dissolved organic matter (CDOM) in Southern North Sea waters: Optical characterization and possible origin. *Estuarine, Coastal and Shelf Science, 85*, 633-640

Astoreca, R., Rousseau, V., Ruddick, K., Knechciak, C., Van Mol, B., Parent, J.-Y., & Lancelot, C. (2008). Development and application of an algorithm for detecting Phaeocystis globosa blooms in the Case 2 Southern North Sea waters. *Journal of plankton research, 31*, 287-300

Atkinson, A., Siegel, V., Pakhomov, E., Jessopp, M., & Loeb, V. (2009). A re-appraisal of the total biomass and annual production of Antarctic krill. *Deep Sea Research Part I: Oceanographic Research Papers, 56*, 727-740

Aumont, O., Maier-Reimer, E., Blain, S., & Monfray, P. (2003). An ecosystem model of the global ocean including Fe, Si, P colimitations. *Global Biogeochemical Cycles, 17*

Azam, F., Fenchel, T., Field, J., Gray, J., Meyer-Reil, L., & Thingstad, F. (1983). The ecological role of water-column microbes in the sea. *Marine ecology progress series. Oldendorf, 10*, 257-263

Babin, M., Stramski, D., Ferrari, G.M., Claustre, H., Bricaud, A., Obolensky, G., & Hoepffner, N. (2003). Variations in the light absorption coefficients of phytoplankton, nonalgal particles, and dissolved organic matter in coastal waters around Europe. *Journal of Geophysical Research: Oceans, 108*

Bailey, S.W., & Werdell, P.J. (2006). A multi-sensor approach for the on-orbit validation of ocean color satellite data products. *Remote Sensing of Environment, 102*, 12-23

Banse, K. (1976). Rates of growth, respiration and photosynthesis of unicellular algae as related to cell size—a review. *Journal of Phycology, 12*, 135-140

Baretta-Bekker, J., Baretta, J., & Ebenhöh, W. (1997). Microbial dynamics in the marine ecosystem model ERSEM II with decoupled carbon assimilation and nutrient uptake. *Journal of Sea Research, 38*, 195-211

Barlow, R., Aiken, J., Holligan, P., Cummings, D., Maritorena, S., & Hooker, S. (2002). Phytoplankton pigment and absorption characteristics along meridional transects in the Atlantic Ocean. *Deep Sea Research Part I: Oceanographic Research Papers, 49*, 637-660

Barlow, R., Cummings, D., & Gibb, S. (1997). Improved resolution of mono-and divinyl chlorophylls a and b and zeaxanthin and lutein in phytoplankton extracts using reverse phase C-8 HPLC. *Marine Ecology Progress Series*, 303-307

Barlow, R., Lamont, T., Gibberd, M.-J., Airs, R., Jacobs, L., & Britz, K. (2017). Phytoplankton communities and acclimation in a cyclonic eddy in the southwest Indian Ocean. *Deep Sea Research Part I: Oceanographic Research Papers, 124*, 18-30

Barlow, R., Stuart, V., Lutz, V., Sessions, H., Sathyendranath, S., Platt, T., Kyewalyanga, M., Clementson, L., Fukasawa, M., & Watanabe, S. (2007). Seasonal pigment patterns of surface phytoplankton in the subtropical southern hemisphere. *Deep Sea Research Part I: Oceanographic Research Papers, 54*, 1687-1703

Barnes, M.K., Tilstone, G.H., Smyth, T.J., Suggett, D.J., Astoreca, R., Lancelot, C., & Kromkamp, J.C. (2014). Absorption-based algorithm of primary production for total and size-fractionated phytoplankton in coastal waters. *Marine Ecology Progress Series, 504*, 73

Barnes, M.K., Tilstone, G.H., Suggett, D.J., Widdicombe, C.E., Bruun, J., Martinez-Vicente, V., & Smyth, T.J. (2015). Temporal variability in total, micro-and nano-phytoplankton primary production at a coastal site in the western English Channel. *Progress in Oceanography, 137*, 470-483

Behrenfeld, M.J., & Falkowski, P.G. (1997). Photosynthetic rates derived from satellite-based chlorophyll concentration. *Limnology and Oceanography, 42*, 1-20

Behrenfeld, M.J., & Milligan, A.J. (2013). Photophysiological expressions of iron stress in phytoplankton. *Annual review of marine science, 5*, 217-246

Bidigare, R.R., Ondrusek, M.E., Morrow, J.H., & Kiefer, D.A. (1990). In-vivo absorption properties of algal pigments. In, *Orlando'90, 16-20 April* (pp. 290-302): International Society for Optics and Photonics

Birchill, A.J., Milne, A., Woodward, E.M.S., Harris, C., Annett, A., Rusiecka, D., Achterberg, E.P., Gledhill, M., Ussher, S.J., & Worsfold, P.J. (2017). Seasonal iron depletion in temperate shelf seas. *Geophysical Research Letters*

Blanchard, J.L., Jennings, S., Holmes, R., Harle, J., Merino, G., Allen, J.I., Holt, J., Dulvy, N.K., & Barange, M. (2012). Potential consequences of climate change for primary production and fish production in large marine ecosystems. *Phil. Trans. R. Soc. B, 367*, 2979-2989

Blondeau-Patissier, D., Gower, J.F.R., Dekker, A.G., Phinn, S.R., & Brando, V.E. (2014). A review of ocean color remote sensing methods and statistical techniques for the detection, mapping and analysis of phytoplankton blooms in coastal and open oceans. *Progress in Oceanography, 123*, 123-144

Bode, A., & Fernandez, E. (1992). Influence of water-column stability on phytoplankton size and biomass succession patterns in the central Cantabrian Sea (Bay of Biscay). *Journal of plankton research, 14*, 885-902

Bonato, S., Breton, E., Didry, M., Lizon, F., Cornille, V., Lécuyer, E., Christaki, U., & Artigas, L.F. (2016). Spatio-temporal patterns in phytoplankton assemblages in inshore–offshore gradients using flow cytometry: A case study in the eastern English Channel. *Journal of Marine Systems, 156*, 76-85

Boney, A.D. (1986). Seasonal studies on the phytoplankton and primary production in the inner Firth of Clyde. *Proceedings of the Royal Society of Edinburgh. Section B. Biological Sciences, 90*, 203-222

Booth, B. (1988). Size classes and major taxonomic groups of phytoplankton at two locations in the subarctic Pacific Ocean in May and August, 1984. *Marine Biology, 97*, 275-286

Boss, E., Swift, D., Taylor, L., Brickley, P., Zaneveld, R., Riser, S., Perry, M., & Strutton, P. (2008). Observations of pigment and particle distributions in the western North Atlantic from an autonomous float and ocean color satellite. *Limnology and Oceanography, 53*, 2112-2122

Bouman, H., Platt, T., Sathyendranath, S., & Stuart, V. (2005). Dependence of light-saturated photosynthesis on temperature and community structure. *Deep Sea Research Part I: Oceanographic Research Papers, 52*, 1284-1299

Bouman, H.A., Nakane, T., Oka, K., Nakata, K., Kurita, K., Sathyendranath, S., & Platt, T. (2010). Environmental controls on phytoplankton production in coastal ecosystems: A case study from Tokyo Bay. *Estuarine, Coastal and Shelf Science, 87*, 63-72

Bouman, H.A., Platt, T., Sathyendranath, S., Li, W.K., Stuart, V., Fuentes-Yaco, C., Maass, H., Horne, E.P., Ulloa, O., & Lutz, V. (2003). Temperature as indicator of optical properties

and community structure of marine phytoplankton: implications for remote sensing. *Marine Ecology Progress Series, 258*, 19-30

Bouman, H.A., Ulloa, O., Scanlan, D.J., Zwirglmaier, K., Li, W.K., Platt, T., Stuart, V., Barlow, R., Leth, O., & Clementson, L. (2006). Oceanographic basis of the global surface distribution of Prochlorococcus ecotypes. *Science, 312*, 918-921

Boyd, P.W., Watson, A.J., Law, C.S., Abraham, E.R., Trull, T., Murdoch, R., Bakker, D.C., Bowie, A.R., Buesseler, K., & Chang, H. (2000). A mesoscale phytoplankton bloom in the polar Southern Ocean stimulated by iron fertilization. *Nature, 407*, 695-702

Bracher, A., Vountas, M., Dinter, T., Burrows, J., Röttgers, R., & Peeken, I. (2009). Quantitative observation of cyanobacteria and diatoms from space using PhytoDOAS on SCIAMACHY data. *Biogeosciences, 6*, 751-764

Brewin, R.J., Devred, E., Sathyendranath, S., Lavender, S.J., & Hardman-Mountford, N.J. (2011). Model of phytoplankton absorption based on three size classes. *Applied Optics, 50*, 4535-4549

Brewin, R.J., Sathyendranath, S., Müller, D., Brockmann, C., Deschamps, P.-Y., Devred, E., Doerffer, R., Fomferra, N., Franz, B., & Grant, M. (2015). The Ocean Colour Climate Change Initiative: III. A round-robin comparison on in-water bio-optical algorithms. *Remote Sensing of Environment, 162*, 271-294

Brewin, R.J.W., Ciavatta, S., Sathyendranath, S., Jackson, T., Tilstone, G., Curran, K., Airs, R.L., Cummings, D., Brotas, V., Organelli, E., Dall'Olmo, G., & Raitsos, D.E. (2017a). Uncertainty in Ocean-Color Estimates of Chlorophyll for Phytoplankton Groups. *Frontiers in Marine Science, 4*

Brewin, R.J.W., Dall'Olmo, G., Pardo, S., van Dongen-Vogels, V., & Boss, E.S. (2016). Underway spectrophotometry along the Atlantic Meridional Transect reveals high performance in satellite chlorophyll retrievals. *Remote Sensing of Environment, 183*, 82-97

Brewin, R.J.W., Tilstone, G.H., Jackson, T., Cain, T., Miller, P.I., Lange, P.K., Misra, A., & Airs, R.L. (2017b). Modelling size-fractionated primary production in the Atlantic Ocean from remote sensing. *Progress in Oceanography*

Bricaud, A., Babin, M., Morel, A., & Claustre, H. (1995). Variability in the chlorophyll-specific absorption coefficients of natural phytoplankton: Analysis and parameterization. *Journal of Geophysical Research: Oceans, 100*, 13321-13332

Bricaud, A., Claustre, H., Ras, J., & Oubelkheir, K. (2004). Natural variability of phytoplanktonic absorption in oceanic waters: Influence of the size structure of algal populations. *Journal of Geophysical Research: Oceans, 109*

Burd, A.B., & Jackson, G.A. (2009). Particle Aggregation. *Annual Review of Marine Science, 1*, 65-90

Butenschön, M., Clark, J., Aldridge, J.N., Allen, J.I., Artioli, Y., Blackford, J., Bruggeman, J., Cazenave, P., Ciavatta, S., & Kay, S. (2016). ERSEM 15.06: a generic model for marine biogeochemistry and the ecosystem dynamics of the lower trophic levels. *Geoscientific Model Development, 9*, 1293

Carr, M.-E., Friedrichs, M.A.M., Schmeltz, M., Noguchi Aita, M., Antoine, D., Arrigo, K.R., Asanuma, I., Aumont, O., Barber, R., Behrenfeld, M., Bidigare, R., Buitenhuis, E.T., Campbell, J., Ciotti, A., Dierssen, H., Dowell, M., Dunne, J., Esaias, W., Gentili, B., Gregg, W., Groom, S., Hoepffner, N., Ishizaka, J., Kameda, T., Le Quéré, C., Lohrenz, S., Marra, J., Mélin, F., Moore, K., Morel, A., Reddy, T.E., Ryan, J., Scardi, M., Smyth, T., Turpie, K., Tilstone, G., Waters, K., & Yamanaka, Y. (2006). A comparison of global estimates of marine primary production from ocean color. *Deep Sea Research Part II: Topical Studies in Oceanography, 53*, 741-770

Carvalho, G.A., Minnett, P.J., Fleming, L.E., Banzon, V.F., & Baringer, W. (2010). Satellite remote sensing of harmful algal blooms: A new multi-algorithm method for detecting the Florida Red Tide (Karenia brevis). *Harmful algae, 9*, 440-448

Cermeno, P., Estévez-Blanco, P., Maranón, E., & Fernóndez, E. (2005). Maximum photosynthetic efficiency of size-fractionated phytoplankton assessed by 14C uptake and fast repetition rate fluorometry. *Limnology and Oceanography, 50*, 1438-1446

Cermeño, P., Marañón, E., Rodríguez, J., & Fernández, E. (2005). Large-sized phytoplankton sustain higher carbon-specific photosynthesis than smaller cells in a coastal eutrophic ecosystem. *Marine Ecology Progress Series, 297*, 51-60

Chen, J., Zhu, W.-N., Tian, Y.Q., & Yu, Q. (2017). Estimation of colored dissolved organic matter from Landsat-8 imagery for complex inland water: case study of Lake Huron. *IEEE Transactions on Geoscience and Remote Sensing, 55*, 2201-2212

Chen, Y.-L.L. (2000). Comparisons of primary productivity and phytoplankton size structure in the marginal regions of southern East China Sea. *Continental Shelf Research, 20*, 437-458

Chisholm, S.W. (1992). Phytoplankton size. *Primary productivity and biogeochemical cycles in the sea* (pp. 213-237): Springer

Ciotti, A.M., Lewis, M.R., & Cullen, J.J. (2002). Assessment of the relationships between dominant cell size in natural phytoplankton communities and the spectral shape of the absorption coefficient. *Limnology and Oceanography, 47*, 404-417

Claustre, H., Babin, M., Merien, D., Ras, J., Prieur, L., Dallot, S., Prasil, O., Dousova, H., & Moutin, T. (2005). Toward a taxon-specific parameterization of bio-optical models of primary production: A case study in the North Atlantic. *Journal of Geophysical Research: Oceans, 110*

Claustre, H., Hooker, S.B., Van Heukelem, L., Berthon, J.-F., Barlow, R., Ras, J., Sessions, H., Targa, C., Thomas, C.S., van der Linde, D., & Marty, J.-C. (2004). An intercomparison of HPLC phytoplankton pigment methods using in situ samples: application to remote sensing and database activities. *Marine Chemistry, 85*, 41-61

Cleveland, J.S. (1995). Regional models for phytoplankton absorption as a function of chlorophyll a concentration. *Journal of Geophysical Research: Oceans, 100*, 13333-13344

Cloern, J.E. (1996). Phytoplankton bloom dynamics in coastal ecosystems: A review with some general lessons from sustained investigation of San Francisco Bay, California. *Reviews of Geophysics, 34*, 127-168

Coupel, P., Matsuoka, A., Ruiz-Pino, D., Gosselin, M., Marie, D., Tremblay, J.-É., & Babin, M. (2015). Pigment signatures of phytoplankton communities in the Beaufort Sea. *Biogeosciences, 12*, 991-1006

Cullen, J., Stewart, E., Renger, E., Eppley, R., & Winant, C. (1983). Vertical motion of the thermocline, nitracline and chlorophyll maximum layers in relation to currents on the Southern California Shelf. *Journal of Marine Research, 41*, 239-262

Cullen, J.J., Neale, P.J., & Lesser, M.P. (1992a). Biological weighting function for the inhibition of phytoplankton photosynthesis by ultraviolet radiation. *SCIENCE-NEW YORK THEN WASHINGTON-*, 646-646

Cullen, J.J., Neale, P.J., & Lesser, M.P. (1992b). Biological weighting function for the inhibition of phytoplankton photosynthesis by ultraviolet radiation. *Science, 258*, 646-650

Dall'Olmo, G., Brewin, R.J.W., Nencioli, F., Organelli, E., Lefering, I., McKee, D., Röttgers, R., Mitchell, C., Boss, E., Bricaud, A., & Tilstone, G. (2017). Determination of the absorption coefficient of chromophoric dissolved organic matter from underway spectrophotometry. *Optics Express, 25*, A1079-A1095

Dam, H.G., Roman, M.R., & Youngbluth, M.J. (1995). Downward export of respiratory carbon and dissolved inorganic nitrogen by diel-migrant mesozooplankton at the JGOFS Bermuda time-series station. *Deep Sea Research Part I: Oceanographic Research Papers, 42*, 1187-1197

de Boyer Montégut, C., Madec, G., Fischer, A.S., Lazar, A., & Iudicone, D. (2004). Mixed layer depth over the global ocean: An examination of profile data and a profile-based climatology. *Journal of Geophysical Research: Oceans, 109*

de Haas, H., van Weering, T.C., & de Stigter, H. (2002). Organic carbon in shelf seas: sinks or sources, processes and products. *Continental shelf research, 22*, 691-717

de Madariaga, I., & Joint, I. (1994). Photosynthesis and carbon metabolism by size-fractionated phytoplankton in the southern North Sea in early summer. *Continental shelf research, 14*, 295-311

Devred, E., Sathyendranath, S., Stuart, V., Maass, H., Ulloa, O., & Platt, T. (2006). A two-component model of phytoplankton absorption in the open ocean: Theory and applications. *Journal of Geophysical Research: Oceans, 111*

Dijkman, N.A., & Kromkamp, J.C. (2006). Photosynthetic characteristics of the phytoplankton in the Scheldt estuary: community and single-cell fluorescence measurements. *European Journal of Phycology, 41*, 425-434

Dixon, J.L., Statham, P.J., Widdicombe, C.E., Jones, R.M., Barquero-Molina, S., Dickie, B., Nimmo, M., & Turley, C.M. (2006). Cadmium uptake by marine micro-organisms in the English Channel and Celtic Sea. *Aquatic Microbial Ecology, 44*, 31-43

Dubinsky, Z., & Stambler, N. (2009). Photoacclimation processes in phytoplankton: mechanisms, consequences, and applications. *Aquatic Microbial Ecology, 56*, 163-176

Durham, W.M., & Stocker, R. (2011). Thin phytoplankton layers: characteristics, mechanisms, and consequences

Duyens, L. (1956). The flattering of the absorption spectrum of suspensions, as compared to that of solutions. *Biochimica et Biophysica Acta, 19*, 1-12

Duysens, L. (1956). Energy transformations in photosynthesis. *Annual review of plant physiology, 7*, 25-50

Eppley, R.W., & Sloan, P.R. (1965). Carbon balance experiments with marine phytoplankton. *Journal of the Fisheries Board of Canada, 22*, 1083-1097

Erga, S.R., Ssebiyonga, N., Hamre, B., Frette, Ø., Rey, F., & Drinkwater, K. (2014). Nutrients and phytoplankton biomass distribution and activity at the Barents Sea Polar Front during summer near Hopen and Storbanken. *Journal of Marine Systems, 130*, 181-192

Falkowski, P.G., Barber, R.T., & Smetacek, V. (1998). Biogeochemical controls and feedbacks on ocean primary production. *Science, 281*, 200-206

Falkowski, P.G., Flagg, C.N., Rowe, G.T., Smith, S.L., Whitledge, T.E., & Wirick, C.D. (1988). The fate of a spring phytoplankton bloom: export or oxidation? *Continental shelf research, 8*, 457-484

Falkowski, P.G., Greene, R., & Kolber, Z. (1993). Light utilization and photoinhibition of photosynthesis in marine phytoplankton. In: Brookhaven National Lab., Upton, NY (United States)

Falkowski, P.G., Katz, M.E., Knoll, A.H., Quigg, A., Raven, J.A., Schofield, O., & Taylor, F.J.R. (2004). The Evolution of Modern Eukaryotic Phytoplankton. *Science, 305*, 354-360

Fasham, M., Holligan, P., & Pugh, P. (1983). The spatial and temporal development of the spring phytoplankton bloom in the Celtic Sea, April 1979. *Progress in Oceanography, 12*, 87-145

Ferreira, A., Stramski, D., Garcia, C.A., Garcia, V.M., Ciotti, A.M., & Mendes, C.R. (2013). Variability in light absorption and scattering of phytoplankton in Patagonian waters: Role of community size structure and pigment composition. *Journal of Geophysical Research: Oceans, 118*, 698-714

Field, C.B., Behrenfeld, M.J., Randerson, J.T., & Falkowski, P. (1998). Primary production of the biosphere: integrating terrestrial and oceanic components. *Science, 281*, 237-240

Finkel, Z., & Irwin, A. (2001). Light absorption by phytoplankton and the filter amplification correction: cell size and species effects. *Journal of experimental marine biology and ecology, 259*, 51-61

Finkel, Z.V., Beardall, J., Flynn, K.J., Quigg, A., Rees, T.A.V., & Raven, J.A. (2009). Phytoplankton in a changing world: cell size and elemental stoichiometry. *Journal of plankton research, 32*, 119-137

Finkel, Z.V., Irwin, A.J., & Schofield, O. (2004). Resource limitation alters the 3/4 size scaling of metabolic rates in phytoplankton. *Marine Ecology Progress Series, 273*, 269-279

Fishwick, J.R., Aiken, J., Barlow, R., Sessions, H., Bernard, S., & Ras, J. (2006). Functional relationships and bio-optical properties derived from phytoplankton pigments, optical and photosynthetic parameters; a case study of the Benguela ecosystem. *Journal of the Marine Biological Association of the United Kingdom, 86*, 1267-1280

Flameling, I.A., & Kromkamp, J. (1997). Photoacclimation of Scenedesmus protuberans (Chlorophyceae) to fluctuating irradiances simulating vertical mixing. *Journal of plankton research, 19*, 1011-1024

Follows, M.J., Dutkiewicz, S., Grant, S., & Chisholm, S.W. (2007). Emergent biogeography of microbial communities in a model ocean. *Science, 315*, 1843-1846

Forget, M.-H., Sathyendranath, S., Platt, T., Pommier, J., Vis, C., Kyewalyanga, M., & Hudon, C. (2007). Extraction of photosynthesis-irradiance parameters from phytoplankton production data: demonstration in various aquatic systems. *Journal of plankton research, 29*, 249-262

Fragoso, G.M., Poulton, A.J., Yashayaev, I.M., Head, E.J., & Purdie, D.A. (2017). Spring phytoplankton communities of the Labrador Sea (2005-2014): pigment signatures, photophysiology and elemental ratios. *Biogeosciences, 14*, 1235

Frederiksen, M., Edwards, M., Richardson, A.J., Halliday, N.C., & Wanless, S. (2006). From plankton to top predators: bottom-up control of a marine food web across four trophic levels. *Journal of Animal Ecology, 75*, 1259-1268

Friedlingstein, P., Cox, P., Betts, R., Bopp, L., von Bloh, W., Brovkin, V., Cadule, P., Doney, S., Eby, M., & Fung, I. (2006). Climate–carbon cycle feedback analysis: results from the C4MIP model intercomparison. *Journal of climate, 19*, 3337-3353

Froneman, P., Laubscher, R., & McQuaid, C. (2001). Size-fractionated primary production in the south Atlantic and Atlantic sectors of the Southern Ocean. *Journal of plankton research, 23*, 611-622

Fujiki, T., & Taguchi, S. (2002). Variability in chlorophyll a specific absorption coefficient in marine phytoplankton as a function of cell size and irradiance. *Journal of plankton research, 24*, 859-874

Furuya, K., Hasegawa, O., Yoshikawa, T., & Taguchi, S. (1998). Photosynthesis-irradiance relationship of phytoplankton and primary production in the vicinity of Kuroshio warm core ring in spring. *Journal of oceanography, 54*, 545-552

Gall, M., & Zeldis, J. (2011). Phytoplankton biomass and primary production responses to physico-chemical forcing across the northeastern New Zealand continental shelf. *Continental shelf research, 31*, 1799-1810

Gallegos, C.L., Platt, T., Harrison, W., & Irwin, B. (1983). Photosynthetic parameters of arctic marine phytoplankton: vertical variations and time scales of adaptation. *Limnol. Oceanogr, 28*, 698-708

García-Martín, E.E., Daniels, C.J., Davidson, K., Davis, C.E., Mahaffey, C., Mayers, K.M.J., McNeill, S., Poulton, A.J., Purdie, D.A., Tarran, G.A., & Robinson, C. (2017). Seasonal changes in plankton respiration and bacterial metabolism in a temperate shelf sea. *Progress in Oceanography*

Garcia-Soto, C., & Pingree, R.D. (2009). Spring and summer blooms of phytoplankton (SeaWiFS/MODIS) along a ferry line in the Bay of Biscay and western English Channel. *Continental shelf research, 29*, 1111-1122

Gaulke, A.K., Wetz, M.S., & Paerl, H.W. (2010). Picophytoplankton: A major contributor to planktonic biomass and primary production in a eutrophic, river-dominated estuary. *Estuarine, Coastal and Shelf Science, 90*, 45-54

Geider, R., MacIntyre, H., & Kana, T. (1997). Dynamic model of phytoplankton growth and acclimation: responses of the balanced growth rate and the chlorophyll a: carbon ratio to light, nutrient-limitation and temperature. *Oceanographic Literature Review, 9*, 974

Geider, R.J., MacIntyre, H.L., & Kana, T.M. (1998). A dynamic regulatory model of phytoplanktonic acclimation to light, nutrients, and temperature. *Limnology and Oceanography, 43*, 679-694

Giering, S., Sanders, R., Martin, A., Lindemann, C., Möller, K., Daniels, C., Mayor, D., & St John, M. (2016). High export via small particles before the onset of the North Atlantic spring bloom. *Journal of Geophysical Research: Oceans, 121*, 6929-6945

Goericke, R., & Montoya, J.P. (1998). Estimating the contribution of microalgal taxa to chlorophyll a in the field—variations of pigment ratios under nutrient-and light-limited growth. *Marine Ecology Progress Series*, 97-112

Gordon, H.R., Brown, O.B., & Jacobs, M.M. (1975). Computed relationships between the inherent and apparent optical properties of a flat homogeneous ocean. *Applied Optics, 14*, 417-427

Gordon, H.R., & Clark, D.K. (1980). Remote sensing optical properties of a stratified ocean: an improved interpretation. *Applied Optics, 19*, 3428-3430

Gordon, H.R., & McCluney, W. (1975). Estimation of the depth of sunlight penetration in the sea for remote sensing. *Applied Optics, 14*, 413-416

Gowen, R.J., Hydes, D., Mills, D., Stewart, B., Brown, J., Gibson, C., Shammon, T., Allen, M., & Malcolm, S.J. (2002). Assessing trends in nutrient concentrations in coastal shelf seas: a case study in the Irish Sea. *Estuarine, Coastal and Shelf Science, 54*, 927-939

Grebmeier, J.M., & McRoy, C.P. (1989). Pelagic-benthic coupling on the shelf of the northern Bering and Chukchi Seas. III. Benthic food supply and carbon cycling. *Marine Ecology Progress Series*, 79-91

Grebmeier, J.M., McRoy, C.P., & Feder, H.M. (1988). Pelagic-benthic coupling on the shelf of the northern Bering and Chukchi Seas. I. Food supply source and benthic biomass. *Marine Ecology Progress Series*, 57-67

Green, J.M., Simpson, J.H., Legg, S., & Palmer, M.R. (2008). Internal waves, baroclinic energy fluxes and mixing at the European shelf edge. *Continental shelf research, 28*, 937-950

Greg Mitchell, B., & Kiefer, D.A. (1988). Chlorophyll α specific absorption and fluorescence excitation spectra for light-limited phytoplankton. *Deep Sea Research Part A. Oceanographic Research Papers, 35*, 639-663

Gregg, W.W., & Carder, K.L. (1990). A simple spectral solar irradiance model for cloudless maritime atmospheres. *Limnology and Oceanography, 35*, 1657-1675

Groom, S., Martinez-Vicente, V., Fishwick, J., Tilstone, G., Moore, G., Smyth, T., & Harbour, D. (2009). The Western English Channel observatory: Optical characteristics of station L4. *Journal of Marine Systems, 77*, 278-295

Guanter, L., Kaufmann, H., Segl, K., Foerster, S., Rogass, C., Chabrillat, S., Kuester, T., Hollstein, A., Rossner, G., & Chlebek, C. (2015). The EnMAP spaceborne imaging spectroscopy mission for earth observation. *Remote Sensing, 7*, 8830-8857

Hallegraeff, G.M. (2010). OCEAN CLIMATE CHANGE, PHYTOPLANKTON COMMUNITY RESPONSES, AND HARMFUL ALGAL BLOOMS: A FORMIDABLE PREDICTIVE CHALLENGE1. *Journal of Phycology, 46*, 220-235

Hama, T., Miyazaki, T., Ogawa, Y., Iwakuma, T., Takahashi, M., Otsuki, A., & Ichimura, S. (1983). Measurement of photosynthetic production of a marine phytoplankton population using a stable 13 C isotope. *Marine Biology, 73*, 31-36

Hamme, R.C., Webley, P.W., Crawford, W.R., Whitney, F.A., DeGrandpre, M.D., Emerson, S.R., Eriksen, C.C., Giesbrecht, K.E., Gower, J.F., & Kavanaugh, M.T. (2010). Volcanic ash fuels anomalous plankton bloom in subarctic northeast Pacific. *Geophysical Research Letters, 37*

Hardin, G. (1960). The competitive exclusion principle. *Science, 131*, 1292-1297

Harding Jr, L.W., Meeson, B.W., & Fisher Jr, T.R. (1986). Phytoplankton production in two east coast estuaries: photosynthesis-light functions and patterns of carbon assimilation in Chesapeake and Delaware Bays. *Estuarine, Coastal and Shelf Science, 23*, 773-806

Harrison, W.G., & Platt, T. (1980). Variations in assimilation number of coastal marine phyto-phytoplankton: Effects of environmental co-variates. *Journal of plankton research, 2*, 249-260

Helbling, E.W., Buma, A.G., de Boer, M.K., & Villafañe, V.E. (2001). In situ impact of solar ultraviolet radiation on photosynthesis and DNA in temperate marine phytoplankton. *Marine Ecology Progress Series, 211*, 43-49

Henriksen, P., Riemann, B., Kaas, H., Sørensen, H.M., & Sørensen, H.L. (2002). Effects of nutrient-limitation and irradiance on marine phytoplankton pigments. *Journal of plankton research, 24*, 835-858

Henson, S.A., Sanders, R., & Madsen, E. (2012). Global patterns in efficiency of particulate organic carbon export and transfer to the deep ocean. *Global Biogeochemical Cycles, 26*

Hessen, D.O., Færøvig, P.J., & Andersen, T. (2002). Light, nutrients, and P:C ratios in algae: Grazer performance related to food quality and quantity. *Ecology, 83*, 1886-1898

Hickman, A.E., Holligan, P.M., Moore, C.M., Sharples, J., Krivtsov, V., & Palmer, M.R. (2009). Distribution and chromatic adaptation of phytoplankton within a shelf sea thermocline. *Limnology and Oceanography, 54*, 525-536

Hickman, A.E., Moore, C., Sharples, J., Lucas, M.I., Tilstone, G.H., Krivtsov, V., & Holligan, P.M. (2012). Primary production and nitrate uptake within the seasonal thermocline of a stratified shelf sea. *Marine Ecology Progress Series*

Hirata, T., Aiken, J., Hardman-Mountford, N., Smyth, T.J., & Barlow, R.G. (2008). An absorption model to determine phytoplankton size classes from satellite ocean colour. *Remote Sensing of Environment, 112*, 3153-3159

Hoepffner, N., & Sathyendranath, S. (1991). Effect of pigment composition on absorption properties of phytoplankton. *Mar. Ecol. Prog. Ser, 73*, l-23

Holligan, P. (1981). Biological implications of fronts on the northwest European continental shelf. *Philosophical Transactions of the Royal Society of London A: Mathematical, Physical and Engineering Sciences, 302*, 547-562

Holligan, P., & Groom, S. (1986). Phytoplankton distributions along the shelf break. *Proceedings of the Royal Society of Edinburgh, Section B: Biological Sciences, 88*, 239-263

Holligan, P., leB. Williams, P., Purdie, D., & Harris, R. (1984). Photosynthesis, respiration and nitrogen supply of plankton populations in stratified, frontal and tidally mixed shelf waters. *Marine Ecology Progress Series*, 201-213

Horton, P., Ruban, A., & Walters, R. (1996). Regulation of light harvesting in green plants. *Annual review of plant biology, 47*, 655-684

Hostetler, C.A., Behrenfeld, M.J., Hu, Y., Hair, J.W., & Schulien, J.A. (2017). Spaceborne Lidar in the Study of Marine Systems. *Annual Review of Marine Science*

Hu, Y., Behrenfeld, M., Hostetler, C., Pelon, J., Trepte, C., Hair, J., Slade, W., Cetinic, I., Vaughan, M., & Lu, X. (2016). Ocean lidar measurements of beam attenuation and a roadmap to accurate phytoplankton biomass estimates. In, *EPJ Web of Conferences* (p. 22003): EDP Sciences

Hunter, P.D., Tyler, A.N., Présing, M., Kovács, A.W., & Preston, T. (2008). Spectral discrimination of phytoplankton colour groups: The effect of suspended particulate matter and sensor spectral resolution. *Remote Sensing of Environment, 112*, 1527-1544

Huot, Y., Babin, M., & Bruyant, F. (2013). Photosynthetic parameters in the Beaufort Sea in relation to the phytoplankton community structure. *Biogeosciences, 10*, 3445

Hutchinson, G.E. (1961). The paradox of the plankton. *The American Naturalist, 95*, 137-145

Iglesias-Rodríguez, M.D., Brown, C.W., Doney, S.C., Kleypas, J., Kolber, D., Kolber, Z., Hayes, P.K., & Falkowski, P.G. (2002). Representing key phytoplankton functional groups in ocean carbon cycle models: Coccolithophorids. *Global Biogeochemical Cycles, 16*

Ioccg (2000). Remote sensing of ocean colour in coastal and other optically-complex waters. *IOCCG Report*, 1-137

Iriarte, A., & Purdie, D.A. (1994). Size distribution of chlorophyll a biomass and primary production in a temperate estuary (Southampton Water): the contribution of photosynthetic picoplankton. *Marine Ecology Progress Series*, 283-297

Irwin, A.J., Finkel, Z.V., Schofield, O.M., & Falkowski, P.G. (2006). Scaling-up from nutrient physiology to the size-structure of phytoplankton communities. *Journal of plankton research, 28*, 459-471

Jackson, T., Sathyendranath, S., & Mélin, F. (2017). An improved optical classification scheme for the Ocean Colour Essential Climate Variable and its applications. *Remote Sensing of Environment*

Jassby, A.D., & Platt, T. (1976). Mathematical formulation of the relationship between photosynthesis and light for phytoplankton. *Limnology and Oceanography, 21*, 540-547

Johnsen, G., & Sakshaug, E. (2007). Biooptical characteristics of PSII and PSI in 33 species (13 pigment groups) of marine phytoplankton, and the relevance for pulse-amplitude-modulated and fast-repetition-rate fluorometry. *Journal of Phycology, 43*, 1236-1251

Johnsen, G., Samset, O., Granskog, L., & Sakshaug, E. (1994). In vivo absorption characteristics in 10 classes of bloom-forming phytoplankton: taconomic characteristics and responses to photoadaptation by means of discriminant and HPLC analysis. *Marine Ecology Progress Series*, 149-157

Johnson, Z.I., Zinser, E.R., Coe, A., McNulty, N.P., Woodward, E.M.S., & Chisholm, S.W. (2006). Niche partitioning among Prochlorococcus ecotypes along ocean-scale environmental gradients. *Science, 311*, 1737-1740

Joint, I., Owens, N., Pomroy, A., & Pomeroy, A. (1986). Seasonal production of photosynthetic picoplankton and nanoplankton in the Celtic Sea. *Marine Ecology Progress Series*, 251-258

Joint, I., & Pomroy, A. (1986). Photosynthetic characteristics of nanoplankton and picoplankton from the surface mixed layer. *Marine Biology, 92*, 465-474

Joint, I., & Pomroy, A. (1993). Phytoplankton biomass and production in the southern North Sea. *Marine Ecology-Progress Series, 99*, 169-169

Joint, I., Pomroy, A., Savidge, G., & Boyd, P. (1993). Size-fractionated primary productivity in the northeast Atlantic in May–July 1989. *Deep Sea Research Part II: Topical Studies in Oceanography, 40*, 423-440

Joint, I., Wollast, R., Chou, L., Batten, S., Elskens, M., Edwards, E., Hirst, A., Burkill, P., Groom, S., & Gibb, S. (2001). Pelagic production at the Celtic Sea shelf break. *Deep Sea Research Part II: Topical Studies in Oceanography, 48*, 3049-3081

Kahru, M., & No¨mmann, S. (1990). The phytoplankton spring bloom in the Baltic Sea in 1985, 1986: multitude of spatio-temporal scales. *Continental shelf research, 10*, 329-354

Kameda, T., & Ishizaka, J. (2005). Size-fractionated primary production estimated by a two-phytoplankton community model applicable to ocean color remote sensing. *Journal of oceanography, 61*, 663-672

Karentz, D., Cleaver, J.E., & Mitchell, D.L. (1991). Cell survival characteristics and molecular responses of Antarctic phytoplankton to ultraviolet-B radiation. *Journal of Phycology, 27*, 326-341

Kempes, C.P., Dutkiewicz, S., & Follows, M.J. (2012). Growth, metabolic partitioning, and the size of microorganisms. *Proceedings of the National Academy of Sciences, 109*, 495-500

Key, T., McCarthy, A., Campbell, D.A., Six, C., Roy, S., & Finkel, Z.V. (2010). Cell size trade-offs govern light exploitation strategies in marine phytoplankton. *Environmental microbiology, 12*, 95-104

Keys, M., Tilstone, G., Findlay, H.S., Widdicombe, C.E., & Lawson, T. (2017). Effects of elevated CO2 and temperature on phytoplankton community biomass, species composition and photosynthesis during an autumn bloom in the Western English Channel. *Biogeosciences*

Kiørboe, T. (1993a). Turbulence, phytoplankton cell size, and the structure of pelagic food webs. *Advances in marine biology, 29*, 1-72

Kiørboe, T. (1993b). Turbulence, phytoplankton cell size, and the structure of pelagic food webs. *Advances in marine biology* (pp. 1-72): Elsevier

Kirk, J. (1975). A theoretical analysis of the contribution of algal cells to the attenuation of light within natural waters II. spherical cells. *New Phytologist, 75*, 21-36

Kirk, J.T. (1994). *Light and photosynthesis in aquatic ecosystems*. Cambridge university press

Kishino, M., Takahashi, M., Okami, N., & Ichimura, S. (1985). Estimation of the spectral absorption coefficients of phytoplankton in the sea. *Bulletin of marine science, 37*, 634-642

Klausmeier, C.A., & Litchman, E. (2001). Algal games: The vertical distribution of phytoplankton in poorly mixed water columns. *Limnology and Oceanography, 46*, 1998-2007

Kratzer, S., Bowers, D., & Tett, P. (2000). Seasonal changes in colour ratios and optically active contituents in the optical Case-2 waters of the Menai Strait, North Wales. *International Journal of Remote Sensing, 21*, 2225-2246

Kulk, G., de Vries, P., van de Poll, W.H., Visser, R.J., & Buma, A.G. (2012). Temperature-dependent growth and photophysiology of prokaryotic and eukaryotic oceanic picophytoplankton. *Marine Ecology Progress Series, 466*, 43-55

Kurekin, A., Miller, P., & Van der Woerd, H. (2014). Satellite discrimination of Karenia mikimotoi and Phaeocystis harmful algal blooms in European coastal waters: Merged classification of ocean colour data. *Harmful algae, 31*, 163-176

Kutser, T. (2009). Passive optical remote sensing of cyanobacteria and other intense phytoplankton blooms in coastal and inland waters. *International Journal of Remote Sensing, 30*, 4401-4425

Kyewalyanga, M., Platt, T., & Sathyendranath, S. (1992). Ocean primary production calculated by spectral and broad-band models. *Marine Ecology Progress Series*, 171-185

Kyewalyanga, M., Platt, T., & Sathyendranath, S. (1997a). Estimation of the photosynthetic action spectrum: implication for primary production models. *Marine Ecology Progress Series, 146*, 207-223

Kyewalyanga, M.N., Platt, T., & Sathyendranath, S. (1997b). Estimation of the photosynthetic action spectrum: implication for primary production models. *Marine Ecology Progress Series, 146*, 207-223

Lancelot, C., & Billen, G. (1984). Activity of heterotrophic bacteria and its coupling to primary production during the spring phytoplankton bloom in the Southern Bight of the North Sea. *Limnology and Oceanography, 29*, 721-730

Laurenceau-Cornec, E.C., Trull, T., Davies, D.M., Bray, S.G., Doran, J., Planchon, F., Carlotti, F., Jouander, M., Cavagna, A.-J., & Waite, A. (2015). The relative importance of

phytoplankton aggregates and zooplankton fecal pellets to carbon export: insights from free-drifting sediment trap deployments in naturally iron-fertilised waters near the Kerguelen Plateau. *Biogeosciences, 12*, 1007-1027

Laurion, I., & Vincent, W.F. (1998). Cell size versus taxonomic composition as determinants of UV-sensitivity in natural phytoplankton communities. *Limnology and Oceanography, 43*, 1774-1779

Lee, J.-Y., Tett, P., Jones, K., Jones, S., Luyten, P., Smith, C., & Wild-Allen, K. (2002). The PROWQM physical–biological model with benthic–pelagic coupling applied to the northern North Sea. *Journal of Sea Research, 48*, 287-331

Legendre, L., Rivkin, R.B., Weinbauer, M.G., Guidi, L., & Uitz, J. (2015). The microbial carbon pump concept: Potential biogeochemical significance in the globally changing ocean. *Progress in Oceanography, 134*, 432-450

Lesser, M.P. (1996). Acclimation of phytoplankton to UV-B radiation: oxidative stress and photoinhibition of photosynthesis are not prevented by UV-absorbing compounds in the dinoflagellate Prorocentrum micans. *Marine Ecology Progress Series, 132*, 287-297

Levin, L.A., Liu, K.-K., Emeis, K.-C., Breitburg, D.L., Cloern, J., Deutsch, C., Giani, M., Goffart, A., Hofmann, E.E., & Lachkar, Z. (2015). Comparative biogeochemistry–ecosystem–human interactions on dynamic continental margins. *Journal of Marine Systems, 141*, 3-17

Lewis, M.R., Warnock, R.E., & Platt, T. (1985a). Absorption and photosynthetic action spectra for natural phytoplankton populations: implications for production in the open ocean. *Limnology and Oceanography, 30*, 794-806

Lewis, M.R., Warnock, R.E., & Platt, T. (1985b). Absorption and photosynthetic action spectra for natural phytoplankton populations: Implications for production in the open ocean1. *Limnology and Oceanography, 30*, 794-806

Li, B., Karl, D.M., Letelier, R.M., & Church, M.J. (2011). Size-dependent photosynthetic variability in the North Pacific Subtropical Gyre. *Marine Ecology Progress Series, 440*, 27-40

Litchman, E., Neale, P.J., & Banaszak, A.T. (2002). Increased sensitivity to ultraviolet radiation in nitrogen-limited dinoflagellates: Photoprotection and repair. *Limnology and Oceanography, 47*, 86-94

Lohrenz, S.E., Fahnenstiel, G.L., Redalje, D.G., Lang, G.A., Dagg, M.J., Whitledge, T.E., & Dortch, Q. (1999). Nutrients, irradiance, and mixing as factors regulating primary

production in coastal waters impacted by the Mississippi River plume. *Continental shelf research, 19*, 1113-1141

Lohrenz, S.E., Weidemann, A.D., & Tuel, M. (2003). Phytoplankton spectral absorption as influenced by community size structure and pigment composition. *Journal of plankton research, 25*, 35-61

Longhurst, A., Bedo, A., Harrison, W., Head, E., & Sameoto, D. (1990). Vertical flux of respiratory carbon by oceanic diel migrant biota. *Deep Sea Research Part A. Oceanographic Research Papers, 37*, 685-694

Longhurst, A., Sathyendranath, S., Platt, T., & Caverhill, C. (1995). An estimate of global primary production in the ocean from satellite radiometer data. *Journal of plankton research, 17*, 1245-1271

Lubac, B., Loisel, H., Guiselin, N., Astoreca, R., Felipe Artigas, L., & Mériaux, X. (2008). Hyperspectral and multispectral ocean color inversions to detect Phaeocystis globosa blooms in coastal waters. *Journal of Geophysical Research: Oceans, 113*, n/a-n/a

Lutz, V.A., Sathyendaranath, S., Head, E.J.H., & Li, W.K.W. (2001). Changes in the In Vivo Absorption and Fluorescence Excitation Spectra with Growth Irradiance in Three Species of Phytoplankton. *Journal of plankton research, 23*, 555-569

Lutz, V.A., Segura, V., Dogliotti, A.I., Gagliardini, D.A., Bianchi, A.A., & Balestrini, C.F. (2009). Primary production in the Argentine Sea during spring estimated by field and satellite models. *Journal of plankton research*, fbp117

MacIntyre, H.L., Kana, T.M., Anning, T., & Geider, R.J. (2002a). Photoacclimation of photosynthesis irradiance response curves and photosynthetic pigments in microalgae and cyanobacteria. *Journal of Phycology, 38*, 17-38

MacIntyre, H.L., Kana, T.M., Anning, T., & Geider, R.J. (2002b). Photoacclimation of photosynthesis irradiance response curves and photosynthetic pigments in microalgae and cyanobacteria1. *Journal of Phycology, 38*, 17-38

MacIntyre, H.L., Kana, T.M., & Geider, R.J. (2000). The effect of water motion on short-term rates of photosynthesis by marine phytoplankton. *Trends in plant science, 5*, 12-17

Mackey, M., Mackey, D., Higgins, H., & Wright, S. (1996). CHEMTAX—a program for estimating class abundances from chemical markers: application to HPLC measurements of phytoplankton. *Marine Ecology Progress Series*, 265-283

Maguer, J.-F., L'Helguen, S., & Waeles, M. (2015). Effects of mixing-induced irradiance fluctuations on nitrogen uptake in size-fractionated coastal phytoplankton communities. *Estuarine, Coastal and Shelf Science, 154*, 1-11

Mahadevan, A., D'Asaro, E., Lee, C., & Perry, M.J. (2012). Eddy-driven stratification initiates North Atlantic spring phytoplankton blooms. *Science, 337*, 54-58

Malone, T., Kemp, W., Ducklow, H., Boynton, W., Tuttle, J., & Jonas, R. (1986). Lateral variation in the production and fate of phytoplankton in a partially stratified estuary. *Marine Ecology Progress Series*, 149-160

Malone, T., & Neale, P. (1981). Parameters of light-dependent photosynthesis for phytoplankton size fractions in temperate estuarine and coastal environments. *Marine Biology, 61*, 289-297

Mannino, A., Russ, M.E., & Hooker, S.B. (2008). Algorithm development and validation for satellite-derived distributions of DOC and CDOM in the US Middle Atlantic Bight. *Journal of Geophysical Research: Oceans, 113*

Manno, C., Stowasser, G., Enderlein, P., Fielding, S., & Tarling, G.A. (2015). The contribution of zooplankton faecal pellets to deep carbon transport in the Scotia Sea (Southern Ocean). *Biogeosciences, 12*, 1955-1965

Mantoura, R., & Llewellyn, C. (1983). The rapid determination of algal chlorophyll and carotenoid pigments and their breakdown products in natural waters by reverse-phase high-performance liquid chromatography. *Analytica Chimica Acta, 151*, 297-314

Marañón, E. (2007). Inter-specific scaling of phytoplankton production and cell size in the field. *Journal of plankton research, 30*, 157-163

Marañón, E., & Holligan, P.M. (1999). Photosynthetic parameters of phytoplankton from 50 N to 50 S in the Atlantic Ocean. *Marine Ecology Progress Series*, 191-203

Marañón, E., Holligan, P.M., Barciela, R., González, N., Mouriño, B., Pazó, M.J., & Varela, M. (2001). Patterns of phytoplankton size structure and productivity in contrasting open-ocean environments. *Marine Ecology Progress Series, 216*, 43-56

Marañón, E., Steele, J., Thorpe, A., & Turekian, K. (2009). Phytoplankton size structure. *Elements of Physical Oceanography: A derivative of the Encyclopedia of Ocean Sciences*, 85

Margalef, R. (1978). Life-forms of phytoplankton as survival alternatives in an unstable environment. *Oceanologica acta, 1*, 493-509

Marra, J., Trees, C.C., Bidigare, R., & Barber, R. (2000). Pigment absorption and quantum yields in the Arabian Sea. *Deep Sea Research Part II: Topical Studies in Oceanography, 47*, 1279-1299

Martin, A.P., & Richards, K.J. (2001). Mechanisms for vertical nutrient transport within a North Atlantic mesoscale eddy. *Deep Sea Research Part II: Topical Studies in Oceanography, 48*, 757-773

McGillicuddy, D., Anderson, L., Doney, S., & Maltrud, M. (2003). Eddy-driven sources and sinks of nutrients in the upper ocean: Results from a 0.1 resolution model of the North Atlantic. *Global Biogeochemical Cycles, 17*

McQuatters-Gollop, A., Raitsos, D.E., Edwards, M., Pradhan, Y., Mee, L.D., Lavender, S.J., & Attrill, M.J. (2007). A long-term chlorophyll dataset reveals regime shift in North Sea phytoplankton biomass unconnected to nutrient levels. *Limnology and Oceanography, 52*, 635-648

Menden-Deuer, S., & Lessard, E.J. (2000). Carbon to volume relationships for dinoflagellates, diatoms, and other protist plankton. *Limnology and Oceanography, 45*, 569-579

Merico, A., Tyrrell, T., Brown, C., Groom, S., & Miller, P. (2003). Analysis of satellite imagery for Emiliania huxleyi blooms in the Bering Sea before 1997. *Geophysical Research Letters, 30*

Mignot, A., Claustre, H., Uitz, J., Poteau, A., D'Ortenzio, F., & Xing, X. (2014). Understanding the seasonal dynamics of phytoplankton biomass and the deep chlorophyll maximum in oligotrophic environments: A Bio-Argo float investigation. *Global Biogeochemical Cycles, 28*, 856-876

Millie, D.F., Fahnenstiel, G.L., Lohrenz, S.E., Carrick, H.J., Johengen, T.H., & Schofield, O.M. (2003). Physical-biological coupling in southern Lake Michigan: influence of episodic sediment resuspension on phytoplankton. *Aquatic Ecology, 37*, 393-408

Mino, Y., Matsumura, S., Lirdwitayaprasit, T., Fujiki, T., Yanagi, T., & Saino, T. (2013). Variations in phytoplankton photo-physiology and productivity in a dynamic eutrophic ecosystem: a fast repetition rate fluorometer-based study. *Journal of plankton research, 36*, 398-411

Mitchell, B.G. (1990). Algorithms for determining the absorption coefficient for aquatic particulates using the quantitative filter technique. In, *Orlando'90, 16-20 April* (pp. 137-148): International Society for Optics and Photonics

Mitchell, B.G., & Kiefer, D.A. (1988). Chlorophyll α specific absorption and fluorescence excitation spectra for light-limited phytoplankton. *Deep Sea Research Part A. Oceanographic Research Papers, 35*, 639-663

Moisan, T.A., & Mitchell, B.G. (1999). Photophysiological acclimation of Phaeocystis antarctica Karsten under light limitation. *Limnology and Oceanography, 44*, 247-258

Moloney, C.L., & Field, J.G. (1991). The size-based dynamics of plankton food webs. I. A simulation model of carbon and nitrogen flows. *Journal of plankton research, 13*, 1003-1038

Moore, C.M., Suggett, D., Holligan, P.M., Sharples, J., Abraham, E.R., Lucas, M.I., Rippeth, T.P., Fisher, N.R., Simpson, J.H., & Hydes, D.J. (2003). Physical controls on phytoplankton physiology and production at a shelf sea front: a fast repetition-rate fluorometer based field study. *Marine Ecology Progress Series, 259*, 29-45

Moore, C.M., Suggett, D.J., Hickman, A.E., Kim, Y.-N., Tweddle, J.F., Sharples, J., Geider, R.J., & Holligan, P.M. (2006). Phytoplankton photoacclimation and photoadaptation in response to environmental gradients in a shelf sea. *Limnology and Oceanography, 51*, 936-949

Moore, J.K., Doney, S.C., Kleypas, J.A., Glover, D.M., & Fung, I.Y. (2001). An intermediate complexity marine ecosystem model for the global domain. *Deep Sea Research Part II: Topical Studies in Oceanography, 49*, 403-462

Moore, L.R., & Chisholm, S.W. (1999). Photophysiology of the marine cyanobacterium Prochlorococcus: ecotypic differences among cultured isolates. *Limnology and Oceanography, 44*, 628-638

Moore, L.R., Rocap, G., & Chisholm, S.W. (1998). Physiology and molecular phylogeny of coexisting Prochlorococcus ecotypes. *Nature, 393*, 464-467

Morán, X.A.G. (2007). Annual cycle of picophytoplankton photosynthesis and growth rates in a temperate coastal ecosystem: a major contribution to carbon fluxes. *Aquatic Microbial Ecology, 49*, 267-279

Morán, X.A.G., & Estrada, M. (2001). Short-term variability of photosynthetic parameters and particulate and dissolved primary production in the Alboran Sea (SW Mediterranean). *Marine Ecology Progress Series, 212*, 53-67

Morán, X.A.G., Fernández, E., & Pérez, V. (2004). Size-fractionated primary production, bacterial production and net community production in subtropical and tropical domains of the oligotrophic NE Atlantic in autumn. *Marine Ecology Progress Series, 274*, 17-29

Morán, X.A.G., & Scharek, R. (2015). Photosynthetic parameters and primary production, with focus on large phytoplankton, in a temperate mid-shelf ecosystem. *Estuarine, Coastal and Shelf Science, 154*, 255-263

Morel, A. (1991). Light and marine photosynthesis: a spectral model with geochemical and climatological implications. *Progress in Oceanography, 26*, 263-306

Morel, A., Ahn, Y.-H., Partensky, F., Vaulot, D., & Claustre, H. (1993). Prochlorococcus and Synechococcus: a comparative study of their optical properties in relation to their size and pigmentation. *Journal of Marine Research, 51*, 617-649

Morel, A., Antoine, D., Babin, M., & Dandonneau, Y. (1996). Measured and modeled primary production in the northeast Atlantic (EUMELI JGOFS program): the impact of natural variations in photosynthetic parameters on model predictive skill. *Deep Sea Research Part I: Oceanographic Research Papers, 43*, 1273-1304

Morel, A., & Bricaud, A. (1981). Theoretical results concerning light absorption in a discrete medium, and application to specific absorption of phytoplankton. *Deep Sea Research Part A. Oceanographic Research Papers, 28*, 1375-1393

Morel, A., Huot, Y., Gentili, B., Werdell, P.J., Hooker, S.B., & Franz, B.A. (2007). Examining the consistency of products derived from various ocean color sensors in open ocean (Case 1) waters in the perspective of a multi-sensor approach. *Remote Sensing of Environment, 111*, 69-88

Morel, A., & Prieur, L. (1977). Analysis of variations in ocean color. *Limnology and Oceanography, 22*, 709-722

Mouw, C.B., Hardman-Mountford, N.J., Alvain, S., Bracher, A., Brewin, R.J., Bricaud, A., Ciotti, A.M., Devred, E., Fujiwara, A., & Hirata, T. (2017). A Consumer's Guide to Satellite Remote Sensing ofMultiple Phytoplankton Groups in the Global Ocean. *Frontiers in Marine Sciecne, 4*

Muller-Karger, F.E., Varela, R., Thunell, R., Luerssen, R., Hu, C., & Walsh, J.J. (2005). The importance of continental margins in the global carbon cycle. *Geophysical Research Letters, 32*, n/a-n/a

Müller, P., Li, X.-P., & Niyogi, K.K. (2001). Non-photochemical quenching. A response to excess light energy. *Plant Physiology, 125*, 1558-1566

Nair, A., Sathyendranath, S., Platt, T., Morales, J., Stuart, V., Forget, M.-H., Devred, E., & Bouman, H. (2008). Remote sensing of phytoplankton functional types. *Remote Sensing of Environment, 112*, 3366-3375

Nechad, B., Ruddick, K., Schroeder, T., Oubelkheir, K., Blondeau-Patissier, D., Cherukuru, N., Brando, V., Dekker, A., Clementson, L., & Banks, A.C. (2015). CoastColour Round Robin data sets: a database to evaluate the performance of algorithms for the retrieval of water quality parameters in coastal waters. *Earth system science data, 7*, 319

Nelson, N.B., & Siegel, D.A. (2013). The global distribution and dynamics of chromophoric dissolved organic matter. *Annual Review of Marine Science, 5*, 447-476

Nelson, N.B., Siegel, D.A., & Michaels, A.F. (1998). Seasonal dynamics of colored dissolved material in the Sargasso Sea. *Deep Sea Research Part I: Oceanographic Research Papers, 45*, 931-957

Ning, X., Cloern, J.E., & Cole, B.E. (2000). Spatial and temporal variability of picocyanobacteria Synechococcus sp. in San Francisco Bay. *Limnology and Oceanography, 45*, 695-702

O'Reilly, J.E., Maritorena, S., Mitchell, B.G., Siegel, D.A., Carder, K.L., Garver, S.A., Kahru, M., & McClain, C. (1998). Ocean color chlorophyll algorithms for SeaWiFS. *Journal of Geophysical Research: Oceans, 103*, 24937-24953

O'Reilly, J.E., Maritorena, S., Siegel, D.A., O'Brien, M.C., Toole, D., Mitchell, B.G., Kahru, M., Chavez, F.P., Strutton, P., & Cota, G.F. (2000). Ocean color chlorophyll a algorithms for SeaWiFS, OC2, and OC4: Version 4. *SeaWiFS postlaunch calibration and validation analyses, Part, 3*, 9-23

Olaizola, M., La Roche, J., Kolber, Z., & Falkowski, P.G. (1994). Non-photochemical fluorescence quenching and the diadinoxanthin cycle in a marine diatom. *Photosynthesis Research, 41*, 357-370

Olenina, I., Hajdu, S., Edler, L., Andersson, A., Wasmund, N., Busch, S., Gobel, J., Huseby, S., Huttunen, M., & Jaanus, A. (2006). Biovolumes and size-classes of phytoplankton in the Baltic Sea. Helcom Baltic Sea Environ Proc No. 106. *Baltic Mar. Environ. Prot. Comm, 144*

Organelli, E., Nuccio, C., Lazzara, L., Uitz, J., Bricaud, A., & Massi, L. (2017). On the discrimination of multiple phytoplankton groups from light absorption spectra of assemblages with mixed taxonomic composition and variable light conditions. *Applied Optics, 56*, 3952-3968

Pace, M., Glasser, J., & Pomeroy, L. (1984). A simulation analysis of continental shelf food webs. *Marine Biology, 82*, 47-63

Palmer, M., Green, M., Inall, M., & Hopkins, J. (2012). Internal Tidal bores and Turbulent Mixing at the Celtic Sea Shelf Break. In, *AGU Fall Meeting Abstracts*

Palmer, M.R., Stephenson, G.R., Inall, M.E., Balfour, C., Düsterhus, A., & Green, J.A.M. (2015). Turbulence and mixing by internal waves in the Celtic Sea determined from ocean glider microstructure measurements. *Journal of Marine Systems, 144*, 57-69

Pauly, D., Christensen, V., Guénette, S., Pitcher, T.J., Sumaila, U.R., Walters, C.J., Watson, R., & Zeller, D. (2002). Towards sustainability in world fisheries. *Nature, 418*, 689-695

Payet, J.P., & Suttle, C.A. (2008). Physical and biological correlates of virus dynamics in the southern Beaufort Sea and Amundsen Gulf. *Journal of Marine Systems, 74*, 933-945

Pemberton, K., Rees, A.P., Miller, P.I., Raine, R., & Joint, I. (2004). The influence of water body characteristics on phytoplankton diversity and production in the Celtic Sea. *Continental shelf research, 24*, 2011-2028

Petrou, K., Kranz, S.A., Doblin, M.A., & Ralph, P.J. (2012). Photophysiological responses of Fragilariopsis cylindrus (Bacillariophyceae) to nitrogen depletion at two temperatures. *Journal of Phycology, 48*, 127-136

Pickett, J.M., & Myers, J. (1966). Monochromatic Light Saturation Curves for Photosynthesis in Chlorella. *Plant Physiology, 41*, 90-98

Pingree, R., Holligan, P., Mardell, G., & Head, R. (1976). The influence of physical stability on spring, summer and autumn phytoplankton blooms in the Celtic Sea. *Journal of the Marine Biological Association of the United Kingdom, 56*, 845-873

Pingree, R.D., Holligan, P.M., & Mardell, G.T. (1978). The effects of vertical stability on phytoplankton distributions in the summer on the northwest European Shelf. *Deep Sea Research, 25*, 1011-1028

Pingree, R.D., Mardell, G.T., Holligan, P.M., Griffiths, D.K., & Smithers, J. (1982). Celtic Sea and Armorican current structure and the vertical distributions of temperature and chlorophyll. *Continental shelf research, 1*, 99-116

Platt, T., Fuentes-Yaco, C., & Frank, K.T. (2003). Marine ecology: spring algal bloom and larval fish survival. *Nature, 423*, 398-399

Platt, T., Gallegos, C., & Harrison, W. (1980a). Photoinhibition of photosynthesis in natural assemblages of marine phytoplankton. *Journal of Marine Research (USA), 38*

Platt, T., Gallegos, C., & Harrison, W. (1980b). Photoinhibition of photosynthesis in natural assemblages of marine phytoplankton

Platt, T., Gallegos, C., & Harrison, W. (1981). Photoinhibition of photosynthesis in natural assemblages of marine phytoplankton

Platt, T., Rao, D.S., & Irwin, B. (1983). Photosynthesis of picoplankton in the oligotrophic ocean. *Nature, 301*, 702

Platt, T., & Sathyendranath, S. (2009). Hikari to Kaiyou no Ichiji Seisan (Light and Marine Primary Production) In Japanese. In (pp. 1-174)

Pomeroy, L.R., le BWilliams, P., Azam, F., & Hobbie, J.E. (2007). The microbial loop. *OCEANOGRAPHY-WASHINGTON DC-OCEANOGRAPHY SOCIETY-, 20*, 28

Pope, R.M., & Fry, E.S. (1997). Absorption spectrum (380–700 nm) of pure water. II. Integrating cavity measurements. *Applied Optics, 36*, 8710-8723

Poulton, A.J., Davis, C.E., Daniels, C.J., Mayers, K.M.J., Harris, C., Tarran, G.A., Widdicombe, C.E., & Woodward, E.M.S. (2017). Seasonal phosphorus and carbon dynamics in a temperate shelf sea (Celtic Sea). *Progress in Oceanography*

Poulton, A.J., Holligan, P.M., Hickman, A., Kim, Y.-N., Adey, T.R., Stinchcombe, M.C., Holeton, C., Root, S., & Woodward, E.M.S. (2006). Phytoplankton carbon fixation, chlorophyll-biomass and diagnostic pigments in the Atlantic Ocean. *Deep Sea Research Part II: Topical Studies in Oceanography, 53*, 1593-1610

Powles, S.B. (1984). Photoinhibition of photosynthesis induced by visible light. *Annual review of plant physiology, 35*, 15-44

Prabhakara, C., Dalu, G., & Kunde, V. (1974). Estimation of sea surface temperature from remote sensing in the 11-to 13-μm window region. *Journal of Geophysical research, 79*, 5039-5044

Qin, P., Simis, S.G., & Tilstone, G.H. (2017). Radiometric validation of atmospheric correction for MERIS in the Baltic Sea based on continuous observations from ships and AERONET-OC. *Remote Sensing of Environment, 200*, 263-280

Racault, M.-F., Sathyendranath, S., Menon, N., & Platt, T. (2017). Phenological responses to ENSO in the global oceans. *Surveys in Geophysics, 38*, 277-293

Racault, M.-F., Sathyendranath, S., & Platt, T. (2014). Impact of missing data on the estimation of ecological indicators from satellite ocean-colour time-series. *Remote Sensing of Environment, 152*, 15-28

Raine, R., & McMahon, T. (1998). Physical dynamics on the continental shelf off southwestern Ireland and their influence on coastal phytoplankton blooms. *Continental shelf research, 18*, 883-914

Raven, J. (1980). Chloroplasts of eukaryotic micro-organisms. In, *The Eukaryotic Microbial Cell—13th Symposium of the Society for General Microbiology* (pp. 181-205)

Raven, J. (1998). The twelfth Tansley Lecture. Small is beautiful: the picophytoplankton. *Functional ecology, 12*, 503-513

Rees, A.P., Joint, I., & Donald, K.M. (1999). Early spring bloom phytoplankton-nutrient dynamics at the Celtic Sea Shelf Edge. *Deep Sea Research Part I: Oceanographic Research Papers, 46*, 483-510

Reid, P.C., Lancelot, C., Gieskes, W.W.C., Hagmeier, E., & Weichart, G. (1990). Phytoplankton of the North Sea and its dynamics: A review. *Netherlands Journal of Sea Research, 26*, 295-331

Retamal, L., Bonilla, S., & Vincent, W.F. (2008). Optical gradients and phytoplankton production in the Mackenzie River and the coastal Beaufort Sea. *Polar Biology, 31*, 363-379

Reul, A., Rodríguez, J., Blanco, J., Rees, A., & Burkill, P. (2006). Control of microplankton size structure in contrasting water columns of the Celtic Sea. *Journal of Plankton Research, 28*, 449-457

Reul, N., Fournier, S., Boutin, J., Hernandez, O., Maes, C., Chapron, B., Alory, G., Quilfen, Y., Tenerelli, J., & Morisset, S. (2014). Sea surface salinity observations from space with the SMOS satellite: A new means to monitor the marine branch of the water cycle. *Surveys in Geophysics, 35*, 681-722

Ridgway, J., & Shimmield, G. (2002). Estuaries as repositories of historical contamination and their impact on shelf seas. *Estuarine, Coastal and Shelf Science, 55*, 903-928

Robinson, A., Bouman, H.A., Tilstone, G.H., & Sathyendranath, S. (2018). Size class dependent relationships between temperature and phytoplankton photosynthesis-irradiance parameters in the Atlantic Ocean. *Frontiers in Marine Science, 4*, 435

Robinson, C., Tilstone, G.H., Rees, A.P., Smyth, T.J., Fishwick, J.R., Tarran, G.A., Luz, B., Barkan, E., & David, E. (2009). Comparison of in vitro and in situ plankton production determinations. *Aquatic Microbial Ecology, 54*, 13-34

Rodriguez, F., Chauton, M., Johnsen, G., Andresen, K., Olsen, L., & Zapata, M. (2006). Photoacclimation in phytoplankton: implications for biomass estimates, pigment functionality and chemotaxonomy. *Marine Biology, 148*, 963-971

Rodríguez, F., Derelle, E., Guillou, L., Le Gall, F., Vaulot, D., & Moreau, H. (2005). Ecotype diversity in the marine picoeukaryote Ostreococcus (Chlorophyta, Prasinophyceae). *Environmental microbiology, 7*, 853-859

Rousseaux, C.S., & Gregg, W.W. (2013). Interannual variation in phytoplankton primary production at a global scale. *Remote sensing, 6*, 1-19

Roy, S. (2000). Strategies for the minimisation of UV-induced damage. *The effects of UV radiation in the marine environment*, 177-205

Roy, S., Sathyendranath, S., & Platt, T. (2011). Retrieval of phytoplankton size from bio-optical measurements: theory and applications. *Journal of the Royal Society Interface, 8*, 650-660

Roy, S., Sathyendranath, S., & Platt, T. (2017). Size-partitioned phytoplankton carbon and carbon-to-chlorophyll ratio from ocean colour by an absorption-based bio-optical algorithm. *Remote Sensing of Environment, 194*, 177-189

Ruf, C.S., Atlas, R., Chang, P.S., Clarizia, M.P., Garrison, J.L., Gleason, S., Katzberg, S.J., Jelenak, Z., Johnson, J.T., & Majumdar, S.J. (2016). New ocean winds satellite mission to probe hurricanes and tropical convection. *Bulletin of the American Meteorological Society, 97*, 385-395

Sathyendranath, S., Aiken, J., Alvain, S., Barlow, R., Bouman, H., Bracher, A., Brewin, R., Bricaud, A., Brown, C., & Ciotti, A. (2014). Phytoplankton functional types from Space. *(Reports of the International Ocean-Colour Coordinating Group (IOCCG); 15)* (pp. 1-156): International Ocean-Colour Coordinating Group

Sathyendranath, S., Brewin, R.J., Jackson, T., Mélin, F., & Platt, T. (2017). Ocean-colour products for climate-change studies: What are their ideal characteristics? *Remote Sensing of Environment*

Sathyendranath, S., Cota, G., Stuart, V., Maass, H., & Platt, T. (2001). Remote sensing of phytoplankton pigments: a comparison of empirical and theoretical approaches. *International Journal of Remote Sensing, 22*, 249-273

Sathyendranath, S., Lazzara, L., & Prieur, L. (1987). Variations in the spectral values of specific absorption of phytoplankton. *Limnology and Oceanography, 32*, 403-415

Sathyendranath, S., & Platt, T. (1989). Computation of aquatic primary production: extended formalism to include effect of angular and spectral distribution of light. *Limnology and Oceanography, 34*, 188-198

Sathyendranath, S., Platt, T., Caverhill, C.M., Warnock, R.E., & Lewis, M.R. (1989). Remote sensing of oceanic primary production: computations using a spectral model. *Deep Sea Research Part A. Oceanographic Research Papers, 36*, 431-453

Sathyendranath, S., Watts, L., Devred, E., Platt, T., Caverhill, C., & Maass, H. (2004). Discrimination of diatoms from other phytoplankton using ocean-colour data. *Marine Ecology Progress Series, 272*, 59-68

Saux Picart, S., Sathyendranath, S., Dowell, M., Moore, T., & Platt, T. (2014). Remote sensing of assimilation number for marine phytoplankton. *Remote Sensing of Environment, 146*, 87-96

Scales, K.L., Miller, P.I., Embling, C.B., Ingram, S.N., Pirotta, E., & Votier, S.C. (2014). Mesoscale fronts as foraging habitats: composite front mapping reveals oceanographic

drivers of habitat use for a pelagic seabird. *Journal of the Royal Society Interface, 11*, 20140679

Schallenberg, M., & Burns, C.W. (2004). Effects of sediment resuspension on phytoplankton production: teasing apart the influences of light, nutrients and algal entrainment. *Freshwater Biology, 49*, 143-159

Schaum, E., Rost, B., Millar, A.J., & Collins, S. (2013). Variation in plastic responses of a globally distributed picoplankton species to ocean acidification. *Nature Climate Change, 3*, 298

Schl, xfc, ter, L., xf, hlenberg, F., Havskum, H., & Larsen, S. (2000). The use of phytoplankton pigments for identifying and quantifying phytoplankton groups in coastal areas: testing the influence of light and nutrients on pigment/chlorophyll a ratios. *Marine Ecology Progress Series, 192*, 49-63

Schlüter, L., Møhlenberg, F., Havskum, H., & Larsen, S. (2000). The use of phytoplankton pigments for identifying and quantifying phytoplankton groups in coastal areas: testing the influence of light and nutrients on pigment/chlorophyll a ratios. *Marine Ecology Progress Series*, 49-63

Schulien, J.A., Behrenfeld, M.J., Hair, J.W., Hostetler, C.A., & Twardowski, M.S. (2017). Vertically-resolved phytoplankton carbon and net primary production from a high spectral resolution lidar. *Optics Express, 25*, 13577-13587

Segura, V., Lutz, V.A., Dogliotti, A., Silva, R.I., Negri, R.M., Akselman, R., & Benavides, H. (2013). Phytoplankton types and primary production in the Argentine Sea. *Mar Ecol Prog Ser, 491*, 15-31

Seppälä, J., Ylöstalo, P., & Kuosa, H. (2005). Spectral absorption and fluorescence characteristics of phytoplankton in different size fractions across a salinity gradient in the Baltic Sea. *International Journal of Remote Sensing, 26*, 387-414

Sharples, J., Moore, C.M., & Abraham, E.R. (2001a). Internal tide dissipation, mixing, and vertical nitrate flux at the shelf edge of NE New Zealand. *Journal of Geophysical research, 106*, 14069-14081

Sharples, J., Moore, C.M., Hickman, A.E., Holligan, P.M., Tweddle, J.F., Palmer, M.R., & Simpson, J.H. (2009). Internal tidal mixing as a control on continental margin ecosystems. *Geophysical Research Letters, 36*

Sharples, J., Moore, M.C., Rippeth, T.P., Holligan, P.M., Hydes, D.J., Fisher, N.R., & Simpson, J.H. (2001b). Phytoplankton distribution and survival in the thermocline. *Limnology and Oceanography, 46*, 486-496

Sharples, J., & Tett, P. (1994). Modelling the effect of physical variability on the midwater chlorophyll maximum. *Journal of Marine Research, 52*, 219-238

Sherr, E., & Sherr, B. (1988). Role of microbes in pelagic food webs: a revised concept. *Limnology and Oceanography, 33*, 1225-1227

Siegel, D., Maritorena, S., Nelson, N., Behrenfeld, M., & McClain, C. (2005). Colored dissolved organic matter and its influence on the satellite-based characterization of the ocean biosphere. *Geophysical Research Letters, 32*

Siemering, B., Bresnan, E., Painter, S.C., Daniels, C.J., Inall, M., & Davidson, K. (2016). Phytoplankton Distribution in Relation to Environmental Drivers on the North West European Shelf Sea. *PLoS One, 11*, e0164482

Silsbe, G.M., Oxborough, K., Suggett, D.J., Forster, R.M., Ihnken, S., Komárek, O., Lawrenz, E., Prášil, O., Röttgers, R., Šicner, M., Simis, S.G.H., Dijk, M.A.V., & Kromkamp, J.C. (2015). Toward autonomous measurements of photosynthetic electron transport rates: An evaluation of active fluorescence-based measurements of photochemistry. *Limnology and Oceanography: Methods, 13*, e10014

Simmons, M.P., Sudek, S., Monier, A., Limardo, A.J., Jimenez, V., Perle, C.R., Elrod, V.A., Pennington, J.T., & Worden, A.Z. (2016). Abundance and biogeography of picoprasinophyte ecotypes and other phytoplankton in the Eastern North Pacific Ocean. *Applied and environmental microbiology, 82*, 1693-1705

Siswanto, E., Ishizaka, J., & Yokouchi, K. (2005). Estimating Chlorophyll-a Vertical Profiles from Satellite Data and the Implication for Primary Production in the Kuroshio Front of the East China Sea. *Journal of oceanography, 61*, 575-589

Siswanto, E., Tang, J., Yamaguchi, H., Ahn, Y.-H., Ishizaka, J., Yoo, S., Kim, S.-W., Kiyomoto, Y., Yamada, K., & Chiang, C. (2011). Empirical ocean-color algorithms to retrieve chlorophyll-a, total suspended matter, and colored dissolved organic matter absorption coefficient in the Yellow and East China Seas. *Journal of oceanography, 67*, 627

Smith, R., Eppley, R., & Baker, K. (1982). Correlation of primary production as measured aboard ship in southern California coastal waters and as estimated from satellite chlorophyll images. *Marine Biology, 66*, 281-288

Smith, R.C., & Baker, K.S. (1978). The bio-optical state of ocean waters and remote sensing. *Limnology and Oceanography, 23*, 247-259

Smyth, T., Tilstone, G., & Groom, S. (2005). Integration of radiative transfer into satellite models of ocean primary production. *Journal of Geophysical Research: Oceans, 110*

Sosik, H.M., & Mitchell, B.G. (1994). Effects of temperature on growth, light absorption, and quantum yield in Dunaliella tertiolecta (Chlorophyceae). *Journal of Phycology, 30*, 833-840

Springer, A.M., & McRoy, C.P. (1993). The paradox of pelagic food webs in the northern Bering Sea—III. Patterns of primary production. *Continental shelf research, 13*, 575-599

Stæhr, P.A., Henriksen, P., & Markager, S. (2002). Photoacclimation of four marine phytoplankton species to irradiance and nutrient availability. *Marine Ecology Progress Series, 238*, 47-59

Steinberg, D.K., Carlson, C.A., Bates, N.R., Goldthwait, S.A., Madin, L.P., & Michaels, A.F. (2000). Zooplankton vertical migration and the active transport of dissolved organic and inorganic carbon in the Sargasso Sea. *Deep Sea Research Part I: Oceanographic Research Papers, 47*, 137-158

Steinberg, D.K., Nelson, N.B., Carlson, C.A., & Prusak, A. (2004). Production of chromophoric dissolved organic matter (CDOM) in the open ocean by zooplankton and the colonial cyanobacterium Trichodesmium spp. *Marine Ecology Progress Series, 267*, 45-56

Stomp, M., Huisman, J., De Jongh, F., Veraart, A.J., Gerla, D., Rijkeboer, M., Ibelings, B.W., Wollenzien, U.I., & Stal, L.J. (2004). Adaptive divergence in pigment composition promotes phytoplankton biodiversity. *Nature, 432*, 104

Stuart, V., Sathyendranath, S., Head, E., Platt, T., Irwin, B., & Maass, H. (2000). Bio-optical characteristics of diatom and prymnesiophyte populations in the Labrador Sea. *Marine Ecology Progress Series, 201*, 91-106

Stuart, V., Sathyendranath, S., Platt, T., Maass, H., & Irwin, B.D. (1998). Pigments and species composition of natural phytoplankton populations: effect on the absorption spectra. *Journal of plankton research, 20*, 187-217

Subramaniam, A., Brown, C.W., Hood, R.R., Carpenter, E.J., & Capone, D.G. (2001). Detecting Trichodesmium blooms in SeaWiFS imagery. *Deep Sea Research Part II: Topical Studies in Oceanography, 49*, 107-121

Suggett, D.J., Moore, C.M., Hickman, A.E., & Geider, R.J. (2009). Interpretation of fast repetition rate (FRR) fluorescence: signatures of phytoplankton community structure versus physiological state. *Mar. Ecol. Prog. Ser, 376*, 1-19

Sullivan, J.M., Donaghay, P.L., & Rines, J.E. (2010). Coastal thin layer dynamics: consequences to biology and optics. *Continental shelf research, 30*, 50-65

Suttle, C.A., & Chan, A.M. (1994). Dynamics and distribution of cyanophages and their effect on marine Synechococcus spp. *Applied and environmental microbiology, 60*, 3167-3174

Tarran, G.A., Heywood, J.L., & Zubkov, M.V. (2006). Latitudinal changes in the standing stocks of nano-and picoeukaryotic phytoplankton in the Atlantic Ocean. *Deep Sea Research Part II: Topical Studies in Oceanography, 53*, 1516-1529

Tett, P., & Barton, E. (1995). Why are there about 5000 species of phytoplankton in the sea? *Journal of plankton research, 17*, 1693-1704

Thakur, K.K., Vanderstichel, R., Barrell, J., Stryhn, H., Patanasatienkul, T., & Revie, C. (2018). Comparison of remotely-sensed sea surface temperature and salinity products with in situ measurements from British Columbia, Canada. *Frontiers in Marine Science, 5*, 121

Thomas, H., Bozec, Y., Elkalay, K., & De Baar, H.J. (2004). Enhanced open ocean storage of CO2 from shelf sea pumping. *Science, 304*, 1005-1008

Thomas, J., O'Reilly, J., Pearce, J., Mahoney, J., Cohn, M., & Marshall, H. (1983). The use of phytoplankton measurements in monitoring environmental trends. *ICES CM*

Tian, T., Merico, A., Su, J., Staneva, J., Wiltshire, K., & Wirtz, K. (2009). Importance of resuspended sediment dynamics for the phytoplankton spring bloom in a coastal marine ecosystem. *Journal of Sea Research, 62*, 214-228

Tilstone, G., Figueiras, F., Fermín, E., & Arbones, B. (1999). Significance of nanophytoplankton photosynthesis and primary production in a coastal upwelling system (Ría de Vigo, NW Spain). *Marine Ecology Progress Series*, 13-27

Tilstone, G., Mallor-Hoya, S., Gohin, F., Couto, A.B., Sá, C., Goela, P., Cristina, S., Airs, R., Icely, J., & Zühlke, M. (2017). Which ocean colour algorithm for MERIS in North West European waters? *Remote Sensing of Environment, 189*, 132-151

Tilstone, G., Smyth, T., Poulton, A., & Hutson, R. (2009). Measured and remotely sensed estimates of primary production in the Atlantic Ocean from 1998 to 2005. *Deep Sea Research Part II: Topical Studies in Oceanography, 56*, 918-930

Tilstone, G.H., Figueiras, F., Lorenzo, L.M., & Arbones, B. (2003). Phytoplankton composition, photosynthesis and primary production during different hydrographic conditions at the Northwest Iberian upwelling system

Tilstone, G.H., Peters, S.W., van der Woerd, H.J., Eleveld, M.A., Ruddick, K., Schönfeld, W., Krasemann, H., Martinez-Vicente, V., Blondeau-Patissier, D., & Röttgers, R. (2012). Variability in specific-absorption properties and their use in a semi-analytical ocean colour

algorithm for MERIS in North Sea and Western English Channel Coastal Waters. *Remote Sensing of Environment, 118*, 320-338

Tilstone, G.H., Smyth, T.J., Gowen, R.J., Martinez-Vicente, V., & Groom, S.B. (2005). Inherent optical properties of the Irish Sea and their effect on satellite primary production algorithms. *Journal of plankton research, 27*, 1127-1148

Tremblay, G., Belzile, C., Gosselin, M., Poulin, M., Roy, S., & Tremblay, J.-É. (2009). Late summer phytoplankton distribution along a 3500 km transect in Canadian Arctic waters: strong numerical dominance by picoeukaryotes. *Aquatic Microbial Ecology, 54*, 55-70

Tweddle, J.F., Sharples, J., Palmer, M.R., Davidson, K., & McNeill, S. (2013). Enhanced nutrient fluxes at the shelf sea seasonal thermocline caused by stratified flow over a bank. *Progress in Oceanography, 117*, 37-47

Uitz, J., Claustre, H., Gentili, B., & Stramski, D. (2010). Phytoplankton class-specific primary production in the world's oceans: seasonal and interannual variability from satellite observations. *Global Biogeochemical Cycles, 24*

Uitz, J., Claustre, H., Morel, A., & Hooker, S.B. (2006). Vertical distribution of phytoplankton communities in open ocean: An assessment based on surface chlorophyll. *Journal of Geophysical Research: Oceans, 111*

Uitz, J., Huot, Y., Bruyant, F., Babin, M., & Claustre, H. (2008). Relating phytoplankton photophysiological properties to community structure on large scales. *Limnology and Oceanography, 53*, 614

Uitz, J., Stramski, D., Gentili, B., D'Ortenzio, F., & Claustre, H. (2012). Estimates of phytoplankton class-specific and total primary production in the Mediterranean Sea from satellite ocean color observations. *Global Biogeochemical Cycles, 26*

Uitz, J., Stramski, D., Reynolds, R.A., & Dubranna, J. (2015). Assessing phytoplankton community composition from hyperspectral measurements of phytoplankton absorption coefficient and remote-sensing reflectance in open-ocean environments. *Remote Sensing of Environment, 171*, 58-74

van de Poll, W.H., Visser, R.J., & Buma, A.G. (2007). Acclimation to a dynamic irradiance regime changes excessive irradiance sensitivity of Emiliania huxleyi and Thalassiosira weissflogii. *Limnology and Oceanography, 52*, 1430-1438

Van den Berg, A., Ridderinkhof, H., Riegman, R., Ruardij, P., & Lenhart, H. (1996). Influence of variability in water transport on phytoplankton biomass and composition in the southern North Sea: a modelling approach (FYFY). *Continental shelf research, 16*, 907919-917931

Vandermeulen, R.A., Mannino, A., Neeley, A., Werdell, J., & Arnone, R. (2017). Determining the optimal spectral sampling frequency and uncertainty thresholds for hyperspectral remote sensing of ocean color. *Optics Express, 25*, A785-A797

Varunan, T., & Shanmugam, P. (2015). A model for estimating size-fractioned phytoplankton absorption coefficients in coastal and oceanic waters from satellite data. *Remote Sensing of Environment, 158*, 235-254

Vaulot, D., Eikrem, W., Viprey, M., & Moreau, H. (2008). The diversity of small eukaryotic phytoplankton (≤ 3 μm) in marine ecosystems. *FEMS microbiology reviews, 32*, 795-820

Veldhuis, M.J., Timmermans, K.R., Croot, P., & van der Wagt, B. (2005). Picophytoplankton; a comparative study of their biochemical composition and photosynthetic properties. *Journal of Sea Research, 53*, 7-24

Verdy, A., Follows, M., & Flierl, G. (2009). Optimal phytoplankton cell size in an allometric model. *Marine Ecology Progress Series, 379*, 1-12

Vidussi, F., Claustre, H., Manca, B.B., Luchetta, A., & Marty, J.C. (2001). Phytoplankton pigment distribution in relation to upper thermocline circulation in the eastern Mediterranean Sea during winter. *Journal of Geophysical Research: Oceans, 106*, 19939-19956

Walsh, J.J., Rowe, G.T., Iverson, R.L., & McRoy, C.P. (1981). Biological export of shelf carbon is a sink of the global CO2 cycle. *Nature, 291*, 196

Warwick, R., & Joint, I. (1987). The size distribution of organisms in the Celtic Sea: from bacteria to metazoa. *Oecologia, 73*, 185-191

Wasmund, N., Andrushaitis, A., Łysiak-Pastuszak, E., Müller-Karulis, B., Nausch, G., Neumann, T., Ojaveer, H., Olenina, I., Postel, L., & Witek, Z. (2001). Trophic status of the south-eastern Baltic Sea: a comparison of coastal and open areas. *Estuarine, Coastal and Shelf Science, 53*, 849-864

Weeks, A., Conte, M.H., Harris, R.P., Bedo, A., Bellan, I., Burkill, P.H., Edwards, E.S., Harbour, D.S., Kennedy, H., Llewellyn, C., Mantoura, R.F.C., Morales, C.E., Pomroy, A.J., & Turley, C.M. (1993). The physical and chemical environment and changes in community structure associated with bloom evolution: the Joint Global Flux Study North Atlantic Bloom Experiment. *Deep Sea Research Part II: Topical Studies in Oceanography, 40*, 347-368

Welschmeyer, N.A. (1994). Fluorometric analysis of chlorophyll a in the presence of chlorophyll b and pheopigments. *Limnology and Oceanography, 39*, 1985-1992

Werdell, P.J., & Bailey, S.W. (2005). An improved in-situ bio-optical data set for ocean color algorithm development and satellite data product validation. *Remote Sensing of Environment, 98*, 122-140

Weston, K., Fernand, L., Mills, D.K., Delahunty, R., & Brown, J. (2005). Primary production in the deep chlorophyll maximum of the central North Sea. *Journal of plankton research, 27*, 909-922

Widdicombe, C.E., Eloire, D., Harbour, D., Harris, R.P., & Somerfield, P.J. (2010). Long-term phytoplankton community dynamics in the Western English Channel. *Journal of plankton research, 32*, 643-655

Williams, C., Palmer, M., Mahaffey, C., & Jardine, J. (2016). Shelf Sea Oxygen Dynamics: A year of Glider Measurements. In, *American Geophysical Union, Ocean Sciences Meeting 2016, abstract# EC44C-1261*

Williams, R.G., & Follows, M.J. (1998). The Ekman transfer of nutrients and maintenance of new production over the North Atlantic. *Deep Sea Research Part I: Oceanographic Research Papers, 45*, 461-489

Wiltshire, K.H., Malzahn, A.M., Wirtz, K., Greve, W., Janisch, S., Mangelsdorf, P., Manly, B.F., & Boersma, M. (2008). Resilience of North Sea phytoplankton spring bloom dynamics: An analysis of long-term data at Helgoland Roads. *Limnology and Oceanography, 53*, 1294-1302

Wisniewski, R.N. (1993). The release of phosphorus during sediment resuspension. In, *Proceedings of the Third International Workshop on Phosphorus in Sediments* (pp. 321-322): Springer

Wolanin, A., Soppa, M.A., & Bracher, A. (2016). Investigation of spectral band requirements for improving retrievals of phytoplankton functional types. *Remote Sensing, 8*, 871

Wright, S., Jeffrey, S., & Mantoura, R. (2005). *Phytoplankton pigments in oceanography: guidelines to modern methods*. Unesco Pub.

Xi, H., Hieronymi, M., Röttgers, R., Krasemann, H., & Qiu, Z. (2015). Hyperspectral differentiation of phytoplankton taxonomic groups: a comparison between using remote sensing reflectance and absorption spectra. *Remote Sensing, 7*, 14781-14805

Xie, Y., Tilstone, G.H., Widdicombe, C., Woodward, E.M.S., Harris, C., & Barnes, M. (2015). Effects of increases in temperature and nutrients on phytoplankton community structure and photosynthesis in the Western English Channel. *Marine Ecology Progress Series, 519*, 61-73

Xing, X., Morel, A., Claustre, H., Antoine, D., D'Ortenzio, F., Poteau, A., & Mignot, A. (2011). Combined processing and mutual interpretation of radiometry and fluorimetry from autonomous profiling Bio-Argo floats: Chlorophyll a retrieval. *Journal of Geophysical Research: Oceans, 116*

Yunev, O.A., Carstensen, J., Moncheva, S., Khaliulin, A., Ærtebjerg, G., & Nixon, S. (2007). Nutrient and phytoplankton trends on the western Black Sea shelf in response to cultural eutrophication and climate changes. *Estuarine, Coastal and Shelf Science, 74*, 63-76

Zinser, E., Johnson, Z., Coe, A., Karaca, E., Veneziano, D., & W. Chisholm, S. (2007). *Influence of Light and Temperature on Prochlorococcus Ecotype Distributions in the Atlantic Ocean*.